JOURNAL OF APPLIED PHYSICS

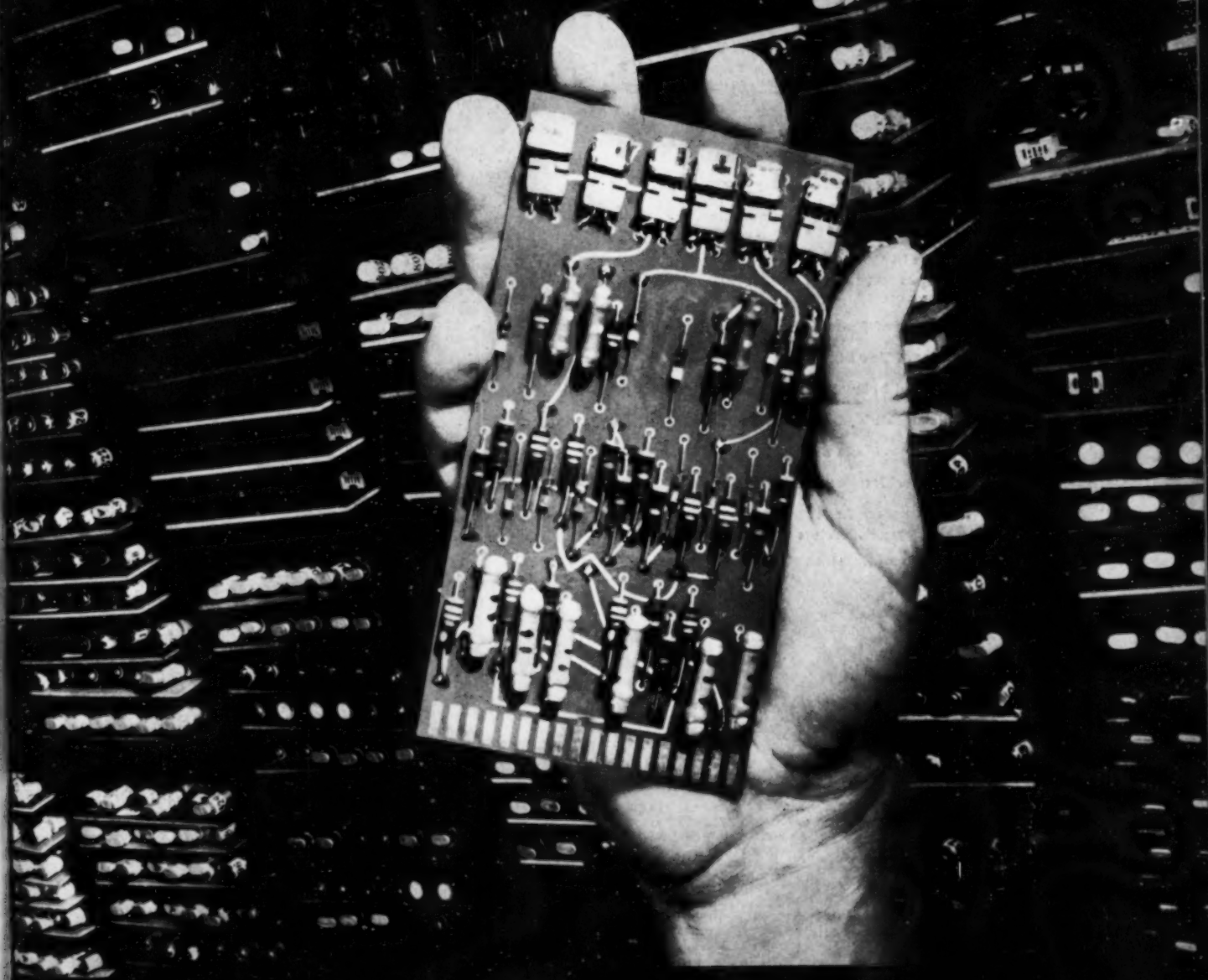

JOURNAL OF APPLIED PHYSICS

Vol. 25, No. 12 DECEMBER, 1954

In This Issue

	Page
Heat Conduction in an Infinite Cylindrical Medium with Heat Generated by a Chemical Reaction — Peter L. Nichols, Jr., and Arthur G. Presson	1469
Current Fluctuation Phenomena in Current-Carrying Sliding Contacts — G. W. Epprecht	1473
Electric Strength and Molecular Structure of Saturated Hydrocarbon Liquids — R. W. Crowe, A. H. Sharbaugh, and J. K. Bragg	1480
Water Vapor Condensation Process in Supersonic Nozzles — Peter P. Wegener	1485
Analysis of Short-Time Tracer Injection in Underground Formations — G. C. Wallick and R. Jenkins	1491
Etching of Single Crystal Germanium Spheres — Ray C. Ellis, Jr.	1497
Equivalent Circuit for a Passive Nonreciprocal Network — H. A. Haus	1500
X-Ray Study of the Graphitization of Carton Black — C. R. Houska and B. E. Warren	1503
Definition of Passive Linear Networks in Terms of Time and Energy — G. Raisbeck	1510
Noise in Transverse-Field Traveling-Wave Tubes — G. Wade, K. Amo, and D. A. Watkins	1514
Measurement of Temperatures in Flames of Complex Structure by Resonance Line Radiation. I. General Theory and Application to Sodium Line Reversal Methods — H. M. Strong and F. P. Bundy	1521
Measurement of Temperatures in Flames of Complex Structure by Resonance Line Radiation. II. Sodium Line Reversal by High-Resolution Spectroscopy — H. M. Strong and F. P. Bundy	1527
Measurement of Temperatures in Flames of Complex Structure by Resonance Line Radiation. III. From Absolute Intensity Measurements at High Resolution — F. P. Bundy and H. M. Strong	1531
Anisotropy of Diffusion in Grain Boundaries — S. R. L. Couling and R. Smoluchowski	1538
On the Effect of Integration in a Pulsed Radar, Randomly Modulated Carrier — W. M. Stone	1543
Letters to the Editor:	
Information Theory and Knowledge: Remarks on a Paper by D. K. C. MacDonald — A. Gamba	1549
On the Interaction of Two Similarly Facing Plane Shock Waves — C. A. Ford and I. I. Glass	1549
Propagation Constant in Rectangular Wave Guide of Finite Conductivity — D. M. Kerns and R. W. Hedberg	1550
Variational and Galerkin's Methods in Compressible Fluid Flow Problems — Pei Chi Chou	1551
Semiconductor Devices Made with Single Crystal Germanium-Silicon Alloys — R. A. Logan, A. J. Goss, and M. Schwartz	1551
Thermodynamic Consideration of Electromagnetic Cavity Resonators — Charles H. Papas	1552
Errata: Modified Luneberg Lens — A. S. Gutman	1553
Comments on Gumowski's Letters on Summation of Slowly Converging Series — E. L. Chu	1553
Experimental Studies of Betatron Orbit Stability — G. C. Baldwin, F. R. Elder, and W. F. Westendorp	1553
Books Reviewed	1554
Books Received	1556
Cover Photograph	1556
Author Index to Volume 25	1557
Subject Index to Volume 25	1565
Index to Advertisers	xxii

ROBERT L. SPROULL
Editor

ELMER HUTCHISSON,
EARLE C. GREGG,
Retiring Editors

Board of Editors
MAURICE A. BIOT
RAY E. BOLZ
WALLACE J. ECKERT
ROBERT D. HEIDENREICH
LOUIS A. PIPES
ROMAN SMOLUCHOWSKI
W. R. SMYTHE
ARTHUR V. TOBOLSKY
ALVIN M. WEINBERG

Publication of the
American Institute of Physics

OFFICERS
FREDERICK SEITZ,
Chairman
GEORGE B. PEGRAM,
Treasurer

GOVERNING BOARD
ROBERT F. BACHER
J. W. BUCHTA
KARL K. DARROW
S. A. GOUDSMIT
DEANE B. JUDD
HUGH S. KNOWLES
C. C. LAURITSEN
W. H. MARKWOOD, JR.
WILLIAM F. MEGGERS
PHILIP M. MORSE
BRIAN O'BRIEN
HARRY F. OLSON
GEORGE B. PEGRAM
ERIC RODGERS
RALPH A. SAWYER
FREDERICK SEITZ
WILLIAM SHOCKLEY
RICHARD M. SUTTON
J. H. VAN VLECK
MARK W. ZEMANSKY

Consultant on Printing
MELVIN LOOS

ADMINISTRATIVE STAFF
HENRY A. BARTON,
Director
WALLACE WATERFALL,
Executive Secretary
THEODORE VORBURGER,
Advertising Manager
RUTH F. BRYANS,
Publication Manager
EDITH I. NEFTEL
Circulation Manager
KATHRYN SETZE
Assistant Treasurer

The JOURNAL OF APPLIED PHYSICS, published monthly at Prince and Lemon Sts., Lancaster, Pa., is devoted to physics in its role as the science basic to other natural sciences and to the arts and industries. Previous to 1937 this publication was known as PHYSICS. The JOURNAL OF APPLIED PHYSICS publishes editorials and reviews, as well as technical papers of applied physics. Articles appearing in it are indexed regularly, according to their field, by Physics Abstracts, Chemical Abstracts, Engineering Index, Inc., Industrial Arts Index, etc.

Manuscripts should be submitted to Robert L. Sproull, Editor, Rockefeller Hall, Cornell University, Ithaca, New York. Unless otherwise stated, submission of a manuscript is a representation that it has been neither copyrighted, published, nor submitted for publication elsewhere. The authors' institutions are requested to pay a **publication charge** of $8 per page which, if honored, entitles them to 100 reprints without further charge. Instructions will be sent with galley proofs.

Subscriptions, renewals, and orders for back numbers should be addressed to the American Institute of Physics, 57 East 55 Street, New York 22, New York.

Subscription Price	U.S. and Canada	Elsewhere
To members of the American Institute of Physics and Affiliated Societies	$10.00	$11.00
To all others	12.00	13.00

Back Number Prices

Yearly back number rate when complete year is available: $14.00. Single copies: $1.25 each.

Changes of address should be sent to the American Institute of Physics; **corrected proofs** should be sent to the Publication Manager, American Institute of Physics. **Advertising rates** supplied on request. Orders, advertising copy, and cuts should be sent to the American Institute of Physics.

Entered as second class matter January 22, 1937, at the Post Office at Lancaster, Pennsylvania, under the Act of March 3, 1879. Accepted for mailing at the special rate of postage provided for in paragraph (d-2), section 34.40, P. L. & R. of 1948, authorized May 2, 1932.

Copyright 1954, by the American Institute of Physics

Journal
of
Applied Physics

Volume 25, Number 12 December, 1954

Heat Conduction in an Infinite Cylindrical Medium with Heat Generated by a Chemical Reaction*

PETER L. NICHOLS, JR., AND ARTHUR G. PRESSON
Jet Propulsion Laboratory, California Institute of Technology, Pasadena, California
(Received February 1, 1954)

The nonlinear partial differential equation for heat conduction in an infinite cylinder with heat generated by a chemical reaction has been solved by means of an electronic differential analyzer. Solutions of the equations in dimensionless variable form have been obtained for a zero-order heat-release term and a first-order heat-release term. Altogether 162 solutions were obtained covering a range of activation energies from 10 to 20 kcal/mole. Empirical relations have been derived for the maximum temperature at the center of the cylinder as a function of the experimental variables involved. Also relations relating to the approximate completion of reaction in terms of the experimental variables were derived from the tabulated data. Several calculations were made to demonstrate the general nature of the numerical solutions.

I. INTRODUCTION

THE general partial differential equation relating to heat conduction in an infinite cylinder containing a medium which generates heat is as follows:

$$\frac{\partial T}{\partial t}=\kappa\left(\frac{\partial^2 T}{\partial r^2}+\frac{1}{r}\frac{\partial T}{\partial r}\right)+\sum_i \frac{\dot{Q}_i}{c}. \tag{1}$$

The term $\sum_i \dot{Q}_i/c$ represents the contribution of various sources of heat generation to the rate of temperature rise at each point throughout the medium. When heat is generated by a chemical reaction, it is usually appropriate to represent the temperature dependence by the Arrhenius expressions $k=B\exp(-A/RT)$. Introduction of such exponential terms in Eq. (1) gives rise to nonlinear partial differential equations which cannot be treated by known analytical methods. Nevertheless, problems requiring solutions of equations of this type are frequently encountered in practice. Seeger[1] has discussed some of the work which has been done on the solution of related problems in one-dimensional rectangular and spherical coordinates. Most attempts at solutions of practical problems have involved the use of linearized forms of such equations.[2] In the present investigation it was found that replacement of the exponential term by linear terms changed the nature of the solutions considerably. Therefore it was decided that systematic numerical solutions of Eq. (1) for heat-release terms corresponding to zero-order and first-order chemical reactions would be useful. The two partial differential equations corresponding to these two cases, respectively, were then expressed in dimensionless variable form as follows:

$$\frac{\partial y}{\partial \tau}=\left(\frac{\partial^2 y}{\partial \rho^2}+\frac{1}{\rho}\frac{\partial y}{\partial \rho}\right)+c_0 e^{-(1/y)}, \tag{2}$$

$$\frac{\partial y}{\partial \tau}=\left(\frac{\partial^2 y}{\partial \rho^2}+\frac{1}{\rho}\frac{\partial y}{\partial \rho}\right)+c_1 e^{-(1/y)} \times\exp\left[-(1/N)\int_0^{\tau} e^{-(1/y)}d\tau\right], \tag{3}$$

where $y=R(T+273)/A$; $\tau=\kappa t/r_0^2$; $\rho=r/r_0$; $y(\rho,0)=y_0$; $y(1,\tau)=y_s$; $c_0=QBr_0^2R/\kappa Ac n_0$; $c_1=QB_1r_0^2R/\kappa Ac$; $N=\kappa/r_0^2B$; $B=B_0$ or B_1; R=gas constant (cal/deg mole); T=temperature (°C); A=activation energy (kcal/mole); κ=thermal diffusivity (cm²/sec); r_0=radius of cylinder; Q=heat liberated by chemical reac-

* This paper presents the results of one phase of research carried out at the Jet Propulsion Laboratory, California Institute of Technology, under Contract No. DA-04-495-Ord 18, sponsored by the Department of the Army, Ordnance Corps.

[1] R. J. Seeger, *Proceedings of Symposium on Large Scale Digital Calculating Machinery* (Harvard University, Cambridge, 1948) pp. 157–168.

[2] H. S. Carslaw and J. C. Jaeger, *Conduction of Heat in Solids* (Clarendon Press, Oxford, 1947).

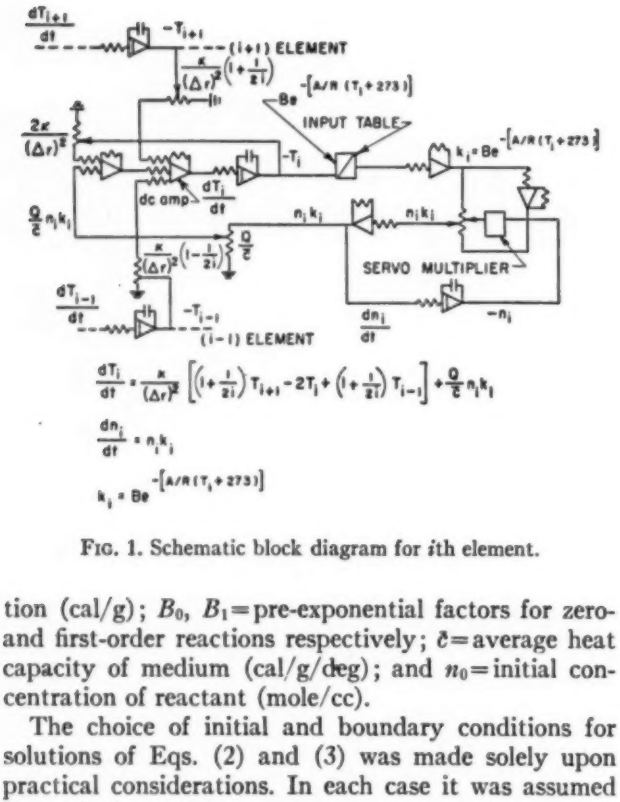

FIG. 1. Schematic block diagram for ith element.

tion (cal/g); B_0, B_1 = pre-exponential factors for zero- and first-order reactions respectively; $\bar{c}$ = average heat capacity of medium (cal/g/deg); and n_0 = initial concentration of reactant (mole/cc).

The choice of initial and boundary conditions for solutions of Eqs. (2) and (3) was made solely upon practical considerations. In each case it was assumed that $y(\rho,0)=y_0$. The constant y_0 was kept in a narrow range around room temperature. The boundary condition most frequently applied in problems to which these differential equations apply can be expressed in the following manner:

$$\frac{\partial y}{\partial \rho}+h(y-y_b)=0. \tag{4}$$

As $h\rightarrow\infty$, the boundary condition approached is that of a prescribed surface temperature.[2] The most general solution of the present problem would require use of the boundary conditions in Eq. (4) when h has a range of values. By assuming a constant temperature at the surface ($h\rightarrow\infty$), however, the number of solutions required for coverage of the variables of the problem is reduced considerably.

II. METHOD OF COMPUTATION

Equations (2) and (3) were solved with the differential analyzer† by using simultaneous equations describing the heat balance in n concentric regions. For the case of first-order heat release, the difference-differential equations corresponding to these elements were as follows:

Central core

$$\frac{dy_0}{d\tau}=\frac{4}{(\Delta\rho)^2}(y_1-y_0)+c_1e^{-(1/y_0)} \times\exp\left[-(1/N)\int_0^\tau e^{-(1/y_0)}d\tau\right]. \tag{5}$$

Outer concentric regions

$$\frac{dy_i}{dt}=\frac{1}{(\Delta\rho)^2}\left[\left(1+\frac{1}{2i}\right)y_{i+1}-2y_i+\left(1-\frac{1}{2i}\right)y_{i-1}\right] +c_1e^{-(1/y_i)}\exp\left[-(1/N)\int_0^\tau e^{-(1/y_i)}d\tau\right]. \tag{6}$$

For convenience in programming, it is possible to use the following auxiliary equations to represent the heat-

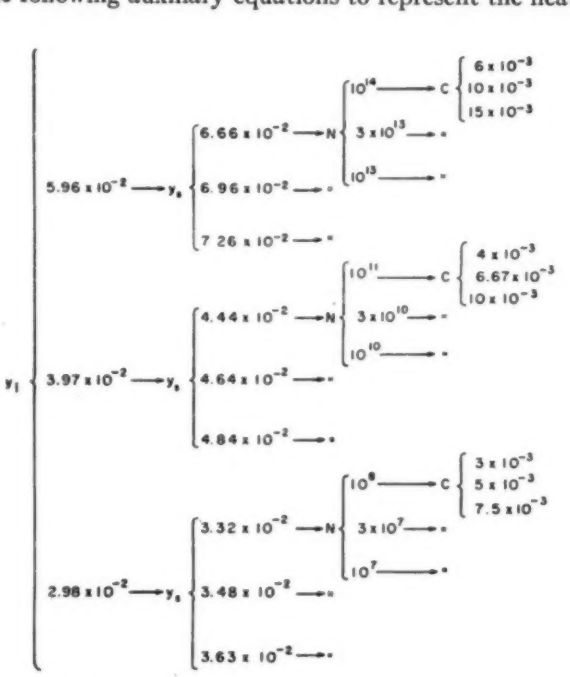

FIG. 2. Scheme chosen for dimensionless variables.

generation term for the ith element:

$$\frac{dn_i}{d\tau}=-n_ik_i, \tag{7}$$

where n_i is the fractional amount of product remaining in the ith element and k_i is a dimensionless reaction-rate constant.

$$\frac{dk_i}{d\tau}=\frac{1}{y_i^2}\frac{dy_i}{d\tau}. \tag{8}$$

Figure 1 is a schematic block diagram of the program of the ith element showing the various components that were used in the mechanized solution. The heat-

† All computations with the electronic differential analyzer were carried out by one of the authors (A. G. Presson) with the assistance of Mrs. E. R. Napp. Helpful suggestions by John Burke of this Laboratory are acknowledged.

generating components of the system for the inner elements were obtained by computing the two ordinary differential equations [Eqs. (7) and (8)] whose solutions are the exponential expressions shown in Eqs. (5) and (6). For elements near the outer surface, the heat-generating components were computed by solving one ordinary differential equation and obtaining the expression $B_1 \exp[-1/y]$ from input tables containing this function plotted against temperature.

Considerable difficulty was encountered in obtaining accurate solutions of the heat-generating components using the input tables to generate the function $B_1 \exp[-1/y]$. Not only has the exponential expression a wide variation in magnitude, but its greatest rate of change occurs near the completion of the reaction. To increase the accuracy of generating this function, the exponential function was removed from the computing system until the temperature of each element reached a sufficient magnitude to generate appreciable heat in the solid. This procedure decreased the slope of the exponential function plotted on the input tables and created only a small error in the initial computation. Relay amplifiers were used to connect the heat-generating components in each element with the computing system at some predetermined temperature. For first-order heat release, the last exponential term in Eqs. (5) and (6) varies from 1 to 0 in a given volume element as the reaction goes toward completion. In the case of zero-order heat release, completion of the reaction in each volume element is indicated when

$$\int_0^{\tau_f} e^{-(1/y)} d\tau = \frac{\kappa}{r_0^2 B_0} = N_0. \qquad (9)$$

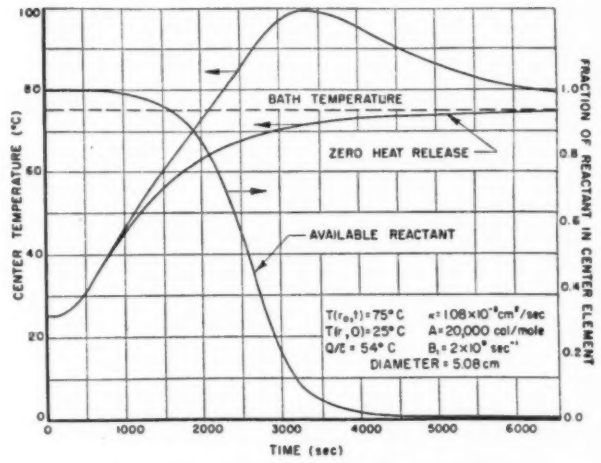

FIG. 3. Rate of cure for first-order heat release.

III. SOLUTIONS OF THE HEAT-CONDUCTION EQUATIONS

The range of parameters chosen for the calculations was dictated by practical considerations. Since a relatively narrow range of surface temperatures and initial medium temperatures was of interest, the particular groupings of parameters shown in Fig. 2 were found to give the best coverage for interpolation of the results.

A number of solutions have been converted to the experimental variables for ready visualization of the physical significance of the solutions obtained. Points of interest were as follows: (1) temperature rise *versus* extent of reaction (Fig. 3), (2) radial temperature distribution throughout medium at various time intervals (Figs. 4 and 5), and (3) effect of varying pre-exponential factor (Fig. 6). A similar variation in the curves was obtained by changing the adiabatic-temperature rise and bath temperature.

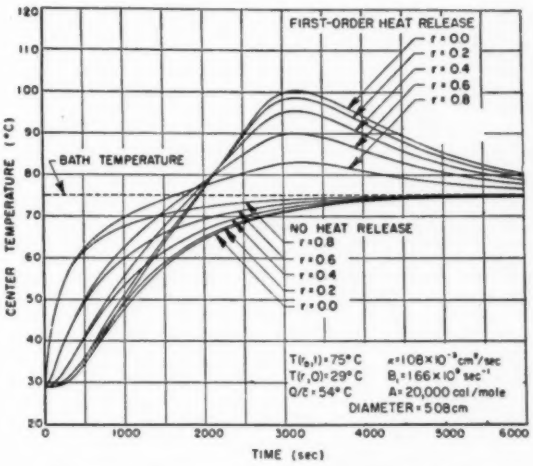

FIG. 4. Radial temperature as function of time.

IV. INTERPOLATION OF DATA

Results of all calculations were summarized by recording the maximum temperature attained at the center of the medium and also the time at which the maximum

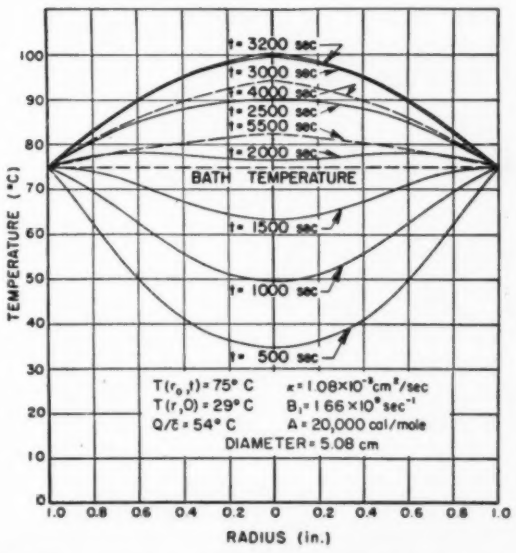

FIG. 5. Temperature distribution at various time intervals.

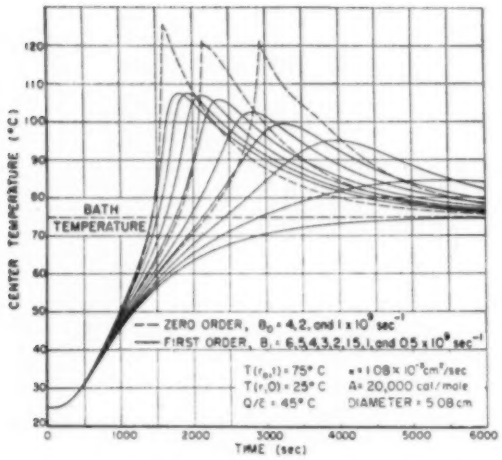
CENTER TEMPERATURE (°C)
TIME (sec)
BATH TEMPERATURE
ZERO ORDER, B_0 = 4,2, and 1 x 10^9 sec^{-1}
FIRST ORDER, B_1 = 6,5,4,3,2,1.5,1, and 0.5 x 10^9 sec^{-1}
$T(r_0,1)$ = 75° C
$T(r,0)$ = 25° C
Q/c = 45° C
κ = 1.08 x 10^{-3} cm^2/sec
A = 20,000 cal/mole
DIAMETER = 5.08 cm

FIG. 6. Effect of varying pre-exponential factor.

temperature rise occurred. The time so chosen often corresponded to practically complete reaction. Accordingly a cooling curve corresponding to no heat release is frequently obtained after the maximum temperature rise.

Equations have been derived empirically which express the maximum temperatures T_m attained and the curing times t_c as functions of the various parameters which enter into the problem. These equations are expressed in terms of the experimental variables and are restricted in the sense that one value (25°C) of the initial medium temperature applies over their range of applicability. This limitation is not serious for the T_m values since they are relatively insensitive variations in the initial medium temperature of ±100 percent. The curing time at an initial medium temperature other than that chosen can be calculated approximately by correcting for the time required for the temperature to change (by conduction alone) from one initial temperature to the other at the given surface temperature T_s. The derived equations are as follows.

Zero-order heat release

$$T_m=62.2T_s^{0.31}\left(\frac{r_0^2B_0}{\kappa}\right)^{0.027}+\frac{Q}{\bar{c}}-\frac{3170}{A^{1.52}}, \tag{10}$$

$$t_c=\left[\frac{30\times10^{0.208A}}{T_s^{0.88}}\left(\frac{r_0^2B_0}{\kappa}\right)^{0.34}-0.0022\frac{Q}{\bar{c}}+0.066\right]\frac{r_0^2}{\kappa}. \tag{11}$$

First-order heat release

$$T_m=62.2T_s^{0.31}\left(\frac{r_0^2B_1}{\kappa}\right)^{0.027}+\frac{Q}{\bar{c}}-\frac{1700}{A^{1.2}}, \tag{12}$$

$$t_c=\left[\frac{45\times10^{0.2A}}{T_s^{0.88}}\left(\frac{r_0^2B_1}{\kappa}\right)^{0.33}-0.0031\frac{Q}{\bar{c}}+0.093\right]\frac{r_0^2}{\kappa}. \tag{13}$$

The average percentage difference of the values of T_m and t_c from the equations and machine calculations are as follows: T_m (Eq. 10) = ±7; T_m (Eq. 12) = ±5; t_c (Eq. 11, A = 15, 20 kcal/mole) = ±6; t_c [Eq. (11), A = 10 kcal/mole] = ±50; t_c [Eq. (13), A = 15, 20 kcal/mole] = ±8; t_c [Eq. (13), A = 10 kcal/mole] = ±50.

The wide discrepancy of t_c values obtained when the activation energy is 10 kcal/mole is partly due to the fact that the solutions of the differential equation have in these cases exceptionally broad maxima, and accordingly it was difficult to determine their position with respect to the time coordinate. The accuracy of the machine calculations is discussed in Sec. V. Despite the approximate nature of the empirically derived formulas for T_m and t_c, it is believed that they will serve as a helpful guide in approaching an otherwise hopelessly complicated heat-transfer problem.

As another means of interpolation, attempts were made to use linear differential equations as approximations to the nonlinear equations [Eqs. (2) and (3)] by placing effective values of Q, k, etc. in the forcing function $\sum_i \dot{Q}_i/\bar{c}$ represented linearly as a constant×T or $\exp(-kt)$, etc. In all cases, no success was obtained even with relatively small changes in the parameters involved.

V. ESTIMATED ACCURACY OF NUMERICAL SOLUTIONS

It would be quite difficult to determine quantitatively the accuracy of numerical solutions obtained with the electronic differential analyzer. An idea of the accuracy which could be expected, however, was gained by solving closely related differential equations which allowed analytical solution, e.g., the heat-conduction equation with no heat release and with heat release of the form $\alpha\exp(-kt)$. In these cases the computed solutions agreed with analytical solutions within 1 percent for 5-, 7-, and 9-element approximations. Because of the wide variations in the exponential function $\exp[-1/y]$, the error in computing only the heat-generating component of the equation was greater than 1 percent. Nevertheless, the error of the complete problem is believed to be within 10 percent although many of the computations are probably accurate within 5 percent.

JOURNAL OF APPLIED PHYSICS VOLUME 25, NUMBER 12 DECEMBER, 1954

Current Fluctuation Phenomena in Current-Carrying Sliding Contacts

G. W. Epprecht
Research Laboratories of the Swiss PTT Administration, Bern, Switzerland
(Received February 12, 1954)

Considerable noise voltages appear across sliding contacts mainly because of the fact that the current across the contact consists of a random series of short pulses, corresponding to the minute, fugacious conducting spots on the contact surface. The properties of this noise within a wide range of contact conditions (i.e., varying sliding speed and operating current) are analyzed theoretically and experimentally. Most of the observed noise characteristics can be explained by various thermic phenomena in the contact interface. Several basic ranges as to operating current and sliding speed may be distinguished, each dominated by a different mechanism.

I. INTRODUCTION

FIXED and sliding contacts have often been subjected to extensive investigations; very satisfactory results have been obtained, particularly in reference to the technological aspects of fixed contacts.[1–13] The basic physical phenomena of current conduction across fixed contacts have in most cases received full theoretical explanation; sliding contacts, however, which involve far more complicated relationships, have not been investigated to the same extent and the theoretical treatment has not been fully developed. Naturally enough, previous research on sliding contacts attacked first, more or less empirically, the problem of finding suitable materials which would exhibit little wear, would withstand high current densities, and would function reliably at low contact resistance under widely varying operating conditions.[4,14,15] Our own investigation approached the contact problem from another standpoint. Sliding contacts frequently act as a source of very undesirable interference voltages. It was the purpose of this research to investigate sliding contacts as a noise source and to determine the relationship between the character of the noise and the varying operating conditions of such contacts. Various experimental and theoretical studies have been carried out and we shall attempt to synthesize our results in a hypothesis which explains most of the observed phenomena.

[1] R. Holm, *Die technische Physik der elektrischen Kontakte.* (Springer, Berlin, 1941).
[2] R. M. Baker, Elec. Eng. **55**, 94 (1936).
[3] J. Brandmüller, und H. Heumann, Z. angew. Phys. **1**, 139 (1948).
[4] W. Burstyn, *Elektrische Kontakte und Schaltvorgänge* (Springer, Berlin, 1942).
[5] E. F. Fullam, and R. H. Savage, J. Appl. Phys. **19**, 654 (1948).
[6] F. Schröter, Arch. Elektrotech. **18**, 111 (1927); **25**, 489 (1931).
[7] P. F. Soper, Beama J. 132, 189, 228 (1946).
[8] P. F. Soper, J. Inst. Elec. Engrs. (London) **96**, II, 645 (1949).
[9] C. van Brunt and R. H. Savage, Gen. Elec. Rev. **47**, 16 (1944).
[10] H. Viehmann, Elektrotech. Z. **70**, 263 (1949).
[11] J. Neukrichen, *Kohlebürsten* (Oldenburg, Munich, 1934).
[12] J. M. Richardson, Bell System Tech. J. **29**, 117 (1950).
[13] R. H. Savage, J. Appl. Phys. **19**, 1 (1948).
[14] B. M. Horton, Low Frequency Electrical Noise Generated in Sliding Contacts, NRL Report P-3408 (1949).
[15] H. Weidemann, Z. Ver. Deut. Ing. **88**, 453 (1944).

II. EXPERIMENTAL APPARATUS

All experiments reported were performed exclusively with the contact combination copper-carbon. The test set consisted essentially of a copper disk, 60 cm in diameter and 1 cm thick, and a carbon brush which was very carefully guided. Sliding speed could be varied from 0.01 mm/sec up to 50 m/sec. An automatic noise analyzer was used to plot the noise spectrum within a frequency range from 2 to 2000 kc (occasionally extended down to 50 cps and up above 10 Mc) on a double log scale. The principal components of the noise analyzer were, as shown in Fig. 1, a broad-band amplifier, feeding 11 filters spaced at intervals of 1 octave, a mechanical switch to scan successively the outputs of the filters, and a logarithmic broad-band amplifier,[21] followed by detector, dc-amplifier, and recording meter. All data reported in this article have been measured on contacts which were, as far as possible, electrically and mechanically in equilibrium (meaning that wear would not change the macroscopic geometry of the contact areas, and that the statistical properties of the electrical noise would not vary during continued operation under constant external contact conditions).

III. OPERATING CURRENT AS A SUMMATION OF SINGLE IMPULSES

It has been shown by Holm[1] that a current across contact surfaces, even if these appear to be perfectly matched, actually passes only at a very few discrete spots as if the interface were some sort of irregular sieve. It follows that as soon as one contact surface starts moving respective to the other, current conduction points of at least one of the surfaces must continually change position and size. This results in fluctuations of current transfer which we call (sliding-) contact-noise. According to this mechanism of ever changing contact spots, we may conceive the total current as consisting of a large number of individual pulses. Such a single current pulse corresponds to the physical elementary phenomenon which takes place if two points of the contact surfaces happen to act as a real electrical connection. It is desirable, of course, to know more about this elementary phenomenon, especially its duration. One way of getting some infor-

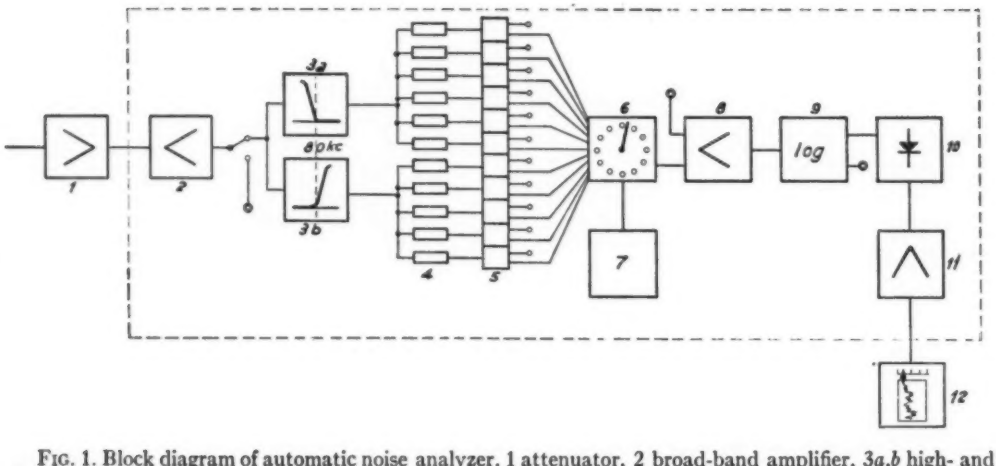

FIG. 1. Block diagram of automatic noise analyzer. 1 attenuator, 2 broad-band amplifier, 3*a*,*b* high- and low-pass filter with 80-kc cut-off frequency, 4 band-pass filter ("*L*" type), 5 attenuators, 6 automatic switch, 7 switching control circuits, 8 broad-band amplifier, 9 logarithmic amplifier, 10 rectifier circuit, 11 dc amplifier, 12 recording meter.

mation consists in analyzing the resulting noise spectrum. It is well known that the time function of the current or voltage is functionally connected to this spectrum. However, current conduction across moving contacts being a random process, there does not exist a single-valued solution for the shape of a current pulse which could be calculated from the measured spectrum. Strictly, only the autocorrelation function of the series of pulses is determined and a single pulse may, theoretically, have almost any shape if only a corresponding distribution function of the pulses be assumed. However, by considering only reasonable physical possibilities of such distributions, we may obtain from spectral analysis some properties of the elementary pulse which are, with great probability, good approximations.[22]

A typical measured noise spectrum of a copper-carbon sliding contact is shown in Fig. 2. Surprisingly, this spectrum changes very little with varying sliding speed and for different kinds of carbon brushes. From the variations of the slope of the spectrum, the following conclusions may be drawn concerning the individual current pulses:

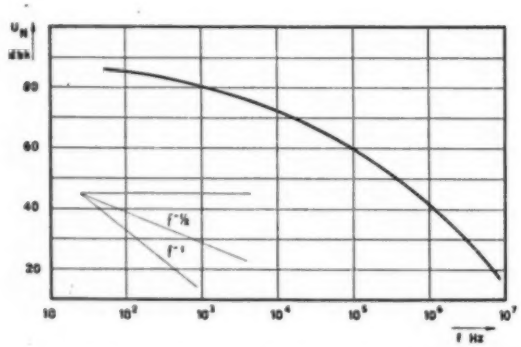

FIG. 2. Typical measured noise spectrum of sliding contacts. ("*dbk*" denotes: "*db* above 1 μv/kc$^{\frac{1}{2}}$ or 1 μa/kc$^{\frac{1}{2}}$" if used in connection with the noise voltage U_N or the noise current I_N, respectively.)

1. The pulses start and/or stop with a very steep slope.

2. Pulse lengths vary over a very wide range but the probability of the lengths has a high peak somewhere around 0.1 to 1 μsec.

3. As a first approximation, the average pulse length is independent of the sliding speed.

IV. THE ELEMENTARY PHENOMENON

Let us first consider a single current pulse and its associated physical phenomena in the interface of the contact. It is known in modern theory of friction that sliding solid bodies are heated up to very high temperatures at minute spots of the contact face.[16–18] We have good reasons to assume that these little hot spots are identical with the ever-changing points of electrical contact. When a current passes through such a spot, the point is not only heated by friction but also by the current loss in its relatively high resistance. The temperature rise in such contact points has been calculated by R. Holm for heating due to friction and due to current.[1,18–20] Although these calculations are based on simplified assumptions, they may be taken as a good approximation. Temperature rise due to friction is somewhat more rapid than that due to resistive heating because in the first case the same amount of produced energy is concentrated in a smaller volume. Application of Holm's calculations yields the following results: friction can always heat a contact spot up to the lower melting point of the two contact materials, assuming that the spot size is small enough. Resistive heating can also heat a point to this melting temperature, but

[16] F. P. Bowden, and D. Tabor, Proc. Roy. Soc. (London) A169, 391 (1939).
[17] F. P. Bowden, and M. A. Stone, Experientia **2**, 186 (1946).
[18] R. Holm, J. Appl. Phys. **19**, 361 (1948).
[19] W. J. Oosterkamp, J. Appl. Phys. **19**, 1180 (1948).
[20] G. H. Wannier, J. Appl. Phys. **19**, 1020 (1948).
[21] G. W. Epprecht, Tech. Mitt. P.T.T. **29**, 161 (1951).

only if a certain minimum voltage is established across the contact. In both cases, the necessary time to reach melting temperature is extremely short.[22] Heating beyond the melting point (i.e. vaporization), though possible by current heating, seems to play a minor role under normal contact conditions; excessive heat is preferentially utilized to increase the dimensions of the molten contact bridge.

We shall see later that there are two operating current ranges in each of which one of these two heating mechanisms dominates.

The elementary phenomenon leading to the production of one pulse may be imagined to take place as follows: when two suitable points of the moving contact surfaces coincide, a sudden temperature rise to the melting point concentrated in a very small region is produced. The dimensions of the molten volume are probably of the order of 10^{-4} to 10^{-5} cm while the temperature rise involves a time period of 10^{-7} to 10^{-6} sec. Most such contact bridges are destroyed immediately after their formation owing to the motion of the surfaces. It is possible that some vaporization of the molten material takes place during this process.

V. THE DEPENDENCE OF CONTACT NOISE ON THE SLIDING SPEED, DELAY-HYPOTHESIS

If the length of an elementary current pulse were determined merely by surface geometry and sliding speed, it follows that the number of pulses per unit time should be directly proportional to the sliding speed; further, the pulse spectrum should be shifted along the frequency axes accordingly. However, measurements have shown that the spectrum form is substantially independent of the sliding speed.

Let us briefly review the basic theory of shot noise. The following relations are valid for any noise consisting of a series of pulses:

$$I_N^2(f_0,\Delta f)=2n\int_{f_0}^{f_0+\Delta f}[S(f)]^2\mathrm{d}f$$

where I_N is the effective noise current, n the average number of pulses per unit time, and

$$S(f)=\int_{-\infty}^{+\infty} i(t)e^{-i2\pi ft}\mathrm{d}t=\mathbf{F}\{i(t)\}, \qquad (1)$$

the latter being the Fourier-transform of a single pulse. If $S(f)$ does not change appreciably within the interval Δf, we may write

$$I_N^2\approx 2n\Delta f S^2(f_0).^*$$

Let us also define a normalized spectral function

$$\Psi(f_0)=S(f_0)/S(f_t)$$

where f_t is some low frequency such that

$$S(f_t)=\int_0^{\infty} i(t)\mathrm{d}t=\delta_m i_m=I/n.$$

δ_m and i_m are the average pulse length and average current, respectively, and $I=\delta_m\cdot i_m\cdot n$ the total operating current. It follows immediately that:

$$I_N^2(f_0)=2\Delta f\Psi^2(f_0)I^2/n. \qquad (2)$$

Experimentally we found that Ψ is independent of the sliding speed v and furthermore that within a large range I_N^2 is proportional to v. This yields for constant load I

$$\begin{aligned} v&\sim 2\Delta f\Psi(f_0)I^2/n \\ v&\sim n^{-1} \\ I_N&\sim\sqrt{v}. \end{aligned} \qquad (3)$$

In other words, the average number of pulses is inversely proportional to the sliding speed, a conclusion which is at variance with the previously mentioned simple geometric picture. However, there is a simple interpretation of this result which also fits well into the rest of our theory.

Imagine again the contact surfaces with their geometrical irregularities, partly covered by various films of nonconducting materials. Some points will always exist of a suitable nature to establish electrical contact, i.e., those points which project above the average surface and which are the least covered with interfering films. Let us call these points *latent contact spots*. In a sliding contact interface, such potential contact spots pass each other and occasionally a current pulse will result. The time interval during which two potential contact spots pass over one another is called *latent contact interval*. We now make the assumption that current conduction cannot take place immediately when such spots meet, but that there is a certain delay in building up a real contact. We do not know exactly by which mechanism a current pulse is finally initiated; it may be a temperature breakdown, the building up of an ionization or an electrolytic process. A delay may also be due to the internal inductivity of the current contraction. In any case, regardless of the true physical cause, we make the following assumption: the mean probability for a current pulse to occur between latent contact spots is proportional to the latent contact interval. Since the latent contact interval is determined mechanically (every single one and thus also its mean) by the surface geometry of the contact electrodes, it is obvious that the contact interval is inversely proportional to v. With decreasing n, the average electrical charge of a pulse must necessarily increase thus resulting in an enlarged radius of the contact spot. It can be shown that this radius is proportional to the pulse current i. Therefore the growth of the contact spot compensates for the decreasing actual contact interval

[22] G. W. Epprecht, Tech. Mitt. P.T.T. **29**, 201, 240 (1951).

* $\approx$ denotes "almost equal," $\sim$ denotes "proportional to."

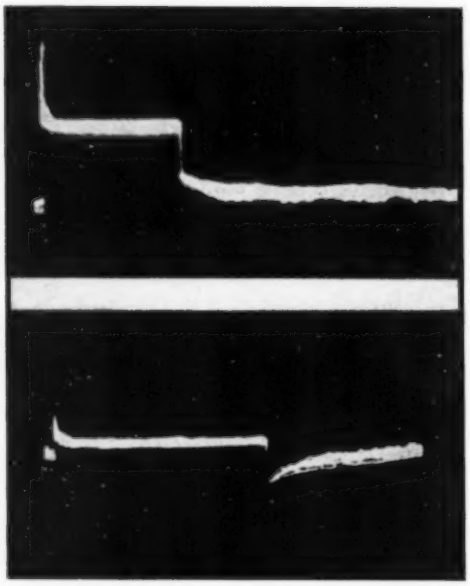

FIG. 3. Oscillogram of the voltage across a sliding contact if fed with a square current pulse. Contact force $P=5$ newtons, contact area $A=8\times8$ mm² pulse length $\delta=30$ μsec, sliding speed $v=10$ cm/sec, dc current superposed to pulse: Fig. 3a: $I=0$, Fig. 3b: $I=10$ ma.

so that the pulse length remains approximately constant with increasing sliding speed. There is a slight rise of contact voltage associated with this increase.

It has been assumed in our delay theory that the probability of an actual contact is proportional to the latent-contact interval. A modification of this hypothesis equally satisfactory in explaining the observed facts consists of the assumption that the building up of a current pulse requires a more or less fixed time; in other words, if the latent-contact interval exceeds this fixed buildup time, a current pulse will result with unit probability while if the latent-contact interval is less than this, the probability for the formation of a current pulse is nil. Because of the wide distribution of latent-contact intervals, with increasing sliding speed, more and more of them will fail to result in a current pulse owing to the lack of buildup time.

To sustain this delay theory, an additional experiment was performed: Instead of feeding dc to the contact, square wave pulses with a short rise time were applied. If the short pulses of which the total operating current is composed actually start only after a short delay, it follows that there will be almost no contact point in a conducting state at the beginning of an applied square wave pulse, but such effective contacts will only develop in size and number during the application of the square wave. Their rapid increase will be associated with a corresponding decrease in the mean contact resistance. This must lead to a sharp voltage peak across the contact at the start of the applied pulse. Such a peak can actually be demonstrated without difficulty by means of an oscilloscope (see Fig. 3).

As to the dependence of the noise on sliding speed, we have seen that the effective noise voltage increases as the square root of the speed. This is only valid up to a certain limiting speed above which there is no more variation in the noise voltage. The critical speed, where the noise attains a saturation value, depends on the operating current, being directly proportional to the latter. The existence of such a critical speed can readily be understood if we remember that the increase in noise is due to a decrease of the pulse number n. It is clear that N the number of contact spots operating in parallel) and n cannot decrease indefinitely as at least one contact point must always exist. It seems quite probable that at high speeds, on the average, the current is carried by not much more than one single spot. As a matter of fact, n does remain constant over a large current-speed range. The number of pulses appears to increase slightly with very high currents. n is also dependent upon the apparent size of the contact area, the critical speed being less for a smaller brush surface area. However, in the $\sqrt{v}$ range (for values of v less than the critical speed), the noise voltage is independent of the contact area.

VI. THE DEPENDENCE OF CONTACT NOISE ON OPERATING CURRENT

The dependence of the noise voltage on the applied load current was investigated over a range wide enough to include all regions of practical significance. Basically, with changing current, a variation of the average number n of pulses per unit time as well as of the average pulse length δ_m can take place. The nature of this dependence can be determined by the alteration of the noise voltage within the operating current range.

We have seen in the last section that there are two distinct ranges of functional relationship between the pulse number n and the sliding speed v; at low speeds, n is inversely proportional to v, whereas at high speeds (above the critical value of v), n attains a constant value. It seems only reasonable to investigate these two ranges separately in order to obtain more information about the variations in n. The results of such

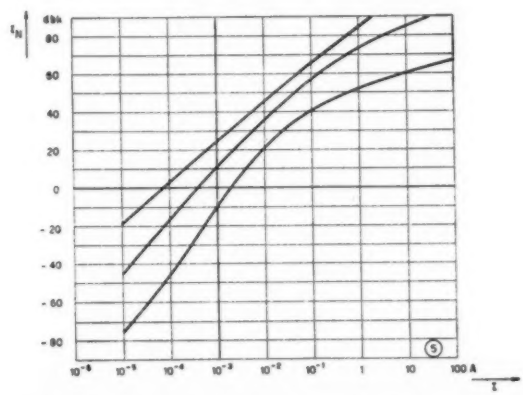

FIG. 4. Typical results for the dependence of noise current I_N on the operating current I, sliding speed $v>v_{crit}$.

measurements are given in Figs. 4 and 5. For normal operating conditions, it is found that the noise current I_N is proportional to $I^{\frac{1}{2}}$ in the lower v range and to $I^{\frac{3}{2}}$ in the higher v range, I being the operating current. An analysis of these results employing relationship (2) leads to the conclusion that n is proportional to I in the lower v range and to $I^{\frac{1}{2}}$ in the upper one.

A more detailed investigation employing various carbon brush materials between extreme load-current limits yielded quantitative differences depending on the brush materials; however, four distinct load ranges with different noise characteristics could almost always be detected. These four ranges are now discussed.

(a) Range of Thermoelectric Noise

If the operating current is extremely small, its associated noise is completely masked by thermoelectric fluctuations which also exist in the absence of any load current. This noise is due to thermoelectric pulses produced in the contact-interface by the frictionally heated contact spots. The thermoelectric noise of sliding contacts is produced by the superposition of short thermovoltage pulses which always have, of course, the same polarity. The average thermoelectric voltage measured at sliding contacts may assume values as high as 150 mv.

(b) Range of Constant n

On increasing the current I above a certain limit, the current noise exceeds the thermoelectric noise. The total effective noise voltage is almost exactly proportional to the load current in this range while the spectrum changes slightly, i.e., the relative amplitude of the higher frequencies is somewhat increased. Therefore, it follows that the average pulse length decreases somewhat with increasing load current. The characteristics of noise in this range indicate that n is essentially constant and that current conduction takes place at the same spots (statistically) that would produce mere thermoelectric noise in the absence of a load current. This indicates that frictional heating of the contact spots is dominating this range. However, the additional heat produced by current flow will accelerate the temperature rise, thus making the elementary pulse shorter. It should be realized that the dc voltage across the contact in this current range is insufficient to bring about melting of a contact spot due to resistive heating alone. The dc contact voltage U, in this range of constant n, increases with the load current I. We may roughly calculate U as a function of I by means of the following considerations. During current heating, larger amounts of copper are melted at the contact spot and, consequently, the current-constriction resistance decreases. The current-constriction resistance is inversely proportional to the diameter of the molten droplet formed while the diameter of the droplet grows approximately as the third root of the available heat.

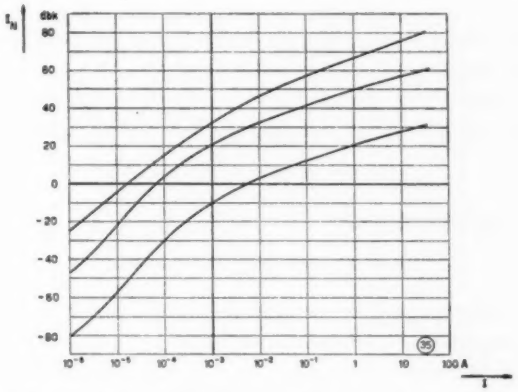

FIG. 5. do., sliding speed $v<v_{crit}$. The curves in Figs. 4 and 5 are plotted for measuring frequencies of 2 kc, 64 kc, 2048 kc.

Thus by assuming

$$\delta_m \sim I^{-\alpha}, \quad (\alpha<1)$$
$$r \sim b^{-1}$$

we get

$$b^3 \sim i_m^2 r \delta_m$$
$$U \sim I^{(\frac{1}{4}+3\alpha/4)} \tag{4}$$

(where r=spot resistance, b=spot diameter, i_m=average spot current, and δ_m=average pulse length). This theoretical result agrees well with our actual observations. As mentioned in the foregoing, the noise current I_N is proportional to the load current I. This is valid for relatively low frequencies; at higher frequencies the increase of I_N is somewhat more rapid than linear due to the shift of the noise spectrum. It is readily seen that also the noise voltage U_N increases with I in this range of constant n. From the assumptions stated above, one obtains for the total contact resistance

$$R \sim I^{-(\frac{1}{4}+\alpha/4)} \tag{5}$$

and consequently,

$$U_N \sim I^{(\frac{1}{4}-\alpha/4)}. \tag{6}$$

Within this range, N, the number of spots operating in parallel at any given instant is small. It does not seem improbable that the average number N is only little more than one.

(c) Range of Constant U

On further increase of the operating current, a point is reached where U attains a value of about 1 volt. This represents the entry of a new current range which we have named as in the title above because of the fact that U remains remarkably constant during large variations of the load current. This U value is the well-known typical voltage of sliding contacts and it is in this range that most industrial copper-carbon contacts are operated. It is a characteristic feature of this constant U range that I_N varies less rapidly with I than in the constant n range, i.e., I_N being approximately proportional to $I^{\frac{1}{2}}$ and $I^{\frac{3}{2}}$ for low and high sliding speeds,

respectively. The upper limit of the range is marked by a new slight rise in U and a flattening of the $I_N(I)$ curve. Furthermore, n is no longer constant but is proportional to I and $I^{\frac{1}{2}}$ for low and high sliding speeds. Analogous to Eqs. (5) and (6), we find for low sliding speeds:

$$n \sim I: \quad R \sim I^{-1}; \quad U_N \sim I^{-\frac{1}{2}} \tag{7}$$

and for high speeds:

$$n \sim I^{\frac{1}{2}}: \quad R \sim I^{-1}; \quad U_N \sim I^{-\frac{1}{4}}. \tag{8}$$

The following interpretation of this behavior is offered: As soon as U attains the critical melting voltage, it becomes possible for molten contact points to be formed not only by frictional heat but also by resistive losses alone. As a result, contact spots which would not contribute significantly to the current conduction if only frictional heating were operating, will now be enlarged by molten material formed during resistive heating. The contact spots which become effective in this manner are probably those which touch only slightly on their opposite contact face or possess too short a contact interval, etc. In any case, it is probable that a large number of latent-contact spots are available.

Further increase of I from the point of entry into the constant U range must result in an increase of either

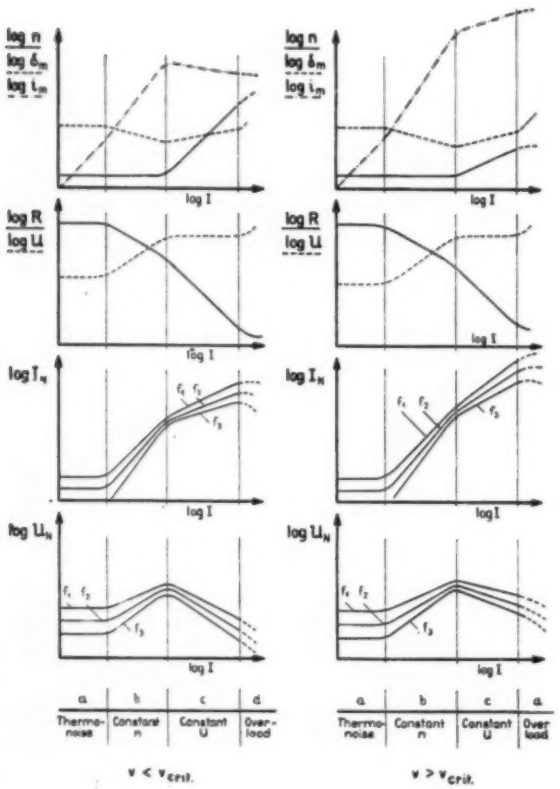

FIG. 6. Electrical behavior of sliding contacts throughout the various current and speed ranges. n = number of pulses per unit time, δ_m = pulse length i_m = av pulse current, R = total contact resistance, U = dc voltage across contact, I_N = noise current, U_N = noise voltage, I = operating current, f = measuring frequency $f_1 < f_2 < f_3$.

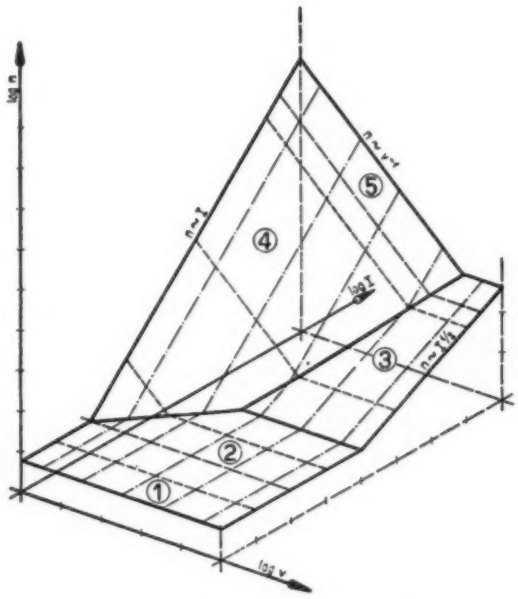

FIG. 7. n, the number of pulses per unit time, plotted *vs* operating current I and *vs* sliding speed v.

n or δ_m, since U is fixed at the melting-voltage. (Any increase in U would result in an increased production of molten copper, thus reducing the dc resistance of the contact and so acting against an additional increase of U). Measurements show that δ_m is lengthened only very slightly, producing a frequency shift of the spectrum of opposite direction to the one observed in the constant n range. The mutual motion of the contact faces appears to prevent an appreciable enlarging of the contact spots, i.e., contact bridges are ruptured as soon as they reach the molten state. Since δ_m does not vary much, it follows that n must necessarily grow with increasing load. As there are many latent-contact spots, this assumption seems to be very reasonable. The good agreement between the predictions of Eqs. (7) and (8) and our experimental data appears to justify our assumptions as to the variation of n, i.e., n is proportional to I and $I^{\frac{1}{2}}$ for the low- and high-speed range, respectively.

(d) The Contact Overload Range

By still further increase of the contact load, a last change in the noise characteristics can be observed before the contact is finally destroyed by thermal overload. This occurs in the interval between 1 and 100 A/cm². The behavior of the various test materials used is less uniform in this range than with lower load currents. However, in all cases, a marked lengthening of the pulses is observed, generally connected with a new rise of the contact voltage U. The noise spectrum is appreciably shifted towards lower frequencies. In addition, I_N increases less rapidly and U_N decreases more rapidly than in the preceding current range. If the load current is slowly increased, an instable range is entered.

Smooth running of the contact may continue for quite a while, but suddenly contact disintegration commences. Even during smooth running, small flat accumulations of copper with a diameter up to 2 mm can be observed on the carbon surface. Probably these copper scales slowly build up owing to the increased melting and perhaps vaporization of metal under the heavy load conditions. As the result of such scale formation, eventually metal will slide on metal. The total current will concentrate at such a spot which can be readily observed as the underlying carbon glows continually. This loosens the structure of the brush. Because of the welding together of such copper scales or the abrasive action of loose, hard carbon particles, the copper contact surface is scratched and roughened, thus leading to the cumulative destruction of the surfaces. Wear rate may be increased by many powers of 10 in this state. This sudden change is easily detected by the whistling and squeaking that occurs. When operated with a negative brush, the contact will generally withstand a current 1.5 to 3 times larger than with a positive brush.

(e) Synthesis of Contact Noise Characteristics for Various Sliding Speeds and Load Currents

The discussions above have brought out that the operating conditions of a sliding contact can be divided into various ranges in reference to load-current and sliding speed. In order to clarify these somewhat complex relations, we have plotted Fig. 6 and the 3-dimensional diagrams Figs. 7, 8, and 9. The first of these plots, Fig. 7, gives the average number of current pulses per unit time as a function of speed and load, while in Figs. 8 and 9, noise current and noise voltage have been plotted *vs* the same variables. Corresponding ranges have been labeled with the same numbers. In the interest of intelligibility, the plots have been simplified.

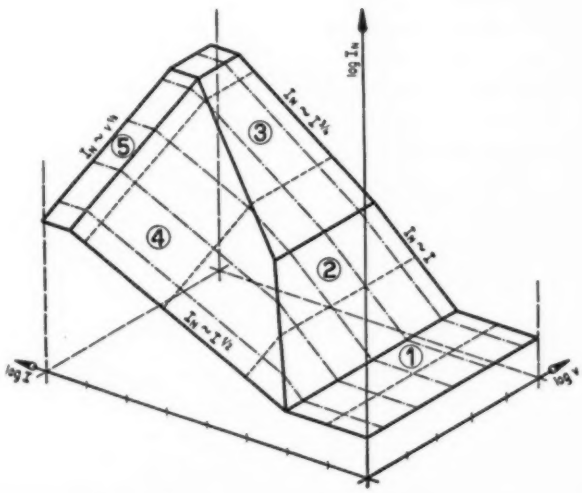

FIG. 8. Noise current I_N *vs* operating current I and *vs* sliding speed v.

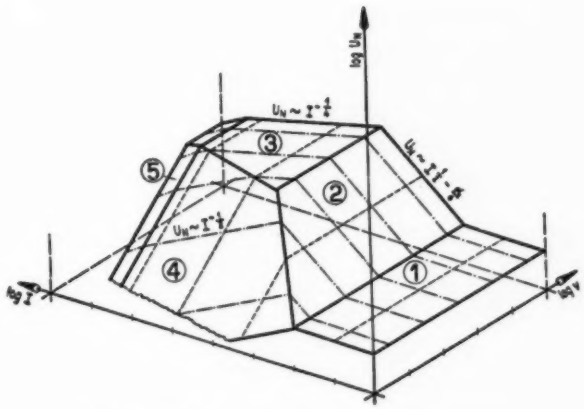

FIG. 9. Noise voltage U_N *vs* operating current I and *vs* sliding speed v.

In reality, there are, of course, no sharp boundaries between the various ranges and the given slopes are only simplified approximations. Further, the diagrams are constructed only for a relatively low frequency (2 kc for instance). In these diagrams, number 1 indicates the range of thermoelectric noise, 2 the constant n range, 3 and 4 the constant U area, and 5 the overload range.

VII. SUMMARY

The results of our investigations may be summarized as follows.

The noise of sliding contacts is a consequence of the fact that the load-current across the contact consists of a series of pulses with statistically distributed starting points and lengths. The mean duration of a single pulse is independent of sliding speed and varies only slightly with changing operating current; it is determined by thermic phenomena at the minute, fugacious conducting spots on the contact surfaces. In the range of weak or zero load current, frictional heat is primarily responsible for the temperature rise of the contact spots, whereas in the range of higher currents, resistive heating predominates. The most important contribution to noise is due to current pulses flowing over contact spots which heat up to the melting point of the metal. These pulses have a duration of about 1 μsec and less. With increasing load current, four characteristic ranges are observed.

(a) the range of predominating thermoelectric noise where the operating current does not contribute significantly to the total noise;

(b) the so-called constant n range, featured by a constant average number of pulses per unit time, and wherein frictional heating of contact spots still governs the process, but current noise exceeds thermoelectric noise;

(c) in the third range, the well-known phenomenon of

a substantially constant contact voltage is observed; further, the heating of the contact spots is dominated by resistive losses at the points of current constriction;

(d) the last range marks the beginning of the overload conditions which soon lead to thermal and mechanical disintegration of the contact surfaces.

The average number of pulses per unit time is inversely proportional to the sliding speed owing to the delay in the buildup of the conducting contact spots (delay-hypothesis). With increasing sliding speed, the pulse number reaches a lower limit. This lower limit is probably reached when there remains only about one significant conducting spot at any given instant.

JOURNAL OF APPLIED PHYSICS VOLUME 25, NUMBER 12 DECEMBER, 1954

Electric Strength and Molecular Structure of Saturated Hydrocarbon Liquids

R. W. Crowe, A. H. Sharbaugh, and J. K. Bragg*
General Electric Research Laboratory, Schenectady, New York
(Received March 3, 1954)

A number of investigators have reported that the apparent electric strengths of straight-chain hydrocarbon liquids increase in a regular manner with increasing molecular chain length. In a recent publication we have presented evidence that this phenomenon is an illustration of a kind of Paschen's law for liquids. An observed *linear* dependence of the electric strengths of such hydrocarbons upon density suggested that chain length variation merely provided a means of changing the electron mean free path in the liquid.

In the present paper we describe the development of an improved technique for measuring electric strengths of liquids, and the application of this technique to a series of pure straight-chain and branched-chain liquid alkanes. As had been observed previously, the strengths of the straight-chain members of the series exhibit a linear relationship with density. The introduction of branches into the hydrocarbon chain, however, results in a definite decrease in strength. Extension of the measurements to hydrocarbons of more complicated structure has apparently introduced a kind of fine structure.

Measurement of the time dependence of electrical breakdown in liquid hydrocarbons shows that the formative time lag is relatively insensitive to changes in viscosity or molecular weight. For an electrode separation of 0.002 inch, it is approximately one microsecond.

I. INTRODUCTION

In 1951, Salvage[1] reported the results of an investigation of the electric strengths of a series of liquid normal alkanes. The measurements were made by placing the liquids between two solid hemispherical electrodes and subjecting them to dc, ac, and impulse voltages. Salvage found that the apparent electric strengths of the liquids increased in a regular manner as the chain length of their constituent molecules was increased. Later Goodwin and MacFadyen,[2] using a technique originally developed by MacFadyen and Edwards[3] and involving the use of single rectangular voltage pulses, were able to reproduce the phenomenon qualitatively. In neither case, however, was an effort made to correlate this observation with any of the physical properties of liquid hydrocarbons which are known to depend on molecular chain length.

In a recent publication,[4] we have presented evidence that this behavior can be associated with the density of the liquid hydrocarbon, which is known to vary over a considerable range depending upon molecular size and shape. Furthermore, we have been able to show, at least qualitatively, why the density should be the controlling factor.

Our experimental results were obtained by applying rectangular voltage pulses to the liquids placed between a mechanically polished stainless steel anode and a liquid mercury cathode. Although such an electrode system yielded results which were quite reproducible, it was always necessary to make a correction for distortion of the mercury surface that takes place during voltage application.[5] For this reason, it seemed desirable to develop an experimental technique which can employ solid electrodes and yet yield results with high precision. We report here the success of this development and extension of the measurements to hydrocarbon liquids consisting of molecules more complicated in structure than those studied earlier.

II. EXPERIMENTAL TECHNIQUES

In order to realize a degree of precision comparable to that obtained with the mercury cathode, it was necessary to refine the experimental techniques considerably. The refinements include both the design of an improved test cell, and the development of a more

---

* Present address: Operations Research, Inc., 8416 Georgia Ave., Silver Spring, Maryland.

[1] B. Salvage, Proc. Inst. Elec. Engrs. **98**, 227 (1951).

[2] D. W. Goodwin and K. A. MacFadyen, Proc. Phys. Soc. (London) **66**, 85 (1953).

[3] K. A. MacFadyen and W. D. Edwards, Nature **163**, 171 (1949).

[4] Crowe, Bragg, and Sharbaugh, J. Appl. Phys. **25**, 392 (1954).

[5] Sharbaugh, Crowe, and Bragg, J. Appl. Phys. **24**, 814 (1953).

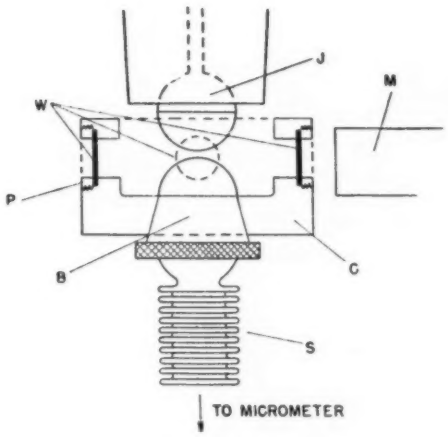

FIG. 1. The breakdown cell.

reliable technique for removing molecular and suspended impurities from the liquids prior to measurement.

A. Breakdown Cell

The cell used for previous measurements in our Laboratory[6] had several disadvantages. Among these were: (1) its large volume made it possible to test only those liquids which were available in relatively large quantities, (2) the ground metal-to-glass joints and the exposed brass bellows were major sources of suspended particles in the test liquids, and (3) it was not designed for effective observation of the spark gap during measurement.

The cell assembly used in the present investigation is shown schematically in Fig. 1. The cell C, of approximately 15-ml liquid capacity, was machined from a solid piece of Teflon. It is equipped with three glass windows W, held in place by Teflon plugs P. This was done so that advantage could be taken of both direct and transverse illumination of the gap.[7] The round hole at the base of the cell is tapered as shown so that a liquid-tight fit could be maintained between the cell and the stainless steel base B. This arrangement permits rotation of the lower electrode without disturbing the location of the cell windows. The upper electrode is lowered to a stationary position in the liquid, and the electrode separation varied by raising or lowering the entire cell and base by means of a micrometer drive in conjunction with the bellows S.

The two hemispherical electrodes, both of mechanically polished stainless steel (one inch in diameter), are offset from the vertical. In addition, the upper electrode is attached to a ball and socket joint J so that it can be rotated at will. Such an arrangement makes it possible to use a pair of electrodes for a number of tests before repolishing is necessary.

[6] Bragg, Sharbaugh, and Crowe, J. Appl. Phys. **25**, 382 (1954).
[7] This improvement was suggested to us by Dr. J. H. Simpson of the National Research Council of Canada.

B. Purification of the Liquids

Past experience has shown us that the presence of minute solid particles, either suspended in the liquid or loosely adhering to the electrode surfaces, often leads to low apparent values of electric strength. As a result, we have made a concentrated effort to eliminate this complication as nearly as possible.

The hydrocarbon liquids used in the present investigation are listed in the first column of Table I. With the exception of *n*-decane and *n*-tetradecane, the liquids were of the *pure* grade (99-mole percent minimum) as obtained from the Phillips Petroleum Company. The straight-chain members of the series were first washed several times with *fuming* sulfuric acid to remove possible sulfur compounds and unsaturates. The branched-chain members were treated in the same manner with *concentrated* sulfuric acid.

The samples were then prepared for testing in the combination distilling and filtering apparatus, a diagram of which is shown in Fig. 2. They were then transferred from the collecting bulb to a well-rinsed flask equipped with a delivery tube and squeeze bulb, and stored until ready to use.

Because of the doubtful purity of the *n*-decane and *n*-tetradecane samples, they were fractionally distilled at reduced pressure in an efficient column following the sulfuric acid treatment.

TABLE I. Electric strengths of liquid hydrocarbons.

Hydrocarbon	Density	E(V/cm)	Pulse duration (μsec)	Std. dev., %	No. of runs
n-Pentane	0.626	1.44×10^6	1.4	3.2	19
n-Hexane	0.659	1.89	0.25	···	4
		1.73	0.5	···	4
		1.63	0.7	2.0	8
		1.55	1.4	2.8	52
		1.54	5.0	3.6	11
n-Heptane	0.684	1.66	1.4	2.7	37
n-Octane	0.703	1.79	1.4	4.0	30
n-Nonane	0.718	2.07	0.25	2.3	6
		1.91	0.5	···	4
		1.88	0.7	4.5	10
		1.83	1.4	2.6	15
		1.84	5.0	5.2	11
		1.83	11.0	4.5	6
n-Decane	0.730	1.92	1.4	4.2	11
n-Tetradecane	0.762	2.00	1.4	3.5	10
2-Methylpentane	0.654	1.49	1.4	3.8	30
2,2-Dimethylbutane	0.649	1.33	1.4	3.4	19
2,3-Dimethylbutane	0.662	1.38	1.4	3.2	20
2,4-Dimethylpentane	0.673	1.44	1.4	2.5	22
2,2,4-Trimethylpentane	0.692	1.40	1.4	2.6	29

Before a given sample was introduced into the breakdown cell for measurement, a careful check was made to determine whether suspended solids had been removed satisfactorily. This was done by shining a narrow beam of white light through the liquid in the storage flask and looking for evidence of suspended materials in the beam. Detection was most effective when the light was allowed to shine almost directly into the eye. It was often necessary to repeat the distillation and filtering procedure several times before the liquid could be considered satisfactory for testing.

C. The Breakdown Measurements

The testing procedure used in the present work was similar to that described in previous papers.[4,6] The cleaned cell was first rinsed thoroughly with the test liquid. It was then filled to a level just above the tops of the three glass windows, and the spark gap scanned carefully by means of the 32× microscope *M* (see Fig. 1). The light source for this step in the procedure was either of two microscope illuminators which directed narrow beams of white light at right angles to each other into the cell through the remaining two windows. If solid particles could be detected by either direct or scattered light, the cell was emptied and rinsed again. When this precaution was taken, breakdown invariably occurred in the center of the gap as it should if solid particles are not interfering. The actual measurements consisted in the application of single voltage pulses of constant duration and gradually increasing amplitude, the amplitude just causing disruption being defined as the breakdown voltage. The electrode spacing for all measurements was 0.002 inch.

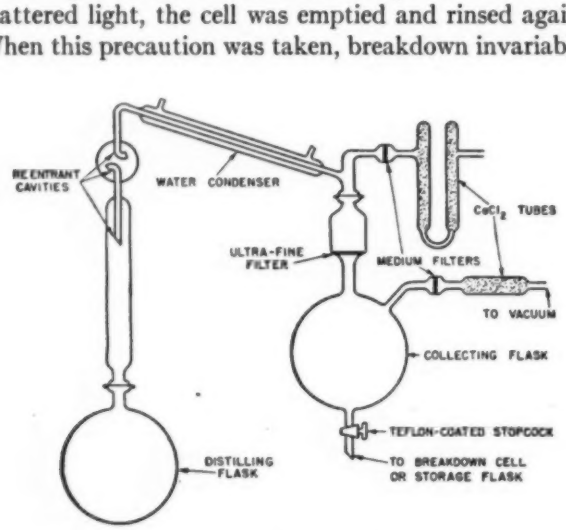

FIG. 2. Apparatus for purifying liquids.

A 2000-ohm noninductive resistor was connected in series with the test cell to limit the current at breakdown. This reduces the pitting of the electrode and the amount of decomposition product formed in the liquid by the breakdown arc.

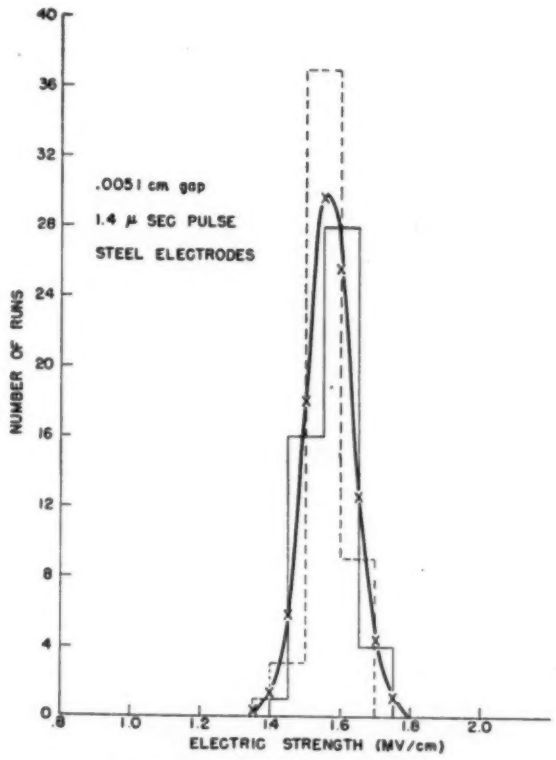

FIG. 3. Distribution of breakdown data for *n*-hexane.

III. EXPERIMENTAL RESULTS AND DISCUSSION

A. Reproducibility of Results

Because the measured electric strengths of liquid hydrocarbons apparently do not change very much with changes in molecular weight and structure, it is necessary to place a great deal of emphasis on reproducibility. Use of the mercury cathode enabled us to obtain results with standard deviations of from 4 to 7 percent. However, as a result of the refinements in technique described in the last section, we are now able to measure electric strengths with even greater precision (see Table I). As a matter of fact, the deviations are so small that they can be accounted for almost entirely by the uncertainties involved in reading the pulse amplitude and measuring the electrode separation.

Because of the fact that solid particles in the spark gap can only result in premature breakdown in liquids, one might expect their presence to yield an unsymmetrical distribution of results. This would be true especially if the concentration of such impurities was sufficiently low that they could not exert their influence in all of the tests. The distribution curve for *n*-hexane as obtained from 52 runs is plotted in Fig. 3. Note the high degree of symmetry. We have obtained sets of data for this and other hydrocarbon liquids which showed a tail, and in some cases another peak, on the lower part of the distribution curve. In all such cases, it was found that the test liquids contained a significant amount of suspended solids. All of the data reported in

this paper represent symmetrical distributions of results such as that shown in Fig. 3.

B. The Dependence of Electric Strength upon Density

We have taken the suggestion of von Hippel[8] that the essential difference between electrical breakdown in condensed phases and gases is involved with the mechanism by which field accelerated electrons lose energy to the dielectric.[4] In gases this retarding barrier is furnished by electronic excitation of the molecules. In the more condensed liquids and solids, on the other hand, vibrational excitation becomes dominant in importance. We have assumed, therefore, that the electric strength E of a liquid ought to obey a law similar to Paschen's Law for gas breakdown, provided one can vary the electron mean free path λ without causing a significant change in the energy ϵ at which the rate of loss of energy of a free electron in the liquid to molecular vibrations is the most severe.[4] For a simple model, it was shown that

$$V/\delta = E \cong K\epsilon/\lambda. \tag{1}$$

It appeared that the liquid hydrocarbons provided a satisfactory method of accomplishing this variation. By assuming that the various atoms of the hydrocarbon molecule are scattered at random throughout the liquid, at least as far as the electron is concerned, it was possible to write,

$$1/\lambda \sim \Sigma n_i a_i = (n_C a_C + n_H a_H), \tag{2}$$

where n_i and a_i represents the number per unit volume and scattering cross section of the ith kind of atom in the liquid, respectively. Then,

$$E = B\epsilon(n_C a_C + n_H a_H). \tag{3}$$

From such a model one should expect a linear dependence of E upon liquid density, provided again that ϵ is the same for all hydrocarbons. Actually, the agreement of our experimental results with Eq. (3) was excellent, much better than we had anticipated.

The electric strengths of the liquid hydrocarbons, as measured in the present investigation, are listed in Table I and plotted in Fig. 4 as a function of liquid density. Here again, the strengths of the straight-chain members of the series fall on a straight line within experimental error. However, those of the branched-chain members fall consistently below this line. Furthermore, the lowering effect associated with branching appears to be more pronounced as the number of branches per molecule is increased.

It will be noted that the electric strengths measured by the present technique are consistently higher than those measured previously with the mercury cathode. This is presumably a result of the difference in the emission properties of steel and mercury and of the greater attention given to the elimination of molecular and suspended impurities in the liquids.

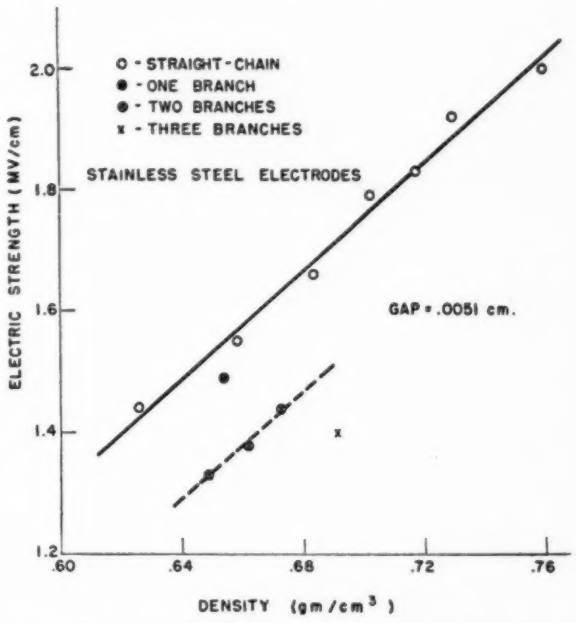

FIG. 4. Dependence of the electric strengths of saturated hydrocarbon liquids upon density.

The failure of the electric strengths of the branched-chain hydrocarbons to fall on the curve described by the straight-chain members of the series is really not surprising in view of the assumptions made in setting up the model. In particular, the assumption that ϵ is the same for all hydrocarbons is undoubtedly not quite true. If ϵ is associated with vibrational excitation in the liquids, one might well expect it to vary as branches are added to the hydrocarbon chain. The fact that the vibrational spectrum of a straight-chain hydrocarbon differs considerably from that of a branched-chain hydrocarbon is strong support for such a conclusion.

We might conclude from this discussion that extension of the measurements to hydrocarbons of more complicated structure has resulted in the appearance of a kind of fine structure. A further extension of the work may lead, ultimately, to a rather broad band of results which show a general increase with increasing density.

Although we cannot deduce with certainty from the present measurements that ϵ is associated with molecular vibrations, we now have experimental evidence that there is a definite difference between the mechanisms of breakdown in gases and liquids. Recent measurements of the sparking voltages of saturated hydrocarbon gases have shown that the ionization potential (which is closely related to the electronic excitation potential) is, as predicted, very definitely of importance in determining the voltage at which breakdown occurs.[9] Of even greater significance, however, is a comparison of the effect of chain branching on the electrical break-

[8] A. von Hippel, J. Appl. Phys. 8, 815 (1937).

[9] J. C. Devins and R. W. Crowe (to be published).

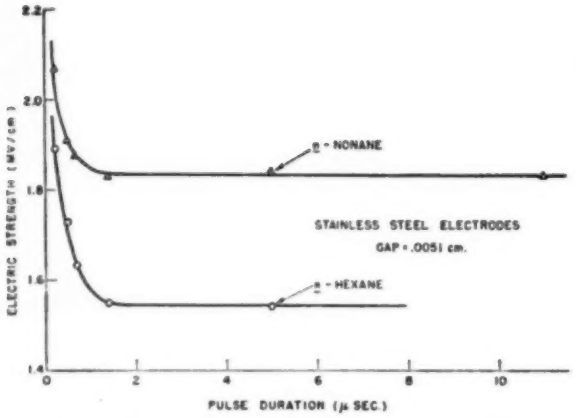

FIG. 5. The time dependence of electrical breakdown in liquid hydrocarbons.

down of liquids and gases. While there is little doubt that branching lowers the electric strength of a liquid hydrocarbon, no such effect is observed in the gas phase. For example, the electric strengths of the four *gaseous* hexane isomers listed in Table I are the same within experimental error at any given pressure and electrode separation.

C. The Time Dependence of the Breakdown Process

The values of electric strength plotted in Fig. 4 were obtained by using a 1.4-microsecond voltage pulse. At the time these measurements were made, we had thought that such a pulse duration was in excess of the formative time lag for the breakdown process in all liquids. The work of Edwards[10] had indicated that the time lag, as measured with electrode spacings comparable with those used here, was approximately one microsecond for a variety of liquids, and therefore was relatively insensitive to the structure and composition of the liquid. However, Goodwin and MacFadyen[2] have presented evidence recently that there is a definite correlation between this time and the molecular weight (or viscosity) of a liquid hydrocarbon. More specifically, they found that it was directly proportional to the time required for positive ions, produced by ionizing collisions between electrons and molecules, to cross the spark gap. On this basis, the time lag varied from about one microsecond for *n*-hexane to about twelve microseconds for *n*-tetradecane. These observations were used as evidence that the mobility of the positive ion plays a major role in the mechanism of electrical breakdown in liquids.

Our concern about the discrepancy described above is obvious. If the formative time lag varies in the manner reported by Goodwin and MacFadyen, then our results might be merely an incomplete representation of this effect, and as such would have little or no meaning in terms of molecular structure. It was necessary, therefore, to reinvestigate the time dependence of breakdown for representative members of the hydrocarbon series studied here. For this investigation two liquids (*n*-hexane and *n*-nonane) of widely different molecular weights and viscosities were selected.

The results of this study are plotted in Fig. 5. In both cases, the measured electric strength is independent of time when the applied pulse is longer than about one microsecond, but rises sharply for shorter pulses. This observation is in complete agreement with the earlier findings of Edwards.[10] We may conclude from these results that the data obtained with the 1.4-microsecond pulse are free from time effects, and represent values of electric strength that would be realized with dc voltages if thermal effects could be avoided. The reason for the discrepancy between our results and those of Goodwin and MacFadyen is not clear at the present time.

[10] W. D. Edwards, Can. J. Phys. **29**, 310 (1951).

Water Vapor Condensation Process in Supersonic Nozzles*†

PETER P. WEGENER
Jet Propulsion Laboratory, California Institute of Technology, Pasadena, California
(Received April 26, 1954)

The history of experimental and theoretical investigations of water vapor condensation phenomena in supersonic nozzles is reviewed. It is then shown empirically for a given experiment that the shocklike disturbance visible in flow pictures delineates the collapse of the supercooled state of the water vapor present in the air. All flow properties are calculated through this extended condensation zone from pressure distribution measurements, and it is seen that no shock waves are involved in the process. Finally a conversion of these data to an equivalent constant-area flow reveals that the latter would be an example of a weak detonation observed in nature as predicted by Burgers and by Reed.

I. SUMMARY OF THE PAST WORK

EARLY investigators of the flow through supersonic nozzles were puzzled by the observation of two oblique shocklike phenomena occurring near the nozzle throat in the supersonic flow. Prandtl[1] showed a beautiful schlieren picture of such a disturbance during the Volta Congress in 1935. Wieselsberger[2] remarked in the discussion that the position of these shock waves was dependent upon the initial humidity of the air. The first systematic investigation of this relationship (Aachen, 1934 to 1936) was published by Hermann,[3] who demonstrated that these disturbances were caused by condensation of the water vapor in the air, and consequently they became known as "condensation thocks." Shocks close to the throat and rather normal so the flow direction were seen at high humidities while they appeared further downstream and more X-shaped for lower moisture content. This important discovery led to the introduction of air-drying equipment into supersonic wind tunnel circuits.

Interestingly enough several years went by before a cross connection to the long known similar phenomena of delayed condensation in steam nozzles and Wilson cloud chambers was recognized. Heybey[4] was the first to apply a thermodynamic treatment of supersonic flow with heat addition to condensation. Oswatitsch[5,6] also presented a general kinetic and thermodynamic theory of condensation in supersonic nozzles. He proved that the number of foreign nuclei present in wind tunnel air is too small to play the customary role of condensation nuclei. Rather, he suggested that supersonic wind tunnel condensation is of the type described by Volmer,[7] Becker and Doering,[8] and others, where triple collisions in the supercooled vapor initiate the formation of tiny stable clusters of molecules. The rate of formation of these clusters, i.e. the nucleation rate, is strongly dependent on the environment, and increases enormously at low temperature. However, Oswatitsch obtained only qualitative agreement of theory and experiment in the case of water vapor in air due to the scanty knowledge of surface tension and other properties at these low temperatures. Also it was impossible to predict accurately the onset of condensation, i.e., the collapse of the metastable state of supersaturation. From this theoretical work and from further experiments[9,10,etc.] it became apparent that the onset of condensation also depended on the time scale of the expansion. It was shown[11] that supercooling up to about 90°C could be achieved in supersonic nozzles when the average temperature gradient of the isentropic expansion between the points of saturation and condensation was about 90°C/cm. These rapid expansions (of about 10^{-4} second duration) prompted renewed investigation of the Becker-Doering theory by Kantrowitz[12] and Probstein[13] to find the time lag associated with the buildup of a steady state nucleation rate, and again the results had to be adjusted empirically. Furthermore, the calculated critical droplet size at such low temperatures suggests that the stable nuclei consist of only a few molecules and application of a continuum theory ought to fail. Efforts were made by Reed[14] and Herzfeld and Reed[15] to understand the initial phases of cluster formation statistically, and to clarify the concept of free energy of tiny drops. The sum total of all these and many other investi-

* The interferograms and pressure distribution measurements were taken for this purpose in December, 1949, by Mr. J. Fuller and Mr. N. M. Shapiro in the 18×18 cm wind tunnel of the U. S. Naval Ordnance Laboratory. Helpful discussion with Mr. M. Sibulkin of the Jet Propulsion Laboratory is gratefully acknowledged.

† This paper presents the results of one phase of research carried out at the Jet Propulsion Laboratory, California Institute of Technology, sponsored by the Department of the Army, Ordnance Corps, and Department of Air Force.

[1] L. Prandtl, Roma Reale Acc. D'Italia **XIV**, 197 (1936).
[2] Reference 1, p. 558.
[3] R. Hermann, Luftfahrt-Forsch. **19** (1942), Part 6, p. 201.
[4] W. Heybey, WVA Archive 66/172 (1942) and Natl. Advisory Comm. Aeronaut. Tech. Mem. No. 1174 (1947).
[5] K. Oswatitsch, Jahrb. Deutsch. Luftfahrt-Forsch. (1941).
[6] K. Oswatitsch, Z. angew. Math. u. Mech. **22**, 1 (1942).
[7] M. Volmer and A. Weber, Z. physik. Chem. **119** (1926).
[8] R. Becker and W. Doering, Ann. Physik. **24**, 719 (1935).
[9] J. Lukasiewicz and J. K. Royle, Reports and Memoranda 2563, 1953 (June, 1948).
[10] R. Head, Guggenheim Aeronautical Laboratory, California Institute of Technology dissertation, 1949.
[11] P. Wegener, Phys. Rev. **76**, 883 (1949).
[12] A. Kantrowitz, J. Chem. Phys. **19**, 1097 (1951).
[13] R. F. Probstein, J. Chem. Phys. **19**, 619 (1951).
[14] S. G. Reed, Jr., Catholic University of America, dissertation, 1951.
[15] K. F. Herzfeld and S. G. Reed, Jr., Z. Elektrochem. **4**, 308 (1952).

gations, however, has not yet led to a quantitative prediction of the onset and rate of water vapor condensation in air flowing in supersonic nozzles.

Parallel to the above development, several authors worked out the flow properties of compressible fluids with heat addition or removal in arbitrary channels. For the case of condensation, it was shown by Heybey[4] and Charyk[16] that the solution of the continuity, momentum, and energy equation (including a heat addition term) allows either a supersonic or a subsonic velocity behind the "shock wave" for supersonic velocity ahead of the shock, and both authors intuitively chose the supersonic velocity solution.

Concurrently the details of the theory of detonations[17] were developed in several countries and it could be shown that for initially supersonic flow (in a coordinate system moving with the detonation), the above two cases were again in accord with the conservation equations and stability considerations. The detonations leading to final subsonic or supersonic velocity were termed "strong" or "weak," respectively. Observed detonations correspond to the case of subsonic velocity after a shock wave and subsequent heat addition from the chemical reaction terminating in sonic velocity at the end of the process. The use of this detonation model led Courant and Friedrichs,[18] Doering,[19] and others to reject the weak detonation as a physically possible process. Historically the word "detonation" has, therefore, become associated with this shock-ignition model. On the other hand, there is no need to limit processes of heat addition in supersonic flow to this model. Such processes can then lead to states in a p-v diagram equivalent to those previously termed the weak detonation. In fact, Burgers[20] remarked in 1948 that "the condensation shock might perhaps be compared with a weak detonation front." Finally, Reed[21] showed theoretically that water vapor condensation in supersonic nozzles is such a process, Oswatitsch[22] describes the same thoughts, and Heybey and Reed[23] go through detailed analysis appending an extensive bibliography on "the search for weak detonations."

In the present work we will attempt to show experimentally that condensation in a nozzle actually occurs at the position where the curved shocklike disturbance is visible in a schlieren photograph. We will then show that it is possible to calculate all flow properties through a condensation zone from pressure distribution measurements. This procedure will enable us to obtain the rate of condensation, i.e., of heat addition. Finally it will be demonstrated experimentally that the condensation process does not involve what is normally considered a shock wave, and is indeed an example of a process corresponding to a weak detonation occurring in nature.

II. LOCATION OF BEGINNING CONDENSATION IN THE SUPERSONIC NOZZLE

Figure 1 shows two schlieren pictures of the flow near the throat of the $M=2.92$ nozzle in the Naval Ordnance Laboratory 18×18 cm supersonic wind tunnel. In the second picture the air had an initial humidity of 46 percent, and a shocklike disturbance is visible very near the throat. Figure 2 shows two interferograms taken with monochromatic light of 5461 A, again for flow with dry and moist air. The condensation zone in the moist air interferogram is visible as an X-shaped region of bent fringes. However, every fringe is continuous through the entire condensation zone. This observation is in marked contrast to that found on interferograms of shock waves in wind tunnels where fringes are discontinuously displaced across the shock whose thickness is of the order of the mean free path of the molecules. From Fig. 2 it is possible to determine the density at any point in the picture. However, we will focus attention on two stream tubes only. Of these one follows the centerline and the second is located near the wall just outside the boundary layer. After determining the density along these two paths in the nozzle from the interferogram in the usual manner for two-dimensional flow, all flow parameters up to the dis-

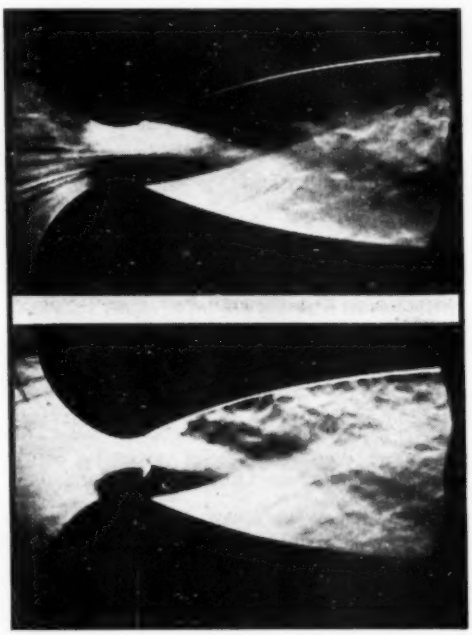

FIG. 1. Schlieren photographs of flow with dry and moist air in the $M=2.92$ nozzle. 18×18 cm tunnel of the U. S. Naval Ordnance Laboratory. (a) Dry air; (b) 46 percent relative humidity. $p_0=1$ atmos. $T_0=285°$K. Flow direction →.

[16] J. V. Charyk, Guggenheim Aeronautical Laboratory, California Institute of Technology dissertation, 1946.
[17] R. Courant and K. O. Friedrichs, *Supersonic Flow and Shock Waves* (Interscience Publishers, Inc., New York, 1948).
[18] Reference 17, p. 231.
[19] W. Doering, Ann. Physik 43, 421 (1943).
[20] J. M. Burgers, Naval Ordnance Lab. Rept. 1130, p. 20 (1949).
[21] S. G. Reed, Jr., J. Chem. Phys. 20, 539 (1952).
[22] K. Oswatitsch, *Gasdynamik* (Wien Springer Verlag, Berlin, 1952), p. 65.
[23] W. H. Heybey and S. G. Reed, Jr., Naval Ordnance Rept. 2779 (1953).

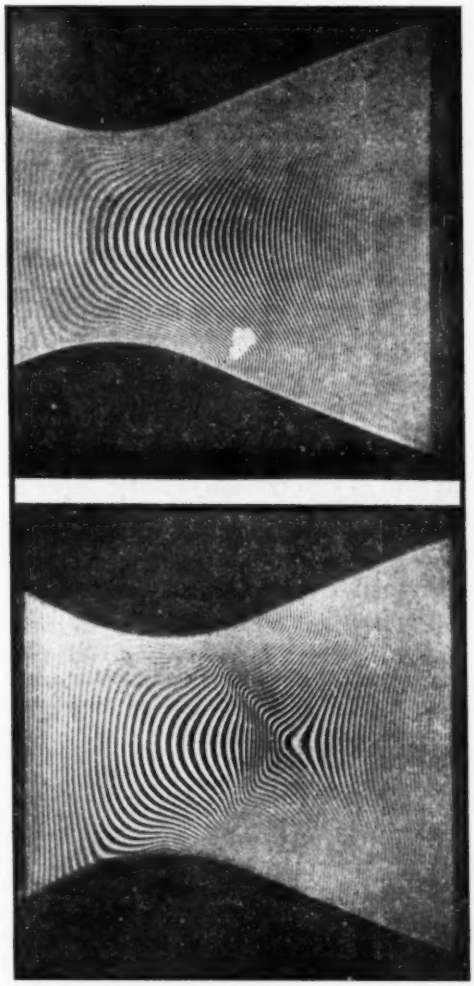

FIG. 2. Interferograms of flow with dry and moist air in the throat region of the $M=2.92$ nozzle. 18×18 cm tunnel of the U. S. Naval Ordnance Laboratory. (a) Dry air; (b) 47 percent relative humidity. $p_0=1$ atmos. $T_0=285°K$. Flow direction →.

turbance may be obtained from an isentropic flow table. The presence of the supercooled water vapor in the air may be neglected because only heat release due to condensation affects the flow properties materially. The question now arises if the outline of the X-shaped disturbance region visible in the photographs coincides with the onset of condensation or if condensation, e.g., first occurs at the nozzle wall and causes an oblique shock system to propagate into the nozzle like that issuing from any other obstacle. Because the start of condensation cannot yet be predicted theoretically, we will compare the expansion on wall and center stream tube with empirical data. As discussed before, we have from previous experiments

$$\Delta T=f\left(\varphi_{or},\frac{\Delta T}{\Delta X}\right), \tag{1}$$

where $\Delta T=T_s-T_k$, the difference of saturation temperature, T_s,[24] and the temperature, T_k, at the beginning of condensation. φ_{or} is the initial relative humidity and $\Delta T/\Delta X$ is the mean temperature gradient in the nozzle between the same two points, where temperature drops about linearly with distance. Figure 3 shows a plot of observed supercooling in nozzles ranging in test section size from one to sixteen inches square. The sources from which these data could be evaluated are indicated on the graph; the scatter is fairly typical of that found in investigations of this sort. The results for wall and center stream tubes of the present test indicate that the solid points fall approximately together, showing that condensation actually occurs where the disturbances are visible in the picture. Also, the Mach number at the beginning of condensation is about 1.28 on wall and center. Assuming the same state of affairs on all stream lines in between the two extremes, we may conclude that the entire visible disturbance front actually delineates the collapse of the supercooled state. This conclusion was further emphasized by qualitative light scattering tests that revealed the presence of droplets throughout the nozzle downstream of this condensation zone.

III. THE RATE OF CONDENSATION

The inspection of available experimental data of measured pressure distributions in nozzles with condensation suggests a discussion of the process in three phases: First the expansion of moist air leads far into the coexistence region of water vapor without any noticeable condensation. Experimentally this means

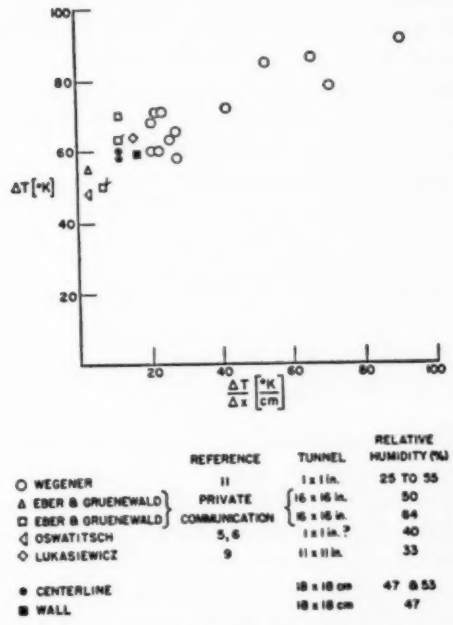

FIG. 3. Observed supercooling as a function of temperature gradient for supersonic tunnels operated with moist air.

[24] *Handbook of Chemistry and Physics* (Chemical Rubber Publishing Company, 1945), twenty-ninth edition, p. 1777.

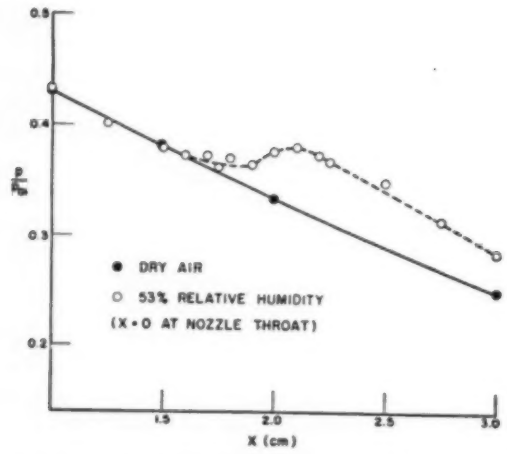

FIG. 4. Pressure distribution measurement with dry and moist air on sidewall centerline. 18×18 cm tunnel of the U. S. Naval Ordnance Laboratory.

that moist and dry air pressure distribution measurements in nozzles are identical up to a certain point. At this point the second phase starts with the collapse of the metastable supercooled state where the pressure of the moist expansion rises markedly above the dry values. In the third and final stage the pressure begins to drop again and we may discuss this part as the equilibrium expansion of air saturated with water vapor. Such a dry and moist pressure distribution measurement taken on the centerline of the sidewall in the throat region of the same $M=2.92$ nozzle is shown in Fig. 4. The x coordinate is placed to give $x=0$ at the throat. Our interest centers on the determination of the flow properties in the collapse region of the condensation zone between $x=x_k=1.6$ cm, the point of deviation of dry and moist air expansions and $x=x_e$, a point downstream of the pressure maximum of the moist air measurement. Oswatitsch[6] derived a system of four equations that closely describe this process. In addition to continuity, momentum, and energy equations applicable to compressible flow with phase change and heat addition in varying area channels (neglecting viscosity and heat conduction), he derives a condensation rate equation. This equation may be written as

$$\frac{dW}{dx}=\int_{x_k}^{x_e}\frac{dD}{dx}J(x')A(x')dx', \tag{2}$$

where dW/dx represents the increase of mass of the liquid (or solid) water along x. The term dD/dx describes the droplet growth law, J is the rate of production of stable condensation nuclei per unit volume, and A represents the known varying nozzle area. The coordinate x' refers to any point at which a stable nucleus was formed and began to grow, since in any given cross section A there will be a multitude of droplets of varying sizes depending on their history and environment at their different origins. So far accurate quantitative calculations using (2) could not be made without adjusting the results empirically because it is difficult to find a suitable droplet growth law where the growth mechanism depends on the initial size of the stable nucleus. Also, accurate determination of the nucleation rate J, where a relative unknown, the surface tension, enters in the third power, is presently impossible. In fact, Oswatitsch[6] suggests turning the experiments around and determining surface tension from wind tunnel experiments. However, a direct calculation of dW/dx from experiment may aid future considerations of the problems entering the right side of (2). We may write

$$\frac{\lambda}{W_{\text{air}}}\frac{dW}{dx}=\frac{dh_0}{dx}, \tag{3}$$

with λ the heat of vaporization of water vapor taken as constant in the small temperature interval through a condensation zone, and W_{air} the mass of air. With air taken as a perfect gas of constant specific heat we obtain

$$\frac{dW}{dx}=W_{\text{air}}\frac{Cp_{\text{air}}}{\lambda}\frac{dT_0}{dx}, \tag{4}$$

and therefore a measurement of the stagnation temperature through a condensation zone will lead directly to a determination of the rate of condensation. The accurate measurement of total temperature in supersonic flow, in particular when a change of phase is involved, is difficult. However, it is possible to determine the flow properties by evaluating the measured dry and moist pressure distributions shown in Fig. 4 according to an approximate method outlined in Appendix A. In this method it is assumed that the flow process in the condensation zone may be treated by a stepwise calculation where every step consists of an isentropic expansion followed by constant area flow with heat addition. It is further assumed that viscosity effects are restricted to the boundary layers, that heat conduction is neglected, and that the droplets move with the flow velocity and are in thermal equilibrium with their surroundings. The results of this calculation are shown in Fig. 5. It is apparent that no shock wave in the ordinary sense is present and that temperature, density, etc., vary continuously throughout the collapse phase of the condensation zone whose extension in the x direction is about 10^4 times the mean free path of the molecules. However, the density gradients are sufficiently strong to produce schlieren pictures like that shown. The expression "condensation-shock" might now be replaced by referring to this phenomenon as a condensation zone. Stagnation temperature increases while stagnation pressure decreases, and the entropy increase, dD/dx, etc., may be calculated from the data. Finally, the Mach number computed throughout the condensation zone remains supersonic with a minimum roughly coinciding with the maximum of static pressure.

It is possible to calculate from the data in Fig. 5 the total heat added to the air stream per unit mass of air, locating $x_k=1.6$ cm and $x_e=2.5$ cm,

$$q=h_{0e}-h_{0k}=Cp_{\text{air}}(T_{0e}-T_{0k}). \tag{5}$$

Independently the dew point in the supply section has been measured and the mass ratio of water to air φ, the mixing ratio, can be determined. If all of the water vapor actually condenses between x_k and x_e, the total heat added to the air stream per unit mass of air could be no larger than

$$q=\varphi\lambda, \tag{6}$$

and we have

$$\varphi\lambda\simeq Cp_{\text{air}}(T_{0e}-T_{0k}). \tag{7}$$

The heat of vaporization is poorly known in the temperature range of our experiment (approximately 220°K), and values applying to supercooled water or those plus the heat of fusion to ice may be chosen.[5] The heat addition was determined by both methods, and it was found that the value obtained assuming sublimation of all water vapor to ice is still about 15 percent lower than that given by Eq. (5). Since this is obviously impossible, an error in the measurement of humidity, inaccuracies of the stepwise calculation, or poor information on λ may account for the discrepancy. At any rate, the direction of the disagreement suggests that ice crystals may be formed in the process. If this suspicion could be proven in further experiments, the theoretical determination of the nucleation rate would become even more formidable.

IV. CONDENSATION STATES IN A *P-V* DIAGRAM

The one-dimensional theory of detonations mentioned in the first section may be discussed in terms of thermodynamic states conforming to the conservation laws

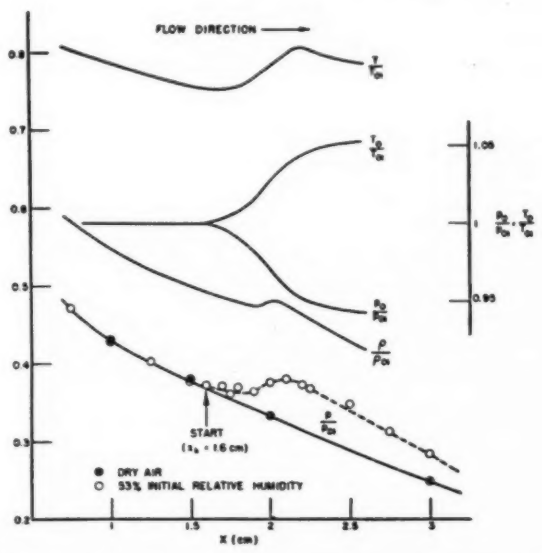

FIG. 5. Measured and derived thermodynamic properties of flow through the condensation zone.

before (index 1) and after the reaction. Selecting specific volume v and pressure p as thermodynamic variables, the results can be given in terms of a pressure-volume diagram. First we consider the continuity and momentum equation for $A=$constant. From these we can derive

$$\frac{p-p_1}{v-v_1}=-\rho_1 u_1^2, \tag{8}$$

the Rayleigh equation,[25] where u_1 is the initial flow velocity. This equation gives a straight line in a p-v diagram and its slope is determined by the conditions ahead of the reaction. All changes of state on this line involve external entropy changes, e.g., heating and cooling of the gas. Introducing $P=p/p_1$ and $V=v/v_1$, and remembering the definition of Mach number and speed of sound, we can rewrite (8) as

$$\frac{P-1}{V-1}=-\gamma M_1^2. \tag{9}$$

Supersonic and subsonic initial Mach numbers are separated in a p-v diagram by the Rayleigh line with the slope $-\gamma$.

Next we want to express the conservation of energy by combining the Rayleigh equation with the energy equation. The latter must now contain a term q describing the addition or removal of heat from the flow. The problem is simplified by our previous assumption that water vapor condensation makes itself felt only by the release of heat and therefore the law of change of internal energy per unit mass of air with temperature is identical on both sides of the reaction. The final result of the derivation[23] is

$$\frac{\gamma+1}{\gamma-1}(p_1v_1-p_2v_2)+(p_2v_1-p_1v_2)+2q=0. \tag{10}$$

If we again employ our dimensionless variables P and V, we may rewrite (10) as

$$\frac{\gamma+1}{\gamma-1}(1-PV)+(P-V)+\frac{2q}{p_1v_1}=0, \tag{11}$$

where q must be expressed in mechanical units. It can be shown[23] that (11) represents a set of hyperbolas for parametric values of q and the common asymptotes in our notation are

$$V=\gamma-1/\gamma+1, \quad \text{and} \quad P=-\gamma-1/\gamma+1.$$

Figure 6 is a plot of (9) and (11) for one set of initial conditions. For $q=0$, (11) is, of course, equivalent to the familiar Rankine-Hugoniot equation going through $P=1$, $V=1$. The upper right quadrant in the p-v diagram between Rayleigh lines for constant volume heat

[25] N. Hall, *Thermodynamics of Fluid Flow* (Prentice-Hall, Inc., New York, 1951), p. 162.

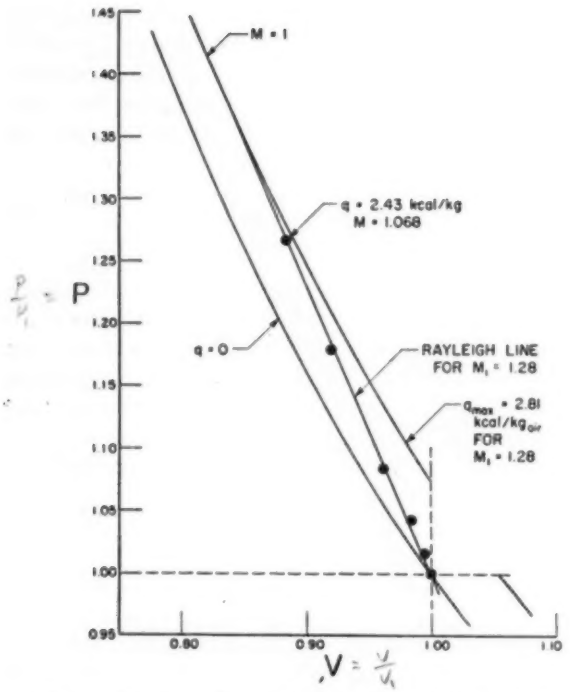

FIG. 6. Pressure-volume diagram of equivalent constant area flow derived from dry and moist air pressure distribution in diverging channel.

addition ($M_1=\infty$), and constant pressure heat addition ($M_1=0$), is devoid of physical meaning. For a given M_1 and $q>0$ the Rayleigh line will be tangent to one Hugoniot curve only, for which $q=q_{max}$ (Fig. 6). The flow speed downstream of the reaction is then sonic. For values $0<q<q_{max}$ we always have two intersections of (11) and (9). The one at the lower P (larger V) corresponds to supersonic speed behind the process, while the one leading to higher P (lower V) yields subsonic speeds. The conservation equations are fulfilled for both cases which were called by definition strong and weak detonation; respectively. Heybey[4] selected the case of $M_2>1$ as the appropriate solution for the condensation process. In order to substantiate this intuitive reasoning we will attempt to show that experimentally obtained thermodynamic states through the condensation zone lie on a Rayleigh line approaching the point of tangency or intersection of (9) and (11) for the appropriate heat release from the supersonic side. This should prove if condensation states are equivalent to those of a weak detonation as predicted by Reed *et al.*

Our task will be to reduce the experimental and derived data (Fig. 5) from observations in a diverging channel to what might be called an equivalent constant-area flow. In order to do this we will assume that the area downstream of $x_k=1.6$ cm is constant for the condensation process. Since we know the actual expansion from the dry pressure distribution, and know A_k at x_k, we may take the diverging channel results obtained at any position x_n and assume that the fluid undergoes an isentropic compression through the area ratio A_n/A_k. Each pair of values of P, $V(x)$ for the expanding nozzle then yields a new pair of values of an equivalent constant area process. These values are plotted starting with $P=1$ and $V=1$ at the beginning of condensation in Fig. 6. Also plotted is a Rayleigh line with the slope $-\gamma M_1^2$ for $M_1=1.28$ ($x_k=1.6$ cm). It can be seen that the calculated points fall on the Rayleigh line which we take as an indication that our conversion was a legitimate one. Aside from the Hugoniot curve for $q=0$, the curve for $q=q_{max}$ corresponding to M_1 is indicated. Flow in a diverging nozzle through a condensation zone may absorb more heat before the velocity is sonic than the q_{max} flow for the $A=$constant case. The converted experimental results (Fig. 6) show no evidence of a shock wave (an intermediate state on the $q=0$ Hugoniot curve) present. The sonic speed is approached from the supersonic side, and therefore the condensation process indeed corresponds to states assigned to the weak detonation.

APPENDIX A

Method of Calculating Thermodynamic Properties through Condensation Zones

Flow properties through condensation zones in a diverging nozzle may be obtained if one property, e.g., the static pressure, has been measured and the channel geometry is known. For our practical case it appears not to be necessary to solve the differential equations mentioned before. Rather, one may use an approximate method by first dividing the condensation zone into small steps in the x direction. Each one of these steps, taken as 0.1 and finally 0.05 cm in our example, can in turn be hypothetically subdivided into an isentropic expansion followed by constant area flow with heat addition (Fig. 7). This procedure permits the successive use of isentropic[26] (I) and Rayleigh[27] (R) flow tables which are readily available for $\gamma=1.4$. The calculation is started at that station in the nozzle where dry and moist pressure distributions begin to deviate from each

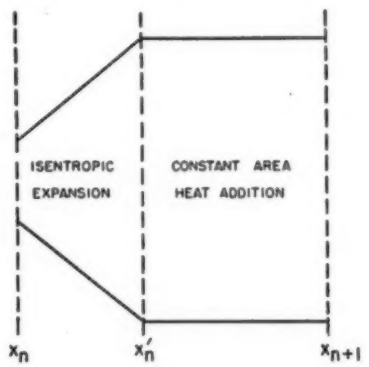

FIG. 7. Scheme for stepwise calculation of flow through condensation zones.

[26] M. Burcher, Natl. Advisory Comm. Aeronaut. Tech. Note No. 1592 (August, 1948).
[27] Reference 25, pp. 256–262.

other ($x_k = 1.6$ cm in Fig. 4). Here at x_k all flow properties are known because up to this station the flow may be taken as isentropic. From the dry air expansion we know M_n, M_{n+1} and the corresponding area ratios from the I table. To calculate the isentropic expansion part of the first step from n to n', we set

$$\frac{A_{n+1}}{A_n}=\frac{A_{n+1}/A^*(\text{dry})}{A_n/A^*(\text{dry})}=\frac{A_n'}{A_n}$$

and find M_n' and p_n'/p_{0n} in the I table since $p_{0n}'=p_{0n}$.

Next we consider the heat addition at constant area portion of the first step. For this process the R table provides us, for every Mach number, with values of pressure, temperature, total pressure, etc., made dimensionless by division through the corresponding values for $M=1$. These Rayleigh functions are p_n'/p^*, T_n'/T^*, etc. The moist pressure distribution measurements provide us with p_{n+1}/p_n and we may obtain

$$\frac{p_{n+1}}{p^*}=\frac{p_{n+1}}{p_n}\frac{p_n}{p_{0n}}\frac{p_{0n}'}{p_n'}\frac{p_n'}{p^*}.$$

M_{n+1} can be found from this in the R table with corresponding values of T_{n+1}/T^*, etc. Like, for example,

$$\frac{T_{n+1}}{T^*}\Big/\frac{T_n}{T^*}=\frac{T_{n+1}}{T_n},$$

the variation of every property may be determined for each step. It is to be noted that stagnation pressure of the flow decreases through the condensation zone and must be recalculated successively for every step using the ratios p_{0n+1}/p_{0n} previously obtained.

JOURNAL OF APPLIED PHYSICS VOLUME 25, NUMBER 12 DECEMBER, 1954

Analysis of Short-Time Tracer Injection in Underground Formations

G. C. Wallick and R. Jenkins
Magnolia Petroleum Company, Field Research Laboratories, Dallas, Texas

(Received December 31, 1953)

A proposed method of determining average underground formation characteristics by means of short-time tracer injection has been investigated both theoretically and experimentally. Streamline travel times for the passage of either an ideal gas or an incompressible fluid through a homogeneous permeable formation, from an injection well to a production well, have been calculated using an electronic digital computer. With only minor modifications, the methods of solution employed could be used in the investigation of more complex well systems. For a fixed ratio of injection well pressure to production well pressure the streamline travel times, expressed in terms of a dimensionless time parameter θ, are approximately independent of the well spacing to well radius ratio. A procedure has been devised for predicting the produced tracer concentration as a function of time using the calculated streamline travel times. Preliminary field tests indicate that the short-time tracer injection method is of practical value, but that additional study is necessary before the method can be used most advantageously.

INTRODUCTION

A NUMBER of attempts have been made to obtain information as to the characteristics of a subsurface geologic formation by adding a detectable material to gas or liquid injected into the formation and observing the additive concentrations and arrival times at one or more wells in the formation. Some of the additives which have been employed are fluorescein, NaCl, and Igepal;[1] boron compounds;[2] helium;[3,4] carbon disulfide;[5] and acetylene.[6] In each of these tests, the additive was injected at constant concentration for a long period of time, e.g., several days. The resultant additive arrival times and final equilibrium concentrations at the observation wells were then used to estimate the flow pattern and the presence of impermeable faults in the formation.

Additional information concerning the characteristics of the formation can be obtained by injecting the additive for a short period of time, e.g., several minutes, and recording both the additive arrival times at the production wells and the concentration of the additive in the produced fluid as a function of time. If the arrival times and the shape of the concentration curves as a function of time as predicted by theory are available for comparison with the experimental data, it is possible to evaluate such quantities as the average formation permeability or the average gas saturation in the formation. This is the most direct method for the determination of these quantities which has thus far been proposed.

[1] P. W. Sturm and W. E. Johnson, Producers Monthly **15**, No. 2, 11 (1950).
[2] Carpenter, Morgan, and Parsons, Producers Monthly **16**, No. 12, 12 (1952).
[3] E. M. Frost, Jr., Bureau of Mines RI 3897 (June, 1946).
[4] E. M. Frost, Jr., Bureau of Mines RI 4715 (August, 1950).
[5] G. G. Bernard and M. Savoy, U. S. Patent No. 2,578,500 (December 11, 1951).
[6] D. C. Bond and M. Savoy, U. S. Patent No. 2,589,219 (March 18, 1952).

This paper describes an idealized theoretical analysis of a short-time tracer injection test in which it is assumed that a detectable tracer is added to a gas injected, under steady-state conditions, into one of two wells in a formation and is detected at the second of the two wells. The formation is assumed to be homogeneous and of infinite lateral extent. A brief description is given of field tests of the proposed method which were carried out in connection with preliminary studies of the new method of oil recovery by "*in-situ* combustion."[7]

BASIC ASSUMPTIONS

The following basic assumptions were made in this study:

1. Steady-state laminar flow conditions are established prior to tracer injection and are maintained during the test.
   a. The mass of gas produced is equal to the mass of gas injected.
   b. The permeability and porosity of the formation are uniform and do not change during the test.
2. Neither the density nor the viscosity of the injected gas is altered by the presence of the tracer; i.e., small tracer concentrations are used.
3. The well spacing is large compared to the well radius.
4. The injected gas is an ideal gas.
5. The tracer is injected directly into the formation and is detected as soon as it enters the production well.
6. There is no mixing of the tracer-tagged gas with the untagged gas as the two gases flow through the formation.

FLOW EQUATIONS

In order to be able to plot tracer concentration curves, it was first necessary to calculate gas transit times along representative streamlines between the injection and production wells. Muskat[8] has shown that, in any porous medium of uniform permeability k and uniform porosity ϕ, the time required for a gas to travel along a streamline from a point s_1 to a point s_2 may be expressed in the form*

$$t=-\frac{\mu\varphi}{k}\int_{s_1}^{s_2}\left(\frac{\partial P}{\partial s}\right)^{-1}ds. \tag{1}$$

In principle, if the pressure distribution along a streamline and the equation of the streamline are known, the travel time along the streamline may be calculated by solution of Eq. (1). In most cases, however, this integral cannot be written in a closed form and it is necessary to resort to numerical methods of solution.

[7] C. S. Kuhn and R. L. Koch, Oil and Gas J. 52, No. 14, 92 (1953).

[8] M. Muskat, *Physical Principles of Oil Production* (McGraw-Hill Book Company, Inc., New York, 1949), pp. 764–768.

* Nomenclature list given at end of the paper.

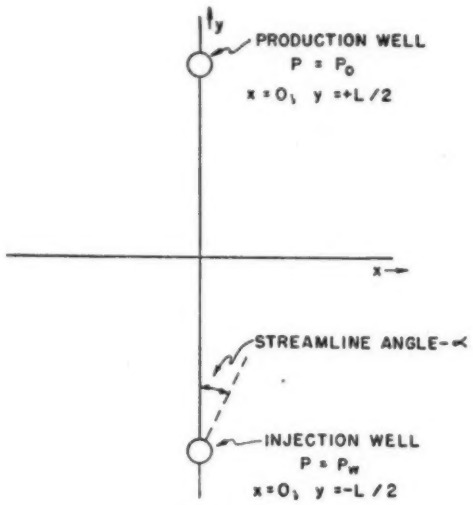

FIG. 1. Well geometry.

If the dimensionless parameters,

$$p=P/P_w,\quad l=s/L,\quad \zeta=x/L,\quad \eta=y/L,$$

and

$$\tau=(kP_w l)/(\varphi\mu L^2),$$

are introduced, Eq. (1) may be written in the form

$$\tau=-\int_{l_1}^{l_2}\left(\frac{\partial p}{\partial l}\right)^{-1}dl. \tag{2}$$

For the well geometry shown in Fig. 1, one obtains

$$p^2(\zeta,\eta)=\frac{N^2-1}{4N^2\ln(L/r)}\ln\left[\frac{\zeta^2+(\eta-0.5)^2}{\zeta^2+(\eta+0.5)^2}\right]+\frac{N^2+1}{2N^2}, \tag{3}$$

where $N=P_w/P_0$. Equation (3) is valid only if the well spacing L is large compared to the well radius r.

For this well system, the streamlines are arcs of circles with centers along the ζ axis and may be represented by an equation of the form

$$(\zeta-c)^2+\eta^2=R^2, \tag{4}$$

where

$$R=(c^2+0.25)^{\frac{1}{2}}. \tag{5}$$

It may be demonstrated by geometrical considerations that

$$c=-0.5/\tan\alpha,\quad \text{and}\quad R=0.5/\sin\alpha \tag{6}$$

where α is the angle at which the streamline leaves the injection well, measured from the η axis as is shown in Fig. 1. It follows from Eq. (3) that

$$\left(\frac{\partial p}{\partial l}\right)^{-1}=p(\zeta,\eta)\frac{4N^2\ln(L/r)}{N^2-1}\times\{[\zeta^2+(\eta-0.5)^2][\zeta^2+(\eta+0.5)^2]\}^{\frac{1}{2}}. \tag{7}$$

METHOD OF SOLUTION

An IBM Card Programmed Calculator was used to calculate gas travel times along the central streamline and along the twenty-four streamlines characterized by the angles α shown in Table II. The method of solution employed in this study could be used, with minor modifications, in the study of well systems more complex than the two well system.

The first step in the solution was to calculate the coordinates, (ζ,η), of points spaced at equal intervals, $\Delta l=0.02$, along each streamline. It may be demonstrated that the ζ coordinate of a point at a distance l along a streamline from the point of intersection of the streamline with the ζ axis is given by

$$\zeta=c+R\sin[(l/R)+\sin^{-1}1]. \tag{8}$$

Equation (8) was used to generate the ζ coordinates by automatically increasing l by $\Delta l=0.02$ from one point to the next. Values for the corresponding η coordinates were calculated using Eq. (4).

A master deck of punched cards was then prepared as follows. Each card of this deck contained the appropriate streamline number, the coordinates of one point, and the factors in Eqs. (3) and (7) which were independent of N and the L/r ratio. It was then possible to calculate the streamline travel times for a given value of N and of L/r in one pass of the master deck through the CPC.

For convenience in this integration, it was assumed that the integration limits were at the centers of the injection and production wells rather than at the circumference of the wells. Direct analytic solution for the travel time of an incompressible fluid along the central streamline demonstrates that for a well spacing of 20 ft and well radii $=3\frac{5}{16}$ in. $(L/r=72.453)$ the error introduced by the above assumption is less than 0.11 percent. This error would be even less for larger values of L/r and for the longer streamline.

STREAMLINE TRAVEL TIMES

Streamline travel times τ were calculated for values of $N=P_w/P_0$ ranging from $N=1.49$ to $N=10.0$ and for values of L/r of 72.453, 144.906, 500, 1000, and 5000. Over the range of the ratio L/r investigated, it was found that, for a fixed value of N, the ratio $\tau/\ln(L/r)$ was approximately a constant for a given streamline. This is illustrated in Fig. 2, which is a plot, for several typical streamlines, of the streamline travel time τ as a function of $\ln(L/r)$ for the pressure ratios $N=2$ and $N=10$.

TABLE I. Dimensionless breakthrough time θ_b for $L/r=1000$.

$N=P_w/P_0$	θ_b	$N=P_w/P_0$	θ_b
1.0000	0.08330	3.0303	0.09265
1.4925	0.08487	4.0000	0.09689
1.7544	0.08629	5.0000	0.09982
2.0000	0.08770	7.6923	0.10479
2.5000	0.09047	10.0000	0.10727

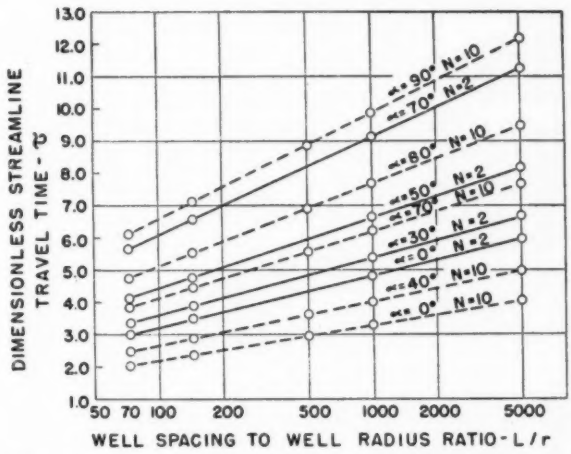
DIMENSIONLESS STREAMLINE TRAVEL TIME - τ
WELL SPACING TO WELL RADIUS RATIO - L/r
α = 90° N=10
α = 70° N=2
α = 80° N=10
α = 50° N=2
α = 70° N=10
α = 30° N=2
α = 0° N=2
α = 40° N=10
α = 0° N=10

FIG. 2. Dimensionless streamline travel time τ *vs* the ratio of well spacing to well radius L/r for representative streamlines. $N=2$ and $N=10$.

Although the ratio, $\tau/\ln(L/r)$, actually increased slightly with increasing values of L/r, the maximum variation observed was less than 0.7 percent of the value for $L/r=1000$. Thus, for practical purposes, the results obtained for this ratio for $L/r=1000$ may be considered to be valid for all values of L/r over the range from 72 to 5000.

It may be demonstrated that if the streamline travel times are expressed in terms of a dimensionless time parameter θ defined by

$$\theta=\frac{k(P_w-P_0)t}{4\mu\phi L^2\ln(L/r)}=\frac{P_aQt}{2(P_w+P_0)\pi\phi hL^2}=\frac{(N-1)\tau}{4N\ln(L/r)} \tag{9}$$

the value of θ obtained in the limit as N approaches unity is equal to an incompressible fluid travel time $\bar{\theta}$, which is independent both of the ratio N and the ratio L/r. The streamline travel times for an incompressible fluid were calculated by a method similar to that described in the previous section.

The dimensionless travel times along the central streamline θ_b for $L/r=1000$ are listed in Table I and times of arrival after breakthrough $\bar{\theta}$ for the remaining twenty-four streamlines are listed in Table II.

In order to estimate the accuracy of the streamline travel times θ shown in Tables I and II, the breakthrough time for an incompressible fluid, $\theta_b=0.08330$, obtained numerically may be compared with the value of $\theta_b=0.08333$ obtained analytically. The difference is seen to be less than 0.04 percent. Since there is more chance for roundoff error in the calculation of the gas travel times, the tabulated values of θ for $N>1$ are probably less accurate than in the example given above.

TRACER CONCENTRATION CURVES

Once the streamline travel times are known it is possible to assume that a tracer is added to the injected

TABLE II. Dimensionless time of arrival $\bar{\theta}$ after breakthrough for $L/r=1000$.

Streamline angle α	Time after breakthrough $\bar{\theta}$				
	$N=1.0000$	$N=2.0000$	$N=3.0303$	$N=5.0000$	$N=10.0000$
10	0.00102	0.00108	0.00114	0.00123	0.00132
20	0.00418	0.00441	0.00465	0.00502	0.00539
30	0.00977	0.01029	0.01087	0.01172	0.01260
40	0.01832	0.01929	0.02039	0.02198	0.02362
50	0.03073	0.03237	0.03421	0.03687	0.03963
60	0.04847	0.05105	0.05396	0.05816	0.06251
70	0.07389	0.07784	0.08031	0.08867	0.09530
80	0.11098	0.11691	0.12357	0.13318	0.14315
90	0.16667	0.17558	0.18560	0.20004	0.21502
100	0.25377	0.26736	0.28262	0.30462	0.32744
105	0.31619	0.33313	0.35215	0.37958	0.40801
110	0.39762	0.41894	0.44287	0.47737	0.51313
116	0.53173	0.56026	0.59228	0.63843	0.68627
120	0.65307	0.68813	0.72748	0.78417	0.84293
124	0.81139	0.85497	0.90388	0.97435	1.04737
127	0.96332	1.01509	1.07318	1.15685	1.24356
130	1.15377	1.21581	1.28540	1.38564	1.48951
133	1.39581	1.47088	1.55511	1.67640	1.80207
136	1.70818	1.80011	1.90322	2.05169	2.20551
138	1.96864	2.07462	2.19348	2.36462	2.54191
140	2.28370	2.40667	2.54459	2.74315	2.94884
142	2.66847	2.81220	2.97340	3.20545	3.44582
144	3.14339	3.31276	3.50269	3.77608	4.05927
145	3.42305	3.60751	3,81437	4.11210	4.42050

gas after some initial time and to make a plot of the volume fraction of tagged gas in the total efflux from the formation as a function of time after breakthrough. The first particle of tagged gas will arrive at the production well at a time after injection θ_b equal to the travel time along the central streamline. At some later time the first tagged gas will arrive along streamline 2 ($\alpha=10°$) and along the corresponding streamline on the opposite side of the central streamline. Since the flow into the production well is essentially radial, the volume fraction of tagged gas in the total efflux from the formation at any time after breakthrough is given by the ratio of the angle between the two streamlines along which the tagged gas is just arriving at that time to the total influx angle of 360°. Such an "arrival" curve is shown in Fig. 3 for $N=2.0$.

If the addition of the tracer to the injected gas is discontinued after a short time, e.g., $\theta=0.01$, it is necessary to consider the time after initial injection that the last particle of tagged gas arrives along the central streamline and subsequently along the longer streamlines. If the arrival curve is displaced to the right through a time $\Delta\theta$ equal to the injection time, it may be considered to represent the contribution to the total efflux of the gas no longer containing the tracer. This curve is shown as a "cut-off" curve in Fig. 3. If the tracer concentration is held constant during the injection period (a square wave injection), the volume fraction of tagged gas in the total efflux from the formation at any time $\bar{\theta}$ after breakthrough will be given by the difference between the "arrival" curve and the "cut-off" curve at that time. The concentration curve for an injection time $\theta=0.01$ obtained in this manner is shown as the broken curve in Fig. 3. It is seen that the concentration curve at first coincides with the "arrival" curve, rises to a maximum value at a time after breakthrough equal to the injection time, and then falls off rapidly for later times.

If the tracer wave form injected into the formation is not a square wave but has some irregular form, it is still possible to determine the concentration curve resulting from this injection if the injected wave form is known. The irregular wave form may be represented approximately to any desired degree of accuracy by a series of square waves. The concentration curve may then be drawn for each component square wave and all of these curves summed to give the resultant concentration curve for the irregular wave form injection. In general, this resultant concentration curve will not have the sharp peak characteristic of a square wave injection, and the maximum concentration will not obtain at a time after breakthrough equal to the injection time.

EXPERIMENTAL APPLICATIONS

General Discussion

Thus far in the theoretical development it has been assumed that the formation in question is homogeneous and infinite in lateral extent. No calculations have been made for fields which are bounded or have some arbitrary permeability distribution. However, an estimate can be made as to the degree of homogeneity of the formation from the shape of a concentration curve obtained experimentally. If there is a direct channel between the two wells, an injected square wave will emerge as a square wave. If the field is homogeneous, the concentration curve will be of the form predicted by theory. For some intermediate case, it would be expected that the concentration curve would both rise and fall more rapidly than the curve for a homogeneous formation and would be flattened in the central portion of the curve.

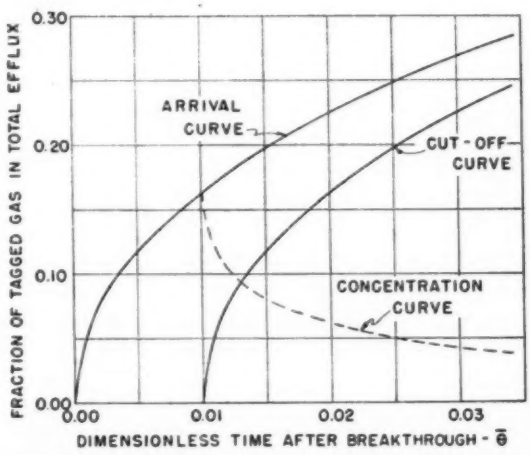

FIG. 3. Method of constructing tracer concentration curves using the theoretical arrival and cut-off curves. Square wave injection. Injection time $\theta=0.01$.

If the shape of the experimental concentration curve indicates that the formation is homogeneous, the following procedure may be used to correlate the observed breakthrough time with the theoretical dimensionless breakthrough time. The theoretical breakthrough times θ_b given in Table I may be plotted as a function of the pressure ratio N and the value for θ_b, corresponding to the known experimental pressure ratio, read from the curve thus obtained. The corresponding time after breakthrough for each of the remaining streamlines may be determined in a similar manner using the data presented in Table II.

It may be shown that, for an ideal gas, Eq. (9) relating the dimensionless breakthrough time θ_b to the observed breakthrough time t_b may be written in the form

$$t_b=\left[\frac{2\pi\phi hL^2(P_w+P_0)}{P_aQ}\right]\theta_b \qquad (10)$$

where h is the formation thickness in cm and Q is the total volume flow rate at atmospheric pressure P_a in cm³/sec. In an actual field test, all of the factors appearing in Eq. (10) would be known with the exception of ϕ and h and thus the product ϕh could be calculated. If an estimate could be made of either φ or h, the other of the two quantities could be determined. Similarly, of the factors appearing in Eq. (9) only k and ϕ would be unknown and one could determine a value for the k/ϕ ratio by relating the experimental and theoretical breakthrough times. Thus if any one of the quantities φ, k, or h were known, the remaining two quantities could be determined from the observed breakthrough time t_b and the calculated dimensionless breakthrough time θ_b. Once the ratio t_b/θ_b had been determined, multiplication of the dimensionless times after breakthrough $\bar{\theta}$ by this ratio would yield the corresponding times $\bar{t}$ in seconds. A theoretical concentration curve could then be constructed by the method described in the previous section and compared with the experimental concentration curve.

Several factors not considered in the present paper limit the usefulness of the above interpretation procedure. At the present time, field techniques have not been developed for bottom hole tracer injection and detection. A square wave injected at the top of the injection well will be distorted by turbulent mixing and will enter the formation in some unknown wave form. There will be a further mixing of the tagged and untagged gas in the production well. Moreover, in this study it has been assumed that there is no mixing of the tracer-tagged fluid with the untagged fluid as the two fluids flow through the formation. At the present time very little is known as to the conditions, if any, under which the above assumption is a valid one.

Description of Field Tests

Several field tests of the proposed short time tracer injection method were carried out in a two well system in which the well separation of forty feet was small compared to the lateral extent of the formation. In these tests, helium was introduced into the injection air from a tank connected to the air line between the compressor and the well head. To initiate a helium injection test, the gas in this tank was bled into the injection air line for a period of approximately one minute. The rate of air injection and the pressure at the injection and production well heads were measured throughout the duration of the test.

Gas samples were taken at the production well head in sample bombs which were then sent to the laboratory for analysis. The number and frequency of samples was varied from one test to the next to allow for differences in air injection rates and breakthrough times. On the average, approximately 75 samples were taken in each of the tests. Analysis for helium in each sample was made using an analyzer similar to the one developed by the Bureau of Mines[9] which is based on the principle that all gases other than helium are adsorbed by charcoal at the temperature of liquid air. With this apparatus one can detect differences in helium concentration of 0.00001 percent. Helium concentrations in atmospheric air, measured with this apparatus, fell between 0.00018 and 0.00022 percent, as compared with an average value of 0.00018 percent reported in the literature.

In each of five tests of the short time tracer injection method, the experimentally determined concentration curves were very smooth and self-consistent. The general characteristics of these curves were in agreement with those predicted by theory for a homogeneous formation. That is, each curve displayed a very low concentration prior to breakthrough, a sharp rise in concentration after breakthrough to some peak value, and an initial sharp drop from this peak value followed by an asymptotic approach to the helium concentration of the injected air. It was thus evident that there was no appreciable channeling between the two wells. As previously indicated, channeling would have been revealed by a more rapid rise and fall in the concentration curve with an attendant flattening of the central portion of the curve.

It was not possible to obtain accurate information as to reservoir characteristics from these experimental concentration curves due to the effects of turbulent mixing of the tagged and untagged gas in the injection and production wells. That this mixing occurred was evident from the fact that although helium was introduced into the injected air for only one minute or less, the observed time interval between breakthrough and peak concentration varied from ten minutes to one hour. According to theory this latter time interval should be equal to the injection time. A comparison of the concentration curve obtained experimentally in the first injection test with the theoretical concentration curve for a square wave injection of a duration

[9] E. M. Frost, Jr., Bureau of Mines RI 3899 (June, 1946).

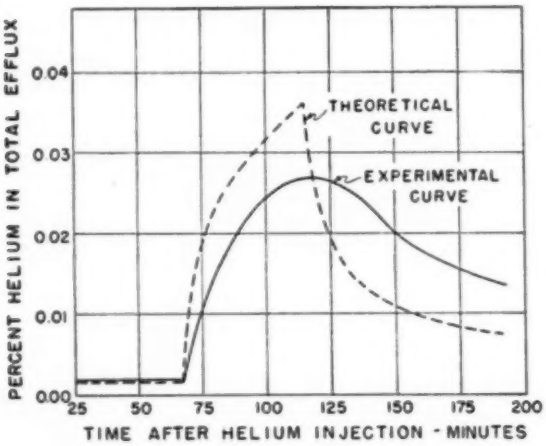

FIG. 4. Comparison of experimental and theoretical helium concentration curves.

equal to the estimated effective injection time is shown in Fig. 4. It is seen that the part of the experimental concentration curve after the peak concentration falls above the theoretically calculated concentration curve. This is exactly the opposite of the effect that would be expected from channeling and is in agreement with theoretical calculations of the type of concentration curve which would result from the injection of a distorted square wave.

Independent estimates were made of the formation thickness h and of the total porosity of the formation. In each test surface measurements were made of the gas flow rate Q and the injection and production well pressures. These quantities, together with the breakthrough times obtained in the field tests, were then substituted in Eq. (10) and values were calculated for the effective porosity to gas ϕ. The percentage of the total pore volume occupied by gas during each test was then calculated from the estimated total porosity and the experimental value for the effective porosity ϕ. The results obtained in five successive field tests increased continuously from 4.4 to 17.7 percent. This increase in gas saturation from one test to the next is in qualitative agreement with the fact that throughout the period of time in which the tests were made, oil was produced from the formation during continuous air injection and, later, by *in-situ* combustion drive.[7]

ACKNOWLEDGMENTS

Acknowledgment is made to the management of the Field Research Laboratories, Magnolia Petroleum Company, for permission to publish the results of this investigation. The authors also wish to express their appreciation to O. D. Ferris for his supervision of the numerical calculations described in this paper, and to the Field Engineering Group of these Laboratories for suggesting the short time tracer injection method and for carrying out the preliminary field tests.

NOMENCLATURE

- c dimensionless constant characterizing a streamline.
- h formation thickness in cm.
- k permeability in darcys.
- L well spacing in cm.
- l dimensionless length parameter equal to s/L.
- N ratio of injection well pressure to production well pressure (P_w/P_0).
- P absolute pressure in atmospheres.
- P_a absolute atmospheric well pressure in atmospheres.
- P_0 absolute production pressure in atmospheres.
- P_w absolute injection well pressure in atmospheres.
- p dimensionless pressure parameter equal to P/P_w.
- Q volume flow rate at atmospheric pressure in cm³/sec.
- R dimensionless radius of circular streamline.
- r well radius in cm.
- s arc length in cm.
- t time in seconds.
- t_b breakthrough time in seconds.
- $\bar{t}$ time after breakthrough in seconds.
- x,y usual rectangular Cartesian coordinates.
- α streamline angle.
- ζ dimensionless coordinate equal to x/L.
- η dimensionless coordinate equal to y/L.
- θ dimensionless time parameter equal to $[(P_w-P_0)kt]/[4\mu\phi L^2 \ln(L/r)]$.
- θ_b dimensionless breakthrough time.
- $\bar{\theta}$ dimensionless time after breakthrough.
- μ viscosity in centipoise.
- τ dimensionless time parameter equal to $(kP_w t)/(\phi\mu L^2)$.
- ϕ effective fractional porosity to gas.

JOURNAL OF APPLIED PHYSICS VOLUME 25, NUMBER 12 DECEMBER, 1954

Etching of Single Crystal Germanium Spheres*

RAY C. ELLIS, JR.
Raytheon Manufacturing Company, Waltham, Massachusetts
(Received January 25, 1954)

Spheres of single crystal germanium have been ground and etched. A series of polyhedra, consistent with the stability of the various crystal planes of germanium, was obtained.
Only (111) plane twins were found in germanium using this method.

I. INTRODUCTION

WHILE studying the etching of germanium, it was found that each etch solution left a characteristic pattern,[1] and that these patterns could be used to identify the orientation of the surface being etched. A polished germanium sphere was etched and then the number and position of areas with like etch patterns were compared. For instance, a certain pattern with a triangular symmetry (Fig. 1) appeared in eight symmetrically located places on such a sphere. The centers of these areas, then, demonstrate typical patterns on (111) planes and the diameters through these points represent the [111] directions.

However, a more interesting direction of investigation was pursued. It is recognized that various etches leave certain crystal planes in their etch pits.[2] It seemed probable that a small sphere etched in such a way would result in a solid bounded by those planes characteristic of the etch. Such polyhedra have been reported.[3]

II. EXPERIMENTAL

Spheres of germanium were made by two methods.

A. Germanium cubes were cut approximately 0.5 cm on a side. These cubes were blown in a circular motion by compressed air at about 35 psi against alundum paper lining a cylinder. Cylinders with inside diameters of 2.5 cm and 5 cm were used. There seemed to be no preference between these sizes. The pressure was regulated in such a way as to derive maximum grinding action with minimum breakage. The average time necessary to convert a cube to a sphere using this method was about 20 minutes. There was considerable wear on the alundum paper and it had to be changed after every 3 or 4 runs. It was found that 2 or 3 spheres could be efficiently ground simultaneously.

B. A cylindrical section with the height approximately equal to the diameter was cut out of a grown single crystal of germanium. The cylinder was then ground to a rough sphere on a power sander. The high points were then removed by rolling the sphere in a V-shaped trough of which one face was the sander belt. When it was found that large and small spheres gave the same results on etching, small spheres were always used. They took less time to prepare and to etch. It was found that the polishing of the surface could be eliminated before etching if the surface had no deep cracks or scratches. As long as the germanium was very symmetrical, the polyhedron would form. Otherwise, an asymmetric solid would develop, exhibiting perhaps 2 to 3 unidentifiable faces. Germanium tends to be etched faster around cracks, thereby forming random shapes.

Spheres to be etched were placed 2 or 3 at a time (one if large) in the bottom of a polyethylene bottle. Polyethylene was used because some of the etches contained fluorides and because polyethylene did not scratch or chip the germanium. The polyethylene bottle was rotated about its axis which was declined about 30° from the vertical. In this way, the small spheres were kept rolling under the surface of the etching liquid. Sufficient etch solution was used in each case so that etching action would not change the concentrations appreciably. High and low resistivity N and P type single crystal germanium gave identical results.

III. RESULTS

Five different polyhedra could be obtained using these methods. (See Table I and Figs. 2–6.)

The crystal planes of the faces of A, D, and E were confirmed by x-ray analysis to be those expected for those polyhedra. The samples B and D were too small for the making of x-ray determinations. It is felt that B

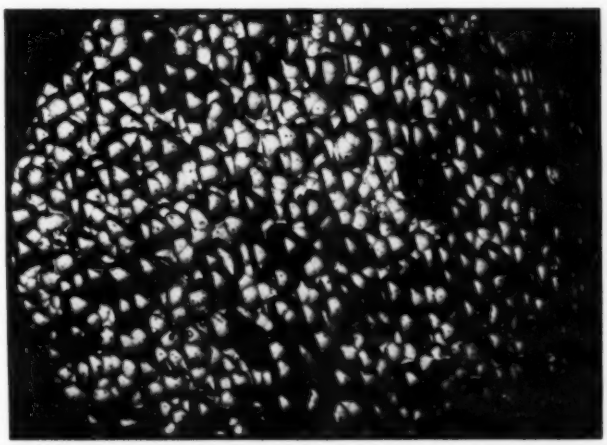

FIG. 1.

* Work supported in part by the U. S. Bureau of Ships, Signal Corps, and Air Corps.
[1] R. C. Ellis and S. P. Wolsky, J. Appl. Phys. 24, 1412 (1953).
[2] R. H. Wynne and C. Goldberg, J. Metals 5, 436 (1953).
[3] P. R. Camp, *Report, Twelfth Annual Conference on Physical Electronics* Massachusetts Institute of Technology, Cambridge, Massachusetts (March, 1952).

TABLE I.

Polyhedron		Crystal plane corresponding to a face
A. Octahedron	(Fig. 2)	(111)
B. Trioctahedron	(Fig. 3)	
C. Rhombic-dodecahedron	(Fig. 4)	(110)
D. Tetrahexahedron	(Fig. 5)	
E. Hexahedron (cube)	(Fig. 6)	(100)

and *D* do not exhibit true stable crystal planes. Rather, the faces are only apparent, being built up of small steps (perhaps even of stomic size) by the stable planes found in the adjacent polyhedra in the sequence.

Sometimes a polyhedron did not develop because the spheres began to roll about one axis in preference to others. In these cases, the sphere became cylindrical along the rolling axis. The ends of the cylinder would develop faces, however.

Typical etches that can be used in obtaining these

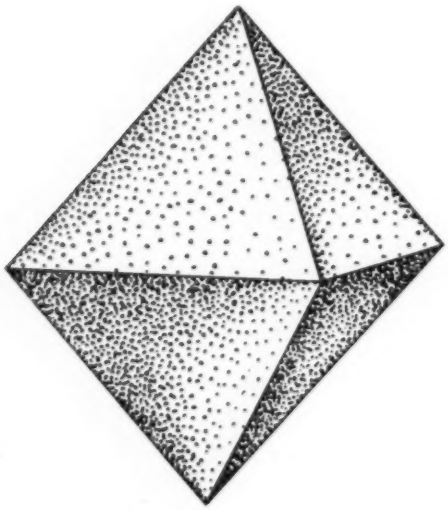

FIG. 2.

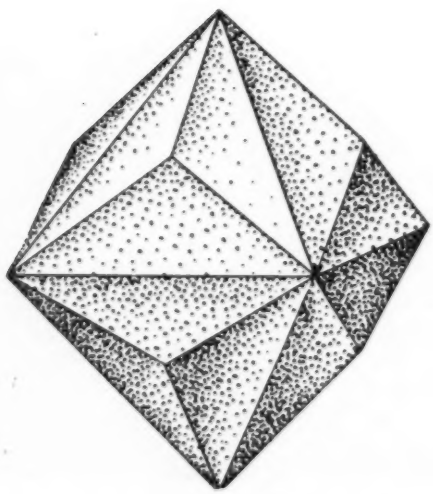

FIG. 3.

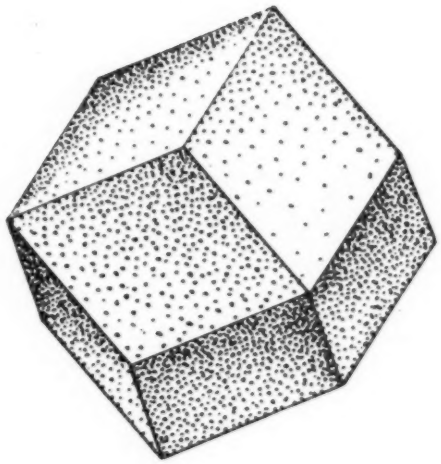

FIG. 4.

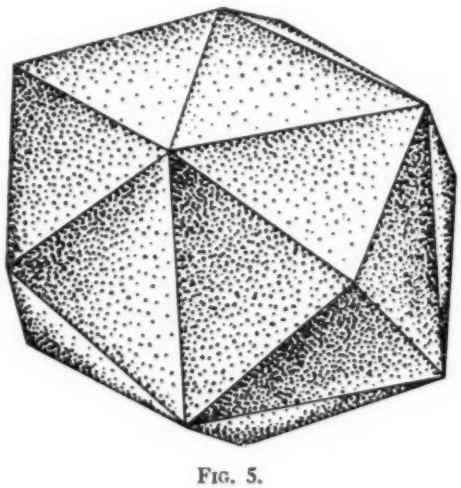

FIG. 5.

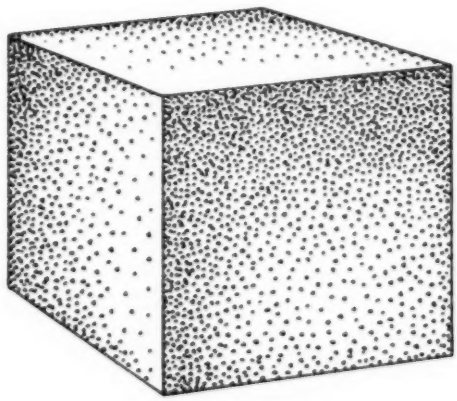

FIG. 6.

polyhedra or etch pits whose faces are the corresponding crystal planes are made up. (See Table II.)

By diluting an etch, a polyhedron resulted that was invariably lower in the sequence than the polyhedron expected. The order of polyhedra is undoubtedly a sequence, for an etch which gave an octahedron would by successive dilutions give the other polyhedra of the

TABLE II.

Polyhedron		ml conc. HNO_3	ml 30% H_2O_2	ml 48% HF	ml glacial acetic acid	gm $AgNO_3$	ml H_2O
A. Octahedron	a.		50	50			
	b.	45		25	30		
	c.	20		40		2	40
B. Trioctahedron	a.	23		13	64		
C. Rhombic-dodecahedron	a.		17	17			66
	b.	13		8	79		
D. Tetrahexahedron	a.	5		3	92		
E. Hexahedron	a.	13		37		2	50
	b.	7		4	89	3	

list in turn. Further dilutions of etches that gave a cube simply slowed the etch rather than changed the polyhedron obtained. Some etches, even in their most concentrated form, did not give an octahedron, but instead would give the dodecahedron. Dilutions of these etches, however, still changed the type of polyhedron obtained in the same direction in the sequence toward the cube.

If a large sphere was etched in a relatively small volume of solution, the expected polyhedron began to form. As the etching continued, different faces began to develop until finally a polyhedron lower in the sequence resulted. Partial use of the etch had an effect similar to dilution. This led to confusion in early experiments and to the erroneous conclusion that a large sphere resulted in a different polyhedron than a small one when etched in the same etch solution. To prevent the etch composition from changing appreciably on such large samples (or when the polyethylene bottle was not large enough to contain all of the etch required), the etch solutions were changed frequently. Continued etching of a polyhedron only reduced its size. If a polyhedron was put in an etch that normally would give a different polyhedron, new faces developed and the polyhedron typical of the etch would finally and distinctly form.

IV. DISCUSSION

The production of the polyhedron from an etch is not a random phenomenon. Once formed, the polyhedron is not stable toward any etch, but can be changed by the application of various different etches. Therefore, it is not only the stability of the various faces that contributes to the formation of a polyhedron, but the potentials involved between the crystal planes in the lattice and the etch solutions. Because of the consistent sequence of the polyhedra formed, it seems probable that the sequence represents the order of the stability of the various simple crystal planes in germanium. Other properties of the diamond lattice such as distance between crystal planes, density of atoms per crystal plane, and bond density between planes vary in the same order.

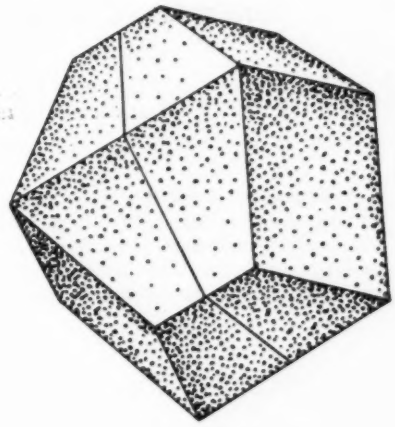

FIG. 7.

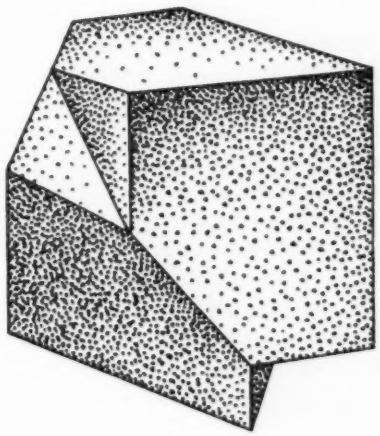

FIG. 8.

V. TWINNING

A brief study of twinning in germanium was made by an extension of the sphere etching technique. Twinned material was cut into spheres in such a way that a twin plane went through the center. Polyhedra whose halves were mirror images were obtained. The figures were strikingly similar to those that would be obtained by cutting a (111) plane through the expected polyhedron and rotating one-half 180° with respect to the other (Figs. 7 and 8). No twins other than this type were found.

ACKNOWLEDGMENT

The author would like to express his appreciation to the personnel of the Research Division of Raytheon Manufacturing Company for their help and cooperation.

JOURNAL OF APPLIED PHYSICS VOLUME 25, NUMBER 12 DECEMBER, 1954

Equivalent Circuit for a Passive Nonreciprocal Network*

H. A. HAUS
Research Laboratory of Electronics and Department of Electrical Engineering, Massachusetts Institute of Technology, Cambridge, Massachusetts
(Received March 25, 1954)

An equivalent circuit is proposed for a linear, passive, nonreciprocal, four-terminal network. It introduces an ideal amplifier and phase shifter. It is shown that the proposed equivalent circuit has certain advantages over equivalent network representations that use gyrators. In particular, standard measuring techniques used on reciprocal networks lead directly to the determination of six elements of the equivalent circuit. One additional measurement gives the remaining two parameters.

INTRODUCTION

TELLEGEN[1] has shown that the addition of a simple passive, nonreciprocal element, called a gyrator, to the existing repertoire of R, L, C elements and ideal transformers enables one to represent any linear, passive, nonreciprocal, four-terminal network. At any given frequency an equivalent circuit can be constructed of three conventional reactances, one resistance, two transformers, and two gyrators.

Tellegen's gyrator is philosophically well founded. It is obvious, however, that the gyrator is not the only imaginable nonreciprocal element. There are many choices that one may take in defining a nonreciprocal element. One choice is particularly expedient, since it results in a considerable simplification of the equivalent circuit. The element chosen in this paper is an ideal amplifier phase shifter characterized by the matrix

$$k\exp(j\phi)I,$$

where $k\exp(j\phi)$ is a complex number and I is the identity matrix. This element has two adjustable parameters, k and ϕ. It may be expected that a passive, nonreciprocal, four-terminal network can be represented by a combination of a passive, reciprocal network with six adjustable parameters (the real and imaginary parts of its matrix elements which satisfy the reciprocity relation) and an ideal amplifier phase shifter.

THE EQUIVALENT CIRCUIT

A general linear, four-terminal network is determined by the matrix of its general circuit parameters.[2]

$$\begin{pmatrix} A & B \\ C & D \end{pmatrix}. \tag{1}$$

The voltage and current at the input are given in terms of the output voltage and current by

$$\begin{aligned} V_1 &= AV_2 + BI_2, \\ I_1 &= CV_2 + DI_2. \end{aligned} \tag{2}$$

For the sign convention consult Fig. 1.

The equation

$$AD - BC = 1$$

is the reciprocity relation. Therefore, a nonreciprocal network has a matrix whose determinant is not equal to unity. Let us set

$$AD - BC = k^2\exp(2j\phi). \tag{3}$$

The original matrix (1) can be written as a product of

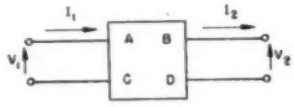

FIG. 1. The sign convention.

two matrices one of which satisfies the reciprocity relation[3]

$$\begin{pmatrix} A & B \\ C & D \end{pmatrix} = \begin{pmatrix} A_0 & B_0 \\ C_0 & D_0 \end{pmatrix} k\exp(j\phi)I, \tag{4}$$

where $A_0 = 1/kA\exp(-j\phi)$, etc.

Equation (4) suggests that an equivalent circuit can be constructed which incorporates a reciprocal network followed by an ideal amplifier and phase shifter characterized by the matrix $k\exp(j\phi)I$. The reciprocal lossy network can be split by standard techniques into a series impedance $jX_s + R_s$ followed by a parallel resistance R_p and a lossless four-terminal network.[4] The resulting circuit is shown in Fig. 2.

The amplifier and phase shifter introduced above has power gain or loss. Indeed, the power put out by a network with the matrix $k\exp(j\phi)I$ is $1/k^2$ times the power fed into its input terminals. The nonreciprocal network of Fig. 2 will be lossy only if k is within limits set by the losses in the network.

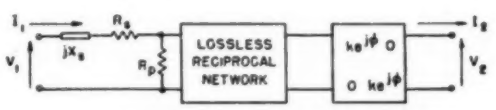

FIG. 2. The equivalent circuit.

* This work was supported in part by the Signal Corps, the Air Materiel Command, and the Office of Naval Research.

[1] B. D. H. Tellegen, Philips Research Repts. 3, 81–101 (1948); 5, 81–86 (1950).

[2] E. A. Guillemin, Communs. Networks (John Wiley and Sons, Inc., New York, 1935), Vol. 2.

[3] H. Schulz, Arch. El. Übertragung 5, 257–266 (1951).

[4] L. B. Felsen and A. A. Oliner, Proc. Inst. Radio Engrs. 42, 477–483 (1954).

A multiplication of a matrix M by the identity matrix satisfies the commutative law: $IM=MI$. Accordingly, the amplifier phase shifter connected to the end of the network in Fig. 2 can be connected any place within the cascade of the reciprocal networks in Fig. 2. We split the matrix $k\exp(j\phi)I$ into the product $kI\exp(j\phi)I$. The first factor is the transfer matrix of an amplifier without phase shift; the second factor appertains to a passive lossless phase shifter. The amplifier can be inserted into the reciprocal part of the network of Fig. 2 as shown in Fig. 3.

The over-all equivalent circuit of Fig. 3 satisfies the condition of power loss inherent in a passive network if the part shown in Fig. 4 is shown to be lossy. The network of Fig. 4 will be lossy if

$$\mathrm{Re}(V_1I_1^*-V_2I_2^*)>0 \tag{5}$$

for any input and output conditions. Equation (5) leads to

$$(R_s+R_p)|I_1|^2+R_p|I_2|^2 -R_p\left(k+\frac{1}{k}\right)|I_1I_2|\cos\psi>0, \tag{6}$$

where ψ is the phase angle between I_1 and I_2. It follows from (6) that the network is lossy if, and only if,

$$\frac{1}{2}\left(k+\frac{1}{k}\right)\leq\left(\frac{R_s+R_p}{R_p}\right)^{\frac{1}{2}}. \tag{7}$$

The network of Fig. 4 can be represented in terms of resistances and two ideal gyrators. The resulting circuit is shown in the appendix. There, it is also demonstrated that the phase shifter connected to the end of the network in Fig. 3 can be formed by reactances and an ideal gyrator.

If $R_s=0$ or $R_p=\infty$ it follows from Eq. (7) that $k=1$. The only nonreciprocal element in the equivalent circuit of a general lossless nonreciprocal network is the phase shifter with the matrix $\exp(j\phi)I$.

THE SIGNIFICANCE OF A K NOT EQUAL TO UNITY

The parameter k can be different from unity only when losses are present in the network. It must be expected that a k not equal to unity accounts for a nonreciprocity in the loss of the network. This fact can be verified most easily through the concepts of iterative impedance and phase function.[2]

A linear, passive, four-terminal network is an impedance transformer. Two passive impedances are invariant with respect to an impedance transformation. They

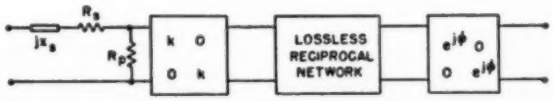

FIG. 3. An alternate equivalent circuit.

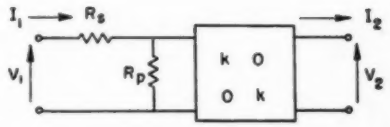

FIG. 4. The nonconservative part of the equivalent circuit.

are the iterative impedances Z_{01} and Z_{02} and can be expressed in terms of the general circuit parameters.

$$Z_{01,2}=\frac{1}{2C}\{[(A+D)^2-4(AD-BC)]^{\frac{1}{2}}\pm(A-D)\}. \tag{8}$$

The signs are chosen so that Z_{01} and Z_{02} have positive real parts. When Z_{01} is connected to the output terminals 2, the ratio of output to input voltage is equal to the ratio of the output and input current

$$V_2/V_1=I_2/I_1=\exp(-\gamma_1), \tag{9}$$

where the "phase function" γ_1 is

$$\gamma_1=\ln\tfrac{1}{2}\{A+D+[(A+D)^2-4(AD-BC)]^{\frac{1}{2}}\}. \tag{10}$$

The impedance Z_{02} connected to the input terminals causes a power flow from the terminal pair 2 to the terminal pair 1. The ratios of the voltages and currents at the two terminal pairs are again related by

$$V_1/V_2=I_1/I_2=\exp(-\gamma_2), \tag{11}$$

where the "phase function" γ_2 is given by

$$\gamma_2=-\ln\tfrac{1}{2}\{A+D-[(A+D)^2-4(AD-BC)]^{\frac{1}{2}}\}.$$

Introducing the definitions of A_0 to D_0 into Eq. (8) one finds

$$Z_{01,2}=(1/2C_0)\{[(A_0+D_0)^2-4]^{\frac{1}{2}}+(A_0-D_0)\}.$$

The factor $k\exp(j\phi)$ has dropped out. In other words, the iterative impedances of the nonreciprocal network are fixed entirely by the reciprocal part of its equivalent circuit in Fig. 2.

Expressing the "phase functions" γ_1 and γ_2 in terms of A_0 to D_0, k, and ϕ, one finds

$$\gamma_{1,2}=\ln\tfrac{1}{2}\{A_0+D_0+[(A_0+D_0)^2-4]^{\frac{1}{2}}\}\pm[\ln k+j\phi].$$

In a reciprocal network we have $k=1$, $\phi=0$; consequently $\gamma_1=\gamma_2$. This means that the insertion loss of the four-terminal network is the same whether Z_{01} is connected to its output or Z_{02} to its input terminals. A value of k different from unity implies that the insertion loss differs in the two cases. The network has a greater insertion loss for a flow of power in the forward direction than for a flow in the reverse direction when $k>1$. The reverse holds true when $k<1$.

MEASUREMENTS

All eight parameters of the equivalent circuit in Fig. 4 are easily measurable by experiment. First, we note that an impedance is invariant with respect to a transforma-

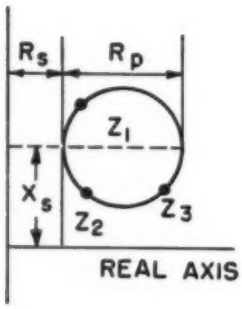

FIG. 5. The impedance plane.

tion by an ideal amplifier and phase shifter. Therefore, the nonreciprocal network of Fig. 3 transforms impedances in exactly the same manner as the reciprocal network obtained from it by omission of the amplifier and phase shifter. Thus, all parameters of the network of Fig. 2 except k and ϕ can be found by standard measurements used to find the parameters of a reciprocal network.[4]

If a variable reactive impedance is connected to the output terminals of the network, the locus of the input impedance is a circle in the impedance plane, as shown in Fig. 5. The values of R_s, R_p, and X_s can be read from such a graph. The knowledge of three output impedances and their transforms determines the lossless reciprocal network in Fig. 3. (Reference 4 gives a detailed description of a method.)

In order to find the values of k and ϕ, a phase and magnitude measurement of the input and output voltages has to be made. Assume, for instance, that the output terminals are open-circuited. Then, we have

$$k\exp(j\phi)=(1/A_0)(V_1/V_2),$$

where V_2 and V_1 are the voltages at the output and input and A_0 is known from the preceding impedance measurements.

CONCLUSIONS

The new equivalent circuit representation offers a simple experimental technique by which the elements of the equivalent circuit can be measured. In particular, six elements of the nonreciprocal network can be found by measurements identical with those used on reciprocal networks. Only one additional measurement is needed to find the nonreciprocal elements in the equivalent circuit.

ACKNOWLEDGMENT

The author is indebted to Mr. L. D. Smullin and his associates in the Microwave Tube Laboratory for many helpful discussions.

APPENDIX

The network of Fig. 4 has the transfer matrix

$$A=k\frac{R_s+R_p}{R_p},\quad B=kR_s,\quad C=\frac{k}{R_p},\quad D=k.$$

Evaluation of the transfer matrix of the network shown in Fig. 6(a) shows that it has the same transfer matrix if

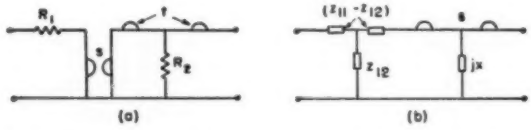

FIG. 6. Representation of the amplifier and phase shifter in terms of gyrators.

$$s=\frac{1}{2}\left(\frac{1}{k}-k\right)R_p,\qquad l=\frac{1-k^2}{1+k^2}R_p,$$

$$R_1=R_s+R_p-\left[\frac{1}{2}\left(k+\frac{1}{k}\right)\right]^2R_p,\quad R_2=\left[\frac{k^2-1}{k^2+1}\right]^2R_p.$$

Whereas R_2 is always positive, R_1 will be positive if condition (7) is satisfied.

Similarly, it can be shown that an ideal phase shifter with the transfer matrix $\exp(j\phi)I$ can be represented by the circuit shown in Fig. 6(b) where

$$\tan^{-1}\frac{s}{X}=\phi.$$

$$Z_{11}=-jX\quad\text{and}\quad Z_{12}=-j(X^2+s^2)^{\frac{1}{2}}.$$

JOURNAL OF APPLIED PHYSICS VOLUME 25, NUMBER 12 DECEMBER, 1954

X-Ray Study of the Graphitization of Carbon Black

C. R. Houska and B. E. Warren
Massachusetts Institute of Technology, Cambridge, Massachusetts
(Received April 26, 1954)

A picture of the early stage of graphitization of a carbon black has been obtained from an x-ray study of a Fine Thermal (FT) carbon black heated for two hours at 2300°C. Nearest neighbor pairs of layers take on the graphite relation independently, producing both ABA and ABC sequences. There are two nearest neighbor layer spacings 3.35 A and 3.44 A corresponding to pairs with the graphite relation and pairs with random orientation. The (00*l*) peaks must be corrected for the distortion broadening resulting from the two spacings, to obtain the parallel layer group thickness L_c. The probability for the ordering of nearest neighbor layers P_1 is defined as the "degree of graphitization." A logarithmic plot is used for a rapid determination of P_1 and the layer diameter L_a from the modulated two dimensional (*hk*) reflections.

I. INTRODUCTION

A TYPICAL carbon black consists of parallel layer groups made up of individual graphite layers which are stacked roughly parallel to one another but random in orientation about the normal to the layer. The diameter of the layer is of the order 20–30 A, and the thickness of the parallel layer groups, measured normal to the layers, is of the order 12–20 A. On heat treating carbon blacks, the dimensions of the parallel layer groups increase, and the x-ray pattern sharpens. There are (00*l*) crystalline reflections, and diffuse (*hk*) two dimensional lattice reflections. In the early stages, the layer diameter grows, and the number of layers in a parallel layer group increases, but the orientation of the layers about the layer normal remains random.

When the layer diameter gets above a certain size of the order $L_a = 100$ A, the layers begin to position themselves with respect to a neighboring layer in the graphite relation. This produces modulations in the (*hk*) reflections, and these modulations become more pronounced the higher the temperature is raised. In the limit these modulations may sharpen into the general (*hkl*) reflections of crystalline graphite. The first appearance of these modulations in the (*hk*) reflections marks the beginning of the process of graphitization.

During the early stages of graphitization there are a number of questions which we hope to be able to answer by an x-ray analysis. Do pairs of nearest neighbor layers position themselves in the graphite relation independent of neighboring layers, or do whole regions of a parallel layer group take on the graphite crystalline structure? Does ordering produce sequences ABC as well as the usual ABA of graphite? How can we measure the number of nearest neighbor pairs of layers which have acquired the graphite relation? How shall we define a quantity "the degree of graphitization" which can be quantitatively measured? Are there two different layer spacings corresponding to random and to graphite like nearest neighbors? When modulations are present in the (*hk*) reflections, how can we measure the layer diameter and the parallel layer group thickness?

II. DIFFRACTION THEORY FOR PARTIALLY ORDERED GROUPS

We assume all layers to be perfect graphite layers with translation vectors $\mathbf{a}_1$, $\mathbf{a}_2$ in the layer, and two atoms per cell in positions 0,0 and $\frac{2}{3}$, $\frac{1}{3}$. The vector $\mathbf{a}_3$ is normal to the layers, and in magnitude equal to the layer separation for pairs with a graphite relation. The position of atom k in cell m_1m_2 of layer m_3 is given by

$$R_m^k=[m_1+X(m_3)]\mathbf{a}_1+[m_2+Y(m_3)]\mathbf{a}_2 +[m_3+Z(m_3)]\mathbf{a}_3+\mathbf{r}_k.$$

$X(m_3)$ and $Y(m_3)$ provide for displacements parallel to the layer, and $Z(m_3)$ for changes in the layer spacing. The intensity in electron units for one parallel layer group is given by

$$I_{eu}=\sum_{kk'}\sum_{m_1m_1'}\sum_{m_2m_2'}\sum_{m_3m_3'} f_kf_{k'} \times\exp\left[\frac{2\pi i}{\Lambda}(\mathbf{s}-\mathbf{s}_0)\cdot(R_m^k-R_{m'}^{k'})\right], \quad (1)$$

where f is the atomic scattering factor, and $\mathbf{s}_0$ and $\mathbf{s}$ are unit vectors in the directions of the primary and diffracted beams. Let

$$\psi^2=\sum_{kk'}\sum_{m_1m_1'}\sum_{m_2m_2'} =F^2\frac{\sin^2\frac{\pi}{\Lambda}(\mathbf{s}-\mathbf{s}_0)\cdot N_1\mathbf{a}_1}{\sin^2\frac{\pi}{\Lambda}(\mathbf{s}-\mathbf{s}_0)\cdot\mathbf{a}_1}\frac{\sin^2\frac{\pi}{\Lambda}(\mathbf{s}-\mathbf{s}_0)\cdot N_2\mathbf{a}_2}{\sin^2\frac{\pi}{\Lambda}(\mathbf{s}-\mathbf{s}_0)\cdot\mathbf{a}_2}, \quad (2)$$

where N_1 and N_2 are the number of cells in the a_1 and a_2 directions, and

$$F^2=4f^2\cos^2\pi(\tfrac{2}{3}h+\tfrac{1}{3}k).$$

In terms of continuous variables $h_1h_2h_3$, the diffraction vector is represented by $(\mathbf{s}-\mathbf{s}_0)/\Lambda=h_1b_1+h_2b_2+h_3b_3$. If N_3 is the number of layers in a parallel layer group, the

intensity can be expressed by

$$I_{eu}=\psi^2\sum_{1}^{N_3}{}_{m_3m_3'}\exp[2\pi i\{[X(m_3)-X(m_3')]h_1 +[Y(m_3)-Y(m_3')]h_2+[Z(m_3)-Z(m_3')]h_3 +(m_3-m_3')h_3\}]. \quad (3)$$

By letting $n=m_3-m_3'$, $X_n=X(m_3)-X(m_3')$, $Y_n=Y(m_3)-Y(m_3')$, and $Z_n=Z(m_3)-Z(m_3')$, we can replace the double sum of Eq. (3) by a single sum

$$I_{eu}=N_3\psi^2\sum_{-(N_3-1)}^{N_3-1}{}_n(1-|n|/N_3) \times\langle\exp[2\pi i(X_nh_1+Y_nh_2+Z_nh_3)]\rangle\exp[2\pi inh_3]. \quad (4)$$

From the form of ψ^2, given by Eq. (2), the intensity is confined to the vicinity of the integral values $h_1=h$ and $h_2=k$. The summation in Eq. (4) represents a modulation in the otherwise uniform hk rods in reciprocal space.

The displacement X_n of a layer with respect to its nth neighbor is made up of the nearest neighbor displacements of all the intermediate layers $X_n=X_1(0,1)+X_1(1,2)+\cdots X_1(n-1,n)$, and hence

$$\langle\exp[2\pi iX_nh_1]\rangle=\langle\prod_{1}^{n}{}_k\exp[2\pi iX_1(k)h_1]\rangle.$$

If the ordering of each nearest neighbor pair is independent of neighboring layers, the average of the product is the product of the averages, and we have the result obtained by Mering.[1]

$$\langle\exp[2\pi i(X_nh_1+Y_nh_2+Z_nh_3)]\rangle =\langle\exp[2\pi i(X_1h_1+Y_1h_2+Z_1h_3)]\rangle^{|n|}. \quad (5)$$

Considering Eq. (4) as a Fourier series whose coefficients can be determined experimentally, we will be able to test for independent ordering of nearest neighbor pairs by testing for the relation of Eq. (5).

We can also interpret Eq. (4) in terms of a probability function $P(X_n,Y_n,Z_n)$ for the displacement of a layer with respect to its nth neighbor by amounts X_n, Y_n, Z_n. The function is normalized by

$$\int\int\int_{-\frac{1}{2}}^{+\frac{1}{2}}P(X_n,Y_n,Z_n)dX_ndY_ndZ_n=1.$$

Represent the probability function as a Fourier series

$$P(X_n,Y_n,Z_n)=\sum_h\sum_k\sum_l C_n(hkl) \times\exp[-2\pi i(hX_n+kY_n+lZ_n)]. \quad (6)$$

The coefficients $C_n(hkl)$ are then

$$C_n(hkl)=\int\int\int_{-\frac{1}{2}}^{+\frac{1}{2}}P(X_n,Y_n,Z_n) \times\exp[2\pi i(hX_n+kY_n+lZ_n)]dX_ndY_ndZ_n, \quad (7)$$

and these are just the values of the coefficients $\langle\exp[2\pi i(X_nh_1+Y_nh_2+Z_nh_3)]\rangle$ of Eq. (4). In principle the coefficients of Eq. (6) can be determined from experiment and the probability function $P(X_n,Y_n,Z_n)$ synthesized. There are presumably two kinds of nearest neighbor relations in partially graphitized carbon black. If the pair of layers is ordered, X_1 and Y_1 have values corresponding to the graphite structure and $Z_1=0$—if disordered, X_1 and Y_1 are random and Z_1 has a definite value. Coefficients $C_n(00l)$ are independent of the translations X_n, Y_n and include contributions from all pairs of layers. Coefficients $C_n(hkl)$ receive contributons only from pairs of layers having ordered X_n, Y_n values and for these $Z_n=0$, hence $C_n(hkl)$ is independent of l for h or k different from zero. Bacon[2] has used this difference between the $00l$ and the hkl reflections to distinguish between the average spacing and that for ordered layers.

For a layer structure there are two interesting projected probabilities.

$$P'(Z_n)=\int\int_{-\frac{1}{2}}^{+\frac{1}{2}}P(X_n,Y_n,Z_n)dX_ndY_n =\sum_l C_n(00l)\exp[-2\pi ilZ_n], \quad (8)$$

$$P'(X_nY_n)=\int_{-\frac{1}{2}}^{+\frac{1}{2}}P(X_n,Y_n,Z_n)dZ_n=\sum_h\sum_k C_n(hk0) \times\exp[-2\pi i(hX_n+kY_n)]. \quad (9)$$

Equation (9) is equivalent to a relation derived by Zachariasen.[3] Although general Fourier equations such as (6), (8), and (9) are attractive as representing direct methods for determination, they are usually very disappointing when applied to substances such as partially graphitized carbon black. In general it is not possible to measure reflections of high enough order to give more than broad poorly defined peaks in the probability function.

Prior to the beginning of graphitization, if all the layers in a parallel layer group have random displacements X_nY_n parallel to the layer, or what is equivalent to this if they have random orientations about the layer normal, Eq. (4) reduces to two kinds of reflections.

1. Sharp crystalline $(00l)$ reflections

$$I_{eu}=N_3\psi^2\sum_{-(N_3-1)}^{N_3-1}{}_n(1-|n|/N_3) \times\langle\exp[2\pi ilZ_n]\rangle\exp[2\pi inh_3]. \quad (10)$$

[1] J. Mering, Acta. Cryst. 2, 371 (1949).

[2] G. E. Bacon, Acta. Cryst. 4, 558 (1951).

[3] W. H. Zachariasen, Phys. Rev. 71, 715 (1947).

2. Diffuse two-dimensional lattice reflections (hk).

For a powder pattern the two-dimensional (hk) reflections give rise to a power per unit length of diffraction circle.[4,5,*]

$$P_{2\theta}'(hk)=Kj\left(\frac{2L_a}{\sqrt{\pi}\Lambda}\right)^{\frac{1}{2}}F^2\Phi(\alpha)\times\frac{(1+\cos^2 2\theta)}{2\sin\theta\,(\sin\theta+\sin\theta_0)^{\frac{1}{2}}},\quad(11)$$

where

$$K=\frac{I_0e^4N_1N_2M\Lambda^2}{m^2c^4 4\pi RA_a},$$

M is the number of layers in the sample,
A_a is the area defined by a_1 and a_2,
j is the multiplicity of the (hk) reflection,
L_a is the effective diameter of the layer

$$\sin\theta_0=|h\mathbf{b}_1+k\mathbf{b}_2|\Lambda/2,$$

$$\Phi(\alpha)=\int_{-\infty}^{+\infty}\exp[-(\alpha-x^2)^2]dx,$$

$$\alpha=(\sin\theta-\sin\theta_0)2\sqrt{\pi}L_a/\Lambda.$$

For α large, due either to large L_a or large $(\sin\theta-\sin\theta_0)$, $\Phi(\alpha)\rightarrow(\pi/4\alpha)^{\frac{1}{2}}$ and Eq. (11) becomes independent of the layer diameter L_c

$$P_{2\theta}'(hk)=\frac{Kj(1+\cos^2 2\theta)}{4\sin\theta\,(\sin^2\theta-\sin^2\theta_0)^{\frac{1}{2}}}.\quad(12)$$

As long as the layers of a parallel layer group have random orientations about the layer normal, the two-dimensional (hk) reflections rise sharply to a peak in the vicinity of θ_0 and then drop off slowly on the high angle side. With the beginning of graphitization, some of the pairs of neighboring layers position themselves in the graphite relation, and the coefficient of Eq. (4) $\langle\exp[2\pi i(X_nh+Y_nk+Z_nl)]\rangle$ is not zero for $n\neq0$. This produces modulation in the (hk) rods in reciprocal space and correspondingly modulations in the two dimensional (hk) reflections. For an (hk) reflection where h and k are not both zero, if we assume that positive and negative values of X_n and Y_n are equally probable, that Z_n is zero for layers in a graphite relation, and that the coefficients decrease rapidly for increasing n, Eq. (4) can be approximated by a Fourier series

$$I_{eu}(hk)=N_3\psi^2\sum_{-\infty}^{+\infty}{}_n\,A_n(hk)\cos 2\pi nh_3,\quad(13)$$

where $A_n(hk)=\langle\exp[2\pi i(X_nh+Y_nk)]\rangle$.

The modulations represented by Eq. (13) exist in the (hk) rods in reciprocal space, and strictly the integrations leading to Eqs. (11), (12) should be redone using (hk) rods which are modulated rather than constant in the h_3 direction. However, to get equations which are simple enough to be useful, we will make the approximation that it is adequate to merely multiply Eqs. (11) and (12) by the modulating factor of Eq. (13). The partial justification for this approximation comes from the fact that modulations in a carbon black (hk) reflection do not appear to any appreciable extent until the layer diameter L_a exceeds 100 A, and the (hk) rods are of correspondingly small diameter.[6,7]

To obtain the Fourier coefficients $A_n(hk)$ without first needing the value of the layer diameter L_a, we use the fact that the modulations of Eq. (13) are periodic along an (hk) rod. An expression which is valid for the outer part of an (hk) reflection is then obtained by combining Eqs. (12) and (13).

$$P_{2\theta}'(hk)=\frac{KjF^2(1+\cos^2 2\theta)}{4\sin\theta\,(\sin^2\theta-\sin^2\theta_0)^{\frac{1}{2}}}\times\sum_{n=-\infty}^{+\infty}A_n(hk)\cos 2\pi nh_3.\quad(14)$$

The linear dimension h_3 along the reciprocal lattice rod is obtained from $h_3=(\sin^2\theta-\sin^2\theta_0)^{\frac{1}{2}}2a_3/\Lambda$. Dividing the measured $P_{2\theta}'(hk)$ by the term preceding the summation in Eq. (14) and normalizing by the condition $A_0(hk)=1$, we obtain the experimental modulating factor $\sum A_n(hk)\cos 2\pi nh_3$ in absolute units. From any reliable half-period in this curve, the coefficients $A_n(hk)$ are then determined in the usual way by use of the Lipson and Beevers strips.

II. EXPERIMENTAL STUDY OF MODULATED (hk) REFLECTIONS

The measurements were made on a Fine Thermal (FT) carbon black which had an electron microscope average particle diameter of 1600 A. The material was heated in an induction furnace in the absence of air for 2 hours at 2300°C to produce partial graphitization.[8] The surface characteristics of similarly heat treated carbon blacks have recently been reported.[9,10] All patterns were run on the Norelco Geiger counter diffractometer using Ni filtered CuKα radiation. The flat faced samples had dimensions 20×10×1.6 mm and were packed to a density of 0.9 g/cc.

Figure 1 shows the modulated two dimensional reflection (10) with the crystalline reflection (004) superimposed on the high angle tail. Figure 2 shows the modulated two dimensional reflection (11) with the weak crystalline reflection (006) superimposed. The two main sources of extraneous broadening result from the unresolved $\alpha_1\alpha_2$ doublet, and the low absorption which

[4] B. E. Warren, Phys. Rev. **59**, 693 (1941).
[5] J. Biscoe and B. E. Warren, J. Appl. Phys. **13**, 364 (1942).
* This equation differs slightly from Eq. (36) of reference 4 due to an improvement in the approximations used in the derivation.

[6] R. E. Franklin, Acta. Cryst. **4**, 253 (1951).
[7] R. E. Franklin, Proc. Roy Soc. (London) **A209**, 196 (1951).
[8] Schaeffer, Smith, and Polley, Ind. Eng. Chem. **45**, 1721 (1953).
[9] Polley, Schaeffer, and Smith, J. Phys. Chem. **57**, 469 (1953).
[10] R. A. Beebe and D. M. Young, J. Phys. Chem. **58**, 93 (1954).

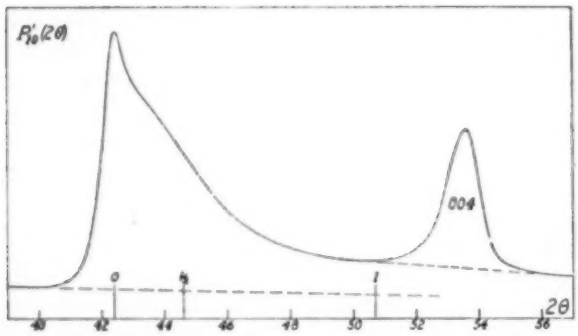

FIG. 1. The (10) reflection from (FT) black heated 2 hours at 2300°C using Ni filtered CuKα.

permits diffraction from the interior of the sample. Although these two effects are small for the (10) reflection, they are both important for the sharp peak part of the (11) reflection. The tail of (11) is sufficiently flat so that no correction is needed. The sharp peak of (11) was separated and given the usual Stokes correction[11] by using the (110) reflection of good crystalline graphite as a standard. Because of the difference in density, an additional correction involving the difference of the low absorption corrections[12] for the two samples was made. The dotted line of Fig. 2 shows the corrected curve and illustrates the importance of the correction. A tentative background level is obtained by extending the background curve on the left of the peak.

We now apply Eq. (14) to that part of the curve to the right of the peak. The experimental curve is divided by the terms preceding the summation, giving the modulating factor $\sum A_n(hk)\cos 2\pi n h_3$ in arbitrary units. The result is normalized by the condition $A_0(hk)=1$. Having obtained the modulating factor in

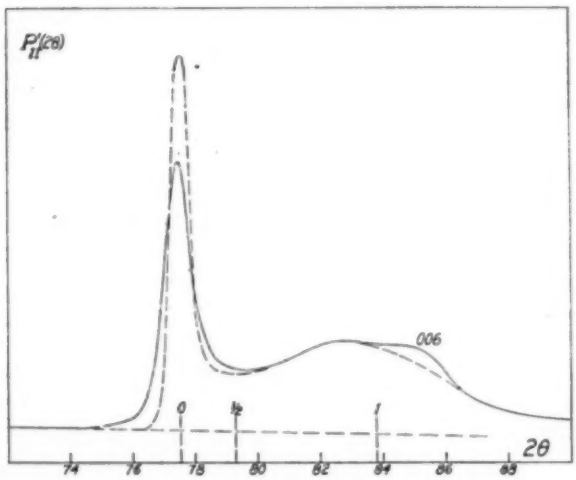

FIG. 2. The (11) reflection from (FT) black heated 2 hours at 2300°C using Ni filtered CuKα. Dashed peak, corrected for instrumental broadening.

[11] A. R. Stokes, Proc. Phys. Soc. (London) **61**, 382 (1948).
[12] D. T. Keating and B. E. Warren, Rev. Sci. Instr. **23**, 519 (1952).

absolute units, we then determine the Fourier coefficients $A_n(hk)$ in the usual way. Only the reflections (10), (11), and (21) were well enough developed to allow an accurate determination. The coefficients obtained are listed in Table I.

Using these coefficients we can now synthesize the projected probability function for neighboring layers $P'(X_1Y_1)$ given by Eq. (9). Although (20) was too weak for accurate measurement, we can assume from the equations for the coefficients that $A_n(20)=A_n(10)$. Using the appropriate multiplicities, we synthesize $P'(X_1Y_1)$ from the values: $A_1(00)=1.00$, $A_1(10)=-0.13, A_1(11)=0.25, A_1(20)=-0.13, A_1(21)=-0.12$. The resulting function is shown by the contours of Fig. 3. We interpret the figure to mean that when ordering takes place between pairs of nearest layers, the pairs have the graphite relation $X_1Y_1=(\frac{2}{3},\frac{1}{3})$ or $(\frac{1}{3},\frac{2}{3})$. Due to the small number of terms in the series, the two peaks are very broad and there is a ghost around the origin. A plot of the function $P'(X_2Y_2)$ would be interesting since it would give the probability of finding ABC as well as ABA ordering for second nearest neighbors. However, the coefficients $A_2(hk)$ of Table I are small, and the information is better obtained from

TABLE I. Coefficients $A_n(hk)$ for (FT) black, heated 2 hours at 2300°C.

n	$A_n(10)$	$A_n(11)$	$A_n(21)$
0	1.00	1.00	1.00
1	−0.13	0.25	−0.12
2	0.02	0.06	0.02

considering their relative values. From Eq. (5) it followed that if nearest neighbor pairs ordered independently $A_n(hk)=[A_1(hk)]^{|n|}$. The coefficients of Table I obey this relation very closely, and this indicates the independent ordering of neighboring layers in the early stage of graphitization. If instead, ordering took place by small regions taking on a graphite structure, the relative values of the coefficients would be quite different, for example $A_2(11)=A_1(11)$.

A quantitative picture of the ordering scheme can be obtained from the values listed in Table I. It is convenient to introduce four probabilities for the displacement of an nth neighbor

P_n^R probability of a random displacement.
P_n^0 probability of zero displacement.
P_n^+ probability of a displacement $X_n=\frac{2}{3}$, $Y_n=\frac{1}{3}$.
P_n^- probability of a displacement $X_n=-\frac{2}{3}$, $Y_n=-\frac{1}{3}$.

In terms of the probabilities

$$A_n(hk)=P_n^R\times 0+P_n^0\times 1+P_n^+\exp[2\pi i(\tfrac{2}{3}h+\tfrac{1}{3}k)]+P_n^-\exp[-2\pi i(\tfrac{2}{3}h+\tfrac{1}{3}k)].$$

Since P_n^+ and P_n^- are equally probable

$$A_n(hk)=P_n^0+(P_n^++P_n^-)\cos 2\pi(\tfrac{2}{3}h+\tfrac{1}{3}k).$$

Since $P_1^0=0$, the coefficients take the following values

n	$A_n(10)$	$A_n(11)$
1	$-\frac{1}{2}(P_1^+ + P_1^-)$	$(P_1^+ + P_1^-)$
2	$P_2^0 - \frac{1}{2}(P_2^+ + P_2^-)$	$P_2^0 + (P_2^+ + P_2^-)$.

The numerical values obtained from the coefficients of Table I are listed in Table II. P_1 is the probability of nearest neighbor pairs ordering in the graphite relation, P_2^0 is the probability of an ABA sequence, and $(P_2^+ + P_2^-)$ is the probability of an ABC sequence. Within the experimental error we can say that one quarter of the nearest neighbor pairs are ordered, one sixteenth of the second neighbor pairs are ordered, and for the latter there is about equal probability of following the ABA and ABC sequences.

IV. THE (00l) REFLECTIONS

Prior to the beginning of graphitization, the parallel layer group thickness L_c is obtained directly from the breadth of the (00l) reflections, and consistent values are obtained from (002) and (004). With the beginning of graphitization, there are two different layer spacings corresponding to ordered and disordered pairs. This produces a distortion broadening in addition to the particle size broadening, and unless proper corrections are made, inconsistent values of L_c are obtained from (002) and (004).

TABLE II. Probabilities of first and second neighbor ordering.

$P_1=(P_1^+ + P_1^-)=0.25$
$P_2^0=0.033$
$(P_2^+ + P_2^-)=0.027$

For (00l) reflections, and independent ordering of the layers, Eq. (4) reduces to

$$I_{eu}=N_3\psi^2 \sum_{-(N_3-1)}^{N_3-1}{}_n (1-|n|/N_3) \times\langle\exp[2\pi i Z_1 h_3]\rangle^{|n|}\exp[2\pi i n h_3].$$

Corresponding to the small values of Z_1, let x be small

$$\langle\exp[ix]\rangle=1+i\langle x\rangle-\tfrac{1}{2}\langle x^2\rangle=(1-\tfrac{1}{2}\langle x^2\rangle)(1+i\langle x\rangle) =\exp[-\tfrac{1}{2}\langle x^2\rangle]\exp[i\langle x\rangle].$$

With this approximation the (00l) peaks are represented by the Fourier series

$$I_{eu}(00l)=N_3\psi^2 \times \sum_{-(N_3-1)}^{N_3-1}{}_n A_n(l)\cos[2\pi n(1+\langle Z_1\rangle)h_3], \quad (15)$$

where $A_n(l)=A_n{}^P\exp[-2\pi^2 l^2|n|\langle Z_1^2\rangle]$ and $A_n{}^P=1-|n|/N_3$. The series represented by Eq. (15) peaks at integral values of $(1+\langle Z_1\rangle)h_3$, and as shown previously by Mering,[1] this corresponds to a new average spacing

$$\bar{a}_3=a_3(1+\langle Z_1\rangle). \quad (16)$$

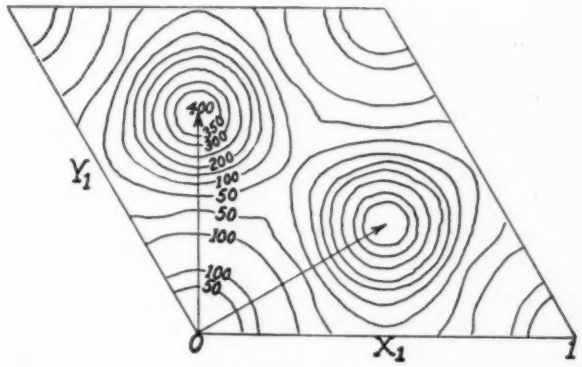

FIG. 3. The probability function $P'(X_1Y_1)$ for ordering of nearest neighbor layers in (FT) black heated 2 hours at 2300°C.

The coefficients $A_n(l)$ can be determined from the measured (00l) reflections. If two orders are available, the particle size and distortion parts can be separated by a log plot.[13]

$$\ln A_n(l)=\ln A_n{}^P-2\pi^2 n\langle Z_1^2\rangle l^2.$$

A plot of $\ln A_n(l)$ *vs* l^2 for the various harmonics n gives the particle size coefficients $A_n{}^P$ from the intercepts and $\langle Z_1^2\rangle$ from the slopes. In the notation we are using, with a_3 the layer spacing, the commonly designated reflections (002) and (004) correspond to $l=1$ and $l=2$.

The reflections (002) and (004) were run on the Norelco diffractometer using Ni filtered CuKα radiation. The correction for instrumental broadening was made by the Stokes method using KBr as a standard, and an additional correction made with the low absorption effect coefficients.[12] The coefficients $A_n(l)=A_n{}^P \times\exp[-2\pi^2 n\langle Z_1^2\rangle l^2]$ for (002) and (004) are shown on

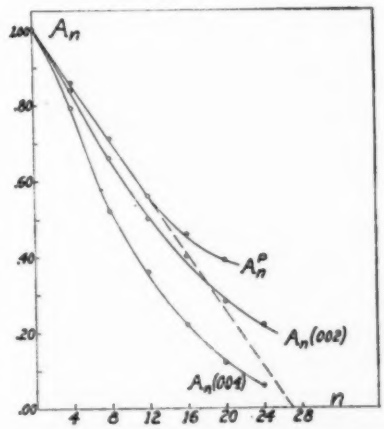

FIG. 4. The Fourier coefficients $A_n(l)$ for (002) and (004) and the particle size coefficient $A_n{}^P$ for (FT) black heated 2 hours at 2300°C.

[13] B. E. Warren and B. L. Averbach, J. Appl. Phys. **23**, 497 (1952).

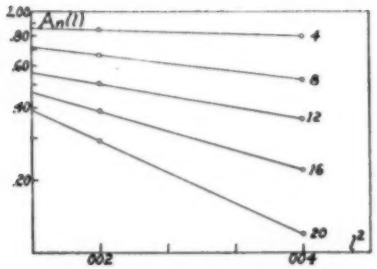

FIG. 5. Plot of $\ln A_n(l)$ *vs* l^2 for the (002) and (004) reflections from (FT) black heated 2 hours at 2300°C.

Fig. 4. The effect of distortion is clearly seen, because if the broadening were due only to particle size, the (002) and (004) curves would coincide.

Using smoothed values from the curves of Fig. 4, we obtain the plots of $\ln A_n(l)$ *vs* l^2 which are shown by Fig. 5. The intercepts on Fig. 5 give the particle size coefficients A_n^P, and these are plotted on Fig. 4. The intercept of the initial slope of the A_n^P *vs* n curve gives the average number of layers in a parallel layer group.[14,15] The value obtained is $\bar{N}_3=27$, and this corresponds to a parallel layer group thickness $L_c=27\times3.42=92$ A.

In terms of the two spacings a_3 and $a_3'=a_3(1+Z_1)$, the average spacing represented by Eq. (16) is given by

$$\bar{a}_3=P_1a_3+(1-P_1)a_3'. \tag{17}$$

From the (002) and (004) reflections $\bar{a}_3=3.42$ A. Using $a_3=3.35$ A and $P_1=0.25$, we obtain from Eq. (17), $a_3'=3.44$ A. This is in good agreement with the value obtained by Franklin[6,7] for the spacing of disordered neighboring layers.

The slope of the curves of Fig. 5 is given by $2\pi^2n\langle Z_1^2\rangle$. An average value $\langle Z_1^2\rangle=0.00066$ is obtained from the $n=16$ and $n=20$ curves. In terms of $Z_1=0$ for ordered layers and $Z_1=Z_1$ for those with random orientation

$$\langle Z_1^2\rangle=P_1\times0+(1-P_1)Z_1^2.$$

Using $P_1=0.25$, $Z_1=(0.00066/0.75)^{\frac{1}{2}}=0.030$, and from this value the spacing for random layers is $a_3'=3.35\times1.030=3.45$ A. In view of the difficulty in separating the distortion broadening, this value is in satisfactory agreement with Franklin's value 3.44 A for layers with random orientation.

V. DETERMINATION OF THE LAYER DIAMETER L_a

Before the start of graphitization, there are no modulations in the (hk) reflections and the layer diameter is given by the two dimensional theory[4,5] $L_a=1.84\Lambda/B\cos\theta$. The effect of modulations on the half-width is to increase (10) and decrease (11), so that quite inconsistent values of L_a are obtained from these reflections. One way of handling the problem is to determine the modulating factor $\sum_n A_n(hk)\cos2\pi nh_3$ by the method of Sec. III and then demodulate the experimental curve by dividing by the modulating factor. The two dimensional particle size equation can then be applied. Treated in this way the (10) and (11) reflections represented by Figs. 1 and 2 gave values of the order $L_a=140$ A.

There is a simpler approximate method for getting both L_a and P_1 which can be applied in the early stages of graphitization when we can assume that each pair of layers orders independently of its neighbors. In terms of $P_1=(P_1^{+}+P_1^{-})$, $A_n(10)=(-P_1/2)^{|n|}$ and $A_n(11)=(P_1)^{|n|}$. Represent the modulating factor of Eq. (13) by

$$M(hkh_3)=\sum_n A_n(hk)\cos2\pi nh_3.$$

With all coefficients expressed in terms of P_1 the sum is readily evaluated

$$M(10h_3)=\frac{1-P_1^2/4}{1+P_1^2/4+P_1\cos2\pi h_3},$$

$$M(11h_3)=\frac{1-P_1^2}{1+P_1^2-2P_1\cos2\pi h_3}.$$

The modulating factor takes simple values for the special cases $h_3=0$, $\frac{1}{2}$, 1, etc. (see Table III). For $h_3=\frac{1}{2}$, the value of the modulating factor is the reciprocal of the value for $h_3=0$ and $h_3=1$. This reciprocal relation suggests the use of a logarithmic plot. By adding a modulating factor, Eq. (11) takes the form

$$P_{2\theta}'(hk)\Big/\left[\frac{F^2(1+\cos^2 2\theta)}{\sin\theta\,(\sin\theta+\sin\theta_0)^{\frac{1}{2}}}\right]\sim\Phi(\alpha)M(hkh_3). \tag{18}$$

At $\sin\theta$ values corresponding to $h_3=0$, $\frac{1}{2}$, 1, etc.

$$\log[\Phi(\alpha)M(hkh_3)]=\log\Phi(\alpha)\pm\log K(hk).$$

Figure 6 shows a plot of $\log\Phi(\alpha)$ *vs* $\log\alpha$ using tabulated values[4] of $\Phi(\alpha)$. It is of course impossible to extend the plot to $\alpha=0$ or to negative values of α. For either (10) or (11) values proportional to $\Phi(\alpha)M(hkh_3)$ at $h_3=0$, $\frac{1}{2}$, 1 are obtained from the experimental curves using Eq. (18). On a piece of tracing paper placed over the log plot these three values are plotted on the $\Phi(\alpha)$

TABLE III. Special values of the modulating factor.

h_3	$M(10h_3)$	$M(11h_3)$
0	$\dfrac{1-P_1}{1+P_1}$	$\dfrac{1+P_1}{1-P_1}$
$\frac{1}{2}$	$\dfrac{1+P_1}{1-P_1}$	$\dfrac{1-P_1}{1+P_1}$
1	$\dfrac{1-P_1}{1+P_1}$	$\dfrac{1+P_1}{1-P_1}$

[14] M. F. Bertaut, Compt. rend. **228**, 493 (1949).
[15] B. E. Warren and B. L. Averbach, J. Appl. Phys. **21**, 595 (1950).

scale. For convenience we represent

$$\log(\alpha)=\log[2\sqrt{\pi}L_a/100\Lambda]+\log[100(\sin\theta-\sin\theta_0)].$$

The abscissas values of the three points are then taken at values of 100 $(\sin\theta-\sin\theta_0)$ computed for $h_3=0$, $\frac{1}{2}$ and 1. Having plotted the three points, the tracing paper is then shifted vertically and horizontally until the three plotted points are equidistant above and below the $\Phi(\alpha)$ curve. For the (10) reflection $h_3=0$, and $h_3=1$ are below, while $h_3=\frac{1}{2}$ is above the curve. For the (11) reflection it is the reverse. Having positioned the tracing paper, the distance of the points above or below the curve is transferred to the ordinate scale giving directly the values $K(10)=(1+P_{\frac{1}{2}})/(1-P_{\frac{1}{2}})$ or $K(11)=(1+P_1)/(1-P_1)$. From the horizontal shift of the tracing paper we get directly the layer diameter L_a. If in the original position we mark the tracing paper at $\alpha=1.0$, the new position of the mark gives $2\sqrt{\pi}L_a/100\Lambda$.

Figure 6 shows the points $h_3=0$, $\frac{1}{2}$, and 1 for the (11) reflection, shifted to a fit where they are equidistant above and below the $\Phi(\alpha)$ curve. The length of the arrows transferred to the ordinate scale gives $(1+P_1)/(1-P_1)=1.70$ and $P_1=0.26$. The horizontal shift gives $2\sqrt{\pi}L_a/100\Lambda=3.5$, $L_a=152$ A. A similar fit for the $h_3=0$, $\frac{1}{2}$, and 1 values from the (10) reflection gives $P_1=0.24$ and $L_a=154$ A. The agreement between these values of P_1 and those obtained in Sec. III from ay analysis of the modulation factor is quite satisfactory.

Although we cannot expect very high accuracy in obtaining P_1 and the layer diameter L_a from a fit on the $\log\Phi(\alpha)$ plot, it is a very quick and simple method. Since it is based on the assumption of independent ordering of the pairs of neighboring layers, it is not safe to use it except in the early stages of ordering. The (11) reflection is probably safe to a higher degree of order than the (10), but in using the (11) reflection, the correction for extraneous broadening is very important.

VI. DISCUSSION

The results reported here have been obtained from the single sample of Fine Thermal (FT) carbon black heated 2 hours at 2300°C. Although not able to show a trend, they give a clear picture of the structure of a carbon black in the early stage of graphitization.

Prior to the beginning of graphitization, the layers of a parallel layer group have random orientations about the layer normal and a spacing of 3.44 A. Presumably there is no incentive for neighboring layers to take on the ordered relation until the layer diameter exceeds a

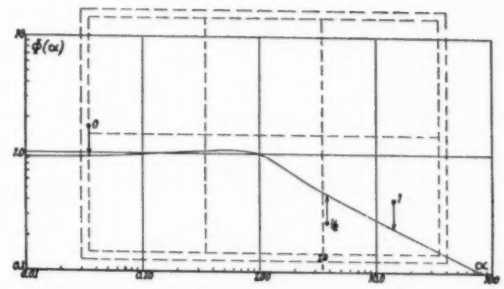

FIG. 6. Plot of $\log\Phi(\alpha)$ *vs* $\log\alpha$ for determination of P_1 and L_a. A fit for the (11) reflection is illustrated.

value of the order $L_a=100$ A. In the early stages of graphitization, some of the pairs of neighboring layers assume the graphite relation, and the spacing decreases to approximately that of graphite 3.35 A. For the sample of Fine Thermal (FT) black heated 2 hours at 2300°C, about 25 percent of the nearest neighbor pairs of layers have ordered. About 6 percent of the second neighbor pairs are ordered, with about equal proportions of the ABA and ABC sequences. In the early stages, each pair of nearest neighbor layers orders independently of the neighboring layers, rather than whole regions taking on the graphite structure. Since independent ordering produces ABC sequences, stacking faults in artificial graphite are to be expected.

When modulations are present in the (hk) two-dimensional reflections, it is not possible to obtain the layer diameter L_a by direct peak width measurements. Some method such as that of demodulation or fitting to a $\log\Phi(\alpha)$ curve must be used. The layer thickness L_c cannot be obtained from the $(00l)$ peaks without first correcting for the distortion broadening due to the existence of two different layer spacings. The accuracy of our measurements of the $(00l)$ spacings was not high enough to distinguish between a linear variation of spacing with ordering, and the slightly curved variation found by Franklin[6] and Bacon.[2]

The quantity P_1, the probability of a pair of nearest layers having a graphite orientation, is readily determined by use of the $\log\Phi(\alpha)$ plot of Fig. 6. It appears to be a suitable quantity to define as the "degree of graphitization."

We wish to acknowledge the sponsorship of this work by Godfrey L. Cabot, Inc., and, in addition, express our thanks to Dr. W. R. Smith and Mr. W. D. Schaeffer of Godfrey L. Cabot, Inc., for their very generous help and advice.

JOURNAL OF APPLIED PHYSICS VOLUME 25, NUMBER 12 DECEMBER, 1954

A Definition of Passive Linear Networks in Terms of Time and Energy

G. RAISBECK
Bell Telephone Laboratories, Inc., Murray Hill, New Jersey
(Received March 3, 1954)

A definition of passive linear network is made:

(a) The network is linear.
(b) If currents of any wave form are fed to the terminals of the network, the total energy delivered to the network is not negative.
(c) No voltages appear between any pair of terminals before a current is fed to the network.

When this definition is applied to two terminal networks, i.e., impedances, a necessary and sufficient condition that a two-terminal network be linear passive is that its impedance function be a positive real function.

An analysis of multiterminal networks yields as a necessary and sufficient condition from the foregoing hypotheses that a certain Hermitian quadratic form be positive definite. In the case of three-terminal networks, it reduces to

$$4R_{11}R_{22}-(R_{12}+R_{21})^2-(X_{12}-X_{21})^2\geq 0,$$

where $R_{ij}+jX_{ij}=Z_{ij}$ are the terms of the matrix of impedances of the network. The relation of this formula to similar but not identical formulas of Gewertz and Llewellyn, and other consequences of the condition, are discussed.

IN a search for a suitable definition of a passive network it seems philosophically desirable to let the definition rest on broad properties involving energy, time, and the like, rather than specific properties such as the analytic or positive character of impedance functions. A good deal is known, however, about passive two-terminal linear networks. Whatever reasonable definition of passivity is assumed, the impedance function is a positive real function.[1] It follows from this fact that if a current is passed through the impedance, the total energy delivered to the impedance is positive, and that no voltage appears across the terminals before a current is impressed. Now these conditions are of the type desirable for a good definition of *linear passive network*. We shall accordingly generalize them for n-terminal networks.

This paper approaches in some respects the work of McMillan[2] from which it differs in one main respect. McMillan deals with realizable networks, and consequently restriction to rational impedance functions and reciprocity (i.e., symmetric impedance matrices) is inevitable. The present paper assumes neither rationality nor reciprocity. The definition of passive linear network which is proposed is apparently much broader than any definition involving realizability, in that the hypotheses are less restrictive; yet it is notable that if a network satisfying the present definition of passive linear network also has a rational symmetric impedance matrix, it satisfies the hypotheses of McMillan for a realizable network. Thus, the restrictions on a passive linear network required to make it realizable are only the obvious conditions that its impedance matrix be rational and symmetrical. Because of this, the chief interest of the paper must lie in its results about nonreciprocal devices and in the fact that the results are cast in a form identical for rational and nonrational impedances.

It will be assumed throughout that the network in question has an impedance matrix. In the case of two-terminal devices, the impedance may be identically zero or the admittance may be identically zero. In either case, if the impedance is not defined, the admittance is, and vice versa. However, a general network may have both kinds of bad behavior at once: it may be that neither the impedance matrix nor the admittance matrix exists. This will happen, for example, if it has one pair of open-circuited and one pair of short-circuited terminals. The classic way to deal with such problems is to suppose infinitesimal external admittances connected among the terminals.

McMillan has shown another way out of the dilemma for networks obeying reciprocity. It seems likely that his technique would also be applicable to nonreciprocal devices. The question is avoided because the chief interest of the present paper is believed to lie in application to cases where there is no question of the existence of the impedance matrix.

Before proceeding to n-terminal networks, we shall first prove a converse of our original statement about positive real impedance functions, to wit:

If a two-terminal network has the following properties: (a) it is linear, (b) if a current of any wave form is impressed on the impedance, the total energy delivered to the impedance is not negative, (c) no voltage appears across the terminals before a current is passed through them; then its impedance function is a positive real function.

A function $Z(\lambda)$, $\lambda=\sigma+j\omega$, is called positive real if[1]

[1] Guillemin, *A Summary of Modern Methods of Network Analysis, Advances in Electronics* (Academic Press, New York, 1951), Vol. 3, pp. 261–303.
[2] McMillan, Bell System Tech. J. **31**, Nos. 2 and 3, pp. 217–279, 541–600, March and May, 1952.

(a′) $Z(\lambda)$ is real for real λ; (b′) $Z(\lambda)$ is analytic in the region $\sigma>0$; (c′) $Re[Z(\sigma+j\omega)]\geq 0$ if $\sigma\geq 0$.

A proof will be outlined, but no attempt will be made at rigor. It is assumed that integrals converge and that limits may be interchanged throughout. These conditions can be assured by more or less stringent assumptions about continuity, boundedness, or absolute integrability, depending on the degree of mathematical sophistication one is willing to assume.

The idea of the proof is as follows.

An expression for the energy delivered to the network will be found (15). An expression for the real part of the impedance in the right-hand half-plane in terms of the impedance on the axis of real frequencies will be found (18). A particular excitation (19) will be found such that the two expressions above are equal. Since the energy delivered to the network is positive, then it follows that the real part of the impedance in the right-hand half-plane is also positive.

Because the circuit is linear we can describe the relation between the voltage $v(t)$ and the current $i(t)$ by

$$v(t)=\int_{-\infty}^{\infty} i(\tau)K(t-\tau)d\tau. \tag{1}$$

Furthermore, because the voltage is zero until the current begins, it follows simply that

$$K(t)=0 \quad \text{for} \quad t<0. \tag{2}$$

In fact, $K(t)$ is no more than the impulse response of the network. The impedance function is simply

$$Z(j\omega)=\int_{-\infty}^{\infty} K(t)e^{-j\omega t}dt. \tag{3}$$

Because of the fact that $K(t)$ vanishes for negative arguments,

$$Z(\sigma+j\omega)=\int_{0}^{\infty} K(t)e^{-\sigma t}e^{-j\omega t}dt \tag{4}$$

is uniformly convergent for $\sigma\geq\delta>0$, and hence is an analytic function of $\sigma+j\omega$ in the right half-plane. Furthermore, inasmuch as $K(t)$ is the pulse response of the impedance, it is a real function, and consequently $Z(\sigma+j\omega)$ is real when $\omega=0$. It remains only to prove that

$$Re[Z(\sigma+j\omega)]\geq 0 \quad \text{for} \quad \sigma\geq 0. \tag{5}$$

Now consider the energy delivered to the impedance

$$E=\int_{-\infty}^{\infty} v(t)i(t)dt. \tag{6}$$

Note that by hypotheses

$$E\geq 0. \tag{7}$$

Form the function

$$e(u)=\int_{-\infty}^{\infty} i(t-u)v(t)dt \tag{8}$$

$$=\int_{-\infty}^{\infty} i(t-u)dt\int_{-\infty}^{\infty} i(\tau)K(t-\tau)d\tau \tag{9}$$

$$=\int_{-\infty}^{\infty}\int_{-\infty}^{\infty} i(t-u)i(\tau)K(t-\tau)dtd\tau. \tag{10}$$

Note that

$$E=e(0). \tag{11}$$

Now take the Fourier transforms of both sides. The right side is the convolution of three functions

$$i(-u)*i(u)*K(u), \tag{12}$$

and its Fourier transform is the product of the transforms of the three separate functions, i.e.,

$$E(\omega)=I^*(\omega)\cdot I(\omega)\cdot Z(j\omega)$$
$$=|I(\omega)|^2\cdot Z(j\omega). \tag{13}$$

Inverting again, we get

$$e(u)=\frac{1}{2\pi}\int_{-\infty}^{\infty} Z(j\omega)|I(\omega)|^2e^{j\omega u}d\omega. \tag{14}$$

Setting $u=0$, we get

$$E=e(0)=\frac{1}{2\pi}\int_{-\infty}^{\infty} Z(j\omega)|I(\omega)|^2d\omega. \tag{15}$$

Now, recalling Poisson's integral for the case of a half-plane,

$$Z(\sigma+j\omega)=\frac{1}{\pi}\int_{-\infty}^{\infty} Z(j\eta)\frac{\sigma}{\sigma^2+(\omega-\eta)^2}d\eta, \quad \sigma>0 \tag{16}$$

for arbitrary ω and arbitrary $\sigma>0$. Inasmuch as Z is typically real,[3] (see Eq. (4))

$$Z(\sigma+j\omega)=Z^*(\sigma-j\omega), \tag{17}$$

we can form both functions, add, and divide by 2 to get

$$Re[Z(\sigma+j\omega)]=\frac{1}{2\pi}\int_{-\infty}^{\infty} Z(j\eta)$$
$$\times\left[\frac{\sigma}{\sigma^2+(\omega+\eta)^2}+\frac{\sigma}{\sigma^2+(\omega-\eta)^2}\right]d\eta. \tag{18}$$

Now let

$$i_0(t)=C_1e^{-\sigma t}\cos\omega(t-C_2), \quad t>0$$
$$=0 \qquad\qquad\qquad\quad t<0. \tag{19}$$

[3] A function is called *typically real* if it assumes conjugate values for conjugate values of its argument.

For suitable real values of C_1 and C_2,

$$|I(\eta)|^2=\frac{1}{2\pi}\left[\frac{\sigma}{\sigma^2+(\omega+\eta)^2}+\frac{\sigma}{\sigma^2+(\omega-\eta)^2}\right]. \quad (20)$$

Hence, from (7), (15), (18), and (20),

$$Re|Z(\sigma+j\omega)|=E\geq 0 \quad \text{for} \quad \sigma>0. \quad (21)$$

The same inequality for $\sigma=0$ follows from continuity arguments. This completes the proof.

Note that the impedance function need not be assumed rational. The rationality of $Z(\lambda)$ arises only when the question of realization with lumped elements is brought up.

Let us now imagine a network having $n+1$ terminals. Suppose it satisfies the following hypotheses.

(a″) It is linear.

(b″) If currents of any wave form are fed to the terminals of the network, the total energy delivered to the network is not negative.

(c″) No voltages appear between any pair of terminals before a current is fed to the network.

We shall call a network satisfying (a″), (b″), and (c″) a *linear passive network*.

It will be proved by a method exactly analagous to the method used for two terminal networks that a certain Hermitian form[4] (34) is positive definite. The steps are: first, to derive an expression for energy delivered to the network (25); second, to assume a special excitation (26) analogous to the one used before; and third to show that the energy in this case is a certain Hermitian form involving only elements of the impedance matrix of the network (28), (34). Because the energy delivered is always positive, the Hermitian form must be positive definite.

Call one terminal a reference terminal and let the currents into and the voltages at the other terminals be called, respectively,

$$i_1(t),\ i_2(t),\ \cdots i_n(t),\ v_1(t),\ v_2(t),\ \cdots v_n(t). \quad (22)$$

Then let $\|i_j(t)\|$ be a vector (i.e., a $1\times n$ matrix) having components $i_1(t)$, $i_2(t)$, $\cdots$, and let $\|v_j(t)\|$ be a vector having components $v_1(t)$, $v_2(t)$, $\cdots$. Then $\|i_j(t)\|$ and $\|v_j(t)\|$ are connected by a matrix relation

$$\|v_j(t)\|=\int_{-\infty}^{\infty}\|k_{jk}(t-\tau)\|\ \|i_k(\tau)\|d\tau, \quad (23)$$

which is analogous to (1). Carrying the analysis through exactly as before, we arrive at

$$e(u)=\frac{1}{2\pi}\int_{-\infty}^{\infty}\|Z_{jk}(j\omega)\|\ \|I_j(\omega)\|\ \|I_k^*(\omega)\|e^{j\omega u}d\omega \quad (24)$$

and

$$E=e(0)=\frac{1}{2\pi}\int_{-\infty}^{\infty}\|Z_{jk}(j\omega)\|\ \|I_j(\omega)\|\ \|I_k^*(\omega)\|d\omega, \quad (25)$$

where $\|Z_{jk}\|$ is the well-known impedance matrix. If now we let

$$i_n(t)=c_n i_0(t-\tau_n), \quad (26)$$

i.e., i_0 multiplied by c_n and delayed by τ_n [i_0 being defined in (19)], then

$$E=Re[\sum_{i,j}c_ic_jZ_{ij}(\sigma+j\omega)e^{j\omega(\tau_i-\tau_j)}], \quad (27)$$

from which it follows that

$$Re[\sum_{i,j}c_ic_jZ_{ij}(\sigma+j\omega)e^{j\omega(\tau_i-\tau_j)}]\geq 0 \quad (28)$$

for all real c's and positive τ's.

If we let

$$\omega\tau_j=\varphi_j \quad (29)$$

$$c_je^{j\omega\tau_j}=u_j=a_j+jb_j \quad (30)$$

$$Z_{ij}'=Z_{ji}'^*=\tfrac{1}{2}[Z_{ij}+Z_{ji}^*]=R_{ij}^s+jX_{ij}^a, \quad (31)$$

then alternative equivalent forms are:

$$\sum_{i,j}c_ic_j[\cos(\varphi_i-\varphi_j)R_{ij}-\sin(\varphi_i-\varphi_j)X_{ij}]\geq 0 \quad (32)$$

$$\sum_{i,j}[(a_ia_j+b_ib_j)R_{ij}^s+(a_ib_j-a_jb_i)X_{ij}^a]\geq 0 \quad (33)$$

$$\sum_{i,j}u_i^*u_jZ_{ij}'\geq 0 \quad (34)$$

for all a_i, b_i, c_i, u_i, and φ_i, where the a's, b's, and c's and φ's are arbitrary real numbers and the u's are arbitrary complex numbers. (The restriction of φ to positive numbers is no restriction at all.) In (31) and (34), * denotes a complex conjugate.

If the matrix of impedances is assumed to be symmetric, this condition reduces to

$$\sum_{i,j}c_ic_jR_{ij}\geq 0$$

for all real c_i, c_j. This is a necessary condition for realizability, and has been stated several times before.[5]

From (31) it follows that (34) is a Hermitian form, and the condition is simply that the Hermitian form (34) is positive definite. From (31) it also follows that the elements of the form Z_{ij}' depend only on the symmetric components of resistance, R_{ij}^s, and the skew-symmetric components of reactance, X_{ij}^a. The skew-symmetric components of resistance, R_{ij}^a, and the symmetric components of reactance, X_{ij}^s, are not involved.

Any one of these inequalities is sufficient to guarantee that $E\geq 0$ for all signals. Take, for example, an arbitrary

[4] A Hermitian form is an expression $F=\Sigma\, x_ih_{ij}x_j^*$ (where * denotes the complex conjugate) in which the matrix of coefficients h_{ij} has the property

$$h_{ij}=h_{ji}^*.$$

See G. Birkhoff and S. McLane, *A Survey of Modern Algebra* (Macmillan, New York, 1946), pp. 256–257.

[5] McMillan, reference 2. McMillan refers to earlier announcements of this result by Y. Ono (1946), himself (1948), and M. Bayard (1949).

set of signals $\|i_n(t)\|$. Let $I_j(\omega)=a_j(\omega)+jb_j(\omega)$. Direct computation shows that

$$Re(\|Z_{ij}(j\omega)\|\,\|I_j(\omega)\|\,\|I_j^*(\omega)\|)$$
$$=\sum_{i,j}[[a_i(\omega)a_j(\omega)+b_i(\omega)b_j(\omega)]R_{ij}(j\omega)$$
$$+[a_i(\omega)b_j(\omega)-a_j(\omega)b_i(\omega)]X_{ij}(j\omega)]\geq 0, \quad (35)$$

by (33) [which is equivalent to (34)]. Hence (25), which is the integral of (35) over frequency [the imaginary part of (25) is zero by symmetry], is also non-negative.

Hence we can deduce a converse. Imagine a network having $(n+1)$ terminals. Suppose it satisfies the following hypotheses.

(a'') It is linear.

(c'') No voltages appear between any pair of terminals before a current is fed to the network.

(d'') The Hermitian quadratic form (34) is positive definite.

Then

(b'') If currents of any wave form are fed to the terminals of the network, the total energy delivered to the network is not negative.

Inequalities (28) and (34) are the analog of (21). The reactive components do not appear for any network obeying reciprocity, because in that case the antisymmetric parts are identically zero. Hence they do not appear in (21), for any two-terminal device obeys reciprocity.

As a practical test, any particular Hermitian form can be reduced to diagonal form.[6]

$$\sum_i y_i^* y_i Z_{ii}'' \quad (36)$$

where all the mixed terms vanish. The form is positive definite if and only if all the numbers Z_{ii}'' are non-negative. For the case $n=2$ (a three-terminal network) this can be done by "completing the square" as follows:

$$\sum_{i,j} u_i^* u_j Z_{ij}'$$
$$=u_1^*u_1Z_{11}'+u_1^*u_2Z_{12}'+u_2^*u_1Z_{21}'+u_2u_2^*Z_{22}' \quad (37)$$
$$=\left[u_1+u_2\frac{Z_{12}'}{Z_{11}'}\right]\left[u_1^*+u_2^*\frac{Z_{21}'}{Z_{11}'}\right]Z_{11}'$$
$$+u_2^*u_2\frac{Z_{11}'Z_{22}'-Z_{12}'Z_{21}'}{(Z_{11}')} \quad (38)$$
$$=y_1^*y_1Z_{11}+y_2^*y_2\frac{Z_{11}'Z_{22}'-Z_{12}'Z_{21}'}{(Z_{11}')}, \quad (39)$$

where

$$y_1=u_1+u_2\frac{Z_{12}'}{Z_{11}'} \quad (40)$$
$$y_2=u_2.$$

The condition reduces then to

$$Z_{11}'\geq 0$$
$$Z_{11}'Z_{22}'-Z_{12}'Z_{21}'\geq 0, \quad (41)$$

(which imply, incidentally, that $Z_{22}'\geq 0$) or simply, by (31),

$$R_{11}\geq 0$$
$$R_{22}\geq 0 \quad (42)$$
$$R_{11}R_{22}-(R_{12^s})^2-(X_{12^a})^2\geq 0.$$

F. B. Llewellyn[7] gives a condition which must be satisfied in order that a two terminal-pair network always have positive input and output impedances for passive terminations. This condition must be satisfied whenever (42) is satisfied. The following argument shows that it is. Llewellyn's condition is

$$4(R_{11}R_{22}+X_{12}X_{21})(R_{11}R_{22}-R_{12}R_{21})$$
$$-(R_{12}X_{21}-R_{21}X_{12})^2\geq 0. \quad (43)$$

In our notation, an equivalent form is

$$[R_{12}R_{22}-(R_{12^s})^2-(X_{12^a})^2][R_{11}R_{22}+(X_{12^s})^2$$
$$+(R_{12^a})^2]+(R_{12^s}R_{12^a}-X_{12^s}X_{12^a})^2\geq 0. \quad (44)$$

The second factor of the first term and the second term are both inherently non-negative. By (42) the first factor of the first term is positive. Hence Llewellyn's condition is satisfied. However, Llewellyn's condition does not imply ours: his is a condition for stability, ours for passivity. All passive networks (according to our definition) are stable, but not all stable networks are passive. Llewellyn himself points out that his condition does not guarantee all the attributes of a passive system.

Gewertz's condition, quoted by Llewellyn, is made under the hypotheses of reciprocity. In our notation, it is

$$R_{11}R_{22}-(R_{12^s})^2\geq 0. \quad (45)$$

Our formula (42) reduces to this when the nonreciprocal term X_{12^a} is removed. This implies that a reciprocal network which is stable under all passive terminations (Gewertz's hypothesis) is passive, but a nonreciprocal network stable under all passive terminations (Llewellyn's hypothesis) need not be passive. The conclusion is made more plausible by the following heuristic consideration. In a given network, a signal traveling

[6] G. Birkhoff and S. McLane, reference 4, Chap. IX.

[7] F. B. Llewellyn, Proc. Inst. Radio Engrs. **40**, No. 3, 281 (March, 1952).

through the network, reflected at the terminals, and returning is stable, provided the signal which reappears is smaller than the one that went in. If the network is reciprocal, this implies that it suffers a loss in both directions. If the network is nonreciprocal, it may increase in one direction of transmission and decrease in the other. Now if we determine the direction of preferred transmission, and provide an external low-loss feedback path for the return transmission, the network plus a passive external feedback path may be unstable. This is just the situation which prevails, for example, in a normal vacuum-tube amplifier.

The relation (34) can be used to derive other unobvious consequences. For example, suppose that for all i, j

$$R_{ij}=0. \tag{46}$$

Then by choosing all a's and b's equal to zero except

$$a_j=1, \tag{47}$$
$$b_j=\pm 1,$$

it follows from (33) that

$$X_{ij}{}^a \geq 0, \tag{48}$$
$$X_{ij}{}^a \leq 0.$$

Hence

$$X_{ij}{}^a=0. \tag{49}$$

That is, if the resistance terms in the matrix of impedances vanish, then so do the nonsymmetric reactance terms, or, in other words, if the matrix of impedances of a passive network contains no resistances, it obeys reciprocity.

Also, for example, if the matrix of impedances of a network is skew-symmetric, as in a gyrator, then the reactive term must vanish if it is to be passive.

In summary, if we accept hypotheses (a″), (b″), and (c″) as the definition of a passive linear network, then a necessary and sufficient condition that a network be linear passive is that the Hermitian form

$$\sum_{i,j} u_i{}^* u_j Z_{ij}'$$

be positive definite. For networks having three terminals this condition reduces to a form which can be compared with similar formulae of Gewertz and Llewellyn. Other nontrivial consequences can be derived from it.

The helpful criticism of J. G. Linvill is gratefully acknowledged.

JOURNAL OF APPLIED PHYSICS VOLUME 25, NUMBER 12 DECEMBER, 1954

Noise in Transverse-Field Traveling-Wave Tubes*

G. Wade, K. Amo, and D. A. Watkins
Stanford University, Stanford, California

(Received March 8, 1954)

From theoretical considerations of the fluctuations in an electron beam, an expression for the noise figure of a transverse-field amplifier is derived. There are found to be three statistically uncorrelated sources of noise in the beam of such a tube—(1) that arising from the fluctuations in the transverse emission velocity of electrons in a direction normal to the surface of the beam, (2) that arising from fluctuations in the transverse emission velocity of electrons in a direction parallel to the surface of the beam, and (3) that arising from fluctuations in the mean position of the beam and depending on its thickness. The analysis shows that the use of a collimator is required to give low noise figures. This is illustrated by the following example: for a tube designed to operate at 1000 mc with a collimator whose width is 0.004 in., the theoretical noise figure is 2 db. Without the collimator, the noise figure would be 11 db.

INTRODUCTION

THIS paper presents a noise analysis for a purely transverse-field traveling-wave amplifier. In this type of tube an electron beam is made to travel in approximate synchronism with a traveling electric field whose longitudinal component is zero at the mean position of the beam. Under the proper conditions for amplification the transverse component of field modulates the transverse position of the beam in such a way that the beam gives up energy to the traveling field. Fluctuations in the transverse positions and in the transverse velocities of the electrons of the beam constitute sources of noise in the amplifier. The effect of each of these sources of noise is considered and a general expression for the noise figure is derived.

Since noise originating in the amplifier results from fluctuations in the transverse positions and in the transverse velocities of the electrons the use of a collimator to limit both the transverse positions and the transverse velocities is a means of reducing the noise figure. The idea of using a well-collimated beam in a transverse-field tube as a possible low-noise device was suggested by Pierce some time ago.[1] The analysis

* The work reported in this paper was made possible through the support extended jointly by the U. S. Navy Office of Naval Research, the U. S. Army Signal Corps, and the U. S. Air Force.

[1] J. R. Pierce, *Traveling-Wave Tubes* (D. Van Nostrand Company, Inc., New York, 1950), Chap. X.

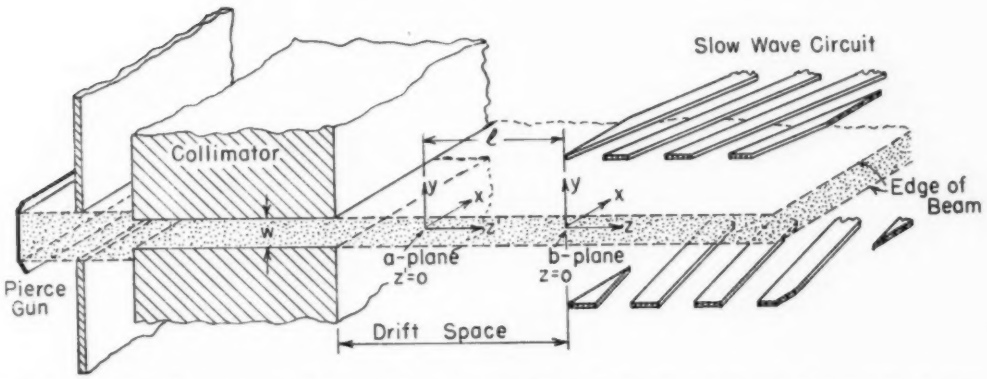

FIG. 1. A portion of a transverse-field traveling-wave amplifier showing the relative positions of the electron gun, the collimator, the drift space, and the slow-wave circuit.

presented here shows quantitatively the effect of a collimator.

Consider a transverse-field tube in which a beam flows through a collimator and a drift space before entering the traveling-wave circuit. The tube is immersed in a uniform magnetic focusing field which is parallel to the direction of current flow. As a result the electrons in the drift region follow helical paths. A Pierce gun produces a beam with a cross section in the form of a narrow rectangular strip. The collimator, whose dimension in the direction of flow is greater than the pitch of the helical paths of the electrons, further reduces the thickness of the beam and puts an upper limit on the magnitude of the transverse velocity of the electrons which are able to pass through it. In the drift space the beam is entirely confined to a region just the width of the collimator. Figure 1 illustrates the setup.

A system of rectangular coordinates is chosen such that the z axis is in the direction of flow and the y axis is in the direction of the short dimension of the beam. A primed z coordinate for the drift region is used in the analysis in order to distinguish between this region and the region of the slow-wave circuit. Let $z'=0$ be located at a plane of the cathode image in the drift region. In subsequent notation this plane will be referred to as the a plane. The plane for which $z=0$ marks the beginning of the circuit region and will be referred to as the b plane.

A glossary of the symbols to be used is given below. The mks system of units is employed in the calculations.

b = Pierce's traveling-wave tube electron speed parameter;
e = electronic charge (magnitude);
f = Pierce's magnetic field parameter $=\beta_m/\beta_e D$;
$j=\sqrt{-1}$;
k = Boltzmann's constant;
l = distance between the a plane and the b plane;
m = electronic mass;
t = time coordinate;
u_0 = electron velocity in the z direction;
w = width of collimator;
x = transverse coordinate shown in Fig. 1; also the total ac variation of position along the x coordinate;
x_n = ac variation of position along the x coordinate in the nth wave;
$\dot{x}_n$ = ac variation of the x component of velocity in the nth wave;
$\dot{x}_a$ = total ac variation of the x component of velocity at the a plane;
$\dot{x}_b$ = total ac variation of the x component of velocity at the b plane;
y = transverse coordinate shown in Fig. 1; also the total ac variation of position along the y coordinate;
y_n = ac variation of position along the y coordinate in the nth wave;
$\dot{y}_n$ = ac variation of the y component of velocity in the nth wave;
$\dot{y}_a$ = total ac variation of the y component of velocity at the a plane;
$\dot{y}_b$ = total ac variation of the y component of velocity at the b plane;
z = axial coordinate for the circuit region;
z' = axial coordinate for the drift region;
B = strength of axial magnetic field;
D = Pierce's gain parameter for a purely transverse electric field (analogous to C in an ordinary tube);
E_y = electric field in the y direction;
F = noise figure;
I_0 = dc beam current;
K = Pierce's impedance parameter;
P = ac power carried by a wave on the circuit in the absence of the beam;
P_t = noise power carried by a wave on the circuit in the absence of the beam;
T = circuit temperature taken to be 290°K;
T_c = cathode temperature;
V = ac circuit voltage acting on the electron beam; also with various subscripts as defined in the text;
V_0 = dc beam voltage;

$\langle V_{1i}^2\rangle_{kw}$ = mean square voltage fluctuations in the growing wave due to thermal noise at the circuit input;
$\langle V_{1x}^2\rangle_{kw}$ = mean square voltage fluctuations in the growing wave due to fluctuations of the x component of velocity at the a plane;
$\langle V_{1y}^2\rangle_{kw}$ = mean square voltage fluctuations in the growing wave due to fluctuations of the y component of velocity at the a plane;
$\langle V_{1w}^2\rangle_{kw}$ = mean square voltage fluctuations in the growing wave due to fluctuations of position along the y coordinate at the a plane;
β = circuit phase constant;
β_e = electronic wave number $=\omega/u_0$;
β_m = cyclotron wave number $=\eta B/u_0$;
δ_n = Pierce's incremental propagation constants;
$\langle\delta\dot{x}^2\rangle_{kw}$ = mean square deviation of the x component of velocity;
$\langle\delta y^2\rangle_{kw}$ = mean square deviation of position along y coordinate;
$\langle\delta\dot{y}^2\rangle_{kw}$ = mean square deviation of the y component of velocity;
η = electronic charge to mass ratio;
λ_m = cyclotron wavelength $=2\pi/\beta_m$;
Φ' = Pierce's symbol for $-E_y/V$;
ω = radian frequency of interest;
Δf = band width;
Γ_1 = circuit propagation constant.

BALLISTIC EQUATIONS FOR THE ELECTRONS IN THE DRIFT SPACE

The equations of motion of the electrons in the drift region are

$$\begin{aligned}&\ddot{z}'=0;\\&\ddot{x}=-\eta B\dot{y};\\&\ddot{y}=\eta B\dot{x}.\end{aligned}\tag{1}$$

This neglects space-charge forces which produce additional acceleration. The equations can be simplified by considering the motion to be separated into various wave components each of which for a single frequency component is characterized by a temporal and spacial variation of $\exp(j\omega t-\Gamma z')$. Hence for each of the waves we can write

$$\begin{Bmatrix}\ddot{x}\\\ddot{y}\end{Bmatrix}=\frac{\partial}{\partial t}\begin{Bmatrix}\dot{x}\\\dot{y}\end{Bmatrix}+\frac{\partial}{\partial z}\begin{Bmatrix}\dot{x}\\\dot{y}\end{Bmatrix}\frac{\partial z'}{\partial t}=u_0(j\beta_e-\Gamma)\begin{Bmatrix}\dot{x}\\\dot{y}\end{Bmatrix}.\tag{2}$$

Likewise

$$\begin{Bmatrix}\dot{x}\\\dot{y}\end{Bmatrix}=u_0(j\beta_e-\Gamma)\begin{Bmatrix}x\\y\end{Bmatrix}.\tag{3}$$

Thus Eqs. (1) can be written

$$\begin{aligned}u_0^2(j\beta_e-\Gamma)^2x&=-\eta Bu_0(j\beta_e-\Gamma)y,\\u_0^2(j\beta_e-\Gamma)^2y&=\eta Bu_0(j\beta_e-\Gamma)x.\end{aligned}\tag{4}$$

The simultaneous solution of Eqs. (4) gives three values for the propagation constant.

$$\Gamma=j\beta_e,\quad j(\beta_e+\beta_m),\quad j(\beta_e-\beta_m).\tag{5}$$

Hence the equations for the transverse position and the transverse velocity are expressible as the summation of three waves

$$\begin{aligned}y&=y_1e^{-i\beta_ez'}+y_2e^{-j(\beta_e+\beta_m)z'}+y_3e^{-j(\beta_e-\beta_m)z'},\\\dot{y}&=\dot{y}_1e^{-j\beta_ez'}+\dot{y}_2e^{-j(\beta_e+\beta_m)z'}+\dot{y}_3e^{-j(\beta_e-\beta_m)z'},\\x&=x_1e^{-j\beta_ez'}+x_2e^{-j(\beta_e+\beta_m)z'}+x_3e^{-j(\beta_e-\beta_m)z'},\\\dot{x}&=\dot{x}_1e^{-j\beta_ez'}+\dot{x}_2e^{-j(\beta_e+\beta_m)z'}+\dot{x}_3e^{-j(\beta_e-\beta_m)z'}.\end{aligned}\tag{6}$$

A time variation of $\exp(j\omega t)$ is understood. From Eqs. (1), (2), and (3) the following relationships are obtained:

$$\begin{aligned}&\dot{y}_1=0,\\&\dot{y}_2=-j\beta_mu_0y_2,\\&\dot{y}_3=j\beta_mu_0y_3,\\&x_2=-jy_2,\\&x_3=jy_3,\\&\dot{x}_1=0,\\&\dot{x}_2=-\beta_mu_0y_2,\\&\dot{x}_3=-\beta_mu_0y_3.\end{aligned}\tag{7}$$

Note that there is no relationship between x_1 and y_1. Combining Eqs. (6) and (7) and taking z' to be zero we get a set of four simultaneous equations in four unknowns

$$\begin{aligned}y_a&=0+y_1+y_2+y_3,\\\dot{y}_a&=0+0-j\beta_mu_0y_2+j\beta_mu_0y_3,\\x_a&=x_1+0-jy_2+jy_3,\\\dot{x}_a&=0+0-\beta_mu_0y_2-\beta_mu_0y_3.\end{aligned}\tag{8}$$

The subscript a indicates the value of the quantity at the a plane ($z'=0$) which is presumed to be known. The simultaneous solution of Eqs. (8) gives x_1, y_1, y_2, and y_3 in terms of y_a, $\dot{y}_a$, x_a, and $\dot{x}_a$. These relationships, substituted back into Eqs. (6), give

$$\begin{aligned}y&=\left[y_a+\frac{\dot{x}_a}{\eta B}\right]e^{-j\beta_ez'}+\frac{1}{2\eta B}[-\dot{x}_a+j\dot{y}_a]e^{-j(\beta_e+\beta_m)z'}\\&\quad+\frac{1}{2\eta B}[-\dot{x}_a-j\dot{y}_a]e^{-j(\beta_e-\beta_m)z'},\\\dot{y}&=0+\tfrac{1}{2}[\dot{y}_a+j\dot{x}_a]e^{-j(\beta_e+\beta_m)z'}+\tfrac{1}{2}[\dot{y}_a-j\dot{x}_a]e^{-j(\beta_e-\beta_m)z'},\\x&=\left[x_a-\frac{\dot{y}_a}{\eta B}\right]e^{-j\beta_ez'}+\frac{1}{2\eta B}[\dot{y}_a+j\dot{x}_a]e^{-j(\beta_e+\beta_m)z'}\\&\quad+\frac{1}{2\eta B}[\dot{y}_a-j\dot{x}_a]e^{-j(\beta_e-\beta_m)z'},\\\dot{x}&=0+\tfrac{1}{2}[\dot{x}_a-j\dot{y}_a]e^{-j(\beta_e+\beta_m)z'}+\tfrac{1}{2}[\dot{x}_a+j\dot{y}_a]e^{-j(\beta_e-\beta_m)z'}.\end{aligned}\tag{9}$$

BEAM INTERACTION WITH THE SLOW-WAVE CIRCUIT

As we have seen, the beam in the drift space supports three forward propagating waves. The unperturbed circuit supports two waves, one propagating in the forward direction and one propagating in the backward direction. Interaction between beam and circuit results in four forward waves and one backward wave. Let us assume that the circuit is terminated in such a way as to give a negligibly small backward wave. Then we need be concerned only with the four forward waves. Four independent boundary conditions at $z=0$ are necessary to determine how the four forward waves are set up. For these we can use the ac variations in V, $\dot{y}$, $\dot{x}$, and y. The variations in x need not be considered since these variations do not couple to the circuit.

Pierce's[2] analysis of amplification in a purely transverse-field traveling-wave tube is useful in the present noise problem. His symbolism will be employed here. For the circuit equation he gets

$$V=\frac{j\omega\Gamma_1 K(I_0/u_0)\Phi' y}{(\Gamma^2-\Gamma_1^2)}. \tag{10}$$

The equations of motion of the electrons in the region of the circuit are slightly different from Eqs. (1), being modified by the circuit electric field in the y direction. Thus

$$\begin{aligned}\ddot{z}&=0,\\ \ddot{x}&=-\eta B\dot{y},\\ \ddot{y}&=\eta(B\dot{x}+\Phi' V).\end{aligned} \tag{11}$$

There will be three waves for which $\Gamma\neq j\beta_e$. Let us designate these waves by the subscripts 1, 2, and 3. A fourth wave exists for which $\Gamma=j\beta_e$. It will be designated by the subscript 4. Pierce's analysis of amplification includes only the first three waves for which he shows that under the assumption of small D

$$\left.\begin{aligned}\dot{y}_n&=\frac{1}{M}\frac{\delta_n}{(\delta_n^2+f^2)}V_n\\ \dot{x}_n&=-\frac{1}{M}\frac{f}{(\delta_n^2+f^2)}V_n\\ y_n&=\frac{1}{M}\left(\frac{1}{u_0\beta_e D}\right)\frac{1}{(\delta_n^2+f^2)}V_n\end{aligned}\right\} n=1,2,3, \tag{12}$$

where

$$M\equiv\frac{u_0\beta_e D}{\eta\Phi'},\quad f\equiv\frac{\eta B}{u_0\beta_e D},$$

and the δ_n's satisfy the relationship

$$1=(j\delta_n-b)(\delta_n^2+f^2). \tag{13}$$

Let the subscript 1 refer to the growing wave or the wave for which δ_n has a positive, real part. For the fourth wave Eqs. (12) and (13) do not hold but Eq. (10) does. Using the relationship $\Gamma=j\beta_e$ and making the small D approximation in Eq. (10) gives

$$y_4=-\frac{b}{Mu_0\beta_e D}V_4. \tag{14}$$

From Eq. (3) it is apparent

$$\dot{y}_4=0. \tag{15}$$

From Eqs. (2) and (11) we obtain

$$\dot{x}_4=-\frac{\Phi'}{B}V_4=-\frac{1}{fM}V_4. \tag{16}$$

Let V_b, $\dot{y}_b$, $\dot{x}_b$, and y_b represent the ac quantities on the circuit and beam at the helix input. Then

$$\begin{aligned}V_1+V_2+V_3+V_4&=V_b,\\ \dot{y}_1+\dot{y}_2+\dot{y}_3+\dot{y}_4&=\dot{y}_b,\\ \dot{x}_1+\dot{x}_2+\dot{x}_3+\dot{x}_4&=\dot{x}_b,\\ y_1+y_2+y_3+y_4&=y_b.\end{aligned} \tag{17}$$

Using Eqs. (12), (14), (15), and (16) in Eqs. (17) and solving for V_1, the voltage at $z=0$ in the growing wave, we have

$$\begin{aligned}V_1=\frac{\delta_1^2+f^2}{(\delta_1-\delta_2)(\delta_1-\delta_3)}\Bigg[&V_b-M(\delta_2+\delta_3)\dot{y}_b\\ &-\frac{M}{f}\left(\delta_2\delta_3-f^2-\frac{\delta_2\delta_3}{bf^2+1}\right)\dot{x}_b+\frac{M}{f}\eta B\frac{\delta_2\delta_3}{bf^2+1}y_b\Bigg].\end{aligned} \tag{18}$$

NOISE EXCITATION OF GROWING WAVES

Fluctuations in V_b are due to thermal noise voltage applied to the helix input. This noise is uncorrelated with the noise originating in the beam. Hence as far as this source is concerned $\dot{y}_b=\dot{x}_b=y_b=0$. From Eq. (18) we may write for the initial mean square fluctuations in the voltage of the growing wave due to input thermal noise

$$\langle V_{1t}^2\rangle_{Av}=\left|\frac{\delta_1^2+f^2}{(\delta_1-\delta_2)(\delta_1-\delta_3)}\right|^2\langle V_b^2\rangle_{Av}. \tag{19}$$

As was previously stated the a plane ($z'=0$) is a cathode image plane. Let l be the distance between this plane and the circuit input. Fluctuations in $\dot{y}$, $\dot{x}$, and y at $z'=0$ will be treated as three uncorrelated sources of noise.† Let these fluctuations be designated by the subscript a. Consider the fluctuations in $\dot{y}_a$ only. Over the distance l these fluctuations are converted into correlated fluctuations in $\dot{y}_b$, $\dot{x}_b$, and y_b in accordance with Eqs. (9). Using Eqs. (9) and (18) we obtain for

[2] Reference 1, Chap. XIII.

† This is strictly true only for an uncollimated beam. The action of the collimator produces some degree of correlation which will be ignored in this treatment.

the initial mean square fluctuations in the voltage of the growing wave due to this noise source

$$\langle V_{1y}^2\rangle_{Av}=\left|\frac{\delta_1^2+f^2}{(\delta_1-\delta_2)(\delta_1-\delta_3)}\right|^2 M^2\langle \dot{y}_a^2\rangle_{Av} \times\left|\frac{1}{f}(\delta_2\delta_3-f^2)\sin\beta_m l-(\delta_2+\delta_3)\cos\beta_m l\right|^2. \quad (20)$$

Following the same procedure with respect to fluctuations in $\dot{x}_a$ and y_a we obtain

$$\langle V_{1x}^2\rangle_{Av}=\left|\frac{\delta_1^2+f^2}{(\delta_1-\delta_2)(\delta_1-\delta_3)}\right|^2 M^2\langle \dot{x}_a^2\rangle_{Av} \times\left|\frac{1}{f}(\delta_2\delta_3-f^2)\sin\beta_m\left(l-\frac{\lambda_m}{4}\right)-(\delta_2+\delta_3) \times\cos\beta_m\left(l-\frac{\lambda_m}{4}\right)+\frac{1}{f}\left(\frac{\delta_2\delta_3}{bf^2+1}\right)\right|^2, \quad (21)$$

$$\langle V_{1w}^2\rangle_{Av}=\left|\frac{\delta_1^2+f^2}{(\delta_1-\delta_2)(\delta_1-\delta_3)}\right|^2 M^2u_0^2\beta_e^2D^2\langle y_a^2\rangle_{Av} \times\left|\frac{\delta_2\delta_3}{bf^2+1}\right|^2, \quad (22)$$

where

$$\lambda_m\equiv 2\pi/\beta_m.$$

THE MAGNITUDE OF THE MEAN SQUARE NOISE FLUCTUATIONS AND THE NOISE FIGURE

The noise figure of the amplifier can be written as

$$F=1+\frac{\langle V_{1y}^2\rangle_{Av}+\langle V_{1x}^2\rangle_{Av}+\langle V_{1w}^2\rangle_{Av}}{\langle V_{1i}^2\rangle_{Av}}. \quad (23)$$

We have yet to determine $\langle V_b^2\rangle_{Av}$, $\langle \dot{y}_a^2\rangle_{Av}$, $\langle \dot{x}_a^2\rangle_{Av}$, and $\langle y_a^2\rangle_{Av}$ in Eqs. (19), (20), (21), and (22), respectively, before the noise figure expression will be resolved.

The gain parameter D is defined as follows

$$D^3\equiv\frac{(\Phi' V)^2}{2\beta_e^2 P}\frac{I_0}{4V_0}. \quad (24)$$

In the case of thermal noise, the power can be written

$$P_t=kT\Delta f, \quad (25)$$

where

k = Boltzmann's constant,
T = circuit temperature in degrees Kelvin taken to be 290°K,
Δf = band width.

For this case the voltage becomes

$$\frac{V^2}{2}=\langle V_b^2\rangle_{Av}. \quad (26)$$

From Eqs. (24), (25), and (26), we obtain

$$\langle V_b^2\rangle_{Av}=\frac{4V_0\beta_e^2D^3kT\Delta f}{I_0\Phi'^2}. \quad (27)$$

Expressions for $\langle \dot{y}_a^2\rangle_{Av}$, $\langle \dot{x}_a^2\rangle_{Av}$, and $\langle y_a^2\rangle_{Av}$, are readily determined by applying the central limit theorem of statistics and a theorem, recently enunciated by MacDonald,[3] relating the frequency distribution of noise to its temporal behavior. The central limit theorem may be stated as follows: "If a population has a finite variance σ^2 then the distribution of the sample mean approaches the normal distribution with variance σ^2/N as the sample size N increases."[4] To derive an expression for $\langle \dot{y}_a^2\rangle_{Av}$ let us consider the electrons of a beam which are emitted from the cathode during a relatively large time interval τ. Let $\langle \delta\dot{y}^2\rangle_{Av}$ be the variance or the mean square deviation from the average y directed component of velocity. According to the central limit theorem the sample variance, or the mean square fluctuation in velocity taken over the time interval τ, is

$$\langle \dot{y}_\tau^2\rangle_{Av}=\frac{\langle \delta\dot{y}^2\rangle_{Av}}{\bar{n}\tau},$$

where $\bar{n}$ is the average number of electrons emitted per second. MacDonald's theorem gives for the frequency distribution corresponding to $\langle \dot{y}_\tau^2\rangle_{Av}$ the following

$$\langle \dot{y}_f^2\rangle_{Av}=\Delta f 4\pi f\int_0^\infty\frac{\partial}{\partial\tau}(\tau^2\langle \dot{y}_\tau^2\rangle_{Av})\sin 2\pi f\tau d\tau,$$

or

$$\langle \dot{y}_f^2\rangle_{Av}=\Delta f\frac{2}{\bar{n}}\langle \delta\dot{y}^2\rangle_{Av}=\frac{2e\Delta f}{I_0}\langle \delta\dot{y}^2\rangle_{Av}.$$

Since the a plane is the plane of the cathode image we have

$$\langle \dot{y}_a^2\rangle_{Av}=\langle \dot{y}_f^2\rangle_{Av}=\frac{2e\Delta f}{I_0}\langle \delta\dot{y}^2\rangle_{Av}. \quad (28)$$

The procedure in the derivation of both $\langle \dot{x}_a^2\rangle_{Av}$ and $\langle \dot{y}_a^2\rangle_{Av}$ is identical to the above. Hence we may write

$$\langle \dot{x}_a^2\rangle_{Av}=\frac{2e\Delta f}{I_0}\langle \delta\dot{x}^2\rangle_{Av}, \quad (29)$$

$$\langle y_a^2\rangle_{Av}=\frac{2e\Delta f}{I_0}\langle \delta y^2\rangle_{Av}. \quad (30)$$

Expressions for the three variances $\langle \delta\dot{y}^2\rangle_{Av}$, $\langle \delta\dot{x}^2\rangle_{Av}$ and $\langle \delta y^2\rangle_{Av}$ are obtained from integrals involving the distribution functions for $\dot{y}$, for $\dot{x}$, and for y, respectively. Consider $\langle \delta\dot{y}^2\rangle_{Av}$ for the case of an uncollimated beam.

[3] D. K. C. MacDonald, Phil. Mag. **40**, 561 (1949).
[4] A. M. Mood, *Introduction to the Theory of Statistics* (McGraw-Hill Book Company, Inc., New York, 1950), p. 136.

The Maxwellian distribution is

$$\left(\frac{m}{2\pi kT_c}\right)^{\frac{1}{2}} \exp\left(-\frac{m}{2kT_c}\dot{y}^2\right).$$

Since the average y-directed velocity is zero, we have

$$\langle \delta\dot{y}^2\rangle_{Av}=\int_{-\infty}^{\infty}\dot{y}^2\left[\left(\frac{m}{2\pi kT_c}\right)^{\frac{1}{2}}\exp\left(-\frac{m\dot{y}^2}{2kT_c}\right)\right]d\dot{y}$$

$$=\frac{kT_c}{m}. \tag{31}$$

A simple, but approximate, way for taking into account the effect of a collimator is to assume that a collimated beam possesses the same distribution function for $\dot{y}$ as does an uncollimated beam (that is, the Maxwellian distribution function) but that the upper limit of $|\dot{y}|$ is finite rather than infinite. This would be strictly true only for a beam emitted from a cathode of zero width which is precisely centered with respect to the upper and lower faces of the collimator. For a cathode whose width is at least as great as the width of the collimator as in Fig. 1 the distribution function is changed by the collimator. For example, all electrons from such a cathode which are emitted at $y=\pm w/2$ (see Fig. 1) and for which $\dot{y}\neq 0$ would be intercepted by the collimator. Hence, the assumption of the Maxwellian velocity distribution implies a properly centered cathode of zero width and, as far as $\dot{y}$ is concerned, ascribes to the collimator less effectiveness than it actually has in intercepting the high transverse velocity electrons. Under such an assumption the maximum value of $|\dot{y}|$ for a collimated beam is that for which the radius of the helical electron path is $w/2$. Hence

$$|\dot{y}|_{\max}=\frac{\eta Bw}{2}$$

and

$$\langle \delta\dot{y}^2\rangle_{Av}=\int_{-(\eta Bw/2)}^{+(\eta Bw/2)}\dot{y}^2\left[\left(\frac{m}{2\pi kT_c}\right)^{\frac{1}{2}}\exp\left(-\frac{m\dot{y}^2}{2kT_c}\right)\right]d\dot{y}$$

$$=\frac{kT_c}{m}Y, \tag{32}$$

where

$$Y\equiv\frac{4}{\sqrt{\pi}}\int_0^{eBw/(8mkT_c)^{\frac{1}{2}}}\alpha^2e^{-\alpha^2}d\alpha.$$

A similar procedure can be followed in determining $\langle \delta\dot{x}^2\rangle_{Av}$. To simplify the analysis we again take as our model a line cathode of zero width located in the x z plane. The electrons are emitted with a Maxwellian x-directed velocity distribution. The effect of the collimator under these conditions is to limit the maximum value of $|\dot{x}|$ to that for which the radius of the helical electron path is $w/4$. Hence

$$\langle \delta\dot{x}^2\rangle_{Av}=\int_{-(\eta Bw/4)}^{\eta Bw/4}\dot{x}^2\left[\left(\frac{m}{2\pi kT_c}\right)^{\frac{1}{2}}\exp\left(-\frac{m\dot{x}^2}{2kT_c}\right)\right]d\dot{x}$$

$$=\frac{kT_c}{m}X, \tag{33}$$

where

$$X\equiv\frac{4}{\sqrt{\pi}}\int_0^{eBw/(32mkT_c)^{\frac{1}{2}}}\alpha^2e^{-\alpha^2}d\alpha.$$

The line cathode assumption in this case involves a somewhat different approximation than in the case for $\langle \delta\dot{y}^2\rangle_{Av}$. In an actual cathode whose width is not zero there are some electrons having an $|\dot{x}|$ greater than the assumed $|\dot{x}|_{\max}$ which nevertheless pass through the collimator. For example, electrons having helical paths of radii as high as $w/2$ may pass through if emitted from positions for which $y=\pm w/2$. On the other hand, many electrons having an $|\dot{x}|$ less than the assumed $|\dot{x}|_{\max}$, and therefore presumed to pass through, actually would be intercepted by the collimator in the case of emission from a wide cathode. Hence these two differences affect the approximation in reverse ways and therefore tend to cancel each other.

It should be pointed out that the procedure of considering $\langle \delta\dot{y}^2\rangle_{Av}$ and $\langle \delta\dot{x}^2\rangle_{Av}$ on a separate basis involves further approximation if the beam is collimated. For example, such a procedure implies that all electrons for which both $|\dot{y}|\leq|\dot{y}|_{\max}$ and $|\dot{x}|\leq|\dot{x}|_{\max}$ are not intercepted by the collimator. However, in actuality any electron for which $|\dot{y}|=|\dot{y}|_{\max}$ and $\dot{x}\neq 0$ will be intercepted. Hence again in this respect the analysis assumes a less well collimated beam than would be the actual beam.

The distribution function for the y position of the emitted electrons is the reciprocal of the width of the cathode. The average y position is the cathode center line, or the line for which $y=0$ in Fig. 1. No electron emitted at $|y|>w/2$ can pass through the collimator. Thus if we neglect the transverse motion of the electrons the effective distribution function for a collimated beam is $1/w$. Hence

$$\langle \delta y^2\rangle_{Av}=\int_{-w/2}^{w/2}y^2\frac{1}{w}dy=\frac{w^2}{12}. \tag{34}$$

For an actual beam $\langle \delta y^2\rangle_{Av}$ is less than this because the transverse motion of the electrons makes it less probable that electrons emitted near $y=\pm w/2$ will be passed by the collimator than electrons emitted near $y=0$.

Note that the use of Eq. (10) is precisely correct only when the undisturbed position of all the electrons is the position of purely transverse field. Since the field can be purely transverse only along a surface this implies a thin beam. However, for reasonable beam thicknesses the equations still are valid to good approximation.

We now have sufficient information to complete the noise figure expression. $\langle V_b^2\rangle_{Av}$, $\langle \dot{y}_a^2\rangle_{Av}$, $\langle \dot{x}_a^2\rangle_{Av}$, and $\langle y_a^2\rangle_{Av}$ are determined from Eqs. (27), (28), (29), (30), (32), (33), and (34). These quantities in turn complete the expressions for $\langle V_{1\epsilon}^2\rangle_{Av}$, $\langle V_{1y}^2\rangle_{Av}$, $\langle V_{1x}^2\rangle_{Av}$, and $\langle V_{1w}^2\rangle_{Av}$ as given by Eqs. (19), (20), (21), and (22), respectively. Entering this information into Eq. (23) and simplifying gives

$$F=1+\frac{T_e}{T}\frac{1}{D}YL_y+\frac{T_e}{T}\frac{1}{D}XL_x+\beta_e^2D\frac{eV_0}{kT}\frac{w^2}{6}\left|\frac{\delta_2\delta_3}{bf^2+1}\right|^2, \quad (35)$$

where

$$L_y\equiv\left|\frac{1}{f}(\delta_2\delta_3-f^2)\sin\beta_m l-(\delta_2+\delta_3)\cos\beta_m l\right|^2,$$

$$L_x\equiv\left|\frac{1}{f}(\delta_2\delta_3-f^2)\sin\beta_m\left(l-\frac{\lambda_m}{4}\right)\right.$$

$$\left.-(\delta_2+\delta_3)\cos\beta_m\left(l-\frac{\lambda_m}{4}\right)+\frac{1}{f}\left(\frac{\delta_2\delta_3}{bf^2+1}\right)\right|^2.$$

EVALUATION OF L_y AND L_x FOR LARGE f AND NEGLIGIBLE LOSS

Under the conditions of f greater than 3 and negligible circuit loss certain approximate expressions for the δ_n's may be used to simplify the noise figure calculations (and incidentally calculations of gain and other amplifier characteristics). Since noise figure decreases with increasing f and decreasing circuit loss the above conditions are desirable in low noise amplifiers.

Under these conditions, the electron velocity for maximum gain is represented by a value of b very nearly equal to f. The corresponding δ_n's are

$$\delta_1=\frac{1}{(2f)^{\frac{1}{2}}}-jf, \quad \delta_2=-\frac{1}{(2f)^{\frac{1}{2}}}-jf, \quad \delta_3=jf. \quad (36)$$

Using Eqs. (36) in the defining expressions for L_y and L_x we obtain

$$L_y=L_x=\frac{1}{2f}. \quad (37)$$

For L_y this follows exactly from Eqs. (36), while for L_x a term of the order of $1/f^2$ has been neglected in comparison with $1/(2f)^{\frac{1}{2}}$.

A SAMPLE CALCULATION ILLUSTRATING THE EFFECT OF THE COLLIMATOR

Consider a low noise amplifier being worked on at Stanford. It is designed to operate with a center frequency of 1000 mcs, a beam current of 1 ma, a beam voltage of 600 volts, and a magnetic focusing field of 0.01 weber per square meter. The collimator width is 0.004 in. (10.16×10^{-5} meter). The slow wave circuit has a transverse impedance parameter ($E_y^2/2\beta^2P$) of 170 ohms. Neglect the circuit losses. Let us take T_c/T to be 3.5 (for the oxide cathode). We obtain for D and f

$$D=\left(\frac{E_y^2}{2\beta^2P}\frac{I_0}{4V_0}\right)^{\frac{1}{3}}=0.0415,$$

$$f=\frac{\beta_m}{\beta_e D}=\frac{\eta B}{\omega D}=6.74.$$

Hence

$$L_y=L_x=\frac{1}{2f}=0.074.$$

For Y and X we have

$$Y=\frac{4}{\sqrt{\pi}}\int_0^{0.508}\alpha^2\exp(-\alpha^2)d\alpha$$

$$=\operatorname{erf}\alpha\Big|_0^{0.508}-\frac{2}{\sqrt{\pi}}\alpha\exp(-\alpha)^2\Big|_0^{0.508}=0.086,$$

$$X=\frac{4}{\sqrt{\pi}}\int_0^{0.254}\alpha^2\exp(-\alpha^2)d\alpha=0.012.$$

Entering Eq. (35) with the above quantities and the relations of Eqs. (36) we have

$$F=1+0.537+0.075+0.007$$

or 2 db. Note that the term resulting from the fluctuations in the transverse positions of the electrons due to the finite thickness of the beam is very small compared with the other terms.

If the collimator is removed $Y=X=1$ and the two terms due to the fluctuations in the transverse velocity components both become 6.25, giving a noise figure of greater than 11 db.

CONCLUSIONS

The noise analysis for the case of a purely transverse-field traveling-wave tube indicates that low noise figures are possible only when the beam is well collimated. For an uncollimated beam the noise figure is worse than that of conventional longitudinal field traveling-wave tubes using velocity-jump noise reduction.[5]

[5] D. A. Watkins, Proc. Inst. Radio Engrs. **40**, 65 (1952).

Measurement of Temperatures in Flames of Complex Structure by Resonance Line Radiation. I. General Theory and Application to Sodium Line Reversal Methods

H. M. Strong and F. P. Bundy
Research Laboratory, General Electric Company, Schenectady, New York
(Received February 24, 1954)

Sodium line reversal temperature measurement by low resolving power spectroscopic instruments on complex flame structures gives temperatures intermediate between the highest and lowest temperature in the line of sight. This intermediate temperature is determined by the temperatures, optical depths and arrangement of the individual zones. By taking into account these factors, it is possible to derive temperatures for the inner zones of a complex flame. The theory, numerical data needed to apply the theory, and experimental examples are given.

1. INTRODUCTION

IN the sodium line reversal* method of flame temperature measurement, a narrow beam of light from a source of bright continuous radiation is passed through the flame which must contain sodium vapor (or some other element having a resonance spectral line in an observable region of the spectrum) and finally onto the slit of a spectroscope. When the background radiation is adjusted to a brightness temperature which is the same as the flame temperature the resonance lines match in brightness with the continuous background. This condition is expressed by the following equation:

$$E_{(\text{lamp})} = E_{(\text{flame})} + (1-A)E_{\text{flame lamp}}, \quad (1)$$

in which E refers to brightness and A refers to fraction of incident radiation absorbed.

The SLR method of flame temperature measurement has been used for about 50 years. The basis for line reversal temperature measurement was discovered in 1857 when Kirchhoff announced the famous laws of thermal radiation bearing his name, as a result of his observations on the reversal of the D lines in the solar spectrum. Practical use of the Kirchhoff law was made by Ch. Féry in 1903[1] who applied it in the measurement of flame temperature by what has come to be called the sodium line reversal method or more generally the line reversal method, since any resonance spectral line can be used for this type of measurement. For flame gases whose various degrees of freedom are in thermal equilibrium, it has been established through the exhaustive work of H. Kohn[2] in 1914 and later by the work of Griffiths and Awbery,[3] that the sodium line reversal method does give the correct flame temperature. The method is now widely used.

What has not been understood about the SLR method is how to interpret its results when the various flame zones in the path of the measuring beam differ from one another in temperature. A good example of a flame having distinct temperature zones is illustrated in Fig. 1 which is a photograph of a rocket motor supersonic flame taken with the D line radiation. In a flame of this type an SLR measurement of temperature on the bright inner zones will be influenced by the cooler zones surrounding it. Griffiths and Awbery[3] demonstrated that SLR temperature readings were influenced by all the different temperature zones in the path of the measuring beam. Lewis and Von Elbe[4] pointed out the need for adding the sodium vapor only to the individual zone whose temperature is to be measured.

Because the results of SLR temperature measurement depend on the shapes of the resonance line intensity contours of the various parts of the flame, the discussion will start with a brief account of sodium D line contours.†

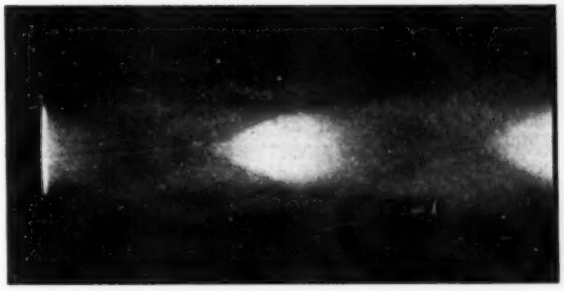

FIG. 1. Photograph of a rocket motor liquid oxygen-alcohol flame in sodium D line radiation. Motor body and nozzle are to the left. Diameter of nozzle exit is three inches.

* Sodium line reversal will be referred to by the symbol SLR throughout this paper.

[1] Ch. Féry, Compt. rend. **137**, 909 (1903).

[2] H. Kohn, Ann. Physik **44**, 749 (1914).

[3] E. Griffiths and J. H. Awbery, Proc. Roy. Soc. (London) **123**, 401 (1929).

[4] B. Lewis and G. Von Elbe, J. Appl. Phys. **11**, 698 (1940).

† Various phases of this work have been previously described by the authors in General Electric Company, Schenectady, New York, Project Hermes Reports as follows: "The Theoretical Shapes and Intensities of Sodium Lines from Flames of Complex Structure" F. P. Bundy and H. M. Strong, Rpt. No. 55 275, September, 1948; "Measurement of Gas Pressures in the Exhaust Flames of Rocket Motor by a Spectroscopic Method" Bundy, Gregg, and Strong, Rpt. No. 55 270, September, 1948.

"The Measurement of Temperature in Complex Flame Structures by Sodium Line Reversal Method" Strong, Bundy, and Larson, Rpt. No. 49A0517, August, 1949; See also papers by Bundy, Strong, and Larson in the book *Third Symposium on Combustion Flame and Explosion Phenomena* (Williams and Wilkins Company, Baltimore, 1949), pp. 641–654. Two papers were presented at June 16–18, 1949 meeting of The American Physical Society at Cambridge, Massachusetts. "Measurement of

2. THERMALLY EXCITED RESONANCE LINE CONTOURS

An outline of the general theory of the intensity contour of a sodium D line has been given in a previous paper, Bundy *et al.*[5] This theory is briefly summarized here. The expression given for the intensity contour of a resonance spectral line from a flame was

$$I(\Delta\lambda)=E_b(\lambda,T)\{1-\exp[-zsf(\Delta\lambda)]\}, \qquad (2)$$

where $E_b(\lambda,T)$ is the emissive power (or brightness) of a blackbody whose temperature is the same as that of the flame. z is the optical depth of the flame at the center of the resonance line ($\Delta\lambda=0$) and sf is the line shape factor. z is proportional to the concentration of sodium atoms and to the path length through the flame. Approximately 10^{13} sodium atoms per cm^2 in the line of sight gives an optical depth of unity for the D_2 line. For flames at extremely low pressure where collisions between the optically active atoms and flame gas molecules do not influence the line shape, the shape factor sf is the doppler broadening of the spectral line.

$$sf_{dopp}=\exp[-\ln 2((\Delta\lambda)^2/W^2_{dopp})].$$

In this expression W_{dopp} is the half-width at the half-intensity level of a spectral line from a very thin flame or one of very low "optical depth" in which absorption broadening does not influence the line shape. The other factor influencing sf is the effect of collisions between optically active atoms and flame gas molecules while the atom is either radiating or absorbing radiation. The shape factor for collision broadening is given by

$$sf_{coll}=\frac{W^2_{coll}}{W^2_{coll}+(\Delta\lambda)^2}.$$

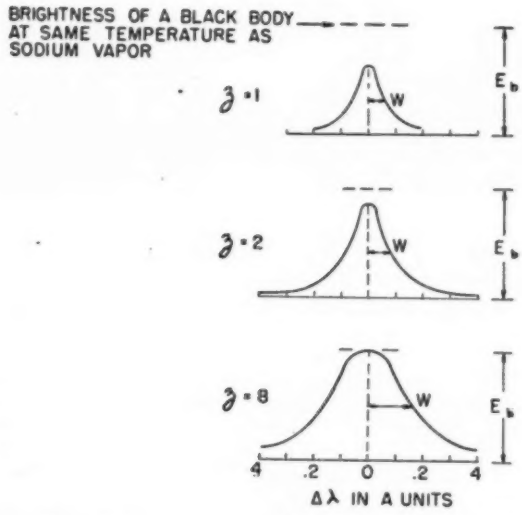

FIG. 2. Intensity contours of sodium D line for three different values of optical depth.

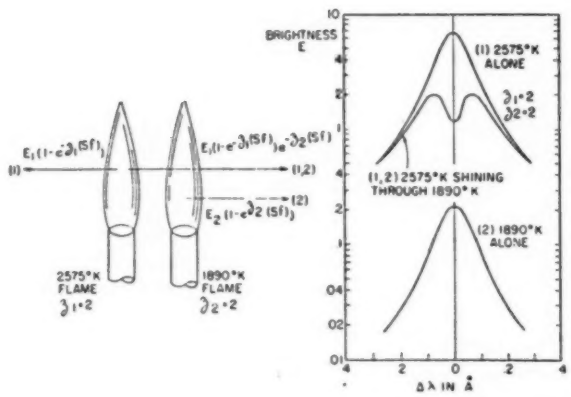

FIG. 3. Sodium D line intensity contours from two flames burning at two different temperatures and from a hot flame as seen through a cooler flame.

This collision factor is usually more influential in determining the shape of a resonance line from flames at atmospheric pressure or above than is the Doppler factor. However, both factors were taken into account in determining the shapes of lines from flames at different temperatures.

The significance of Eq. (2) is illustrated in Fig. 2 in which intensity contours of a sodium D line are plotted for three different values of the optical depth z. In these intensity contour plots, sf was taken to be exclusively of the collision type.

In a flame where the sodium atoms are thermally excited, the brightness of the D lines can never exceed that corresponding to a blackbody whose temperature is the same as the flame temperature. Thus, as the amount of sodium in the line of sight is increased, the center of the D line reaches blackbody brightness first and as the sodium density is further increased the intensity in the wings of the line approach this same brightness.

These characteristics of the intensity contours of the D lines apply for both emission and absorption of radiation.

3. SODIUM D LINE INTENSITY CONTOURS IN COMPLEX FLAMES

When the radiation from a region of sodium vapor having optical depth z_1 and uniform temperature T_1 passes through another zone of optical depth z_2 and temperature T_2, the D line intensity contours have quite a different appearance than for either of these two regions taken separately. This is illustrated in Fig. 3 for the case of two uniform flames; flame 1 burning at 2575°K and shining through flame 2 burning at 1890°K. The radiation from flame 1 is selectively transmitted through flame 2 and when this modified flame 1 radiation is added to flame 2 radiation, the result is the dimpled contour illustrated.

The intensity contour of the radiation from both flames is given by an expression in which the intensity of radiation from flame 1 is multiplied by the selective

---

Temperatures in Complex Flame Structures by High Resolution Spectroscopy of the Sodium D Lines, I" by F. P. Bundy, and "II" by H. M. Strong.

[5] Bundy, Strong, and Gregg, J. Appl. Phys. **22**, 1069 (1951).

transmission factor of flame 2 and added to the intensity of radiation from flame 2. The selective transmission factor of flame 2 is $\exp[-z_2 sf]$. The equation for the distribution of intensity in the dimpled contour is

$$I(\Delta\lambda)=E_1\{1-\exp[-z_1 sf]\}\exp[-z_2 sf] + E_2\{1-\exp[-z_2 sf]\}, \quad (3)$$

where E_1 and E_2 are the blackbody brightnesses in the neighborhood of 5893 A corresponding to the true temperatures of flames 1 and 2, respectively.

This effect is further illustrated in Fig. 4 for an actual case of a flame at 2575°K (vertical interference pattern) shining through a second flame burning at 1890°K (slanting pattern). The optical arrangement for obtaining the interference pattern is illustrated in Fig. 4(a). A plain photograph of flames in sodium D line radiation only is shown in Fig. 4(b) and the interference patterns obtained in Fig. 4(c). The interferometer used was adjusted so that the two D lines were superimposed (see reference 5). Each interference fringe represents the intensity contour resulting from superimposing the D_1 line on the D_2 line.

The D_2 line has an optical depth twice as great as the D_1 line. Hence when the D lines are superimposed in this manner, the effective optical depth is intermediate between z_{D_1} and z_{D_2}. This will be explained further in Part II.[6]

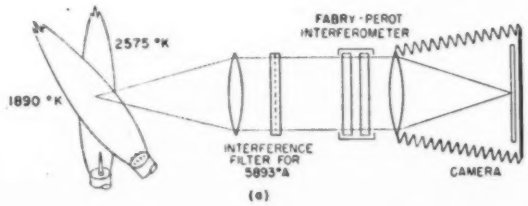

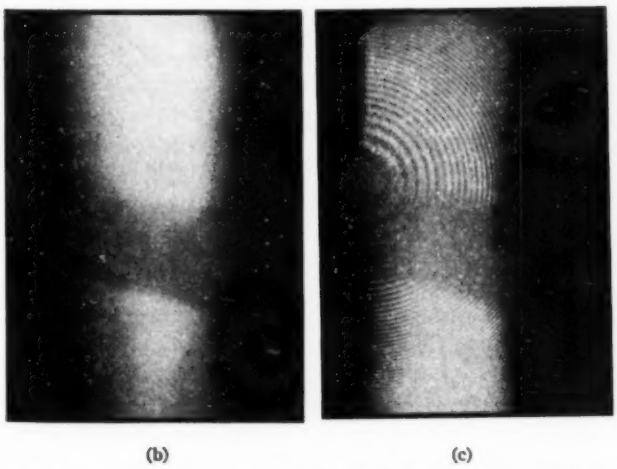

FIG. 4. Interference pattern for a 2575°K flame shining through an 1890° flame. (a) Optical arrangement, (b) photo of flames taken in D line radiation, without interferometer, (c) interference pattern of flames as photographed through Fabry-Perot interferometer.

[6] See H. M. Strong and F. P. Bundy, J. Appl. Phys. **25**, 1527 (1954), following paper.

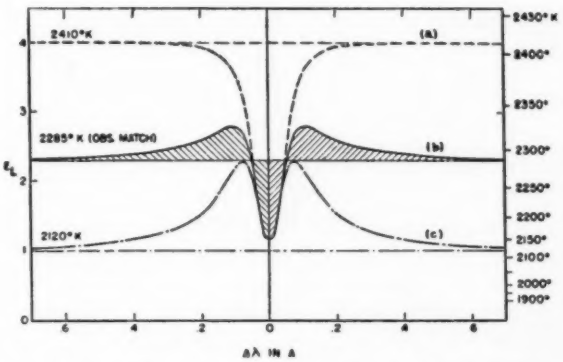

FIG. 5. Theoretical intensity distribution in a SLR observation of temperature on two flames in series each of optical depth 2 burning at 1890°K and at 2575°K. The 1890°K flame was closer to the spectroscope with the hotter flame directly behind it: (a) Background too bright, (b) D lines appear to match background if resolution of lines is poor, (c) background is weaker than D lines.

The effects illustrated here cannot be observed unless the resolving power, $\lambda/\Delta\lambda$, of the spectroscopic instrument is of the order of at least 10^5. A Fabry-Perot type interferometer having a resolving power of this magnitude was used in this work.

4. SODIUM LINE REVERSAL PHENOMENA IN COMPLEX FLAMES

In the case of a uniform flame, SLR matching condition exists between the background and the D lines at every point on the intensity contour of both D lines when the background brightness temperature is equal to the flame temperature. This is the result of the fact that every point on the D line contour is emitted by the flame to exactly the same extent that it absorbs radiation out of the background.

When the flame is complex in its temperature structure, the preceding statement no longer applies. Then what is observed in the low resolving power spectroscope normally used in SLR work is an intermediate matching temperature resulting from the spreading and blending of the detailed structure of the D lines. This will be described in more detail.

First, consider an SLR measurement on the two flames already referred to in Fig. 3. The intensity contour resulting from passage of radiation from say a tungsten ribbon lamp through both of these flames is given by the following expression:

$$I(\Delta\lambda)=E_l\exp[-(z_1+z_2)sf] + E_1\{1-\exp[-z_1 sf]\}\exp[-z_2 sf] + E_2\{1-\exp[-z_2 sf]\}. \quad (4)$$

E_l is the blackbody brightness of the tungsten ribbon lamp, E_1, E_2, etc. have the same meaning as in Eq. (3). The condition for an SLR match in a low resolving power instrument is that the total radiant energy observed in the region of the D lines is equal to the total radiant energy in the background in this same region.

This condition is expressed in the following equation:

$$\int_{\Delta\lambda=0}^{\infty} E_l d\lambda = \int_{\Delta\lambda=0}^{\infty} I(\Delta\lambda) d\lambda. \tag{5}$$

For practical purposes the upper limit of integration is the limit beyond which the D lines are not observable, usually one angstrom unit from the line center.

Typical SLR intensity patterns are illustrated in Fig. 5 for background brightnesses corresponding to 2120, 2285 and 2410°K. In curve (a) the background is decidedly too bright so that a distinct dark line would be observed. In curve (c) the background is decidedly too weak and the D line stands out bright against it. In curve (b) the wings of the D line are above background level while the center is below the background level, and the amount of over-intensity is almost exactly offset by the amount of under-intensity. The SLR spectroscope does not reveal all the detail shown here, but it does show conditions (a) and (c) as nonmatching and condition (b) as matching because the over and under intensities become lumped together.

In tests on flames of the type described, the observed SLR match point on ordinary SLR apparatus was 2285°K, agreeing with the theoretical value very closely.

This description for the simple example of two zones of temperature shows how the theory of sodium line intensity contours may be applied to analyzing SLR results in complex flame structures. The analysis will now be made more general and this will lead to the description for a method of measurement in complex flames to be given in the next section.

Equation (5) may be modified so that factors of the form $\exp[-zsf]$ do not appear but are replaced by factors of the form $\{1-\exp[-zsf]\}$. For example, Eq. (5) applying to two flames can be written in the following manner:

$$E_l \int_0^{\infty} d\lambda = \frac{\int_0^{\infty} (E_1[\{1-\exp[-(z_1+z_2)sf]\}-\{1-\exp[-z_2sf]\}]+E_2\{1-\exp[-z_2sf]\})d\lambda}{\int_0^{\infty}\{1-\exp[-(z_1+z_2)sf]\}d\lambda}. \tag{6}$$

The terms $\int_0^{\infty}\{1-\exp[-zsf]\}d\lambda$ have been evaluated for sfs for combinations of Doppler and collision type factors appropriate to flames of different temperatures at atmospheric pressure. The results of these integrations are given in Fig. 6.

Referring to the appropriate curve, the values of

$$\int_0^{\infty}\{1-\exp[-(z_1+z_2)sf]\}d\lambda$$

and

$$\int_0^{\infty}\{1-\exp[-z_2sf]\}d\lambda$$

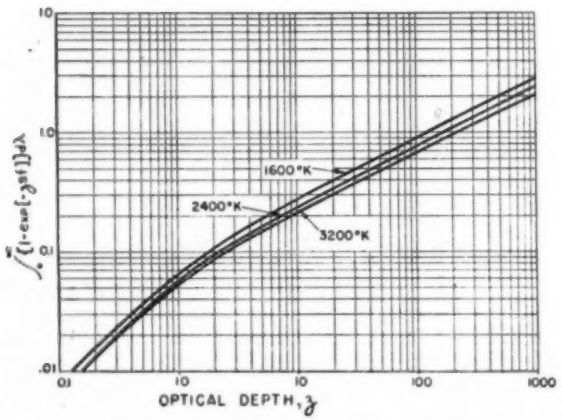

FIG. 6. $\int_0^{\infty}\{1-\exp[-zsf]\}d\lambda$ plotted as a function of z for ambient flame pressure of one atmosphere (absolute) and temperatures of 1600, 2400, and 3200°K.

may be obtained and substituted in Eq. (6). Calling these values A and B respectively, Eq. (6) becomes,

$$E_l = \frac{E_1(A-B)+E_2B}{A}. \tag{7}$$

A flame having a cool outer shell and hot inner core is illustrated in Fig. 7. Analysis of SLR in this flame leads to the equation,

$$E_l = \frac{E_2(X-Y)+E_1(Y-Z)+E_2Z}{X}, \tag{8}$$

$$X = \int_0^{\infty}\{1-\exp[-(z_1+2z_2)sf]\}d\lambda,$$

$$Y = \int_0^{\infty}\{1-\exp[-(z_1+z_2)sf]\}d\lambda,$$

$$Z = \int_0^{\infty}\{1-\exp[-z_2sf]\}d\lambda.$$

Following this reasoning, similar equations can be written for flames having more than two zones. If zones are unsymmetrically located in the flame, it is necessary to allow for the lack of symmetry by appropriate assignment of z values. In a given zone, the value of z is proportional to the length of path in the zone.

The concentration of sodium vapor in a complex flame influences the intermediate temperature result obtained

by SLR only when the concentration is very low. This can be shown by use of Eq. (8). Consider a flame like that shown in Fig. 7(a) whose core is 2575°K and outer shell at 1890°K. With an optical depth ratio, core to shell, of $z_1/z_2=4$. Substitution of different values of z_1 and z_2 and solving for the value of E_l, the blackbody brightness of a comparison lamp that will produce an effective SLR match, shows that at very low values of z_2, E_l at first declines with increase of z_2 then remains constant with further increases, as shown in the graph in Fig. 7(b).

5. EXPERIMENTAL PART

Equation (7) has been tested on two flames in an optical arrangement designed to measure the temperatures of the flames separately and in combination, with the hot flame behind the cool flame, by an ordinary SLR test. Simultaneously the optical depths of the flames were measured by obtaining the highly resolved D lines

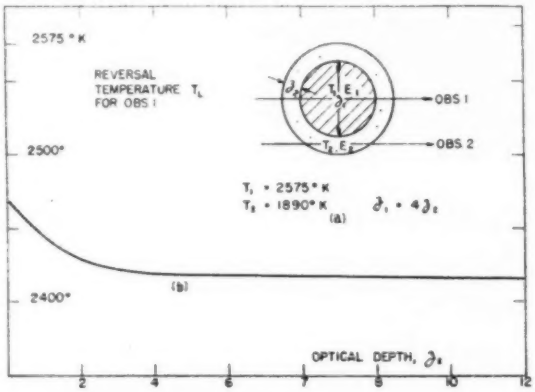

FIG. 7. Theoretical values of the SLR temperature on a complex flame as a function of optical depth. (a) Cross section of flame. (b) Graph of temperature τs optical depth of outer zone z_2 by observation 1.

resulting from a sodium vapor lamp‡ shining through the flames.

The optical arrangement is shown in Fig. 8(a). The horizontal optical train is an SLR apparatus. A carbon arc illuminates an optical density wedge which is imaged first between the two flames and then again on the photographic plate in the spectrograph camera. The wedge gradient is parallel to the slit so that somewhere along the sodium lines, which come from the flame radiation, a match between sodium lines and carbon arc background is obtained. A SLR spectrogram is reproduced in Fig. 8(b). An arrow points to the match point. The arrangement for measuring optical depths is represented in the slanting optical train. It consists of an SVL, an interference filter for 5893 A, a Fabry-Perot interferometer and camera. The SVL is also imaged in the flames and again on the camera plate. An interference pattern is shown in Fig. 8(c). The photographic plate of Fig. 8(c) was calibrated by auxiliary equipment not shown in Fig. 8(a) so that by taking microdensitometer traces across various parts of the interference pattern, the required light intensity values could be obtained. In the next paper,[6] it is explained how, from a photograph of this type, the correct z values for D_1 and D_2 lines in each of the flames may be derived from intensities measured on the photographic plate.

‡ "Sodium vapor lamp" will be referred to in the remainder of the paper by the symbol SVL.

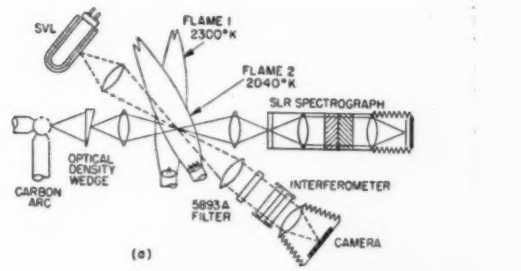

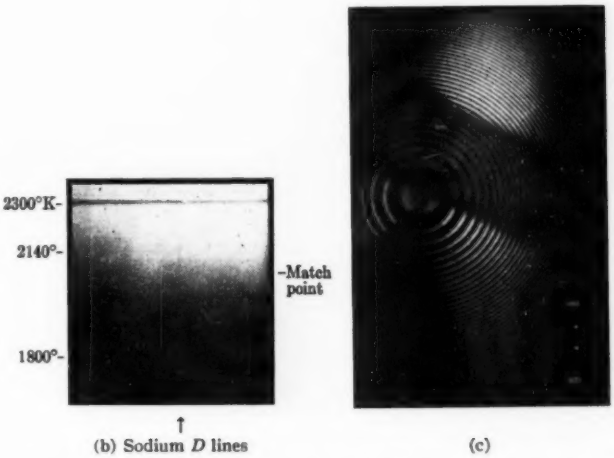

FIG. 8. (a) Optical arrangement for simultaneous observation of SLR temperature and optical depths of flames. (b) Photo of SLR test on the two flames. (c) Interference pattern of SVL shining through both flames.

The data obtained and the result of calculating the temperature of flame 1 together with the directly measured temperature of this flame are given in Table I. The values of A and B were taken from Fig. 6.

In this case, the agreement with experiment was very close because the optical depths of the two flames were experimentally determined. Ordinarily, one would not

TABLE I. Data for determination of temperature of flame 1 (Fig. 8).*

Flame 1 $z_1(D_2)$	Flame 2 $z_2(D_2)$	T_2=2040°K A	B	E_2	$T_{1,2}$=2140°K E_1 calc	T_1(°K) calc	T_1 obs
1.6	2.3	0.150	0.110	0.63	2.4	2300	2300 to 2310°2

* The transmission of the superimposed D lines from the SVL through flames 1 and 2 together, representing a complex flame, and through flame 2 alone representing the outer zone of a complex flame zone gave the data needed to compute z (effective) for flame 2 and for flame 1 (see reference 6 for details of procedure).

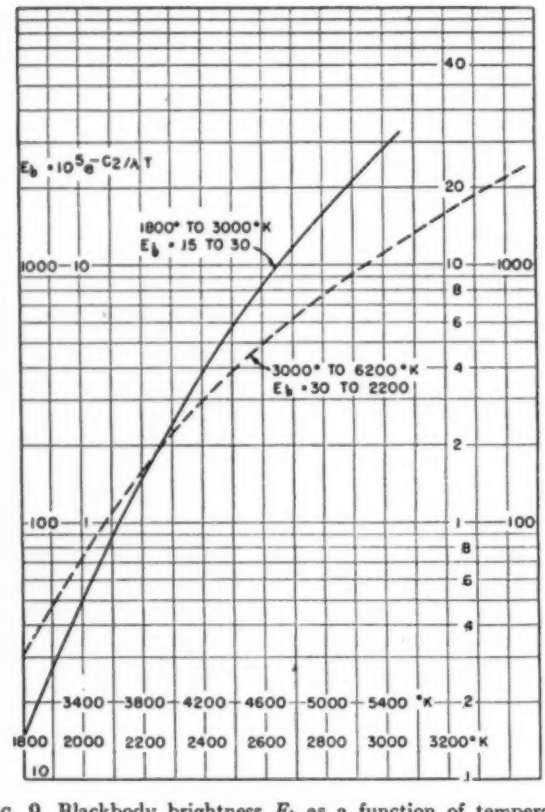

FIG. 9. Blackbody brightness E_b as a function of temperature from 1800° to 6200°K.

be equipped with high resolution spectroscopic apparatus to measure optical depths in this fashion. Even so, a fair idea of the inner zone temperatures can be obtained with ordinary SLR apparatus by making an assumption about the distribution of sodium vapor in the flame.

A photograph of a complex flame may be used to measure the relative thicknesses of the individual flame zones and to estimate their optical depths. If sufficient sodium to give $z=2$ in the thinnest zone is mixed in the fuel and it can be assumed to be evenly distributed in the flame, the optical depths of the different zones will be in the same ratio as their thicknesses. However, due to differences in pressure and temperature of the different zones the ratio of effective thicknesses of zones will differ a little from the measured thicknesses. It is therefore necessary to estimate the correction needed to improve the accuracy of the temperature calculation.

The next step is to assign a value of the optical depth to one of the zones and compute the z values for the other zones from the corrected ratios of zone thickness. The smallest z value assigned should be at least 2. In assigning z values in this way, one takes advantage of the fact that the flame has had sufficient sodium vapor added to it to make the optical depth high. Then the effective flame temperature remains constant for variations in optical depth as explained in the previous section and illustrated in Fig. 7.

Having assigned z values, the values of X, Y, Z, etc. may be obtained by reference to the appropriate curve, Fig. 6.

For convenience, a plot of blackbody brightness E as a function of temperature T in degrees absolute (Kelvin scale) has been prepared and is given in Fig. 9.

An observation of temperature is made with ordinary SLR apparatus through the flame center (obs 1). Other observations are made at such distances away from the center that each successive test includes one less flame zone. The last observation is made on the outer zone alone [obs. 2 in Fig. 7(a)]. The number of observations required is equal to the number of zones.

The procedure just described was used to estimate the temperatures in the different zones of a 3-in. rocket motor flame burning liquid oxygen and alcohol. A diagram of the flame with the temperatures of each zone as found by SLR is shown in Fig. 10.

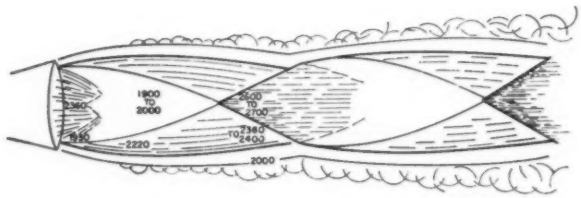

FIG. 10. Drawing of a rocket motor flame with observed temperatures in degrees Kelvin marked in the various zones.

The SLR method of flame temperature measurement is applicable only to gases containing atomic sodium vapor and at temperatures in excess of about 1400°K. It will not detect pockets of relatively cool unmixed gases in case these are present in the flame.

The successful use of the SLR method is dependent upon the sodium line spectrum standing out prominently in comparison to the continuous background spectrum of the flame. Thus, it works best on nonluminous flames and becomes progressively less sensitive as the general luminosity of the flame increases.

This work was sponsored by Project Hermes and the rocket flame measurements were made at the Malta Test Station. The authors gratefully acknowledge the help and cooperation of the staff at the Test Station.

JOURNAL OF APPLIED PHYSICS VOLUME 25, NUMBER 12 DECEMBER, 1954

Measurement of Temperatures in Flames of Complex Structure by Resonance Line Radiation. II. Sodium Line Reversal by High-Resolution Spectroscopy

H. M. Strong and F. P. Bundy
Research Laboratory, General Electric Company, Schenectady, New York

(Received February 24, 1954)

Sodium line reversal temperature measurement by low resolving power spectroscopic instruments on complex flame structures gives temperatures intermediate between the highest and lowest temperature in the line of sight. An apparatus is described which was designed especially for determining the temperature structure in a complex flame by a modified sodium line reversal technique. Experimental data testing the validity of the method and a description of how it may be applied to complex flames is given.

1. INTRODUCTION

THE previous paper[1] has shown how the different zones in a complex flame influence sodium line reversal[2] temperature. There will now be described a modified type of SLR apparatus suitable for determining temperatures in the various zones of a complex flame structure.

In the conventional type of SLR apparatus a source of continuous radiation, such as a tungsten ribbon lamp, is directed through the flame containing sodium vapor and into a small prism spectroscope where the D lines of the flame may be observed against the background radiation. The background brightness is adjusted to match the D lines to obtain a temperature reading.

The same principles are used in the modified SLR apparatus with the difference that the test is performed under conditions that yield highly resolved D lines. Instead of a background of continuous radiation, a sodium vapor lamp[3] shining through a rotating spiral disk is used to produce a background of graded brightness. In place of a prism spectroscope a Fabry-Perot interferometer is used to give highly resolved D lines. The data are recorded photographically and brightness comparisons obtained from microdensitometer tracings. Normally, one pair of photographs should suffice to determine the temperatures in the various zones of a complex flame structure.

It is essential to use a monochromatic source of background radiation such as an SVL in order to obtain interference fringes.

One of the principle advantages in the modified method is that the optical depths of the different flame zones can be determined. It is then possible to calculate the temperature structure quite accurately and simply. A further advantage is that by suitable optical arrangement, a large portion of the flame can be recorded in one pair of photographs.

The theory and an experimental example for the case of a measurement taken through two uniform flames of different temperatures arranged in series will be given. After this, the method of procedure for the more general case will be described.

2. THEORY

The observation of SLR temperature through two flames burning at two different temperatures was described in the previous paper.[1] The brightness of the tungsten lamp required to match the D lines in a low resolving power instrument for these two flames is given by

$$E_l=\frac{E_1(A-B)+E_2B}{A}, \tag{1}$$

in which E = the blackbody brightness of the tungsten lamp that matches the D lines, E_1 = blackbody brightness[4] of flame 1, E_2 = blackbody brightness of flame 2,

$$A=\int_0^\infty \{1-\exp[-(z_1+z_2)sf]\}d\lambda,$$

$$B=\int_0^\infty \{1-\exp[-z_2sf]\}d\lambda.$$

z_1 and z_2 are optical depths of flames 1 and 2, respectively, and sf is the appropriate D line shape factor. This Eq. (1) is Eq. (7) of the preceding paper.

Equation (1) takes a simpler form when the optical depths z_1 and z_2 are made small. As z_1 and z_2 approach zero Eq. (1) becomes

$$E_l=\frac{z_1E_1+z_2E_2}{z_1+z_2}. \tag{2}$$

This equation is quite accurate for values of z up to 0.3. However, for practical purposes, Eq. (2) is satisfactory to use for values of z_1+z_2 up to about 2. This is because the brightness changes so rapidly with temperature that some error in the determination of the brightness can be tolerated.

[1] H. M. Strong and F. P. Bundy, J. Appl. Phys. **25**, 1521 (1954) (preceding paper).
[2] The symbol SLR will be used to mean sodium line reversal.
[3] The symbol SVL will be used to mean sodium vapor lamp.
[4] The brightness of a blackbody whose temperature is the same as that of the flame at the wavelengths of the D lines. E is Wien's blackbody radiation distribution function of λ and T.

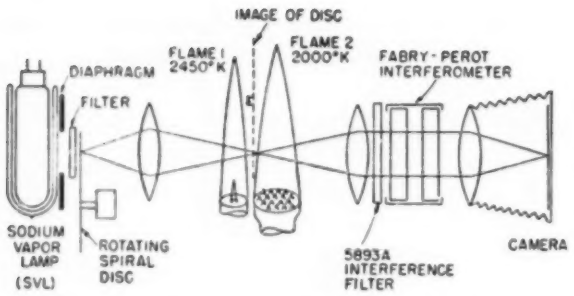

FIG. 1. Apparatus for sodium line reversal by high-resolution spectroscopy.

In order to apply Eq. (2), the z's and E's should be measured with reasonably good accuracy and the optical depths of the flames should be kept somewhat lower than that which is usually required for the observation of SLR with a conventional type of apparatus. In case the optical depth is too great at the line center, measurements of E should be made at a selected value of $\Delta\lambda$ on the line shoulders where the optical depth is low. The z's can always be determined by comparison of brightnesses at the line centers if desired, since the ratios of the z's in different parts of the flame structure are practically the same at the line center as at any selected value of $\Delta\lambda$ on the D line contours.

The required measurements can be made if the spectroscopic instrument used has a resolving power of $\lambda/\Delta\lambda \geqq 10^5$. A suitable apparatus and the method will be described in the next section.

3. EXPERIMENTAL

An apparatus for high resolution SLR work is shown in Fig. 1. It is quite similar to conventional SLR apparatus but with the difference that a sodium vapor lamp has been substituted for a tungsten ribbon lamp and a Fabry-Perot interferometer for the usual prism spectroscope. Instead of the interferometer, one could use a large prism or grating instrument but certain advantages in the use of the interferometer would be lost.

If a Fabry-Perot interferometer is used, the plate spacing should be adjusted to superimpose the D_1 and D_2 lines[5]; otherwise the wings of the D_1 and D_2 lines merge together too much in the field of observation. The effective optical depths for the superimposed D lines can be resolved into separate optical depths for the D_1 and D_2 lines as will be shown later. First the general procedure will be described.

With the apparatus shown in Fig. 1 the SVL furnishes a background of D_1 and D_2 lines of nearly equal brightness. The blackbody brightness at the centers of these lines can be as high as that corresponding to 4000 to 5000°K. The effective brightness of the background is best controlled by an optical density wedge or a rotating spiral disk imaged on a photographic plate. In the work to be described, a rotating spiral disk was used.

[5] Bundy, Strong, and Gregg, J. Appl. Phys. 22, 1069 (1951).

The lens system illustrated in Fig. 1 is such that an image of a section of the brightly illuminated spiral disk is formed in the flame and again in the camera after passage through the interferometer. Thus, an image of the flame is formed in the camera also, but one which differs from images in the ordinary sense in that the only portions illuminated are those which are located at the fringes of the interference pattern. In this system, to get a fair comparison of intensities, it is necessary for all the radiation leaving lens 1 to pass through lens 2. The Fabry-Perot interferometer permits the images desired to be formed whereas a grating or prism instrument is not well adapted to this purpose.

To get the required data for testing the method with the arrangement in Fig. 1, a series of photographs, all of equal time duration, were taken. These are illustrated in Fig. 2. The subjects of each of the 6 exposures were as follows:

Exposure 1: SVL shining through rotating spiral disk, flames 1 and 2.

Exposure 2: Flames 1 and 2 without the SVL and spiral disk.

Exposure 3: Repeat of exposure 1.

Exposure 4: SVL shining through spiral disk and flame 2.

Exposure 5: Flame 2 alone. Because of its relatively low temperature, the brightness was about $\frac{1}{4}$ that of the other exposures. This exposure does not reproduce satisfactorily with the others.

Exposure 6: SVL shining through spiral disk only.

Note the intensity grading effect of the rotating disk in Exposure 6.

In order to establish the spiral disk density gradient in the photograph, two index marks were provided by cutting a series of slots in the disk at two different radii. These index marks show up as unusually bright streaks in the photograph. However, in the illustration of Fig. 2, the top index mark does not show as clearly as it does on the original negative.

Microdensitometer records were made of each exposure by traversing the fringe patterns from the center of the fringe pattern out along a diameter of the circular

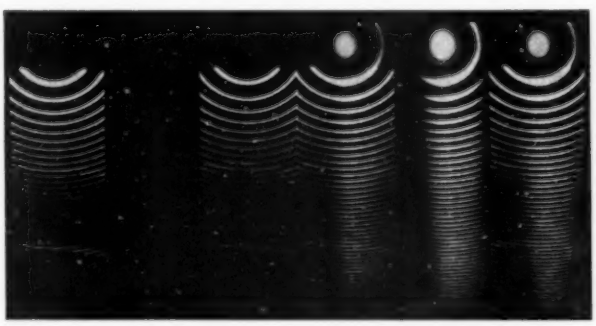

6 5 4 3 2 1

FIG. 2. Interference patterns obtained in test of SLR by high-resolution spectroscopy.

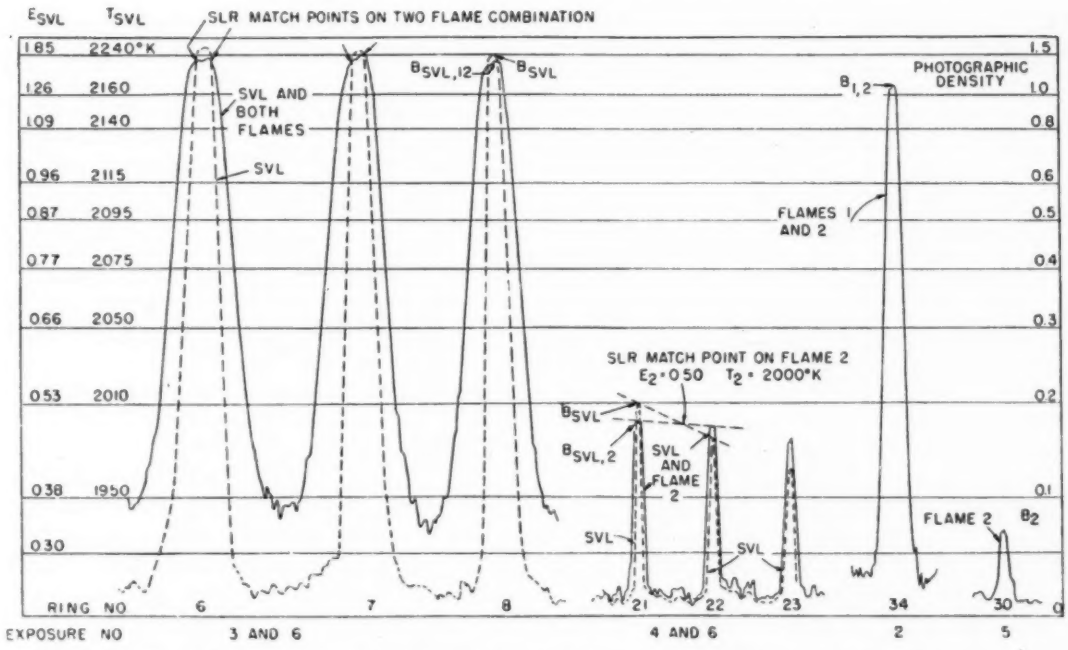

FIG. 3. Segments of microdensitometer traces taken on interference patterns in Fig. 2.

fringes. In Fig. 2 this trace extends from the top center of each photograph vertically downwards. Parts of each of these traces are shown in Fig. 3. By superimposing the trace for the SVL alone, which represents background brightness, on top of a trace for the vapor lamp shining through the flames, the places where the two traces cross represent points of equal brightness or in other words they represent the SLR matching condition.

In Fig. 3, the vertical scale is marked both in terms of the blackbody brightness of the background, E_{SVL}, and temperature.

The brightness temperature of the SVL was determined in the following manner: first, the temperature of the flame of a Meker burner, burning propane gas, was determined by an ordinary SLR test using a calibrated tungsten ribbon lamp and prism spectroscope. This flame was then used as flame 2 in the experimental test of the modified SLR apparatus as shown in Fig. 1. The interference patterns for SLR on this flame by itself are exposures 4 and 6 of Fig. 2. The superimposed microdensitometer traces of exposures 4 and 6 are included in Fig. 3. The position of the match point was taken to be the previously determined temperature of flame 2, 2000°K, corresponding to a blackbody brightness of 0.5. Using the known transmission gradient of the rotating spiral disk and the 0.5 reference brightness point, the brightness scale on the microdensitometer trace was established.

The brightness of the SVL was so great that the rotating spiral disk alone was insufficient to bring its brightness level down to the range of the flames. The brightness level was brought down to the desired range by insertion of a filter between the SVL and spiral disk. The combined transmission of filter and spiral disk at the match point for the 2000°K flame was 0.0011. Hence the full brightness of the SVL was 450, corresponding to a temperature of 4500°K. Its brightness temperature was quite steady despite small variations in current. (See Fig. 9, Paper I.)

The optical depths, z_1 and z_2, were determined by comparing the intensity of the SVL alone with its intensity after transmission through the flames. For example, the transmission of flame 1 and flame 2 taken together, from which the value of (z_1+z_2) may be obtained, is

$$e^{-(z_1+z_2)}=\frac{B_{SVL,1,2}-B_{1,2}}{B_{SVL}}\cdots. \tag{3}$$

In this equation, the symbol B has been substituted for E previously used so as not to confuse the determination of the z's with the determination of blackbody brightness and temperature. The values of the B's are usually taken at the line center whereas the E's will be taken at the place where the intensity contour curves intersect. B_{SVL} signifies the brightness of the sodium vapor lamp. $B_{SVL,1,2}$ means the brightness due to radiation of the SVL shining through both flames, plus flame 1 shining through flame 2, plus the radiation from flame 2. $B_{1,2}$ is the brightness resulting from flame 1 shining through flame 2 plus the radiation from flame 2. Similarly,

$$e^{-z_2}=\frac{B_{SVL,2}-B_2}{B_{SVL}}. \tag{4}$$

Finally,

$$e^{-z_1}=\frac{e^{-(z_1+z_2)}}{e^{-z_2}}. \tag{5}$$

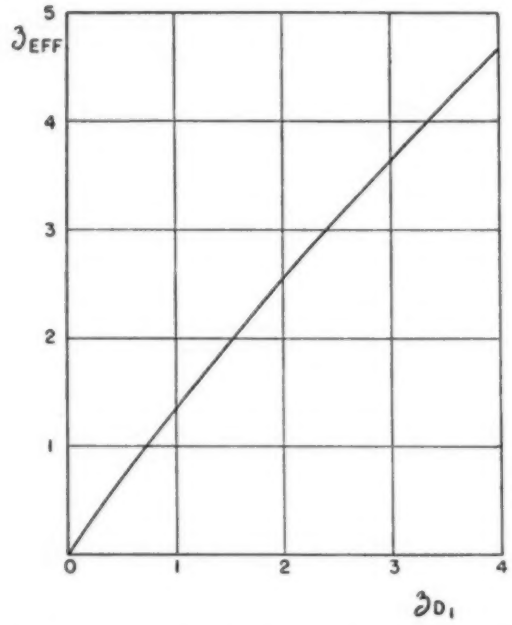

FIG. 4. Effective optical depth, $z_{(eff)}$, of superimposed D_1 and D_2 lines plotted against optical depth of D_1 line.

From these relations z_1 and z_2 are obtained. These z's are due to the combined absorptions of the D_1 and D_2 lines and should be called effective z's (or z_{eff}). The relation connecting z_{eff} with the correct z_{D_1} and z_{D_2} values for D_1 and D_2 lines in the flames is

$$e^{-z_{eff}}=\frac{\exp(-z_{D_1})+\exp(-2z_{D_1})}{2}. \tag{6}$$

For thermally excited D lines as in flames $z_{D_2}=2z_{D_1}$. In the SVL the two D lines have nearly equal brightness. In deriving Eq. (6) to be used in connection with the experimental data, the SVL background D_1 and D_2 lines were taken to be of equal brightness. Figure 4 shows a plot of z (D_1 line) against z_{eff} based on Eq. (6) from which the correct z_{D_1} and z_{D_2} values for the flame may be obtained. In Eq. (3) (z_1+z_2) is z_{eff} for both flames. Reference to Fig. 4 gives the value of z_{D_1} (flame 1) $+z_{D_1}$ (flame 2). Similarly, z_2 in Eq. (4) leads to z_{D_1} (flame 2) and z_1 Eq. (5) leads to z_{D_1} for flame 1.

In the example illustrated, the data obtained and the calculated and measured temperatures are given in Table I.

While the example illustrated indicates that a high degree of accuracy is possible the limitations in the resolving power of the interferometer and of accuracy of photographic intensity measurements would generally limit the accuracy of such measurements to an estimated ± 3 percent at this temperature level.

TABLE I. Experimental values of quantities in Eq. (2).

E_{SVL}	E_2	$z_{1(eff)}$	$z_1(D_1)$	$z_{2(eff)}$	$z_2(D_1)$	E_1 calc	T_1 calc °K	T_1 meas. °K
1.71	0.50	0.43	0.29	1.02	0.72	4.55	2440°	2430°

4. APPLICATION TO COMPLEX FLAME STRUCTURES

This method can be used on complex flame structures in the manner illustrated in Fig. 5. Also illustrated in Fig. 5 are the interference patterns that would be obtained for the SVL shining through the wedge only and for the SVL shining through the optical density wedge and flame. In the latter, the wedge image is clearly outlined in the interference pattern. Densitometer traces taken along the dotted arrows (1), (2), and (3) give the data needed to obtain the temperature in the outer shell, the temperature for a line of sight through both zones of the flame, and the various brightness values needed for computing optical depths of each zone of the flame. The blackbody brightness of the inner zone of the flame may be obtained from the following equation:

$$E_{SVL}=\frac{z_2E_2+z_1E_1+z_2E_2}{z_1+2z_2}\cdots. \tag{7}$$

All quantities are experimentally determined except E_1.

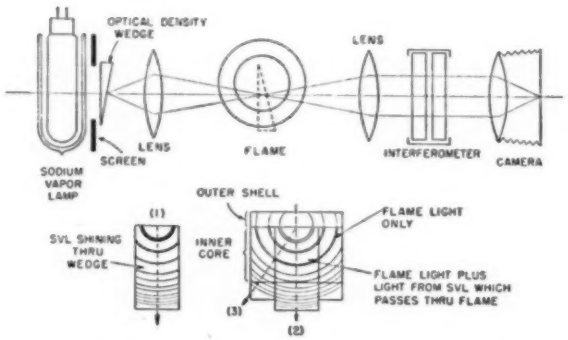

FIG. 5. Illustration of how SLR by high resolution spectroscopy may be applied to measure temperature of a complex flame.

For the more general case this equation can be expressed as

$$E_{SVL}=\frac{\sum_{r=1}^{n} z_rE_r}{\sum_{r=1}^{n} z_r}\cdots, \tag{8}$$

where each value of r represents a discreet zone. When r is larger than 2, then temperatures must be determined by stages, working from the outside towards the center.

This method is limited for use on nonluminous flames only.

Measurement of Temperatures in Flames of Complex Structure by Resonance Line Radiation. III. From Absolute Intensity Measurements at High Resolution

F. P. Bundy and H. M. Strong
Research Laboratory, General Electric Company, Schenectady, New York

(Received February 24, 1954)

A method for measuring flame temperatures is described which requires the determination of the intensity and emissivity of the flame at wavelengths within the intensity contour of a resonance spectral line such as a *D* line of sodium. An experiment is cited to illustrate the method in which a Fabry-Perot interferometer was used as the spectroscopic dispersion instrument. The emissivities were determined by comparing the brightnesses of the mirrored and unmirrored flame. The theory, procedure, and an example of using the method to find the temperature of a submerged zone of a flame are given.

1. INTRODUCTION

IN a hot gas which is in thermal equilibrium the radiation emitted at any given wavelength cannot exceed the brightness of a blackbody at the same temperature and same wavelength. The actual intensity of radiation from such a gas is given by the product of its emissivity at the particular wavelength and the blackbody intensity for the same temperature and wavelength. Thus, if both the intensity of radiation and the emissivity of a hot cloud of gas, or a flame, can be determined at a given wavelength, then its blackbody intensity can be calculated. From the latter the temperature can be determined by use of the radiation laws. Because of the difficulty of measuring absolute values of radiation a more workable method is to determine the spectral brightnesses and emissivities of a standard flame of known temperature and of a flame of unknown temperature in arbitrary units, then from the ratio of their deduced blackbody brightnesses (in the same arbitrary units) determine the temperature of the flame of unknown temperature.

The method which will be described in this paper makes use of the ratio of the blackbody radiation intensities of two flames, one of known temperature and the other unknown, at a particular wavelength within the intensity contour of a resonance-type spectral line such as a *D* line of sodium. A particular advantage of the method is that it can be used to determine the temperature of the zones within a flame having a complex temperature structure, such as a supersonic rocket flame which contains a series of shock cones having higher temperature than other parts of the flame. A spectroscopic instrument of very high resolving power is required because the detailed intensity structure of the spectral line being used must be well resolved.

2. THEORY

The intensity contour of a resonance-type spectral line emitted from a flame of uniform temperature is illustrated in Fig. 1, and has the analytical form:

$$I(\Delta\lambda)=E_b(\lambda,T)\{1-\exp[-zsf(\Delta\lambda)]\}, \qquad (1)$$

where $\Delta\lambda$ is the wavelength interval from the center of the spectral line, $E_b(\lambda,T)$ is the blackbody radiation intensity at the wavelength λ and absolute temperature T, z is the "optical depth" of the flame at $\Delta\lambda=0$, and $sf(\Delta\lambda)$ is the "shape factor" of the distribution of intensity of primary radiation from the atoms (i.e., the shape caused by thermal motion doppler shift and by collision broadening). Since $sf(\Delta\lambda)$ is maximum (unity) at the line center ($\Delta\lambda=0$), and decreases rapidly as $|\Delta\lambda|$ increases, the optical depth $zsf(\Delta\lambda)$ of the flame becomes quite small in the extremities of the line contour. The emissivity at different places in the spectral line contour is given in terms of the optical depth by the expression which appears in Eq. (1), $\{1-\exp[-zsf(\Delta\lambda)]\}$. Experimentally the quantities which may be determined are $I(\Delta\lambda)$ and $zsf(\Delta\lambda)$. From these the blackbody radiation intensity may be determined from Eq. (1) in the form:

$$E_b(\lambda,T)=\frac{I(\Delta\lambda)}{1-\exp[-zsf(\Delta\lambda)]}. \qquad (2)$$

If a flame has zones of different temperatures, such as a hot core with a relatively cool sheath, the intensity contour of a resonance-type spectral line emitted from it is complicated and depends upon the temperatures, depths and arrangement of the zones. A typical example is shown in Fig. 2. In the center of the line the intensity is cut down by the selective absorption of the relatively cool sheath, while at some distance from the line center

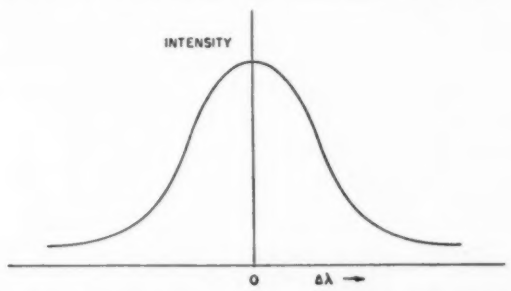

FIG. 1. Intensity contour of resonance-type spectral line emitted from a flame of uniform temperature.

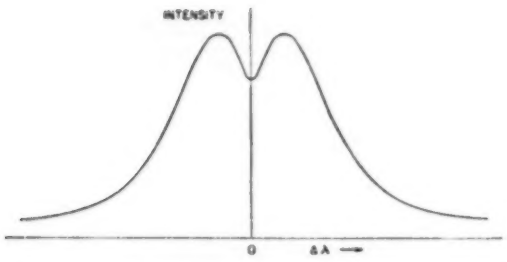

FIG. 2. Intensity contour of a resonance-type spectral line emitted from a flame with a hot core and cooler sheath.

the optical depth of the cool sheath becomes so small that it is quite transparent to the radiation originating in the hot core. This causes the maximum intensity to occur a little way out from the line center.

If a flame has a cross section of the type shown in Fig. 3 the intensity of radiation is distributed across the spectral line region according to the relation

$$I^*(\Delta\lambda)=E_b(T_3)\{1-\exp[-z_3sf(\Delta\lambda)]\}+E_b(T_2)\times\{1-\exp[-z_2sf(\Delta\lambda)]\}\cdot\exp[-z_3sf(\Delta\lambda)]+E_b(T_1)\{1-\exp[-z_1sf(\Delta\lambda)]\}\cdot\exp[-(z_2+z_3)sf(\Delta\lambda)]. \quad (3)$$

An effective temperature T^* can be defined for this case on the basis of the total intensity of radiation $I^*(\Delta\lambda)$ and the total optical depth, $z_1+z_2+z_3$ by the relation,

$$E_b(T^*)=\frac{I^*(\Delta\lambda)}{1-\exp[-(z_1+z_2+z_3)sf(\Delta\lambda)]}. \quad (4)$$

This effective temperature is that which would be indicated by a simple sodium line reversal apparatus using the same light path through the flame.[1] If the optical depths $zsf(\Delta\lambda)$ are less than about 0.3 the $\{1-\exp[-zsf(\Delta\lambda)]\}$ terms are approximated very closely by $zsf(\Delta\lambda)$. Hence in this case,

$$E_b(T^*)\doteqdot\frac{z_1E_b(T_1)+z_2E_b(T_2)+z_3E_b(T_3)}{(z_1+z_2+z_3)}. \quad (5)$$

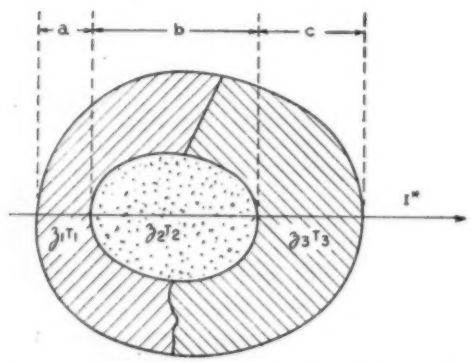

FIG. 3. Cross section of flame with hot core and unsymmetrical sheath.

[1] F. P. Bundy and H. M. Strong, J. Appl. Phys. 25, 1521 (1954), Part I of this series.

As blackbody brightness $E_b(T)$ increases so rapidly with temperature (see Fig. 9, reference 1) it is found in practice that flame zone temperatures may be deduced with satisfactory accuracy by this method for optical depths as high as 1 or even 2 in some cases. If the radiating vapor is uniformly distributed in the zones the z's of the different zones are proportional to their geometric distances a, b, c along the line of sight, in which case

$$E_b(T^*)\doteqdot\frac{aE_b(T_1)+bE_b(T_2)+cE_b(T_3)}{a+b+c}. \quad (6)$$

If the zones of the flame are known to have widely different pressures and temperatures the geometrical thicknesses can be modified in proportion to the absolute pressure and inversely to the absolute temperature. In many cases the concentration of the spectrally active element in the flame is great enough that the optical depth at the center of the spectral line is considerably greater than 1.0. In such cases the intensity and emissivity measurements can be made at a wavelength far enough from the line center that the optical depth $zsf(\Delta\lambda)$ is small enough to make the approximations in Eqs. (5) and (6) sufficiently accurate.

In the case illustrated in Fig. 3 three sets of measurements are required to determine the temperatures of all three flame zones: one along a light path that passes through all three zones, one which passes through zone 1 only, and one which passes through zone 3 only. The latter two observations yield temperatures T_1 and T_3. The first observation yields temperature T^*. The distances a, b, and c are known from the flame geometry. Temperature T_2 is then found from Eq. (6) in which it is the only unknown.

In general it would be quite difficult to measure the spectral intensities $E_b(T)$ in absolute units. For this reason it is more convenient to calibrate the intensity readings in terms of a flame of known temperature using some convenient arbitrary intensity units. To find the ratio of the true blackbody intensities of the calibrating flame and the flame being measured the true optical depths of each of the flames must be determined.

One of the most direct methods of determining the optical depth of a flame is to make two measurements on it, one with, and another without a mirror behind it. A mirror of reflectivity R placed behind the flame makes the flame appear effectively $(1+R)$ times as deep along the line of sight. However the ratio of the observed spectral brightnesses with and without the mirror in place varies with the emissivity or optical depth of the flame. For flames of nearly zero emissivity the presence of the mirror causes the intensity to increase to nearly $(1+R)$ that of the bare flame whereas if the flame has high emissivity the presence of the mirror has practically no effect on the observed intensity.

As will be described later under experimental appa-

ratus, the spectroscopic instrument used in the authors' experiments was a Fabry-Perot interferometer so adjusted that the fringes of the D_1 and D_2 resonance radiations of sodium were superposed. The effect of the mirror on the brightness ratio in this special case was analyzed as follows: Under thermal conditions of excitation in flames the probability of excitation of sodium atoms for D_2 radiation is twice that for D_1 radiation, both according to theory and as checked experimentally. Hence $z_{D_2}=2z_{D_1}$, and the ratio of intensities for the superposed radiations for mirrored *vs* unmirrored conditions is:

$$\mathcal{R}(\Delta\lambda)=\frac{I_M(\Delta\lambda)}{I_0(\Delta\lambda)}$$

$$=\frac{\{1-\exp[-z_{D_1}(\Delta\lambda)]\}\{1+R\exp[-z_{D_1}(\Delta\lambda)]\}+\{1-\exp[-2z_{D_1}(\Delta\lambda)]\}\{1+R\exp[-2z_{D_1}(\Delta\lambda)]\}}{\{1-\exp[-z_{D_1}(\Delta\lambda)]\}+\{1-\exp[-2z_{D_1}(\Delta\lambda)]\}}, \quad (7)$$

where I_M is the intensity when the flame is backed by a mirror and I_0 is for the bare flame without the mirror. This brightness ratio is plotted against z_{D_1} for various values of mirror reflectivity, R, in Fig. 4. This method of determining optical depth is most sensitive and accurate in the range of $z=0.07$ to $z=3.0$ which fortunately is also the region of most practical interest. Thus from the ratio of intensities in the mirrored and unmirrored conditions the emissivities for both the D_1 and D_2 radiations can be determined. The total intensity divided by the sum of the D_1 and D_2 emissivities gives the blackbody intensity which is required for comparison between two independent flames. [See Eq. (2).]

3. EXPERIMENTAL METHOD AND RESULTS

This spectroscopic method of determining flame temperatures required the measurement of intensities at particular wavelengths within the intensity contour of a resonance-type spectral line. The spectroscopic instrument used therefore had to have enough resolving power and dispersion to produce the detailed fine structure of spectral lines in a form suitable for measurement. The authors had available a high quality Fabry-Perot interferometer which was easily adapted for use in this method. The optical systems are shown in Fig. 5. Figure 5(a) shows the arrangement used for calibrating the photographic plates for density of blackening *vs* intensity of exposure while Fig. 5(b) shows the arrangement for flame temperature measurement.

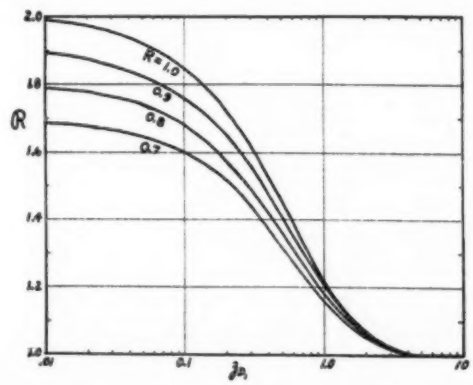

FIG. 4. Ratio of intensities of superposed sodium D_1 and D_2 radiations *vs* z_{D_1} for different values of mirror reflectivity, R.

Whenever light intensities are determined by blackening of photographic emulsions it is always necessary to calibrate each plate directly by subjecting it to a series of exposures of known intensity. In addition care must be taken to avoid ranges of exposure times and intensities which involve "reciprocity failure." In the apparatus used in this investigation the photographic plate was calibrated by use of a sodium vapor lamp and a rotating spiral disk optical density wedge. Lens 1, Fig. 5(a), formed a real image of the optical density wedge at the place later occupied by the flames to be studied. Lens 2 was placed at its focal distance from the image so that it rendered parallel the rays from the image. Lens 2 and the camera lens together formed a second image of the optical density wedge on the photographic plate. The interferometer interposed between lens 2 and the camera has no effect on the shape or size of the image on the camera plate except that it transmits the nearly monochromatic light only at certain angles to its optic axis. Thus the only parts of the image which show are those which fall in the circles described by those critical angles. In addition to the interference fringes, the index marks on the density wedge also appear on the camera plate. The apertures on lenses 1 and 2 were adjusted so that the light cone angle was the same as when the flames were in place and so that no stray light entered the system. An interference-type filter was placed in front of the aperture of lens 2 to

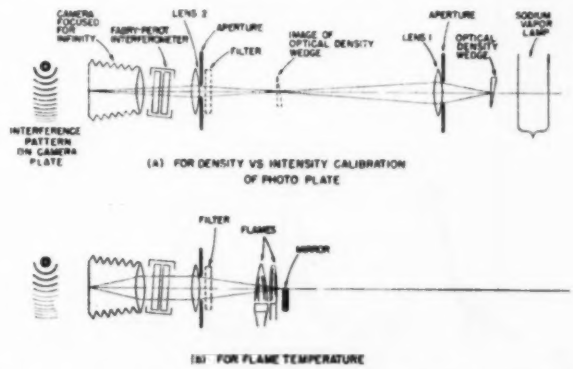

FIG. 5. Optical setup. (A) Arrangement for photographic density calibration. (B) Arrangement for flame temperature measurement.

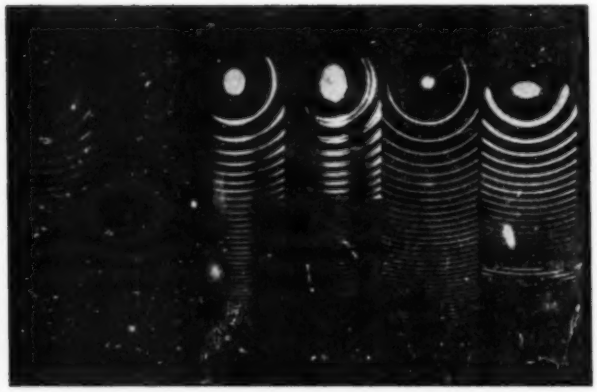

FIG. 6. Typical set of exposures for determining flame temperatures.

minimize passage of radiation of wavelengths other than that near the 5890-angstrom sodium *D*-line radiation. In addition, other neutral filters of known transmission were used with the brighter flames to equalize exposure times. The axis of the interferometer was deliberately tipped to throw the center of the interference pattern off to the edge of the picture so that the fringes would be more evenly spaced in the important part of the picture.

The flame pictures were taken with the flames and mirrors placed at the focal point of lens 2. The settings of lens 2, the interferometer, camera, aperture and interference filter were left as they were for the calibration photographs. The apparatus was carefully shielded to prevent stray light from entering the optical system. The required pictures were taken on different exposure areas of the same photographic plate. Eastman 103-T spectroscopic plates were used because of their rather selective high sensitivity in the sodium yellow region and their relatively fine grain size.

To test the applicability of this method of flame temperature measurement for the determination of the temperatures of cores of zoned flames the following experiment was done: A photographic plate was given the intensity calibration exposures described above. Other successive exposures were made of a standard Meker burner propane-air flame of known temperature (1950°K),[2] a hot gas-oxygen blast lamp flame alone, (2490°K),[2] and the hot gas-oxygen blast lamp flame viewed through the Meker propane-air flame (to show that the temperature of the hot flame can be calculated from the observations on the combination flame and the cool flame). A typical plate is shown in Fig. 6. Exposure 1 is a wedge calibration pattern. Exposure 2 is the same as 1 except with optical density wedge removed to test the uniformity of illumination of the field. Exposure 3 is the hot gas-oxygen flame seen through the Meker propane-air flame (note the radial streaks which are part of the flame structure; also the dimpled interference fringes which are characteristic of this flame zone arrangement as shown in Fig. 2). Exposure 4 is the hot gas-oxygen flame alone (note the bright and dark streaks). Exposures 5 and 6 are of the Meker propane-air flame alone. In Exposures 3 through 6 the mirrored part of the flames appears in the first seven fringes at the top.

The patterns shown in Fig. 6 were run on a microdensitometer to obtain the plots of photodensity along radial paths. The tracings from Exposures 6, 4, and 3 are

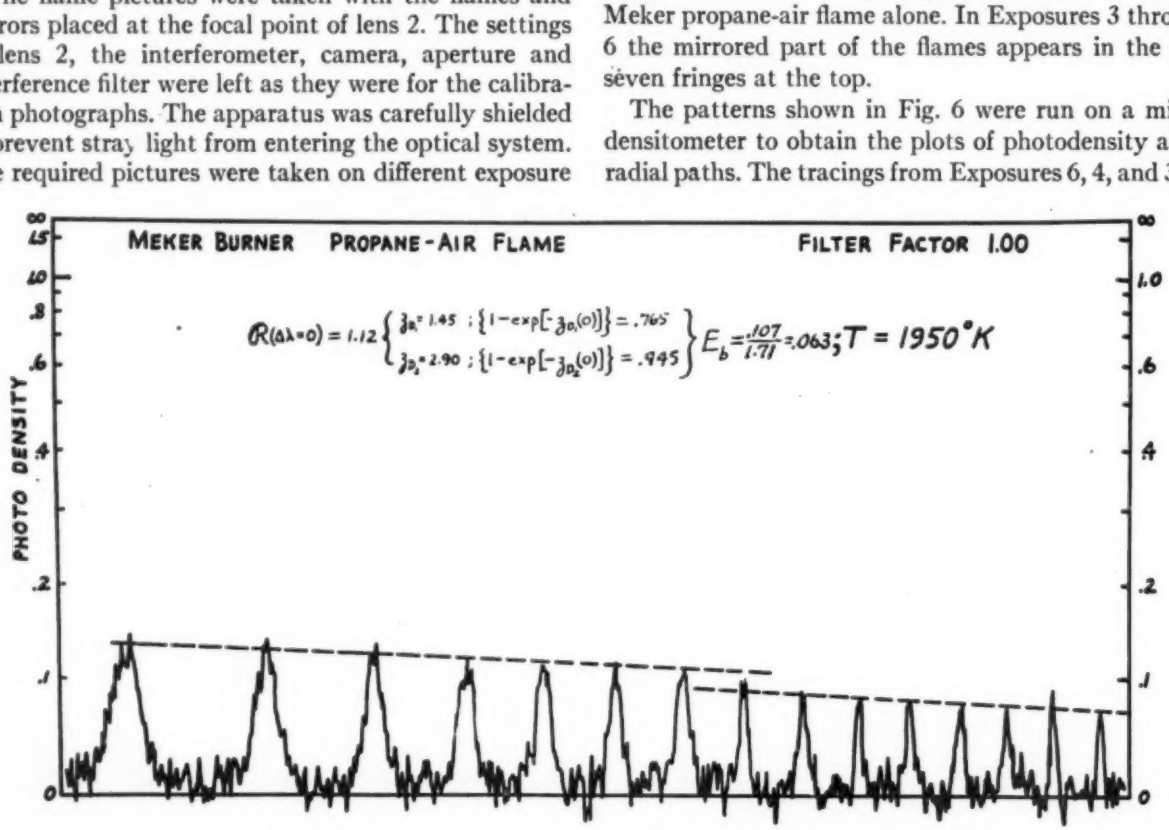

FIG. 7. Densitometer tracing of pattern from Meker flame alone.

[2] These temperatures were measured by the sodium line reversal method.

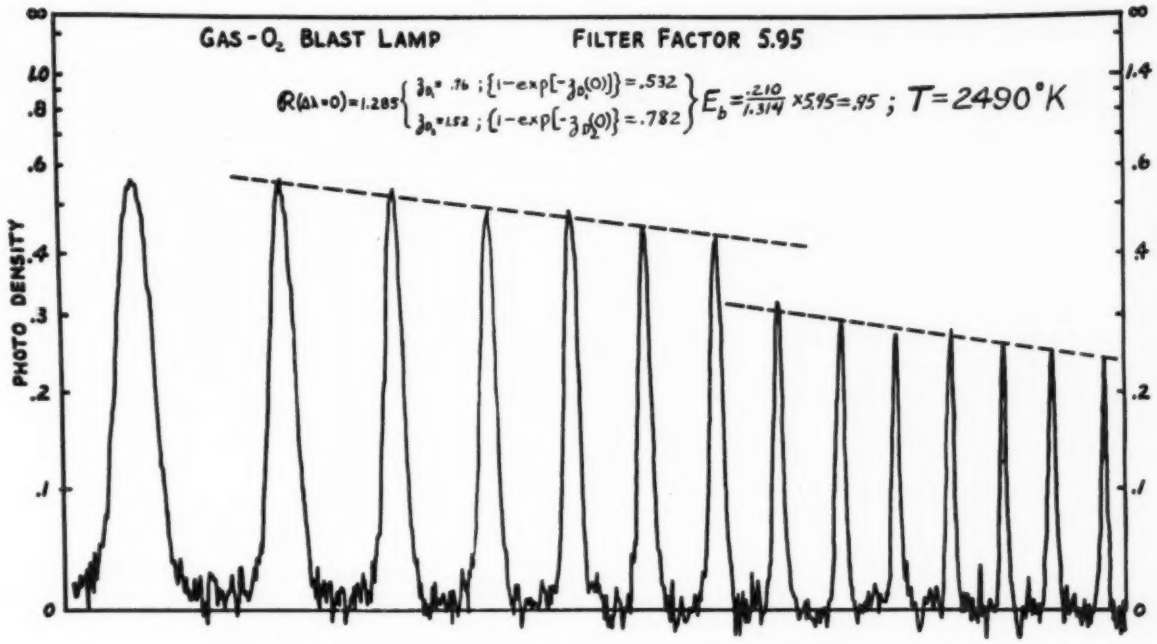

FIG. 8. Densitometer tracing of pattern from gas-oxygen flame alone.

shown in Figs. 7, 8 and 9, respectively. In each of the densitometer tracings the step between the mirrored and unmirrored part of the flame is quite distinct. It occurs between the seventh and eighth fringes from the left. Another characteristic common to the three tracings is the decrease of density from left to right which corresponds to bottom to top of the flames. This is to be expected as the flames become a little cooler and more narrow toward their tops. That this gradation was not caused by the optical system was proved by the peak densities of all the fringes in Exposure 2 being the same.

In Fig. 7 the intensity ratio, $I_M/I_0=1.12$, of the mirrored *vs* unmirrored parts at the $\Delta\lambda=0$ points indicated an optical depth of 1.45 for the D_1 line and 2.90 for the D_2. This gives emissivities of 0.765 and 0.945 for the centers of the D_1 and D_2 lines, respectively. The observed intensity of 0.107 arbitrary unit (indicated in Fig. 7) divided by the sum of these emissivities gives a blackbody intensity of 0.063 arbitrary units for this 1950°K flame which is the standard of reference.

In Fig. 8, the intensity ratio for the gas-oxygen flame, $I_M/I_0=1.285$, indicates emissivities of 0.532 and 0.782 for the centers of the D_1 and D_2 lines, respectively. The observed intensity divided by the sum of these emissivities and multiplied by the filter factor of the neutral filter used leads to a blackbody intensity of 0.95. This is 15.1 times that of the 1950°K calibration flame. From the ratio given by Wien's law,

$$\frac{E_b(T_1)}{E_b(T_2)}=\exp c_2\left(\frac{1}{T_2}-\frac{1}{T_1}\right) \tag{8}$$

this gives a temperature of 2490°K. This value agrees with value obtained by the sodium line reversal method.

The tracing in Fig. 9 shows the typical dimpled spectral line structure characteristic of a hot flame shining through a cooler one. In this case at the line center, $\Delta\lambda=0$, the optical depth of the cool flame is large enough to nearly mask the effect of the hot flame. Hence the chief advantage of this method is made use of by making the measurements at $\Delta\lambda=0.1$ angstrom unit where the optical depth is small enough to show the effects of both flames. These measuring points occur at about the "shoulders" of the line contours. The intensity ratio, $I_M/I_0=1.645$, gives emissivities of 0.190 and 0.342 for the D_1 and D_2 radiations, respectively. The measured intensity level divided by the sum of the emissivities and multiplied by the filter factor leads to a blackbody intensity of 0.387 arbitrary unit which by comparison with the intensity of the standard flame yields an effective temperature for the combination flame of 2290°K.

The information available on the cool flame alone and the combination of flames should, by the method described in the theory above, lead to the temperature of the hot flame alone. This will now be tested. In this case the Meker flame was about 2.5 cm thick, the gas-oxygen flame about 1.25 cm thick and the optical depth measurements show the sodium vapor density to be about the same in both flames as would be the case if they were separate zones of the same flame. Taking these dimensions and the blackbody intensities (in arbitrary units) which have been derived above, inserting these in Eq. (6) it is found that the blackbody intensity of the hot flame is 16.4 times that of the 1950°K standard (cool) flame. This gives 2510°K which

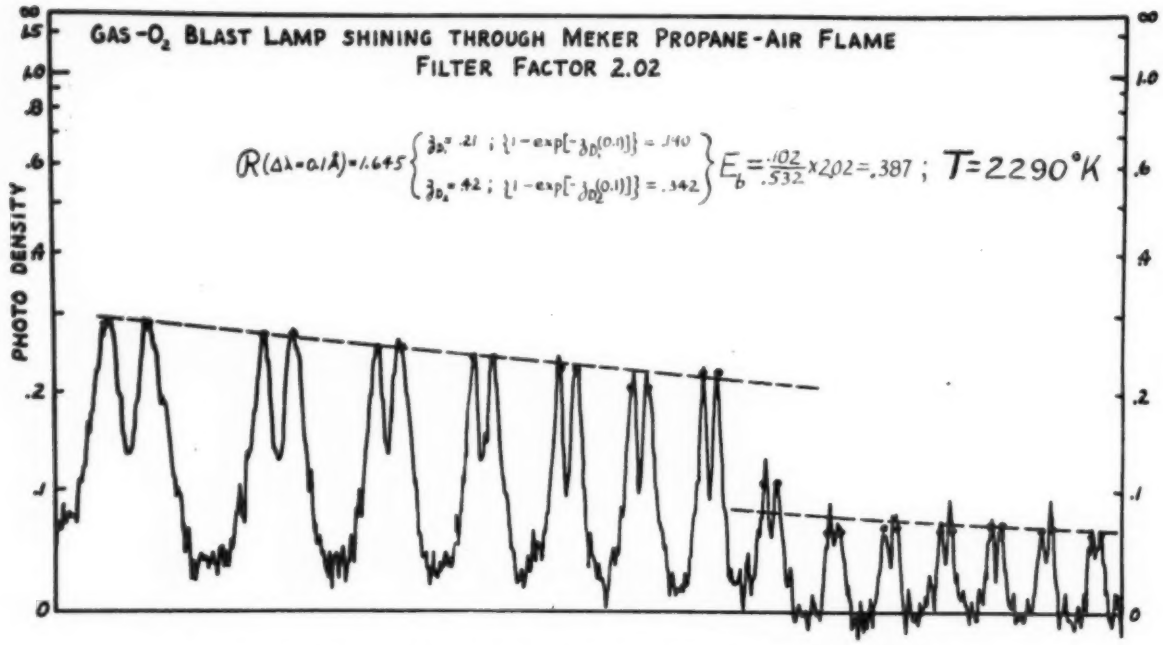

FIG. 9. Densitometer tracing of pattern from gas-oxygen flame behind the Meker flame.

is to be compared to the 2490°K determined by measuring the hot flame alone. This is a fairly satisfactory check and demonstrates the utility of the method for determining the temperatures of internal zones of a flame.

Another possible use of the method which might be of interest in some cases is to determine the flame temperatures at different places in the field of view of the second zone. For example, in Fig. 6, Exposures 3 and 4, the bright and dark streaks in the gas-oxygen flame are clearly shown. By taking densitometer tracings along paths that include the zone of interest and the mirror line the temperature of the zone at the mirror line can be derived. Then the temperatures in other parts of the flame can be derived by comparing the brightnesses at the other places with that on the mirror line. Thus the temperatures of all the parts of the flame that show in the picture can be deduced with fair accuracy.

4. DISCUSSION

The theory of this method of flame temperature measurement and the procedure for carrying it out appear to be sound and direct. However, those who are experienced in photographic densitometry and high-resolution spectroscopy will recognize some of the sources of possible error and the great care required to minimize them. Some of the possible sources of error are: (1) reciprocity failure of exposure of the photograph plate; (2) variation of transmission factor of the filters with wavelength of light and aperture angle of the optical system; (3) scattering and absorption of light by the reflecting films on the interferometer plates; (4) difficulty of getting a steady and uniform distribution of active sodium in all parts of the flames; (5) difficulty of placing the mirror close enough to the flames to give the ideal reflection relationships which are assumed in the theory.

The authors made a rather extensive test of the reciprocity of intensity and time of exposure *versus* the photographic density produced on the plates used. It was concluded that for accurate results in this method it is best to hold to a constant exposure time and compensate for variation of source brightness by the insertion of filters. Careful tests of the Wratten filters used showed that their transmission factors should be measured with the same light (wavelength band) as is used in the flame temperature measurements, and with the filter in place in the same optical system.

Scattering and absorption of light by the reflecting metal films on the interferometer plates cause a reduction of the resolving power of the instrument and hence an indicated distribution of intensity in the interference fringes which is smeared out more than the ideal. Consequently it is not safe to measure an optical depth at one $\Delta\lambda$ in one exposure and compare it with the optical depth derived from another exposure at a different $\Delta\lambda$. The interferometer plates used by the authors in the tests reported above had aluminum reflecting coatings. The authors have learned since that silver coatings are much better in that they have less scattering and absorption.

Several methods of introducing sodium salts into the flame gases were tried. The method finally adopted was essentially the salt spray chamber system of Lundegärdh.[3] At the best it is difficult to get repro-

[3] H. Lundegärdh, *Die Quantitative Spektralanalyse der Elemente* (Jena, 1929).

ducible and steady salt concentrations in the flames because of variations in the action of the spray chamber and sensitivity of the mixing of the fuel and oxidizer gases in the burners.

The theory assumes that the mirror is at the back edge of the flame and that the reflection is the same as for a parallel light beam. That is, the light which originates in a given part of the flame reflects back through the same part. In practice the mirror must be kept at a safe distance to prevent overheating, cracking and corrosion. Also with the optical system that is used the rays emitted by a given part of the flame do not reflect back through the same part of the flame on the path to the camera. In a broad uniform flame this would not be important, but for a slender zoned flame the error can be appreciable.

Obviously this high-resolution method cannot work well for flames which emit a strong continuous spectrum in the wavelength region near the resonance spectral lines because such background radiation would mask out the interference pattern. A limited amount of continuous spectrum radiation can be corrected for by subtracting off the background which appears in the interference pattern. However, the method works best on flames which are nearly colorless before the sodium salt is added to produce the required sodium yellow resonance radiation.

Methods other than the mirrored flame may be used to determine the spectral emissivity. For example, the method described in Part II, reference 1, would be applicable. This consists of comparing the brightness of a sodium vapor lamp as seen alone and as seen through the flames, taking into account the radiation from the flames themselves.

A distinct advantage of this over many other methods of measuring flame temperatures optically is that there is no upper limit to the temperatures that can be measured which are set by the temperature limits of the comparison light or flame. Extremely wide variations in brightness can be compensated for by use of filters of proper transmission, and thus flames many times brighter and hotter than the hottest comparison light can be measured.

This method, like any other method which depends upon equilibrium between the thermal motion of the gas molecules and the thermal excitation of the atoms or molecules which emit and absorb the resonance radiation, will work satisfactorily only under equilibrium or near-equilibrium conditions. If the flame is being excited by electrical discharges or by active chemical reaction the results cannot be trustworthy.

JOURNAL OF APPLIED PHYSICS VOLUME 25, NUMBER 12 DECEMBER, 1954

Anisotropy of Diffusion in Grain Boundaries

S. R. L. COULING* AND R. SMOLUCHOWSKI
Carnegie Institute of Technology, Pittsburgh, Pennsylvania
(Received April 16, 1954)

Grain boundary penetrations of radioactive silver into copper bicrystals having a common cubic direction have been measured using an autoradiographic technique. Diffusion occurred along directions forming an angle $\varphi=0°$, 45°, and 90° with the common cubic direction. For very low angles of disorientation θ, no preferential intergranular penetration was observed; for low and intermediate relative orientations, grain boundary diffusion was found to be most rapid along the common direction ($\varphi=0°$); for high angles of misfit, little anisotropy of boundary diffusion was detected. The observed asymmetry about $\theta=45°$ of the curves of grain boundary penetration *versus* θ is in agreement with the known dependence of the density of boundary dislocations on the angle between grains and on grain boundary direction. The anisotropy measurements may be qualitatively explained in terms of the distribution and relative amounts of elongated areas of "fit" and "misfit" in the grain boundary, and they confirm the earlier proposed model of grain boundaries in the region of angles where the simple dislocation model does not apply.

1. INTRODUCTION

A METALLIC grain boundary may be regarded as a region of transition between the lattices of its two neighboring grains. The properties of the boundary depend, therefore, upon the relative orientation, or more specifically, the degree of fit between the grains. By measuring the effect of variation of the relative orientation on some measurable phenomenon such as relative grain boundary energy, intergranular corrosion, intergranular diffusion, etc., it has been possible to obtain an insight into the actual structure of a simple grain boundary. Such studies have provided evidence of the true nature of low-angle boundaries ($\theta\lesssim 15°$) but have not yet given sufficient information to clarify the structure of boundaries of higher angle.

In 1940, Burgers[1] proposed that a low angle tilt boundary between two simple cubic grains having a common [001] axis could be thought of as composed of a series of edge dislocations running parallel to the common cube direction. If the difference in relative orientation between the grains is a small angle of rotation, θ, about their common axis, then the distance between dislocations, d, is given approximately by the relation

$$d=b/\theta,$$

where b is the Burgers vector of the lattice. This expression provides an indication of the angular range of validity of the ideal Burgers model since one would not expect the dislocations to preserve their identity when their regions of atomic misfit overlap. This occurs at a separation of about three lattice translation vectors which for a simple cubic lattice corresponds to $\theta\sim 15°$. Experimental confirmation of the validity of the model for small angles of misfit is very good. Using this model, Read and Shockley[2] calculated the dependence of relative grain boundary energy on orientation; their theoretical expression agrees well with measurements later made by various investigators on iron,[3,4] tin[5] and lead.[6] Another confirmation of the Burgers model has been recently provided by Vogel *et al.*,[7] who noted that etched lineage boundaries in nearly perfect germanium single crystals were visible as a series of regularly spaced conical etch pits. Assuming each pit to correspond to the termination of an edge dislocation and measuring θ by precision x-ray determination, the authors found that the measured pit spacings agreed excellently with those calculated from the Burgers model. Bubble models of low angle boundaries such as those of Lomer and Nye[8] clearly show the individual dislocations making up the boundary and give further evidence of the validity of the model.

The structure of a boundary of higher angle is still not definitely known. Mott[9] has suggested that a large angle boundary may be thought of as "islands where the fit is reasonably good" separated by "lines near which fit is bad," while Achter and Smoluchowski[10] thought that a description of the boundary as "coherent areas" and "areas of misfit" was more appropriate. It has been later proposed[11] that each of these areas of "misfit" can be ideally considered as formed by coalescence of two (or more) dislocations. Such coalescence of dislocations forms elongated strings or clusters of vacancies and of generally distorted material. The onset of this distorted grain boundary material with increasing θ would be

* Now at the Dow Chemical Company, Midland, Michigan. Submitted in partial fulfillment of the requirements for the degree of Doctor of Science at Carnegie Institute of Technology, 1953.

[1] J. M. Burgers, Proc. Phys. Soc. (London) **52**, 23 (1940).

[2] W. T. Read and W. Shockley, Phys. Rev. **78**, 275 (1950).

[3] C. G. Dunn and F. Lionetti, Trans. Inst. Mining Met. Engrs. **185**, 125 (1949).

[4] Dunn, Daniels and Bolton, Trans. Inst. Mining Met. Engrs. **188**, 1245 (1950).

[5] K. T. Aust and B. Chalmers, Proc. Roy. Soc. (London) **201**, 210 (1950).

[6] K. T. Aust and B. Chalmers, Proc. Roy. Soc. (London) **204**, 359 (1950).

[7] Vogel, Pfann, Corey, and Thomas, Phys. Rev. **90**, 489 (1953).

[8] W. M. Lomer and J. F. Nye, Proc. Roy. Soc. (London) **212**, 576 (1952).

[9] N. F. Mott, Proc. Phys. Soc. (London) **60**, 391 (1948).

[10] M. R. Achter and R. Smoluchowski, J. Appl. Phys. **22**, 1260 (1951).

[11] R. Smoluchowski, Phys. Rev. **87**, 482 (1952).

rather sharp because the repulsion between like dislocations results in a uniform spacing between them. The recent soap bubble studies[8] clearly illustrate this transition from individual dislocations to highly distorted areas. In terms of this model, a grain boundary should be considered as one of three cases:

(a) Small θ (0°–15°); Burgers model applicable.
(b) Intermediate θ (15°–35°); dislocations collect in bunches and form rod-like regions of highly distorted lattice. "Rods" are parallel to common cube direction and separated by relatively undistorted areas.
(c) High θ (35°–45°); rods coalesce into large islands of misfit.

This latter grain boundary model suggests that for small and intermediate values of θ, the boundary should be anisotropic since the dislocations or rods are all roughly parallel to one another and to the common cube direction. A possible method of demonstrating the existence of such anisotropy would be to diffuse atoms intergranularly parallel to and perpendicular to the columnar axis of a bicrystal, expecting that for intermediate values of θ, diffusing atoms would be able to penetrate the boundary faster along the dislocations or rods than they could across them.

2. EXPERIMENTAL METHODS AND RESULTS

The Cu—Ag system was chosen for the investigation. This same system was used previously by Achter and Smoluchowski[10] in determining the effect of relative orientation on intergranular diffusion, the extent of silver penetration into columnar copper boundaries being measured by an etch technique. In the present work,[12] columnar bicrystals of copper were prepared and radioactive silver diffused in different directions of the bicrystals boundaries, the depths of penetration being determined by an autoradiographic method.

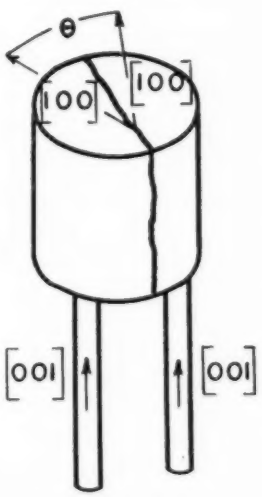

FIG. 1. Bicrystal of relative orientation θ having a common cubic direction.

[12] S. R. L. Couling and R. Smoluchowski, Phys. Rev. **91**, 245(A) (1953).

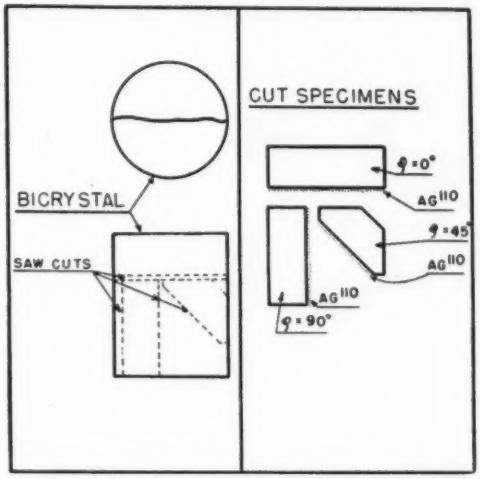

FIG. 2. Orientation of specimens (φ=0°, 45°, 90°) cut from a bicrystal with Ag^{110} plated on the appropriate faces.

A. Preparation of Samples

Using "seeds" with [001] axes, columnar bicrystals of copper (Westinghouse O.F.H.C. grade) of predetermined orientation were grown from the melt in graphite crucibles in a Bridgman vacuum furnace (Fig. 1). The exact orientation difference between grains of a bicrystal was later measured by Laue back-reflection technique, θ being taken as the angle between [100] directions in each grain; by proper pre-orientation of the seeds it was possible to make the grain boundary direction a bisector of the angle between [100] axes, so that the relative orientation could be expressed in terms of only one parameter, θ. The (001) poles of bicrystal grains were always parallel to one another within 4° and closely parallel to the plane of the grain boundary. Altogether, 14 bicrystals, covering the range θ=14° to θ=84° in approximately 5° increments, were used in the investigation.

Using a fine-bladed jeweller's saw and steel blocks mitered at appropriate angles for guides, three specimens were cut from each bicrystal at the following angles (Fig. 2).

(a) φ=0°: cut perpendicular to the common [001] direction of the bicrystal grains.
(b) φ=45°: cut at 45° to the common [001] direction and normal to the plane of the boundary.
(c) φ=90°: cut parallel to the common [001] direction and normal to the plane of the boundary.

The three samples were heavily etched in 50 percent HNO_3 to remove all cold-worked layers, and the surfaces to be plated were polished through 3/0 emery paper, electropolished, and electroplated to a thickness of ~0.05 mm with silver containing radioactive Ag^{110}. The concentration of Ag^{110} in the silver plate was the same for all samples (approximately 1 atom Ag^{110} per 6.5×10^6 atoms ordinary Ag). The specimens were then

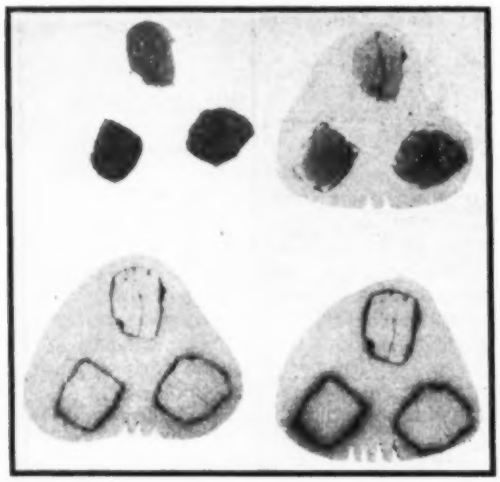

FIG. 3. Typical autoradiographs from a set of specimens having $\theta=19°$. Starting at the top of each autoradiograph and proceeding clockwise, the order of specimens is $\varphi=0°$, $\varphi=45°$, $\varphi=90°$: (a) 0.05 mm from interface; 0.5 hr exposure (b) 0.12 mm from interface; 6 hr exposure (c) 0.20 mm from interface; 40 hr exposure (d) 0.23 mm from interface; 95 hr exposure. Volume diffusion appears as general darkening in the first two layers.

sealed in evacuated Vycor tubes and diffused 336 hours (2 weeks) at 675°C.

B. Autoradiography

After diffusion, the samples were polished down to the Cu−Ag interface and the three specimens of a common orientation ($\varphi=0°$, 45°, 90°) mounted together in a Bakelite block. The reverse side of the mount was ground so as to be plane-parallel to the front and the thickness measured with a micrometer. Grain boundary penetrations of silver into each of the boundaries were then determined by making contact autoradiographs at successive distances from the interface, care being taken to be sure that the face of the block remained parallel to the back within 0.005 mm.

Eastman Kodak No-Screen x-ray film was used for all autoradiographs. Distance from the interface was the determining factor for autoradiograph exposure time: those right at the interface were exposed only about 10 minutes, while those near the limits of silver penetration were exposed 100 hours. The final diffusion distance for a specimen was taken as the average of depths, 0.025 mm apart, where a faint boundary trace could and could not be detected.

C. Results

Selected autoradiographs from a set of specimens ($\theta=19°$) which showed considerable anisotropy of grain boundary diffusion are shown in Fig. 3. At each level, the intensity of film darkening from the boundary of the $\varphi=0°$ specimen is seen to be greater than that from $\varphi=45°$ or $\varphi=90°$, indicating that penetration is deepest along the columnar direction. Because silver carried by vapor transfer diffused into the backs and sides of the specimens during diffusion *in vacuo*, the outer peripheries of the samples are clearly outlined.

Observed grain boundary penetrations, y, are plotted *versus* θ for $\varphi=0°$, 45°, 90° in Fig. 4. In general, intergranular penetrations were measured as $y(\varphi=0°) \geqslant y(\varphi=45°) \geqslant y(\varphi=90°)$ although exceptions to this behavior were noted in the sets of specimens having $\theta=46°$ and $\theta=53°$. Some scatter is seen to be present in the results, probably attributable to small departures from perfect columnarity and possible "cusp" (good fit) orientations in the bicrystals, errors in measuring θ, minor fluctuations in diffusion time and temperature, and errors in determining final diffusion penetrations.

3. DISCUSSION

A. Comparison with Previous Work

The upper solid curve of Fig. 4 (corresponding to diffusion in the columnar direction, $\varphi=0°$) would be expected to be in some way comparable to results reported by Achter and Smoluchowski since in both cases measurements were made of the penetrations of silver into copper boundaries as a function of relative orientation between grains. Qualitatively, there is agreement in curve form: both sets of data show penetrations to be a maximum at $\theta=45°$, to fall off sharply on either side of the peak as the disorientation decreases, and to be zero at low angles of misfit. In the present work, however, the use of the autoradiographic technique enabled the detection of smaller amounts of boundary silver than did the etch method; as a result, preferential penetrations at smaller angles of misfit and deeper penetrations at identical orientations were recorded. These are in accord with the results on self-diffusion in silver.[13]

It is to be noted that the present curve for $\varphi=0°$ is not symmetrical about $\theta=45°$. Read and Shockley[2] predicted an energy cusp at $\theta=53°$ for a face-centered cubic lattice, corresponding to twinning on the (210)

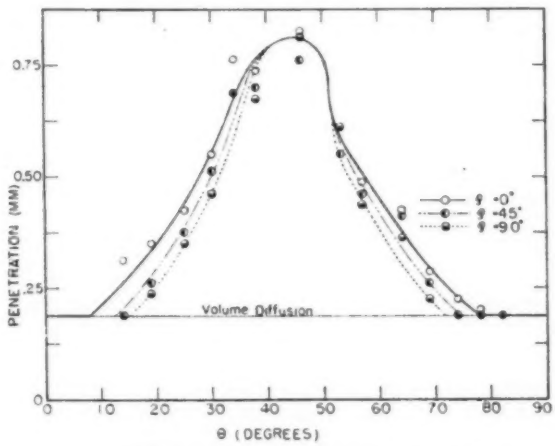

FIG. 4. Grain boundary penetrations as a function of θ for $\varphi=0°$, 45°, 90°.

[13] D. Turnbull and R. E. Hoffman, Acta Metall. 2, 419 (1954).

plane. It is reasonable, therefore, to expect that diffusion penetrations will be lower for $\theta \approx 50°$–$60°$ than for corresponding $\theta \approx 40°$–$30°$; data points indicate that this is actually the case, although no pronounced penetration minimum was observed for $\theta = 53°$. It is to be seen that the points are also consistently lower for $\theta \approx 60°$–$80°$ than for corresponding $\theta \approx 30°$–$10°$. This behavior will be discussed below in detail.

B. Grain Boundary Diffusion Anisotropy

The curves of Fig. 4 definitely indicate the existence of observable anisotropy of grain boundary diffusion over wide ranges of relative orientation. If penetrations into the boundaries are expressed by an equation of the form

$$y^2 = kD,$$

where y = boundary penetration, D = boundary diffusion coefficient, and k = a constant, then

$$2y\Delta y = k\Delta D$$

or

$$\Delta y/y = \tfrac{1}{2}\Delta D/D,$$

where $\Delta y = y(\varphi=0°) - y(\varphi=90°)$ and $\Delta D = D(\varphi=0°) - D(\varphi=90°)$. Values of y and Δy are obtained from Fig. 4 and $\Delta y/y$ is plotted as a function of θ in Fig. 5. The uncertainty in Δy is considerable since it is obtained as a difference between two comparatively large diffusion distances; ranges of $\Delta y/y$ have, therefore, also been plotted assuming the error in determining a particular boundary penetration to be ± 0.012 mm. Points for $\theta = 14°$, $74°$, and $78°$ (full circles) do not belong on the curve because $\varphi = 90°$ grain boundaries of these specimens were never discernible on their respective autoradiographs; for these points, $y(\varphi=90°)$ has been taken equal to volume penetration, 0.187 mm.

It is seen from Fig. 5 that relative grain boundary diffusion anisotropy is very low near $\theta = 45°$, indicating that diffusion coefficients for $\varphi = 0°$ and $\varphi = 90°$ are very nearly identical at high angles of misfit. Maximum observed diffusion anisotropy occurs at $\theta \approx 20°$ or $70°$; for these orientations

$$\frac{\Delta y}{y} \approx 0.3 \approx \frac{1}{2}\frac{D(\varphi=0°) - D(\varphi=90°)}{D(\varphi=0°)},$$

$$D(\varphi=90°)/D(\varphi=0°) \approx 0.4.$$

C. Grain Boundary Structure

It is believed that the observed anisotropy measurements for low angles of misfit may be best explained in terms of the grain boundary structure proposed in reference (11). According to this model, preferential intergranular diffusion will become significant when the grain boundary dislocation density increases to the point where dislocations collect in elongated clusters and permit the rapid passage along them of diffusing

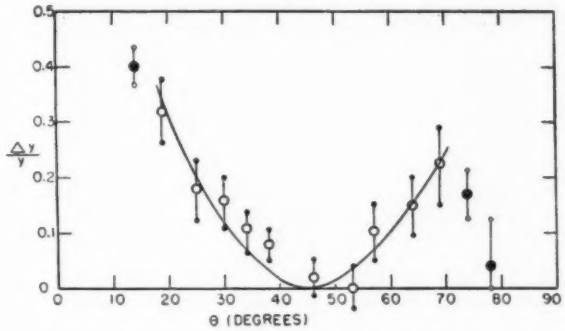

FIG. 5. Relative grain boundary diffusion anisotropy (for $\varphi = 0°$ and $\varphi = 90°$) as a function of θ.

atoms. An examination of the curve for $\varphi = 0°$ of Fig. 4 shows that no boundary penetration is observed when $\theta \lesssim 8°$ or $\theta \gtrsim 78°$. At these two critical orientations the density of boundary dislocations should be identical; using an analysis due to Read and Shockley,[14] it may be shown that such is the case. Considering two face-centered cubic crystallites having a common [001] axis and small-angle of misfit θ', where the grain boundary is allowed to rotate about [001] making an angle α with the mean of the [100] directions in the two grains, Read and Shockley obtain the following expression relating boundary dislocation density, ρ, and grain boundary direction:

$$\rho = \frac{\cos\alpha' + \sin\alpha'}{b}\theta',$$

where b is the Burgers vector of the lattice equal to $a_0/\sqrt{2}$ and $\alpha' = \alpha \pm 45°$, the sign of 45° being so chosen that both α and α' lie between 0° and 90°. For relative orientations $0° \leq \theta \leq 8°$ we have $\theta' = 0$, $\alpha = 0$, $\alpha' = 45°$, and $\rho_1 = 2\theta/a_0$. For relative orientations $78° \leq \theta \leq 90°$ we have $\theta' = 90° - \theta$, $\alpha = 45°$, $\alpha' = 0$, and $\rho_2 = \sqrt{2}(90° - \theta)/a_0$. Since $2(8°) \sim \sqrt{2}(90° - 78°)$, dislocation densities are very nearly identical at the two critical orientations and are given by $0.28/a_0$. Thus when preferential intergranular penetration is first detected, the dislocations are approximately 3.5 lattice constants apart.

Since grain boundary penetration is, in a broad sense, a measure of the dislocation density in the boundary, it is possible to explain why penetrations for $\theta \approx 10°$–$35°$ are consistently higher than they are for corresponding $\theta \approx 80°$–$55°$. The density of boundary dislocations is higher by a factor $\sqrt{2}$ for a low orientation difference θ than it would be if the boundary were rotated 45° about [001] giving an identical disorientation but with relative orientation $(90° - \theta)$.

When elongated clusters of dislocations or rods begin to collect in the boundary, one would expect to be able to observe preferential penetration along the columnar direction because diffusing atoms would be

[14] W. T. Read and W. Shockley, *Imperfections in Nearly Perfect Crystals* (A Symposium held at Pocono Manor, 1950) (John Wiley and Sons, Inc., New York, 1952).

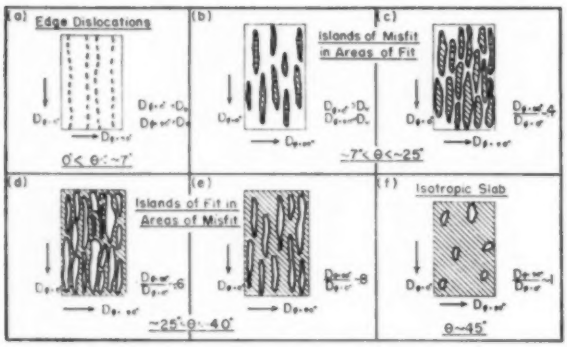

FIG. 6. Grain boundary structure for various relative orientations of grains.

able to travel along the rods faster than they could diffuse in the relatively undistorted material between them. However, for such a configuration, one would not observe penetration perpendicular to the rods because diffusing atoms have no consistently easy path for fast diffusion; it is not until rod density increases appreciably that preferential transverse penetration would be detected. At such a stage it is probably best to think of the boundary as areas of "fit" and "misfit," or "coherency" and "incoherency." Various topological configurations of these areas can be proposed to explain the anisotropy. Perhaps the simplest way is to think of the rods as long, more or less elliptical islands of misfit imbedded in relatively undistorted areas of fit (Figs. 6b and c). The continuous "phase" in the boundary is the region of coherency and an anisotropy of diffusion is observed because the long elliptical islands of misfit offer an easy diffusion path along their major axis. Such a stage may well correspond to disorientations as high as 20°–25°, with the amount of misfit increasing continuously from $\theta \sim 8°$.

At approximately $\theta = 25°$ it may be expected that the boundary will have so much area of misfit that the misfit "phase" of the boundary becomes continuous, i.e., the boundary is then best described as areas of fit surrounded by areas of misfit (Fig. 6d). Such a structure has been proposed previously by Achter and Smoluchowski.[15] An anisotropy of boundary diffusion is still observed because of the long elliptical shape of the coherent areas. As disorientation increases further, the areas of misfit increase at the expense of the coherent areas, causing the latter to decrease in width and possibly shorten the average length of their major axis (Fig. 6e). This means that the boundary exhibits less and less diffusion anisotropy. Finally, at $\theta = 45°$, where the boundary becomes isotropic with respect to diffusion, islands of fit will disappear completely, be distributed in an isotropic manner, or become so widely separated that the boundary is essentially uniform. It follows that the use of the uniform slab model in a theory of grain boundary diffusion is not permissible until the highest angles of disorientation are reached.

ACKNOWLEDGMENT

The financial assistance supplied to one of the authors (S. R. L. Couling) by the U. S. Atomic Energy Commission and the General Electric Company is gratefully acknowledged. Thanks are also due to C. W. Haynes and R. W. Turner for helpful discussion and D. G. Shafer for laboratory assistance in the preliminary phases of the work.

Research was supported by a U. S. Atomic Energy Commission contract.

[15] M. R. Achter and R. Smoluchowski, Phys. Rev. **83**, 163 (1951).

On the Effect of Integration in a Pulsed Radar, Randomly Modulated Carrier

W. M. STONE
Boeing Airplane Company, Seattle, Washington, and Oregon State College, Corvallis, Oregon
(Received January 11, 1954)

The method of Marcum for finding the probability density function associated with a pulsed radar with integration and a square law detector is extended to include the case of a randomly modulated sinusoidal signal. Two mathematical procedures are developed, the well-known Edgeworth asymptotic series and a convergent series suggested by Varma. Sets of curves are drawn for probability of detection *vs* average signal-to-noise power ratio.

Some previous work has shown very high values for probability of detection resulting if it is assumed necessary to detect only one out of many pulses. Such probability levels are reduced if a slowly varying random amplitude of signal is postulated.

I. INTRODUCTION

THIS paper is an extension of the results of the author's "On the Statistical Theory of Detection of a Randomly Modulated Carrier"[1] to include the case of integration of N pulses before a decision is reached by the detecting device associated with a pulsed radar system. The development closely follows that of Marcum,[2] who considered the amplitude of signal to be constant. Kac and Siegert[3] obtained the probability density of noise and constant sinusoidal signal after rectification and arbitrary filtering. The results of Emerson,[4] based on certain orthonormal expansions, seem to indicate that $(1+2\gamma^2)^{\frac{1}{2}}$ can be interpreted as approximately equal to Marcum's N, γ being the ratio of the band widths of the Gaussian video and audio filters.

Rice[5] and others have shown that the envelope R associated with a sinusoidal signal of constant amplitude A in the presence of Gaussian noise is distributed according to the probability density function

$$f(R,A)=\begin{cases}\dfrac{R}{\psi_0}\exp\left(-\dfrac{R^2+A^2}{2\psi_0}\right)I_0\left(\dfrac{RA}{\psi_0}\right), & R\geq 0,\\ 0, & R<0,\end{cases} \quad (1)$$

where ψ_0 is the average noise power of the receiver and the $I_N(x)$ is the modified Bessel function of the first kind, Nth order. To obtain a closed expression it is necessary to postulate a square law detector, equivalent to introducing the dimensionless variables

$$x=R^2/2\psi_0, \quad u=A^2/2\psi_0. \quad (2)$$

That is, the probability that an observed value of a random variable ξ lies between x and $x+dx$ is written

$$P(x<\xi<x+dx)=f(x,u)dx$$
$$=\begin{cases}\exp(-x-u)I_0[2(xu)^{\frac{1}{2}}]dx, & x\geq 0,\\ 0, & x<0.\end{cases} \quad (3)$$

The probability density function associated with a new random variable x,

$$x=x_1+x_2+\cdots+x_N, \quad (4)$$

where x represents the sum or integration of N such variables as appear in (3), has been developed by Marcum. Equation (4) requires an idealized integrating circuit device which actually performs the implied addition without weighting the N original variates in any way.

A characteristic function is defined as the Fourier transform of a given probability density function:

$$\varphi(z)=E(e^{i\xi z})=\int_{-\infty}^{\infty}e^{ixz}f(x)dx. \quad (5)$$

If the same probability density function $f(x,u)$ is associated with each x_i, the Fourier transform of $f(x,u,N)$, the probability density function associated with the new variable x, is the Nth power of the transform of $f(x,u)$ above;

$$\varphi(z,u,N)=E(e^{i\xi z})=[\varphi_1(z,u)]^N, \quad (6)$$

where

$$\xi=\xi_1+\xi_2+\cdots+\xi_N. \quad (7)$$

Since the random variables involved can take on positive values only, it is easier to use the Laplace transform formulas of Churchill.[6]

$$\varphi_1(s,u)=\int_0^{\infty}\exp(-sx-x-u)I_0[2(xu)^{\frac{1}{2}}]dx$$
$$=\frac{1}{s+1}\exp\left(-\frac{su}{s+1}\right) \quad (8)$$

[1] W. M. Stone, J. Appl. Phys. **24**, 935–939 (1953).
[2] J. I. Marcum, "A Statistical Theory of Target Detection by Pulsed Radar; Mathematical Appendix," the RAND Corporation, Research Memorandum RM-753 (1948).
[3] M. Kac and A. J. F. Siegert, J. Appl. Phys. **18**, 383–397 (1947).
[4] R. C. Emerson, J. Appl. Phys. **24**, 1168–1176 (1953).
[5] S. O. Rice, Bell System Tech. J. **23**, 282–332 (1944); **25**, 46–156 (1945).
[6] R. V. Churchill, *Modern Operational Mathematics in Engineering* (McGraw-Hill Book Company, Inc., New York, 1944).

and

$$\varphi(s,u,N)=\frac{1}{(s+1)^N}\exp\left(-\frac{sNu}{s+1}\right). \quad (9)$$

The inverse transformation yields at once

$$f(x,u,N)=\begin{cases}\exp(-x-Nu)(x/Nu)^{(N-1)/2} \\ \qquad\times I_{N-1}[2(Nxu)^{\frac{1}{2}}], \quad x\geq 0, \\ 0, \quad x<0.\end{cases} \quad (10)$$

Marcum's criterion of detection is that the sum of N samples of the normalized and squared envelope shall exceed a certain bias level, say x_0. The probability that this event occurs is

$$P(x>x_0)=P(x_0,N,u)$$
$$=\int_{x_0}^{\infty}\exp(-x-Nu)(x/Nu)^{(N-1)/2}\times I_{N-1}[2(Nxu)^{\frac{1}{2}}]dx. \quad (11)$$

The bias level must be chosen in terms of the probability that a false alarm will occur. From (11) the probability that noise alone will exceed the bias level is

$$P(x_0,N,0)=\frac{1}{(N-1)!}\int_{x_0}^{\infty}e^{-x}x^{N-1}dx. \quad (12)$$

The false alarm time is the time in which the probability is P_0 that noise alone will not exceed the bias. Hence,

$$P(x_0,N,0)=1-P_0^{N/n}, \quad (13)$$

where Marcum defines n as the false alarm number in terms of false alarm time and the filter band width of the system. Since N/n is small in practice it is permissible to write

$$P(x_0,N,0)=1-\exp\left(-\frac{N}{n}\log\frac{1}{P_0}\right)$$
$$\approx\frac{N}{n}\log\frac{1}{P_0}=NP(x_0,1,0). \quad (14)$$

In the construction of curves of probability of detection an arbitrary choice of x_0 for $N=1$ establishes the value of $P(x_0,1,0)$; successive applications of (13) and (12) determine the bias levels associated with other values of N. The Pearson[7] table of the incomplete gamma function is readily available for this procedure, provided $N\leq 50$.

II. RANDOMLY MODULATED CARRIER

Section I was a statement of results obtained by Marcum and Kaplan and McFall.[8] The next step is to study the effect of taking the normalized amplitude of signal to be itself a random variable, $y(t)=A(t)/\psi_0^{\frac{1}{2}}$, in particular, a slowly varying random variable. The last remark is important to the theory below and is well substantiated by field measurements. By a rigorous development Middleton[9] has shown that it is permissible to "average over all phases" of the amplitude; hence it is necessary to postulate a probability density function associated with y, say $g(y,M,\sigma)$, $y\geq 0$. The mean M and the standard deviation σ of y are placed in evidence because of the great importance of their relative magnitudes. The new form of the probability density function associated with the envelope is

$$P(x<\xi<x+dx)=f(x,N,M,\sigma)dx$$
$$=e^{-x}dx\int_0^{\infty}g(y,M,\sigma)\exp(-Ny^2/2)(2x/Ny^2)^{(N-1)/2}\times I_{N-1}[y(2Nx)^{\frac{1}{2}}]dy. \quad (15)$$

The choice of bias level is independent of signal so the probability of detection takes the form

$$P(x>x_0)=P(N,M,\sigma,x_0)=\int_{x_0}^{\infty}f(x,N,M,\sigma)dx. \quad (16)$$

(a) Edgeworth Series Representation

As indicated in reference (1) a logical procedure is to expand $f(x,N,M,\sigma)$ in an Edgeworth series. This requires knowledge of the various moments associated with x; it is sufficient to develop a general formula for the nth moment,

$$\alpha_n=E(x^n)=\int_0^{\infty}x^nf(x,N,M,\sigma)dx. \quad (17)$$

The easiest method is to apply the Laplace transformation:

$$\varphi(s,N,M,\sigma)=\int_0^{\infty}e^{-sx}f(x,N,M,\sigma)dx$$
$$=\frac{1}{(s+1)^N}\int_0^{\infty}g(y,M,\sigma)\times\exp[-Nsy^2/2(s+1)]dy. \quad (18)$$

There is no question about the validity of interchanging the order of integration in (18). The expansion of a Laplace transform in a Taylor series is always possible;

$$\varphi(s,N,M,\sigma)=\sum_{n=0}^{\infty}\frac{a_ns^n}{n!}, \quad (19)$$

where

$$a_n=(-1)^n\alpha_n. \quad (20)$$

The Taylor series in question is quickly obtained by a

[7] K. Pearson, *Tables of the Incomplete Gamma Functions* (Cambridge University Press, Cambridge, 1946).

[8] S. M. Kaplan and R. W. McFall, Proc. Inst. Radio Engrs. **39**, 50–60 (1951).

[9] D. Middleton, Quart. Appl. Math. **5**, 445–498 (1948).

simple rearrangement of terms

$$\varphi(s,N,M,\sigma)=\int_0^\infty g(y,M,\sigma)\sum_{k=0}^\infty \frac{(-1)^k}{2^k k!}\frac{(Nsy^2)^k}{(s+1)^{k+N}}dy$$

$$=\int_0^\infty g(y,M,\sigma)\sum_{k=0}^\infty \frac{(-1)^k}{2^k k!}(Ny^2)^k \times\sum_{r=0}^\infty \binom{-k-N}{r}s^{r+k}dy. \quad (21)$$

If $r+k=n$, $0\leq k\leq n$, an interchange of the order of summation yields

$$\varphi(s,N,M,\sigma)=\int_0^\infty g(y,M,\sigma)\sum_{n=0}^\infty \frac{(-s)^n}{n!} \times\sum_{k=0}^n (Ny^2)^k \frac{n!(N+k)\cdots(N+n-1)}{2^k k!(n-k)!}dy$$

$$=\int_0^\infty g(y,M,\sigma)\sum_{n=0}^\infty \frac{(N)_n(-s)^n}{n!} \times\sum_{k=0}^n \binom{n}{k}\frac{(Ny^2)^k}{2^k(N)_k}dy, \quad (22)$$

where

$$(N)_n=N(N+1)\cdots(N+n-1), \quad (N)_0=1. \quad (23)$$

Referring to (19), the form of the nth moment associated with the $f(x,N,M,\sigma)$ is

$$\alpha_n=(N)_n\sum_{k=0}^n \binom{n}{k}\frac{N^k}{2^k(N)_k}\int_0^\infty y^{2k}g(y,M,\sigma)dy. \quad (24)$$

(b) Normal Law Distribution of Carrier Amplitude

A logical assumption is that the carrier amplitude is normally distributed about a mean value of M with standard deviation σ. The random variable y is essentially non-negative; hence

$$g(y,M,\sigma)=\begin{cases} B\exp\left(-\dfrac{(y-y_0)^2}{2a^2}\right), & 0\leq y<\infty, \\ 0, & y<0, \end{cases} \quad (25)$$

where B is a normalizing constant,

$$u(r)=(Ba)^{-1}=(2\pi)^{\frac{1}{2}}[\tfrac{1}{2}+\varphi^{(-1)}(1/r)], \quad r=a/y_0. \quad (26)$$

TABLE I. $C_k(r)=[Q_{2k}(r)/Q_2^k(r)]$.

n_0	2	2.5	3	3.5	4	5	6
$1/r$	1.728	2.410	2.975	3.494	4.000	5.000	6.000
k							
2	1.80916	1.53276	1.38349	1.29108	1.22834	1.15089	1.10665
3	4.53057	3.05316	2.38013	2.00383	1.76480	1.48726	1.33716
4	14.3068	7.39222	4.84549	3.60158	2.88295	2.12261	1.74658
5	54.1909	20.9427	11.3276	7.31748	5.25419	3.30562	2.44716

Here $\varphi^{(-1)}(x)$ is the error function,

$$\varphi^{(-1)}(x)=(2\pi)^{-\frac{1}{2}}\int_0^x \exp(-t^2/2)dt. \quad (27)$$

To evaluate the integral in (24) for this choice of $g(y,M,\sigma)$ it is convenient to define a set of functions

$$u(r)Q_k(r)=\int_0^{1/r}\exp(-x^2/2)(1-rx)^k dx + \int_0^\infty \exp(-x^2/2)(1+rx)^k dx. \quad (28)$$

A recurrence formula is easily obtained

$$u(r)[Q_k(r)-Q_{k-1}(r)] =\int_0^{1/r}\exp(-x^2/2)[(1-rx)^k-(1-rx)^{k-1}]dx + \int_0^\infty \exp(-x^2/2)[(1+rx)^k-(1+rx)^{k-1}]dx$$

$$=-r\int_0^{1/r} x\exp(-x^2/2)(1-rx)^{k-1}dx + r\int_0^\infty x\exp(-x^2/2)(1+rx)^{k-1}dx. \quad (29)$$

Integration by parts leads to

$$Q_k(r)-Q_{k-1}(r)=r^2(k-1)Q_{k-2}(r), \quad (30)$$

with

$$Q_0(r)=1, \quad Q_1(r)=1+\frac{r}{u(r)}\exp(-1/2r^2). \quad (31)$$

A table of the Q functions is easily constructed. Equation (24) now takes the form

$$\alpha_n=(N)_n\sum_{k=0}^n \binom{n}{k}[(Ny_0^2)^k/2^k(N)_k]Q_{2k}(r). \quad (32)$$

This notation is more concise than that of reference (1).

The parameters y_0 and a may be determined by conditions that the ratio of the mean of y to the standard deviation is some fixed number n_0 and that the average signal-to-noise power ratio z,

$$z=E(y^2/2)=(y_0^2/2)Q_2(r), \quad (33)$$

may be taken as the independent variable. It is easy to show that

$$E(y^2)/[E(y)]^2=1+1/n_0^2=Q_2(r)/Q_1^2(r), \quad (34)$$

from which r must be obtained by trial and error. As a function of z the nth moment is

$$\alpha_n=(N)_n\sum_{k=0}^n \binom{n}{k}[(Nz)^k/(N)_k]C_k(r), \quad (35)$$

where

$$C_k(r)=[Q_{2k}(r)/Q_2^k(r)]. \quad (36)$$

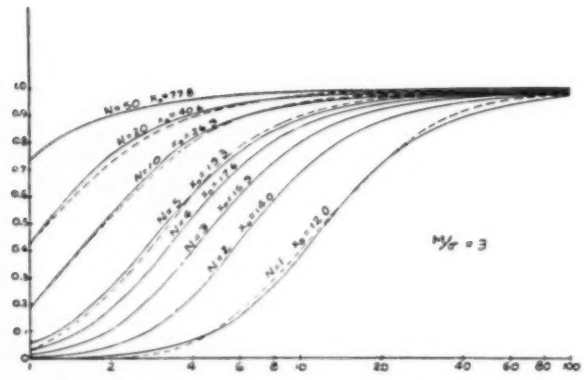

FIG. 1. Probability of detection vs average signal-to-noise power ratio, normally distributed carrier amplitude $M/\sigma=3$, Edgeworth, approximate Varma.

The $C_k(r)$ are tabulated in Table I for various values of n_0.

Equation (16) may be rewritten in the form

$$P(N,n_0,z,x_0)=\int_{x_0}^{\infty} f(x,N,n_0,z)dx. \tag{37}$$

Curves of this probability of detection have been sketched by the Edgeworth series method in Fig. 1 for the case $n_0=3$, N and x_0 taking on various values. The Edgeworth series is actually not convergent for the case under discussion. However, the curves in Fig. 1 may be checked by other methods discussed below.

III. VARMA SERIES REPRESENTATION

A convergent series representation of the probability of detection may be obtained by a method closely following that of Varma.[10] Equation (37) may be written in the form

$$1-P=\int_0^{x_0} e^{-z}dx\int_0^{\infty} g(y,M,\sigma)\exp(-Ny^2/2)\times(2x/Ny^2)^{(N-1)/2}I_{N-1}[y(2Nx)^{\frac{1}{2}}]dy. \tag{38}$$

The definite integral form of the Bessel function,

$$I_{N-1}(x)=\frac{x^{N-1}}{2^{N-1}\Gamma(\frac{1}{2})\Gamma(N-\frac{1}{2})}\int_0^{\pi}\times\exp(x\cos\theta)\sin^{2N-2}\theta d\theta, \tag{39}$$

leads to a triple integration for $1-P$. Expansion of the exponential factor and term-by-term integration with respect to θ yields

$$1-P=(\pi)^{-1}\int_0^{x_0} e^{-z}dx\int_0^{\infty} g(y,M,\sigma)\exp(-Ny^2/2)\times\sum_{k=0}^{\infty}\frac{(2Nxy^2)^k}{(2k)!}\frac{\Gamma(k+\frac{1}{2})}{\Gamma(N+k)}dy, \tag{40}$$

which may be reduced to

$$1-P=\int_0^{\infty} g(y,M,\sigma)\exp(-Ny^2/2)dy\times\sum_{k=0}^{\infty}\frac{(Ny^2)^k}{2^k k!\Gamma(N+k)}\int_0^{x_0} e^{-x}x^{N+k+1}dx. \tag{41}$$

Let

$$G(N+k,x_0)=\frac{1}{\Gamma(N+k)}\int_0^{x_0} e^{-x}x^{N+k-1}dx, \tag{42}$$

a form slightly different from the Pearson Incomplete Gamma function. Finally,

$$1-P=\sum_{k=0}^{\infty}\frac{N^kG(N+k,x_0)}{2^k k!}\int_0^{\infty} y^{2k}\times\exp(-Ny^2/2)g(y,M,\sigma)dy. \tag{43}$$

(a) Rayleigh Distributed Amplitude

Quite a simple result is obtained if the amplitude of signal is assumed to be distributed as the square root of the sum of squares of m normal variates (see Cramér,[11] p. 236),

$$g(y,M,\sigma)=\begin{cases}\dfrac{2y^{m-1}\exp(-y^2/2b^2)}{2^{m/2}b^m\Gamma(m/2)}, & 0\le y<\infty.\\ 0, & y<0.\end{cases} \tag{44}$$

This yields $z=E(y^2/2)=mb^2/2$. Table II lists n_0 as a function of m, based on the relationship

$$\frac{1}{n_0^2}=\frac{\sigma^2}{M^2}=\frac{m\Gamma^2(m/2)}{2\Gamma^2(m+1/2)}-1. \tag{45}$$

The integral factor of the kth term in the series of (43) is easily evaluated:

$$\int_0^{\infty} y^{2k+m-1}\exp\left[-\frac{y^2(1+Nb^2)}{2b^2}\right]dy=\frac{1}{2}\left(\frac{2b^2}{1+Nb^2}\right)^{k+m/2}\int_0^{\infty} e^{-u}u^{k-1+m/2}du, \tag{46}$$

and, finally,

$$1-P=\frac{1}{\Gamma(m/2)(1+2Nz/m)^{m/2}}\sum_{k=0}^{\infty}\left(\frac{2Nz}{m+2Nz}\right)^k\times\frac{\Gamma(k+m/2)}{k!}G(N+k,x_0). \tag{47}$$

TABLE II. $n_0=M/\sigma$.

m	2	3	4	5	6	7	8	9	10
n_0	1.913	2.370	2.755	3.049	3.400	3.681	3.943	4.189	4.420
m	11	12	13	14	15	16	17	18	
n_0	4.640	4.851	5.053	5.247	5.432	5.616	5.790	5.961	

[10] R. S. Varma, Quart. J. Mech. Appl. Math. 5, 361–363 (1952).

[11] H. Cramér, *Mathematical Methods of Statistics* (Princeton University Press, Princeton, 1946).

Because of the binomial expansion

$$(1-x)^{-m/2}=\frac{1}{\Gamma(m/2)}\sum_{k=0}^{\infty}\frac{x^k}{k!}\Gamma(k+m/2), \quad (48)$$

it follows that

$$\lim_{x_0\to\infty} P(N,n_0,z,x_0)=0, \quad (49)$$

a check on the derivation since probability of detection is zero for an arbitrarily high bias. The Rayleigh case, $m=2$, $n_0=1.913$, is of special interest.

$$P(N,n_0,z,x_0)=1-\frac{1}{1+Nz}\sum_{k=0}^{\infty}\left(\frac{Nz}{1+Nz}\right)^k G(N+k,c_0). \quad (50)$$

Figure 2 constitutes a set of such Rayleigh curves for various values of N and x_0. For low values of N the series of (50) may be summed at once to a simple exponential expression.

(b) Normally Distributed Amplitude

The assumption that $g(y,M,\sigma)$ is the normal probability density function defined by (25) leads to an integral which is evaluated at once. Taking $\beta^2=1+Na^2$, the integral factor in (43) is

$$B\int_0^{\infty}\exp\left[-\frac{(y-y_0)^2}{2a^2}-\frac{Ny^2}{2}\right]y^{2k}dy$$

$$=\frac{\exp(-Ny_0^2/2\beta^2)}{\beta^{k+1}u(r)}\int_{-1/\beta r}^{\infty}\exp(-u^2/2)(\beta au+y_0)^{2k}dy$$

$$=\exp(-Ny_0^2/2\beta^2)\frac{u(\beta r)}{\beta u(r)}\left(\frac{y_0}{\beta^2}\right)^{2k}Q_{2k}(\beta r). \quad (51)$$

The Varma series representation of the probability of detection (37) is, therefore,

$$P(N,n_0,z,x_0)=1-\exp(-Ny_0^2/2\beta^2)\frac{u(\beta r)}{\beta u(r)}\times\sum_{k=0}^{\infty}\left(\frac{Na^2}{\beta^2}\right)^k\frac{G(N+k,x_0)}{2^k k!}\frac{Q_{2k}(\beta r)}{(\beta r)^{2k}}. \quad (52)$$

This form of the probability function must satisfy the condition that

$$\lim_{x_0\to\infty} P(N,n_0,z,x_0)=0=1-\exp(-Ny_0^2/2\beta^2)\frac{u(\beta r)}{\beta u(r)}\times\sum_{k=0}^{\infty}\left(\frac{Na^2}{\beta^2}\right)^k\frac{Q_{2k}(\beta r)}{2^k k!(\beta r)^{2k}}. \quad (53)$$

From the definition of $u(x)Q_{2k}(x)$ in (28) it is easy to establish that

$$d/dx[u(x)Q_{2k}(x)]=2k(2k-1)xu(x)Q_{2k-2}(x). \quad (54)$$

It follows that the more general expression

$$F(x,t)=u(x)\sum_{k=0}^{\infty}\frac{t^k}{2^k k!}\frac{Q_{2k}(x)}{x^{2k}}, \quad 0\le t<1, \quad x>0, \quad (55)$$

is the solution of the partial differential equation

$$xF_x(x,t)=t[F(x,t)+2(t-1)F_t(x,t)]. \quad (56)$$

Straightforward differentiation shows that

$$F(x,t)=C(1-t)^{-1/2}\exp t/2x^2(1-t), \quad (57)$$

where C is an arbitrary constant determined by the use of (53). Setting $x=\beta r$ and $t=Na^2/\beta^2$ establishes the result

$$\frac{u(\beta r)}{\beta u(r)}\sum_{k=0}^{\infty}\left(\frac{Na^2}{\beta^2}\right)^k\frac{Q_{2k}(\beta r)}{2^k k!(\beta r)^{2k}}=\exp(Ny_0^2/2\beta^2). \quad (58)$$

(c) Approximate Methods

The series in (47) or (50) are slowly convergent, some 30 to 50 terms being required for values of N between 1 and 20. This suggests that the approximation of $G(N+k,x_0)$ by a sum of exponential functions might be advantageous since it would lead to closed forms for the probability of detection. Excellent results have been obtained by taking

$$G(N+k,x_0)\approx\sum_{s=1}^{s_0}c_s\exp(-ks/n), \quad (59)$$

where the parameter n can usually be chosen by inspection of the tabulated values of $G(N+k,x_0)$. The least-squares method yields a set of s_0 equations for the determination of the c's,

$$\sum_{s=1}^{s_0}c_s\sum_{k=0}\exp[-k(s+j)/n]=\sum_{k=0}\exp(-kj/n)G(N+k,x_0), \quad (60)$$

where $j=1, 2, \cdots, s_0$ and k is continued until the $G(N+k,x_0)$ is negligible. The approximation to (47) takes the form

$$P(N,n_0,z,x_0)\approx 1-\sum_{s=1}^{s_0}\frac{c_s}{[1+(2Nz/m)(1-q^s)]^{m/2}}, \quad (61)$$

where $q=\exp(-1/n)$. Except for low values of z and N this yields curves which are quite indistinguishable from those in Fig. 2 obtained by laboriously exact summation of the Rayleigh series in (50), the case $m=2$. For values of $N\le 20$ it was found that n might be chosen to be 12 or 16. It is possible to save labor by taking, say, every third value of the $G(N+k,x_0)$, equivalent to choosing n to be one-third as large. This would be advisable for values of N so large that $G(N+k,x_0)$ could not be evaluated entirely from Pearson's tables.

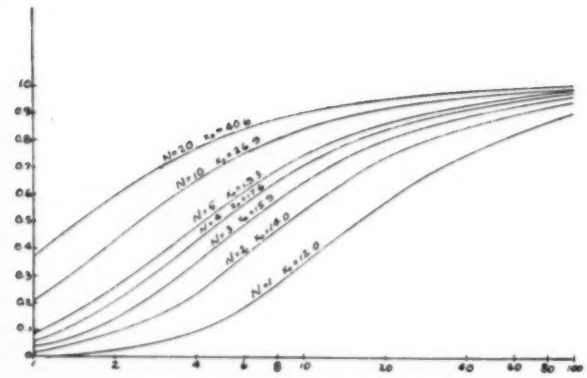

FIG. 2. Probability of detection *vs* average signal-to-noise power ratio, Rayleigh distributed carrier amplitude $M/\sigma=3$.

Equation (52) for the normally distributed case is quite impractical for computation but the use of (59) leads to the simple form

$$P(N,n_0,z,x_0)\approx 1-\sum_{s=1}^{s_0}\frac{c_s\exp\left(\dfrac{-Ny_0^2(1-q^s)}{2[1+Na^2(1-q^s)]}\right)}{[1+Na^2(1-q^s)]^{\frac{1}{2}}}. \quad (62)$$

The dotted curves in Fig. 1 were obtained by use of (62) with $s_0=3$. Apparently not much is gained by taking $s_0=4$ or more. Except for low values of z and N this appears to be as accurate as the nonconvergent Edgeworth series method and is certainly less laborious.

IV. SIMPSON METHOD

It was pointed out in reference (1) that for a normalized constant amplitude of signal y the probability of failure to detect, unintegrated case, is

$$1-p=\int_0^{x_0}\exp(-t-y^2/2)I_0[y(2t)^{\frac{1}{2}}]dt$$

$$=F(x_0,y^2/2), \quad (63)$$

where $F(x,y)$ is a function tabulated by Brinkley, Edwards, and Smith.[12] The probability of n successive failures to detect would be $(1-p)^n$. The joint probability element that a randomly modulated signal lies between y and $y+dy$ and that n successive failures to detect occur is

$$d(1-P)=g(y,M,\sigma)dyF^n(x_0,y^2/2). \quad (64)$$

Finally, the probability that a signal is detected at least once out of n examinations of a pulse return is

$$P(n,n_0,z,x_0)=1-\int_0^\infty g(y,M,\sigma)F^n(x_0,y^2/2)dy. \quad (65)$$

For various choices of $g(y,M,\sigma)$ the integral may be evaluated by Simpson's rule without excessive difficulty. The results are presented in Fig. 3 for the normally distributed case, $n_0=3$. The form of (65) may be easily altered to include other criteria of detection, such as requiring that at least two of n pulses show the presence of a signal. The curves in Fig. 3 approach unity more slowly than indicated by previous theory. This is because a slowly varying signal amplitude implies a finite probability that at the instant of contact the signal is in a deep fade. And a high scanning rate will not allow time for an appreciable change of signal strength.

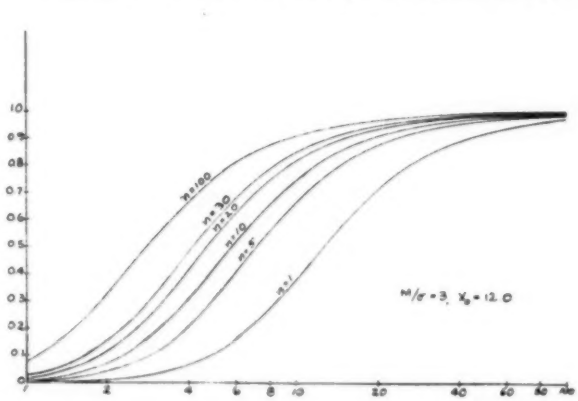

FIG. 3. Probability that at least one of n pulses is detected *vs* average signal-to-noise power ratio, normally distributed carrier amplitude $M/\sigma=3$, $x_0=12$.

ACKNOWLEDGMENTS

The research in this paper has been supported by the Unites States Air Force. The author wishes to acknowledge that the ideas of Sec. IV were originally put forth by Warren Leyde. The graphical and numerical work was done by Gladys Williams and N. W. Stone.

[12] Brinkley, Edwards, and Smith, "Table of the Temperature Distribution Function for Heat Exchange between a Fluid and a Porous Solid" (U. S. Bureau of Mines, Pittsburgh, Pennsylvania).

Letters to the Editor

Information Theory and Knowledge: Remarks on a Paper by D. K. C. MacDonald

A. GAMBA
Istitu to di Fisica dell'Università, Turin, Italy
(Received July 20, 1954)

THE physical implications of the recently developed theory of communication[1] have been discussed by Brillouin,[2] who has shown that the second principle of thermodynamics can be consistently enlarged in order to take into account "information." Information is equivalent to negentropy (negative entropy), and the generalized second principle of thermodynamics states that in any transformation of a closed system the quantity "entropy minus information" must always increase or, at best, remain constant;

$$\Delta(S-I)\geqslant 0. \tag{1}$$

Communication theory is that part of thermodynamics which deals with the transformations negentropy$\rightleftarrows$information.

In an interesting paper MacDonald[3] suggested recently that the usual definition of information, as given by Shannon,[1] does not seem adequate for the case of "new" knowledge (for example the knowledge one gets by discovering a natural law). He tentatively proposed, therefore, a different formula for this case. However, if such a proposal were to be accepted, the information would no longer be an additive quantity, and the generalized second principle of thermodynamics Eq. (1) would break down.

In order to solve this difficulty let us examine a particularly simple case. Consider a system of N classical particles distributed among k cells in such a way that n_1 are in the first, n_2 in the second, $\cdots$, n_k in the kth cell. The number of different configurations is

$$P_1=\frac{N!}{n_1!\,n_2!\cdots n_k!}, \quad \text{with } N=n_1+n_2+\cdots+n_k,$$

and thus the entropy of the system is (using Stirling's formula)

$$S_1=k\ln P_1=-kN\Sigma p_i\ln p_i, \tag{2}$$

where $p_i=n_i/N$. This formula is to be compared with Shannon's definition of information. Therefore, if we determine the actual state of the system, i.e., which particle is in which cell, we obtain an amount of information

$$I_1=S_1$$

which must be paid for by an over-all increase in the entropy of the measuring apparatus

$$\Delta S\geqslant I_1. \tag{3}$$

Let us now assume that there is a natural law which states that only the 1st, 2nd, 3rd, $\cdots$, n_1th particle can go into the first cell. By the same arguments as above, the entropy would then be given by

$$S_2=S_1-A, \tag{4}$$

where A is a positive constant, and if we determine the state of the system by a measurement we get an amount of information

$$I_2=S_2$$

which must be paid for by an over-all increase in the entropy of the measuring apparatus

$$\Delta S'\geqslant I_2. \tag{5}$$

In the case of an optimum measurement, i.e., when the equality sign holds in Eqs. (3) and (5),

$$\Delta S-\Delta S'=I_1-I_2=A.$$

It seems, therefore, that in the latter case we have determined the state of the system saving an amount of entropy A with respect to the first case. If the number of such systems is n, we can save an amount of entropy nA, which in turn can be used to obtain other information. So, by letting n go to infinity, it seems that the amount of information we can get by knowing a natural law is actually infinite.

The example chosen is rather artificial, but it seems particularly suited in pointing out where the basic incorrectness of this kind of argument lies. A reassessment of the initial *a priori* probabilities does not mean a *real* change of entropy (or information) from S_1 to S_2: it simply means that the entropy we assigned to the system the first time was wrong. The very definition of entropy by means of the Boltzmann formula holds true, provided that the *a priori* probabilities are correctly assigned. And the same argument, of course, holds for information. Therefore, the discovery of a natural law does not mean a gain in information or negentropy, but simply means that we are then able to correct some previous mistakes. In principle, the existence of a natural law could be inferred just through inconsistencies due to a wrong assignment of entropies.

We may, therefore, conclude by saying that there seems to be no reason to define information due to new knowledge. In any case, such a definition would fall outside the domain of physics, whereas the usual concept of information cannot be separated from the concept of entropy without leading to inconsistencies.

[1] C. E. Shannon and W. Weaver, *Mathematical Theory of Communication* (University of Illinois Press, Urbana, Illinois, 1949).
[2] L. Brillouin, J. Appl. Phys. **24**, 1152 (1953); **25**, 595 (1954). See also D. Gabor, Phil. Mag. **41**, 1162 (1950).
[3] D. K. C. MacDonald, J. Appl. Phys. **25**, 619 (1954).

On the Interaction of Two Similarly Facing Plane Shock Waves

C. A. FORD AND I. I. GLASS
Institute of Aerophysics, University of Toronto, Toronto, Canada
(Received August 13, 1954)

AN ingenious method of generating the interaction of two similarly facing plane shock waves has been described by Laporte and Turner.[1] We would like to draw attention to two alternate methods of producing the same interaction which have been used at the Institute of Aerophysics since 1952. These

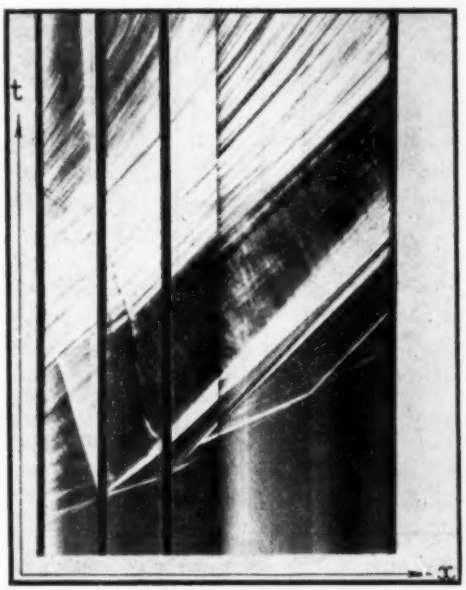

FIG. 1. Double refraction of a plane shock wave at a helium layer and subsequent overtaking of two similarly facing shock waves. Case air ‖He‖ air. Microfilm method. (Composite photograph of two (x,t)-plane schlieren records.)

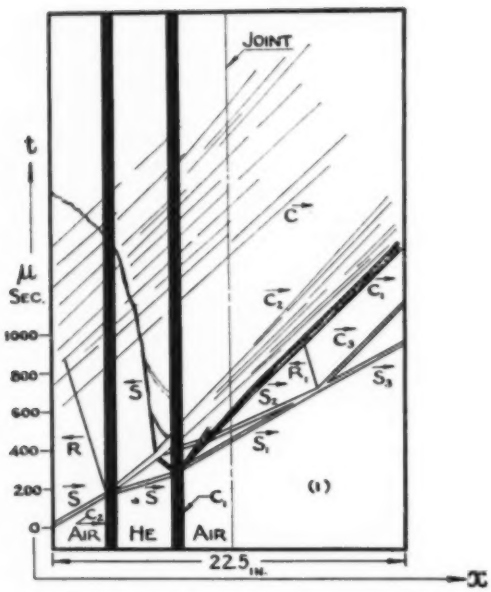

FIG. 2. Double refraction of a plane shock wave at a helium layer and subsequent overtaking of two similarly facing shock waves. Case air ‖He‖ air. Microfilm method. (Explanatory line diagram of actual (x,t)-plane schlieren records shown on Fig. 1.) Air‖He‖air initially at rest. $p_1=747$ mm Hg; $a_1=1130$ ft/sec; S_1=incident shock (1.69 a_1); S_2=overtaking shock (1.23 a_1); S_3=transmitted shock (1.69 a_1); R_1=head of reflected rarefaction wave (0.28 a_1 at a pressure ratio of 0.97); C_2=contact front (0.90 a_1); C_1, C_2 microfilm contact surfaces.

methods possess in addition the desirable advantage of having the coalesced or transmitted shock wave travel in a gas at rest whose state is initially known.

Figure 1 is an (x,t)-plane schlieren photograph composed of two records matched in the center and covers a distance of 22.5 in. of the shock-tube flow. It shows the wave system before and after the interaction on a single plate. Figure 2 is an explanatory line diagram of Fig. 1. A plane shock wave strikes a microfilm (nitrate dope, 3000 A thick) contact film C_2, separating air and helium at rest. A transmitted shock wave and a reflected rarefaction wave separated by a contact front result after the collision. The transmitted shock wave then strikes a similar contact film C_1, separating the helium from the air (1) at rest. A transmitted shock S_1 and a reflected shock separated by a contact front are formed after this interaction. The reflected shock recedes and strikes C_2. It is reflected, collides with C_1, forming the transmitted shock S_2. The similarly facing shocks S_1 and S_2 then overtake, interact, and generate the transmitted shock wave S_3, the reflected rarefaction wave R_1, and between them the "ideal" contact front C_3. The overtaking shock waves are thus formed as a result of a double refraction of a plane shock wave at a layer of helium. Theoretical and experimental details of this investigation have been reported previously.[2,3]

Figure 3 is composed of an actual (x,t)-schlieren record and an explanatory line drawing of the wave system before and after the same type of interaction. It is produced essentially by utilizing three shock-tube chambers at successively higher pressures.[3] When the two diaphragms are ruptured, two overtaking shock waves are generated.

An analysis of the wave-speed records for the overtaking shock wave problem gave very good agreement with theory.[4]

It should be noted that all the wave elements appear on the present records—even the head of the rarefaction wave.

As observed in reference 1, the contact front on (x,t)-schlieren photographs also appears extremely sharp, despite the small density change. The sharpness is probably due to the large gradient of the density profile of the "ideal" contact front which is formed by the overtaking of two similarly facing shock waves.

[1] Otto Laporte and G. B. Turner, J. Appl. Phys. 25, 678 (1954).
[2] Glass, Martin, and Patterson, "A Theoretical and Experimental Study of the Shock Tube," Institute of Aerophysics, University of Toronto, UTIA Report No. 2 (November, 1953).
[3] C. A. Ford and I. I. Glass, "An Experimental Study of Shock-Wave Refraction," UTIA Report No. 29 (to be published in 1954).
[4] Bull, Fowell, and Henshaw, "The Interaction of Two Similarly-Facing Shock Waves," UTIA Report No. 25 (January, 1953).

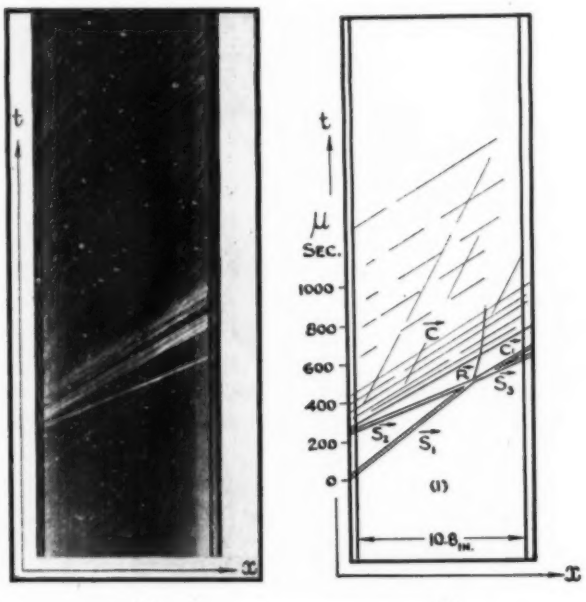

FIG. 3. The overtaking of two similarly facing plane shock waves. (Schlieren photograph and explanatory line diagram of the interaction in the (x,t)-plane.) State (1). Air at rest. $p_1=15$ mm Hg; $a_1=1133$ ft/sec; S_1=incident shock (1.250 a_1); S_2=overtaking shock (2.325 a_1); S_3=transmitted shock (2.259 a_1); R_1=head of reflected rarefaction wave (0.260 a_1); C_1=contact front (1.578 a_1).

Propagation Constant in Rectangular Wave Guide of Finite Conductivity

D. M. KERNS AND R. W. HEDBERG
National Bureau of Standards, Washington, D. C.
(Received July 8, 1954)

THE purpose of this letter is to present a complete first-order expression for the propagation constant for the lowest mode in rectangular wave guide having walls of finite conductivity. The expression is "complete" in the sense that it holds both above and below cutoff and contains both the real and the imaginary parts of the correction to the value of the propagation constant for infinite conductivity. The conventional method of taking finite conductivity into account, given in many texts, yields only the above-cutoff attenuation term. Apparently only this part of the more complete result has appeared in the literature previously. (In some texts it is erroneously stated that the correction to the phase constant above cutoff vanishes to the first order.)

The derivation of the present result was undertaken primarily to enable evaluation of the correction to the attenuation constant for a wave-guide-below-cutoff attenuator in rectangular wave guide used as a standard.

The conditions of the problem and the notation employed (rationalized mks units) are as follows. The medium in the wave guide is homogeneous, isotropic, and nondissipative, and has permeability μ and dielectric constant ϵ. The metal (or other material) of the wave-guide walls has permeability μ_m and conductivity σ. It is assumed that in the metal the conduction current greatly exceeds the displacement current. The angular frequency is denoted by ω and the skin depth in the metal by $\delta\{\delta=[2/(\omega\mu_m\sigma)]^{\frac{1}{2}}\}$. It is assumed that the wall thickness and the cross-sectional dimensions $a,b(a>b)$ as well are large compared

with the skin depth. The desired propagation constant γ is defined by the statement that for a progressive wave the field quantities vary with coordinate z and time t in accordance with the factor $\exp[j(\omega t-\gamma z)]$, where j is the imaginary unit.

Then, for the lowest mode in the wave guide, we find

$$\gamma=\gamma_0\left[1+(1-j)\frac{\mu_m\delta}{\mu\gamma_0^2}\left(\frac{\pi^2}{a^3}+\frac{k^2}{2b}\right)\right]$$

where $k^2=\omega^2\mu\epsilon$ and $\gamma^2{}_0=k^2-(\pi/a)^2$. This result is correct to the first order in δ.

It is interesting to note that far below cutoff ($k\ll\pi/a$) the attenuation term becomes approximately

$$\frac{\pi}{a}\left(1-\frac{\mu_m\delta}{\mu a}\right)\cong\frac{\pi}{a+(\mu_m\delta/\mu)}.$$

When, in particular, $\mu_m=\mu$, the correction to the attenuation constant far below cutoff corresponds to an increase of the larger dimension of the guide by an amount equal to δ.

The result given above was first obtained by a perturbation method.[1] The tangential electric field E_w on the wave-guide walls was calculated to the first order by a well-known method.[2] Then considering E_w as a secondary exciting source the lowest-mode component of the corresponding field in the wave guide was calculated and combined with the original unperturbed field. From the combined field the corrected γ was obtained.

The result was checked by an independent derivation. It was found that a method outlined by Slater[3] for the parallel plate problem could be adapted to a first-order calculation of the rectangular wave-guide problem.

[1] R. W. Hedberg, "Skin-depth correction for a rectangular-waveguide below cutoff attenuator," M. S. thesis, 1952, University of Denver, Denver, Colorado (unpublished).
[2] See, e.g., J. C. Slater, *Microwave Transmission* (McGraw-Hill Book Company, Inc., New York, 1942), p. 139.
[3] See reference 2, p. 150.

Variational and Galerkin's Methods in Compressible Fluid Flow Problems

PEI CHI CHOU
Drexel Institute of Technology, Philadelphia, Pennsylvania
(Received September 2, 1954)

VARIATIONAL and Galerkin's methods have been applied to compressible flow problems by Wang and Brodsky[1,2] in 1948 and 1949. As numerical examples, the problem of steady, perfect, compressible fluid flow past a circular cylinder without circulation has been solved in both cases.

The purpose of this note is to show that the variational integral used by Wang yields an Euler equation which is not exactly the potential equation of compressible fluid, but the potential equation multiplied by a factor equivalent to the density. Consequently, in following Rayleigh-Ritz procedure, if the same series of the velocity potential is assumed, the variational and Galerkin's methods will give different results in general. However, if the value of γ is taken to be 2, then variational and Galerkin's methods will give identical results.

The potential equation for two-dimensional inviscid compressible fluid in Cartesian coordinates is

$$\phi_{xx}(a^2-\phi_x^2)-2\phi_{xy}\phi_x\phi_y+\phi_{yy}(a^2-\phi_y^2)=0, \quad (1)$$

where a is the velocity of sound and can be expressed as

$$a^2=\frac{\gamma-1}{2}(q_m^2-\phi_x^2-\phi_y^2). \quad (2)$$

The variational integral, introduced by Bateman[3] and applied by Wang, can be written in terms of ϕ as follows:

$$J=\int\int_S[q_m^2-\phi_x^2-\phi_y^2]^{\gamma/(\gamma-1)}dxdy. \quad (3)$$

The vanishing of the first variation of J, $\delta J=0$, leads to the following Euler equation,

$$[q_m^2-\phi_x^2-\phi_y^2]^{1/(\gamma-1)}\left[\phi_{xx}\left(1-\frac{\phi_x^2}{a^2}\right)-2\phi_{xy}\frac{\phi_x\phi_y}{a^2}+\phi_{yy}\left(1-\frac{\phi_y^2}{a^2}\right)\right]=0. \quad (4)$$

Since $[q_m^2-\phi_x^2-\phi_y^2]^{1/(\gamma-1)}$ is an expression for the density ρ, which is always larger than zero, it follows that Eq. (1) is satisfied.

In applying the Rayleigh-Ritz procedure, ϕ is assumed in a series form with undertermined coefficients A_{mn}. The equation $\delta J=0$ now can be expressed as

$$\frac{\partial J}{\partial A_{mn}}\delta A_{mn}=0$$

or

$$\frac{\partial J}{\partial A_{mn}}=\frac{4\gamma}{(\gamma-1)^2}\int\int_S\frac{\partial\phi}{\partial A_{mn}}[q_m^2-\phi_x^2-\phi_y^2]^{(2-\gamma)/(\gamma-1)}\times[\phi_{xx}(a^2-\phi_x^2)-2\phi_{xy}\phi_x\phi_y+\phi_{yy}(a^2-\phi_y^2)]dxdy=0. \quad (5)$$

On the other hand, in applying Galerkin's method to the same problem, and using the same series for ϕ, the resulting equations are

$$\int\int_S\frac{\partial\phi}{\partial A_{mn}}[\phi_{xx}(a^2-\phi_x^2)-2\phi_{xy}\phi_x\phi_y+\phi_{yy}(a^2-\phi_y^2)]dxdy=0. \quad (6)$$

A study of Eqs. (5) and (6) shows that if a variational integral yields an Euler equation which is exactly the differential equation to be solved, then the variational and Galerkin's methods will give identical results. In the case of Eq. (3) the Euler equation is the desired differential equation (1) multiplied by

$$[q_m^2-\phi_x^2-\phi_y^2]^{(2-\gamma)/(\gamma-1)}.$$

Therefore the variational and Galerkin's methods give different answers for the same problem using same series.

In reference 1, the value of the ratio of specific heats γ is taken as 2 instead of 1.407. It is interesting to note that when $\gamma=2$, Eq. (5) and Eq. (6) are identical and the variational and Galerkin's methods will give identical results. The slight discrepancy in numerical results shown in Table I of reference 2 is probably due to errors in numerical computation.

[1] Chi-Teh Wang, J. Aeronaut. Sci. **15**, 675–685 (1948).
[2] Chi-Teh Wang and R. F. Brodsky, J. Appl. Phys. **20**, 1255 (1949).
[3] H. Bateman, Proc. Natl. Acad. Sci. U. S. **16**, 816–825 (1930).

Semiconductor Devices Made with Single Crystal Germanium-Silicon Alloys

R. A. LOGAN, A. J. GOSS, AND M. SCHWARTZ
Bell Telephone Laboratories, Murray Hill, New Jersey
(Received September 13, 1954)

WE have recently grown large single crystals of germanium-silicon alloys. The forbidden energy gap of these alloys varies continuously from that of pure germanium (0.7 ev) to that of pure silicon (1.1 ev) as the silicon content is increased.[1] Carrier mobility and other physical and chemical properties pertinent to device fabrication show a similar continuous variation. For example, a single crystal alloy of 95 percent Ge+5 percent Si[2] has an energy gap of 0.8 ev and a Hall mobility of 2100 $cm^2\ v^{-1}\ sec^{-1}$. By choosing alloys of the proper composition it has been possible to obtain single crystalline material which has many of the advantages of the larger energy gap of silicon but also retains a good portion of the best properties of germanium.

With present technology the usual techniques used in the formation of p-n junctions in single crystal germanium and silicon are difficult to apply to the single crystal alloy. The

technique of double doping while the crystal is being grown is not easily applicable since exceedingly slow, uninterrupted growth rates are required to form the single crystal alloy. The process of alloying impurity metals on the surface of the semiconductor is limited in the same manner since slow cooling rates must be employed to produce a coherent single crystal regrowth layer. However, the formation of p-n junctions by solid phase diffusion[3] of impurities into the crystal is a process which is well suited to this new material.

Vapor phase diffusion of arsenic into p-type germanium-silicon alloys was performed in a closed quartz system. Heating for one hour at 750°C produced an n-type layer 0.18 mil in depth in a single crystal alloy of 94 percent Ge+6 percent Si, whereas in

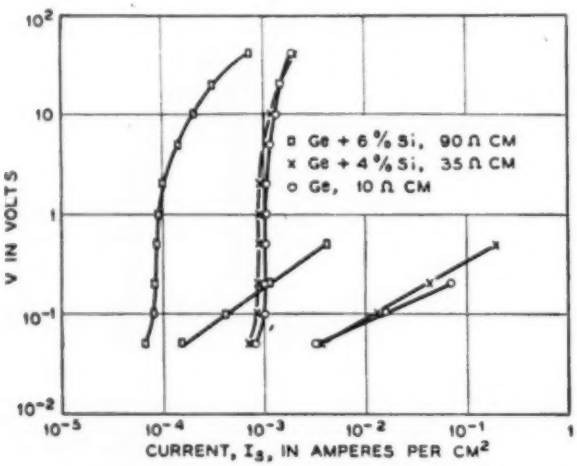

FIG. 1. Direct current voltage-current relations for junctions of area ~0.03 cm² made by diffusion of arsenic into Ge and Ge-Si alloys.

pure germanium, a 0.36-mil layer is obtained. Since thermal conversion is as serious a problem in these alloys as it is in germanium, exacting standards of cleanliness were maintained,[4] and the alloy retained its original resistivity and a high lifetime of minority carriers. For example, near a diffused junction in 90-ohm-cm alloy of 94 percent Ge+6 percent Si, the lifetime, as determined by carrier injection techniques, was in excess of 15 μ, the limit of the measuring apparatus.

The electrical characteristics of these diodes are shown in Fig. 1. If a comparison is made for material of equal resistivity and lifetime, there is a marked decrease in the saturation current

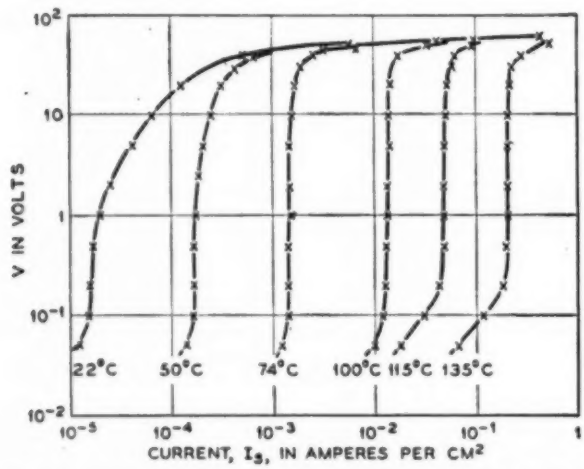

FIG. 2. Temperature dependence of dc characteristics of diode of area 0.015 cm² made by arsenic diffusion into 95 percent Ge+5 percent Si alloy of 2 ohm-cm resistivity.

I_s as the silicon content of the alloy is increased. For example, in Fig. 2, I_s in an alloy of 95 percent Ge+5 percent Si is about 02 times smaller than in pure germanium diodes, and this factor is maintained as the ambient temperature is raised to 135°C. Infrared absorption measurements indicate an energy gap of 0.8 ev for this alloy which is in good agreement with the observed reduction in I_s.

Experimental junction transistors have been made with the Ge-Si alloys using diffused junctions for the emitter and collector. The base contacts were made by electroplating with rhodium and overplating with gold or soldering directly to the Ge-Si alloy with a Pb-In solder. For ease of fabrication, the base layers were about 5 mils wide, and the observed α's (which were in excess of 0.9) were probably limited by recombination in the base layer.

[1] Levitas, Wang, and Alexander, Phys. Rev. 95, 846 (1954), also presented at American Institute of Mining Engineers Conference in New York, N. Y., February, 1954; Davis, Demars, Rubin, and Straub, Phys. Rev. 95, 597 (1954); E. R. Johnson and S. M. Christian, Phys. Rev. 95, 597 (1954).
[2] In this paper, all percentages are expressed as atomic percentages.
[3] G. L. Pearson and C. S. Fuller, Proc. Inst. Radio Engrs. 42, 760 (1954).
[4] R. A. Logan, Phys. Rev. 91, 757 (1953).

Thermodynamic Consideration of Electromagnetic Cavity Resonators*

CHARLES H. PAPAS
California Institute of Technology, Pasadena 4, California
(Received June 3, 1954)

IF a cavity resonator has a "simple shape" and is filled with a homogeneous, isotropic medium, to calculate its resonant frequencies and mode functions is a straightforward task in principle. However, it is sometimes of interest to determine the oscillatory properties of a cavity that differs by a small amount in one or more of its physical characteristics from a cavity the oscillatory properties of which are known. For example, the calculation of resonant frequency shift accompanying the introduction of a small foreign body into the cavity's volume is necessary in certain measurement techniques.

A most general formula which allows the calculation of the shift in resonant frequency produced by a foreign body of given size, shape, dielectric constant, and permeability was first deduced by Müller[1] and several years later by Slater[2] who used a different derivation.

It is the purpose of this letter to invite attention to a most simple derivation of the Müller-Slater formula based on thermodynamic considerations. The derivation consists of first recognizing that the change of the resonant field configuration produced by a small foreign body is adiabatic, and then applying the Boltzmann-Ehrenfest adiabatic theorem. The change produced by a foreign body is said to be adiabatic when it leaves the number of nodal surfaces unchanged. If the region occupied by a foreign body is *small compared to spatial variations of the field*, the undisturbed field is homogeneous throughout the volume and the disturbing influence of the foreign body is not sufficiently strong to force a jump from the original mode to an adjacent one. Hence, the restriction that the foreign body be small in the above sense is tantamount to limiting the allowable changes to adiabatic ones.

According to the Boltzmann-Ehrenfest[3] adiabatic theorem, if the state of any oscillating system is changed adiabatically, the product of the period and the time average energy remains invariant. That is,

$$W\tau = \text{constant}, \tag{1}$$

where W = time average energy, $\tau = 2\pi/\omega$ = period, ω = angular frequency. It follows from Eq. (1) that

$$\frac{\delta W}{W} = \frac{\delta\omega}{\omega}. \tag{2}$$

The change in time average energy produced by the foreign body is δW, and $\delta\omega$ is the corresponding change of resonant frequency. If the foreign body is placed at a position within the cavity where the electric field is E and the magnetic field is H, and thereby becomes endowed with a magnetic moment m and an electric moment p, the change in time average energy can be written as

$$\delta W = -\tfrac{1}{4}m^*\cdot H - \tfrac{1}{4}p^*\cdot E, \tag{3}$$

where the asterisk indicates the conjugate complex value of the quantity to which it is attached. And it follows from Eqs. (2) and (3) that

$$-\frac{\delta\omega}{\omega} = \frac{m^*\cdot H + p^*\cdot E}{4W}. \tag{4}$$

This is the Müller-Slater formula. It applies to anisotropic foreign bodies as well as to isotropic ones.[4]

[1] J. Müller, Hochfrequenztechnik und Elektroakustik **54**, 157–161 (1939), F. Borgnis, Hochfrequenztechnik und Elektroakustik **59**; H. Casimir; Philips Research Repts **6**, 162–182 (1951).
[2] J. C. Slater, *Microwave Electronics* (D. Van Nostrand Company, Inc., New York, 1950), Chapter 4.
[3] L. Brillouin, *Les Tenseurs* (Dover Publications, New York, 1946), pp. 183–185.
* This research was supported by the Office of Naval Research.
[4] C. H. Papas, Technical Reports No. 3 and No. 5, Department of Electrical Engineering, California Institute of Technology.

Errata: Modified Luneberg Lens

[J. Appl. Phys. 25, 855 (1954)]

A. S. Gutman
Air Force Cambridge Research Center, Cambridge, Massachusetts

THE equation in the third paragraph, first column, page 855 should be corrected to read

$$n = [2-(r/a)^2]^{\frac{1}{2}}.$$

Change Eq. (3) to read

$$n = (1/f)(a^2+f^2-r^2)^{\frac{1}{2}}.$$

The second group of equations in the first column on page 857 should read as follows:

$$K_1 = -f,$$
$$K_2 = a\cos\alpha,$$
$$K_3 = 0,$$
$$K_4 = a\sin\alpha.$$

Change the equation following the above group to read

$$x = -f\cos(ct/f) + a\cos\alpha\sin(ct/f).$$

In the last equation of the first column on page 857, the $\pm$ sign should be changed to a minus sign.

Acknowledgment is made to Mr. George D. M. Peeler of the Naval Research Laboratory, Washington, D. C., for directing the attention of the author to these errata.

Comments on Gumowski's Letters on Summation of Slowly Converging Series

E. L. Chu
W. W. Hansen Laboratories of Physics, Stanford University, Stanford, California
(Received September 3, 1954)

IN his first letter[1] Gumowski derives a summation formula for slowly converging series, and in a second letter,[2] replying to a criticism by Braun,[3] he discusses his result further. He illustrates his points by applying his result to the summation of the series, $f_n = 1/n^k$, $k>0$.

Regarding this topic, I would like to point out that Euler's formula is applicable to a series of the above type, provided $k>1$, as exemplified in Knopp's book,[4] p. 561, Ex. 226(d), (e), and (f). In applying Euler's formula to such series, the lower limit of the summation integral is 1, not 0. If $k\leqq 1$, the series diverge and so cannot be summed by any formula.

For series whose general term $f(x)$ has poles or other singularities at positive real nonintegral values of x, the summation integral will be divergent if the lower limit of integration is not properly chosen. In such cases one can first split the series and then sum it.

The essential difference between Gumowski's result and Euler's formula is that the latter formula has a remainder term, while the former has none. With no remainder term and without its asymptotic behavior having been ascertained, a summation formula may not always be meaningful, because the series in the formula is usually divergent.

It may also be mentioned that in Chapter XIII, Section 13.12 of Hardy's book,[5] one operational and several other different methods of deriving Euler's formula are described, and the use of a proper lower limit for the integral in the formula, to avoid divergence difficulty, is discussed with particular clarity.

[1] I. Gumowski, J. Appl. Phys. **24**, 1068 (1953).
[2] I. Gumowski, J. Appl. Phys. **25**, 133 (1954).
[3] J. H. Braun, J. Appl. Phys. **25**, 132 (1954).
[4] K. Knopp, *Theory and Application of Infinite Series* (Blackie and Son, Limited, London, England, 1946).
[5] G. H. Hardy, *Divergent Series* (Oxford University Press, New York, 1949).

Experimental Studies of Betatron Orbit Stability

G. C. Baldwin, F. R. Elder, and W. F. Westendorp
Research Laboratory, General Electric Company, Schenectady, New York
(Received August 2, 1954)

IN the design of a betatron or synchrotron, an important parameter is the guide field exponent, defined by

$$n = -\frac{r}{B}\frac{\partial B}{\partial r} = -\frac{\partial(\log B)}{\partial(\log r)},$$

where r is the radial position coordinate, and B the flux density of the magnetic guide field. This parameter determines the relative strengths of the axial and radial restoring forces which cause focussing oscillations about the instantaneous circle, with frequencies, respectively, $n^{\frac{1}{2}}$ and $(1-n)^{\frac{1}{2}}$ times the orbital revolution frequency, $\dot{\theta}$. The guide field exponent is determined largely by the polepiece profile. Its value is chosen from considerations of relative axial and radial tube apertures or from the standpoint of facilitating gun clearance during injection. We have found no experimental data in the literature on the effect of choice of n on betatron performance, since it is difficult to vary n in continuously excited machines.

In order to study the behavior of electrons guided by fields of various n values, experiments have been made with a small betatron of simple design. The polepiece profile generates a guide field in which $n=0.69$, independent of radius for a range of one inch on either side of the 5.25-inch equilibrium orbit radius, and the magnet is designed to accommodate a standard sealed-off doughnut employed in General Electric 15-Mev industrial radiographic betatrons. Four concentric shading coils on each polepiece, at radii of 3.75, 4.5, 5.25 and 6.00 inches, respectively, in conjunction with additional turns about the centerpieces to stabilize the orbit radius, permit linear control of n through a range of $0.5<n<0.9$ when connected to adjustable taps on a current transformer excited by the main magnetizing coil current. To avoid special cooling of these coils, the machine is operated discontinuously by thyratron switching to a capacitor bank. The electron gun is pulsed by a transformer excited through a delay network by the abrupt rise of voltage across the magnetizing coils at the start of the acceleration cycle. The orbit is shifted to the target by the reduction in orbit radius caused by current passed

through centerpiece windings in series, with a capacitor and a thyratron switch triggered by reversal of magnetizing coil voltage at the end of the acceleration cycle, approximately one millisecond after injection. Relative x-ray output is indicated by the ballistic throw of a survey type ionization monitor.

When the output intensity is measured as a function of shading coil current, both with and without orbit shifting, it is found that the output with orbit shifting shows a slow trend, rising slowly as n is increased from 0.5 to just under 0.75. There is evidence for maxima near $n=0.69$ and $n=0.75$. At $n=0.77$, the output disappears completely. (The region of zero output for a range of values of n above 0.75 is believed caused by transient effects early

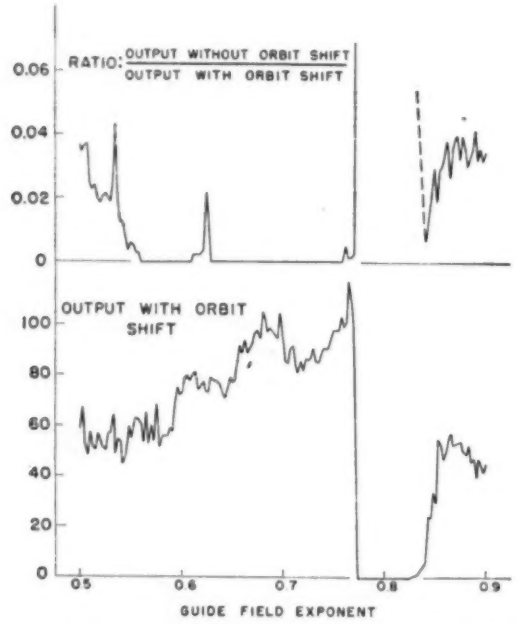

FIG. 1. Results of measurements with a variable-exponent betatron. The upper curve is a measure of orbit stability. Data from which the two curves were plotted are averages of ten acceleration cycles at each of 160 different shading current settings. Abscissa is here plotted as field exponent, determined by separate search coil calibration with the doughnut removed.

in the cycle, which cause n to be initially lower than its steady-state value.) Weak radiation appears in the absence of orbit shifting for discrete-n values of 0.53, 0.62, and 0.76. This is found by oscilloscopic observation to occur diffusely throughout the acceleration cycle. It indicates instability of the orbit at these n values.

Similar phenomena have been predicted for synchrotrons.[1,2] It can be shown by analysis of the motion that the observed instability is caused by azimuthal guide field variation, which introduces a periodic coefficient into the radial equation of motion. At n values of 0.56, 0.64 and 0.75, the radial oscillation pattern is stationary (i.e., nonprecessing) with respect to the guide field and the perturbation is resonant.

Measurements made with deliberately introduced azimuthal field variations support this interpretation. Further work is in progress.

It is evident that the familiar stability condition,[3] $0<n<1$, although necessary, is not sufficient if the guide field departs from complete azimuthal uniformity.

The polepiece profile and shading coil system in the above-described machine were developed with the assistance of Mr. Howard Kasch.

[1] D. M. Dennison and T. Berlin, Phys. Rev. **70**, 58 (1946).
[2] E. Courant, J. Appl. Phys. **20**, 611 (1949).
[3] D. W. Kerst and R. Serber, Phys. Rev. **60**, 53 (1941).

Books Reviewed

Selected Papers on Noise and Stochastic Processes. NELSON WAX (editor). Pp. 337, Dover Publications, New York, 1954. Price $2.00 (paper) or $3.95 (cloth).

This is a group of six classic papers on stochastic processes. They are unabridged reprints of review articles by Chandrasekhar, Uhlenbeck, Ornstein, Ming, Rice, Kac, and Doob. The collection is intended as a reference for workers in the field of noise, Brownian motion, and statistical mechanics. It is also intended as an introduction to advanced noise theory and fluctuation phenomena.

Analog Methods in Computation and Simulation. W. W. SOROKA. Pp. 390 + xii. McGraw-Hill Book Company, Inc., New York, 1954. Price $7.50.

This book, primarily a graduate level text and reference, represents an initial attempt to compile and present a wealth of material on analog computation and simulation methods. Basic theory and applications are presented for mechanical, electrical, and electronic computing elements as well as for the solution of simultaneous linear algebraic equations and nonlinear algebraic equations. Equivalent circuits for ordinary and partial differential equations by finite difference methods are also thoroughly treated.

There is, in addition, a chapter on the analogies of the stretched membrane and the electrical conducting sheet. The object here is to set up an experimental system which obeys a given equation and boundary conditions and from which solutions are obtained by direct measurement. Quite often this process is simpler and quicker than extensive computation.

The text emphasizes basic understanding of each method. It also supplies a collection of some 340 references to practical applications of these methods.

Elements of Statistical Mechanics. D. TER HAAR. Pp. 468 +xix. First edition. Rinehart and Company, New York, 1954. Price $8.50.

This text was designed to encompass two broad aspects of statistical mechanics, the basic elements and various applications in which these elements have been successful. Written in four parts, the first two deal with fundamental ideas. Part A, called *Statistics of Independent Particles*, is presented as the elementary approach to statistical mechanics and deals with the Maxwell and Maxwell-Boltzmann distributions as well as quantum statistics and Bose-Einstein and Fermi-Dirac statistics. Ensemble theory is developed in Part B; a discussion of petit and classical grand ensembles precedes a treatment of the ensembles in quantum statistics.

This theoretical background serves to introduce a consideration of the second aspect of statistical mechanics, applications. Some of the more familar subjects treated are the equation of state (including both classical and quantum mechanical theories thereof), electron theory of metals, and semiconductors. A discussion of eight distinct applications in all constitutes Part C of the book.

Approximately 100 pages are devoted to a series of appendixes—Part D—which represent an exposition of several more advanced concepts, such as the H theorem and the ergodic theorem, in addition to topics like relativistic statistics and intermolecular forces.

This text is intended primarily for graduate students with a clear understanding of classical mechanics, quantum theory, thermodynamics, nuclear theory, and calculus. The author hopes, however, that the book will also be a useful research tool. To that end extensive bibliographical references are included at the end of each chapter.

Gmelin's Handbuch der Anorganische Chemie. Selen (Part 3), Pp. 184. Price $26.64. **Bor** (Supplement volume), Pp. 253. Price $34.80. **Gold** (Part 2), Pp. 306. Price $40.32. **Gold** (Part 3), Pp. 558. Price $74.88.

These new volumes in the Gmelin's Handbook of Inorganic Chemistry series are available in the United States through Walter J. Johnson, 125 East 23 Street, New York 10, New York, or Stechert-Hafner, 31 East Tenth Street, New York 3, New York.

The volume on selenium (1953) is devoted exclusively to the selenium rectifier and selenium photocell. Parts 1 and 2, published earlier, presented the chemical and physical properties of the element and its compounds. The literature on selenium devices is covered to the year 1953. This volume is illustrated with 158 line drawings, and includes the theory, properties, and manufacture of selenium rectifiers and photocells.

The volume on boron (1954) is a supplement to the 1926 volume and covers the literature to 1950. Fluoroboron compounds, crystalline boron, boron carbide, boranes, borides, and many other boron compounds are discussed.

The gold volumes (1954) complete the new series on gold which started in 1950. Since Part I (1950) contained only the history of the element, these two new volumes are essentially the whole series. Part 2 has sections on occurrence, manufacture, and "special modifications," which includes colloidal gold. Part 3 presents the physical, electrochemical, chemical, and physiological properties of the element, its compounds, and alloys.

Millimicrosecond Pulse Techniques. I. A. D. LEWIS AND F. H. WELLS. Pp. 310+xiv. McGraw-Hill Book Company, Inc., New York, and Pergamon Press Ltd., London, 1954. Price $7.50.

This volume collects relevant material from known fields of electrical engineering plus recent developments in the millimicrosecond range for the physicist or electronic engineer wishing to use these techniques. It treats the theory and design of electronic circuits and devices useful in the range of time intervals between the microsecond region, where the linear dimensions of the apparatus are very short compared to the wavelength of the electromagnetic radiation, and the microwave region, where electron transit time phenomena form the basis of operation of the tubes employed. The emphasis is placed on systems of large band width. Conventional pulse circuits with lumped circuit elements are pushed to their limit of speed, and systems where circuit parameters are deliberately distributed in space are developed.

A brief theoretical introduction is provided for the nonelectronic physicist. This is followed by chapters on transmission lines, with a discussion of the Laplace transform treatment; transformers, including an account of tapered line transformers; pulse generators; amplifiers; cathode-ray oscilloscopes; and two chapters of specific applications, mostly on nuclear physics instrumentation. Fourteen pages of references to recent literature are included.

Linear Equations in Applied Mechanics. H. F. P. PURDAY. Pp. 240+xiv. Interscience Publishers, Inc., New York, 1953. Price $3.50.

Designed for the student or research worker with an elementary knowledge of the calculus, this text presents the basic aspects of linear algebraic and difference equations, ordinary and partial differential equations, and integral equations. The emphasis is on the mathematics encountered in the theoreies of mechanical vibration, elasticity, mechanics of fluids, and conduction and convection of heat. Analysis of these theories is facilitated by the use of matrices, determinants, invariants, vectors, tensors, conjugate and orthogonal functions, and series. These mathematical devices are explained and much numerical work is presented to clarify their use further.

Harmonic functions of various types are discussed; included are circular, hyperbolic, and Bessel functions, and spherical harmonics.

Also reviewed are methods of solution of problems in applied mechanics by numerical, mechanical, and electrical means of computation. The method of relaxation and analog devices such as the soap bubble and the electrolytic tank receive attention.

The textural material is supplemented by a comprehensive list of books and papers which offer more detailed information on all the mathematics and physics treated in the book.

Flames, Their Structure, Radiation and Temperature. A. G. GAYDON AND H. G. WOLFHARD. Pp. 340+xi. The Macmillan Company, New York, 1953. Price $11.00.

The authors have attempted to present an advanced discussion of part of the science of combustion, that dealing with stationary flames. Purely mathematical treatment has been avoided, the emphasis being placed on the basic physical concepts involved, with the chemical aspects of the subject receiving less attention.

The book was designed as a reference work. It considers such topics as the measurement of flame velocity, the theories of flame propagation, the method of carbon formation in flames, flame radiation, the measurement of high flame temperatures, and ionization in flames. The subject of flame temperature, in particular, is dealt with at some length. Various techniques of temperature measurement are discussed including the spectrum-line reversal method.

There are eight pages of references and a set of eighteen plates, both colored and black and white.

A. G. Gaydon is a Warren Research Fellow of the Royal Society and member of the Chemical Engineering Department of London's Imperial College. H. G. Wolfhard is Principal Scientific Officer of the Royal Aircraft Establishment at Farnborough.

The Physics of Viruses. E. C. POLLARD. Pp. 230+xi. First edition. Academic Press, Inc., New York, 1953. Price $5.50.

The author, a nuclear physicist at Yale University, has attempted "···to present what is known about viruses from the viewpoint of a physicist," to use his own words. The terminology and mathematics of the physicist have been used to describe the techniques employed in determining the shape and structure of viruses. A really thorough appreciation of the material in this book demands a somewhat advanced knowledge of the methods of modern physics.

The effects produced on viruses by various types of ionizing radiation are discussed. The actions of fast charged particles and x-rays, in this respect, are described in detail. A complete chapter is devoted to the reaction of viruses to ultraviolet light. Other topics discussed are thermal inactivation of viruses, sonic and osmotic effects on viruses, and virus genetics and multiplication. The nature of the virus surface receives considerable attention.

Written for the physicist, this account should, the author hopes, be of interest to "···that growing body of students who admit to being virologists as well." As such, the book could conceivably be used as a text as well as a reference work.

The Man in the Thick Lead Suit. DANIEL LANG. Pp. 207+xi. Oxford University Press, New York, 1954. Price $3.50.

This book presents ten of Daniel Lang's chronicles of the "atomic age."

These articles have been integrated and brought up to date since their original appearance in the *New Yorker*. They are

mostly concerned with scientists and the effect of "the bomb" on their lives. The profiles of S. A. Goudsmit, W. G. Pollard, and Wernher von Braun appear here, as well as "Reporter at Large" pieces on the Yucca Flats bomb tests, uranium hunting, civil defense, and Oak Ridge and Savannah River communities, and the Air Force investigation of "flying saucers." Throughout the book, the author is concerned with people and the extent to which the human imagination can deal with the destructive possibilities of nuclear energy. There is an introduction by Eric Sevareid.

Television. V. K. ZWORYKIN AND G. A. MORTON. Pp. 1020 +xv. Second edition, John Wiley and Sons, Inc., New York. Price $17.50.

This edition of *Television* represents an extensive revision and enlargement of the authors' original publication. Each chapter has been revised or completely rewritten and several new chapters on color and industrial television have been added.

The book presents the problems of television in terms of basic physical processes, yet maintains a wide technical coverage of practical details. This is accomplished by partitioning the material into four sections. Part 1 discusses the fundamental principles of physical electronics, electron optics, and fluorescent materials. Part 2 covers the principles of television, discussing properties of pickup devices, video transmitters, and picture-reproducing systems. Part 3 is concerned with the many component elements of an electronic television system. Here the authors discuss primarily the problems of the camera tubes, such as the Vidicon and the image orthicon, and the viewing tube or kinescope. Part 4 consists of five chapters on color television, industrial television, and practical television systems. Three of these chapters treat the fundamentals, principles, and practice of color television.

Although the casual reader can gain considerable useful information on the theory and practice of television from this treatise, the authors' emphasis on the basic physics and electronics of television necessarily assumes an adequate background on the part of the reader. A working knowledge of circuit theory, calculus, and the physics of electron motion will be found helpful.

Books Received

Symposium on Fluorescent X-Ray Spectrographic Analysis. Presented at the 56th Annual Meeting of the American Society for Testing Materials. Pp. 72, American Society for Testing Materials, Philadelphia, 1954. Price (paper cover) $1.75.

Index to the Literature on Spectrochemical Analysis. BOURDON F. SCRIBNER AND WILLIAM F. MEGGERS. Part III, 1946–1950. Pp. 226, American Society for Testing Materials, Philadelphia, 1954. Price (paper cover) $4.50.

Television. V. K. ZWORYKIN AND G. A. MORTON. Second edition. Pp. 1037+xv, John Wiley and Sons, Inc., New York, 1954. Price $17.50.

Modern Physics for the Engineer. LOUIS N. RIDENOUR (editor). Pp. 499+xix, McGraw-Hill Book Company, Inc., New York, 1954. Price $7.50.

Elementary Meteorology. GEORGE F. TAYLOR. Pp. 364+ viii, illus., Prentice-Hall, Inc., New York, 1954. Price $7.95.

Atomic Energy and Its Applications. J. M. A. LENIHAN. Pp. 265+xiii, illus., Pitman Publishing Corporation, New York, 1954. Price $4.00.

Perceptualistic Theory of Knowledge. PETER FIREMAN. Pp. 50+xii, Philosophical Library, New York, 1954. Price $2.75.

Quantum Mechanics. F. MANDL. Pp. 233+viii, Academic Press, Inc., New York, 1954. Price $5.80.

Introduction to Atomic and Nuclear Physics. HENRY SEMAT. Pp. 561+xii, Rinehart and Company, New York, 1954. Price $6.50.

Cover Photograph

The cover shows one panel of an experimental calculator developed at the IBM research laboratory at Poughkeepsie, New York. The ends of similar panels can be seen in the background. Each panel contains transistors, semiconductor diodes, and resistors. Connections within the panel are made by "printed circuit" techniques. There are 595 such panels in the calculator.

The experimental calculator has a speed and capacity comparable to the IBM Type 604, which uses 1250 vacuum tubes. The new calculator uses 2200 transistors. The use of transistors permits a drastically reduced size and a reduction of power requirements by a factor of 20.

Author Index to Volume 25

(References with (L) are to Letters to the Editor)

Aarset, B., R. W. Cloud, and J. G. Trump. Electron emission from metals under high energy hydrogen bombardment—1365

Adler, Fred P. Measurement of the conductivity of a jet flame—903

Ahrens, Tino. Estimating differential scattering cross sections in gases—505

Akeley, E. S. (see Jacobs, Ira)—572

Albers-Schoenberg, E. Ferrites for microwave circuits and digital computers—152

Aldrich, R. (see Marvin, R. S.)—1213

Allen, Wm. A., Joe M. Mapes, and Wesley G. Wilson. Effect produced by oblique impact of a cylinder on a thin target—675(L)

—— **and W. Goldsmith.** Spall effects produced by a cylindrical and a spherical charge of high explosive—813(L)

Alexander, Leroy. Synthesis of x-ray spectrometer line profiles with application to crystallite size measurements—155

Alpert, D. (see Rogers, W. A.)—868

—— **and R. S. Buritz.** Ultra-high vacuum. II. Limiting factors on the attainment of very low pressures—202

Alpher, Ralph A. and Robert J. Rubin. Normal reflection of shock waves from moving boundaries—395

Amick, J. A. (see Johnson, E. R.)—1204(L)

Amin, M. R. Fast time analysis of intermittent point-to-plane corona in air. I. The positive point burst pulse corona—210

—— Fast time analysis of intermittent point-to-plane corona in air. II. Positive pre-onset streamer corona—358

—— Fast time analysis of intermittent point-to-plane corona in air. III. The negative point Trichel pulse corona—627

Amo, K. (see Wade, G.)—1514

Andrews, R. D. Measurement of orientation in polystyrene monofilaments by means of double refraction—1223

Ang, C. and C. Wert. Torsional pendulum of low thermal inertia—1061(L)

Armstrong, H. L. Erratum: Thermal effects in point contact rectifiers—136

—— Additional observation on thermal effects in point contact rectifiers—1345(L)

Arnold, S. M. (see Koonce, S. Eloise)—134(L)

Aronin, Lewis R. Radiation damage effects on order-disorder in nickel-manganese alloys—344

Aronofsky, J. S. Effect of gas slip on unsteady flow of gas through porous media Part I—48

—— **and O. D. Ferris.** Transient flow of non-ideal gases in porous solids—one-dimensional case—1289

Arthur, George R. Statistical properties of the output of a frequency sensitive device—1185

Asaro, Frank. (see Martin, A. B.)—364

Aseltine, J. A. Transform method for linear time-varying systems—761

Ash, E. A. (see Watkins, D. A.)—782

Bailey, E. D. (see Sittel, K.)—1312

Baker, D. K. Flicker noise in germanium rectifiers at very low- and audio-frequencies—922

Baldwin, G. C., F. R. Elder, and W. F. Westendorp. Experimental studies of betatron orbit stability—1553(L)

Balluffi, R. W. and L. L. Seigle. Diffusion in bimetal vapor-solid couples—607

—— **and L. L. Seigle.** Conditions for porosity formation during diffusion—1380

Bardeen, John (see Letaw, Harry, Jr.)—600

Bath, Hubert M. (see Cutler, Melvin)—1440(L)

Battey, J. F. (see Visvanathan, S.)—99

Baumann, N. P. and G. G. Wiseman. Electrical noise pulses from polarized dielectrics—1391

Beaver, W. L. (see Muller, M. W.)—542(L)

Becker, H. On shock propagation in brass—1066(L)

Bekefi, G. Comments on J. H. Crysdale's "Letter to the Editor"—808(L)

Berry, Clifford E. Ion trajectories in the omegatron—28

Bestul, A. B. Composition of apparent shearing forces during shear degradation of polymers—1069

Bills, A. E. and R. Lefker. Shadowing technique for electron microscopy—a possible substitute for the high-vacuum evaporation technique—901

Biot, M. A. Theory of stress-strain relations in anisotropic viscoelasticity and relaxation phenomena—1385

Birdsall, T. G. (see Middleton, David)—128(L)

Birk, M., Y. Manheimer, and G. Nahmani. Note on the propagation of explosion-produced air shocks—1208(L)

Bittmann, C. A. (see Carman, J. N.)—543(L)

Blackwell, J. H. Transient-flow method for determination of thermal constants of insulating materials in bulk. Part I. Theory—137

Blois, M. S., Jr., and L. M. Rieser, Jr. Apparent density of thin evaporated films—338

Bobalek, Edward G. (see Powell, Allen S.)—757

Boettcher, A., R. Thun, and H. Treupel. Continuously recording electron diffraction camera for studies of crystal structure transitions—926(L)

Boyer, Raymond F. Relationship of first- to second-order transition temperatures for crystalline high polymers—825

Bozorth, R. M. (see Nesbitt, E. A.)—1014

Bracken, J. T. and F. E. Senftle. Change of isotopic abundance ratio within a sphere due to diffusion—267(L)

Bragg, J. K., A. H. Sharbaugh, and R. W. Crowe. Cathode effects in the dielectric breakdown of liquids—382

—— (see Crowe, R. W.)—392

—— (see Crowe, R. W.)—1480

Brand, F. A. (see Jacobs, Harold)—1406

Braun, Julian H. Comments on summation of slowly converging series—132(L)

Brewer, George R. On the focusing of high-current electron beams—243

Brillouin, L. Negentropy and information in telecommunications, writing, and reading—595

—— Information theory and uncertainty principle—887

Brinkman, John A. On the nature of radiation damage in metals—961

Brophy, James J. Current noise in thermistor bolometer flakes—222

Brown, Alexander (see Reding, F. P.)—848

Brown, Sanborn C. (see Hsieh, Hsi-Teh)—302

Bryant, P. J., H. U. Rhoads, and A. H. Weber. Electron beam effects on thin evaporated bismuth films—1343(L)

Buehler, William J. (see Nachman, Joseph F.)—307

Bulette, F. E. Spin-coated polyvinyl alcohol replicas for electron microscope use—810(L)

Bundy, F. P. (see Strong, H. M.)—1521

—— (see Strong, H. M.)—1527

—— **and H. M. Strong.** Measurement of temperatures in flames of complex structure by resonance line radiation. III. From absolute intensity measurements at high resolution—1531

Bunn, C. W. Molecular structure and the crystallinity of long-chain polymers—820
Burford, T. M. Analysis of systems involving difference-differential equations—1145
Buritz, R. S. (see Alpert, D.)—202
—— (see Rogers, W. A.)—868
Button, Kenneth J. (see Lax, Benjamin)—1413

Camp, Paul R. Resistivity striations in germanium crystals—459
Carley, James F. Flow of melts in "crosshead"-slit dies; criteria for die design—1118
Carman, J. N., P. E. Stello, and C. A. Bittmann. Regrowth of silicon through a low melting zone of silicon-gold eutectic—543(L)
Cassen, Benedict (see Dunne, Brian)—569
Catsiff, E. and A. V. Tobolsky. Relation between stress-relaxation studies and dynamic properties of polyisobutylene—145
—— **and A. V. Tobolsky.** Elastoviscous properties of amorphous polymers in the transition region. II. Stress-relaxation of butadiene-styrene copolymers—1092
Chapin, D. M., C. S. Fuller, and G. L. Pearson. New silicon *p-n* junction photocell for converting solar radiation into electrical power—676(L)
Chen, Henry S. C. Note on "Effect of filament voltage on the plate current of a diode"—929(L)
Chen, Henry S. Erratum: A note on "Effect of filament voltage on the plate current of a diode"—1345
Chou, Pei Chi. Variational and Galerkin's methods in compressible fluid flow problems—1551(L)
Chow, Shou-Hsien. Parallel-connected magnetic amplifiers—216
—— On a nonlinear diffusion equation applied to the magnetization of saturable reactors—377
—— Erratum: On a nonlinear diffusion equation applied to the magnetization of saturable reactors—930(L)
—— Analyses of basic dielectric amplifier circuits—1297
Christian, R. H. (see Shreffler, R. G.)—324
—— **and R. G. Shreffler.** Equation of state of argon—1341(L)
—— Comments on Gumowski's letters on summation of slowly converging series—1553(L)
Clogston, A. M. and H. Heffner. Focusing of an electron beam by periodic fields—436
Cloud, R. W. (see Aarset, B.)—1365
Cochardt, A. W. Method of measuring magnetostriction—91
—— New magneto-mechanical torsion experiments—670
Cohen, Julius. Semiconducting films of antimony—798
Cohen, Marshall H. On the band width of cavity antennas—582
Cohn, George I. and Bernard Saltzberg. Solution of nonlinear differential equations by the reversion method through the first thirteen terms—252
Coleman, Paul D., Murray D. Sirkis, and Irving Kaufman. Crossed electron beam technique for measuring space-charge effects in beams—679(L)
Colli, L., U. Facchini, E. Gatti, and A. Persano. Dynamics of corona discharge between cylindrical electrodes—429
Cope, A. D. and A. Rose. X-ray noise observation using a photoconductive pickup tube—240
Couling, S. R. L. and R. Smoluchowski. Anisotropy of diffusion in grain boundaries—1538
Crowe, R. W. (see Bragg, J. K.)—382
——, **J. K. Bragg, and A. H. Sharbaugh.** On the electric strengths of aliphatic hydrocarbons—392
——, **A. H. Sharbaugh, and J. K. Bragg.** Electric strength and molecular structure of saturated hydrocarbon liquids—1480
Crowley, T. H. On reciprocity theorems in electromagnetic theory—119
Crysdale, J. H. Comments on diffraction of electromagnetic waves by an aperture in a large screen—269(L)
Cunningham, J. R. and I. Hlynka. Relaxation time spectrum of dough and the influence of temperature, rest, and water content—1075
Curtis, C. W. Second mode vibrations of the Pochhammer-Chree frequency equation—928(L)
Cutler, Melvin and Hubert M. Bath. Surface leakage current in rectifiers—1440(L)

Dalman, G. C. Effect of cathode and anode resistance on the retarding potential characteristics of diodes—1263
Danielson, G. C. (see Sidles, P. H.)—58
Danielson, W. E. (see Pierce, J. R.)—1163
Davis, R. C. On the detection of sure signals in noise—76
Deb, S. and G. S. Sanyal. Amplification factor and perveance of an elliptic triode—1196
Decker, Richard W. All-glass valves for use in obtaining ultra-high vacua—1441(L)
de Hoop, A. T. Erratum: On the propagation constant in gentle circular bends in rectangular wave guides—matrix theory—136
Demorest, H. L. (see Higatsberger, M. J.)—883
Deresiewicz, H. (see Mindlin, R. D.)—21
—— (see Mindlin, R. D.)—25
—— (see Mindlin, R. D.)—1329
Destriau, G. Brightness waves and transitory phenomena in the quenching of luminescence by alternating electric fields—67
DeWitt, T. W. (see Padden, F. J.)—1086
Dexter, F. D. Rotational plastometry applied to molten polyethylene—1124
Dieke, G. H. (see Riesz, R.)—196
Ditzenberger, J. A. (see Fuller, C. S.)—1439(L)
Dolan, W. W. (see Dyke, W. P.)—106
Domenicali, Charles A. Stationary temperature distribution in an electrically heated conductor—1310
Dow, W. G. (see Sicinski, H. S.)—161
Dowling, P. H. and J. R. Sewell. Effect of organic vapor on the secondary emission of phosphors—228
Drougard, M. E., H. L. Funk, and D. R. Young. Dielectric constant and loss measurements on barium titanate single crystals while traversing the hysteresis loop—1166
Drucker, D. C. and W. B. Woodward. Interpretation of photoelastic transmission patterns for a three-dimensional model—510
Dunlap, W. C., Jr. Germanium diodes from spherical pellets—448
Dunn, C. G. Analysis of quantitative pole-figure data—233
Dunne, Brian and Benedict Cassen. Phenomena associated with supersonic liquid jets—569
Dyke, W. P., J. K. Trolan, W. W. Dolan, and F. J. Grundhauser. Field emission current-density distribution—106

Edmonson, R. B., H. L. Olsen, and E. L. Gayhart. Application of ideal gas theory to the gaseous expansion from an electric spark—1008
Ehrlich, Paul. Direct-current transients in polymethyl methacrylate and in polystyrene—1056(L)
Eisenstein, A. S. (see Russell, Paul N.)—954
Elder, F. R. (see Baldwin, G. C.)—1553(L)
Ellis, Ray C., Jr. Etching of single crystal germanium spheres—1497
Epprecht, G. W. Current fluctuation phenomena in current-carrying sliding contacts—1473
Ergen, William K. Kinetics of the circulating-fuel nuclear reactor—702

Ernst, E. W. and H. VonFoerster. Electron bunches of short time duration—674(L)
Eshelby, J. D. Distortion of a crystal by point imperfections—255
Ewald, A. W. Germanium-stabilized gray tin—1436(L)

Facchini, U. (see Colli, L.)—429
Farnsworth, H. E. (see Schlier, R. E.)—1333
Ferris, O. D. (see Aronofsky, J. S.)—1289
Fine, M. E., H. Van Duyne, and Nancy T. Kenney. Low-temperature internal friction and elasticity effects in vitreous silica—402
Fischer, Robert B. Decompositions of inorganic specimens during observation in the electron microscope—894
Fisher, Edward. Period and amplitude of the Van Der Pol limit cycle—273
Flammer, Carson. Errata: Vector wave function solution of the diffraction of electromagnetic waves by circular disks and apertures. II. The diffraction problems—543
Flory, P. J. (see Mandelkern, L.)—830
Ford, C. A. and I. I. Glass. On the interaction of two similarly facing plane shock waves—1549(L)
Forray, M. (see Mindlin, R. D.)—12
Forster, H. K. and N. Zuber. Growth of a vapor bubble in a superheated liquid—474
—— On the conduction of heat into a growing vapor bubble —1067(L)
Fowler, C. M. Symmetry as a factor in finite difference approximations—293
Freudenthal, A. M. Effect of rheological behavior on thermal stresses—1110
—— **and E. J. Gumbel.** Failure and survival in fatigue—1435(L)
Friedman, Henry D. Coincidence of pulse trains—1001
Friedmann, N. E. (see Rosenthal, D.)—1059(L)
Fuller, C. S. (see Chapin, D. M.)—676(L)
—— **and J. A. Ditzenberger.** Diffusion of boron and phosphorus into silicon—1439(L)
Funk, H. L. (see Drougard, M. E.)—1166

Gabor, D. and C. V. Nelson. Determination of the resultant dipole of the heart from measurements on the body surface—413
Gamba, A. Information theory and knowledge: Remarks on a paper by D. K. C. MacDonald—1549(L)
Garder, A. O. (see Meyer, H. I.)—1400
Garoff, Kenton (see Reingold, Irving)—537
Gatti, E. (see Colli, L.)—429
Gayhart, E. L. (see Edmonson, R. B.)—1008
Geckler, R. D. (see Sweeny, K. H.)—1135
Geisler, A. H. Spurious areas in pole figures—1245
Germer, L. H. Arcing at electrical contacts on closure. Part IV. Activation of contacts by organic vapor—332
Gilardini, Aldo. Measurement of electromagnetic field in resonant cavities by introduction of small metallic rings—1064(L)
Ginzbarg, Arthur S. Comments on the paper of Alan G. Mencher, "Epicentral displacement due to elastic waves in an infinite slab"—804(L)
Glass, I. I. (see Ford, C. A.)—1549(L)
Glauz, R. D. and E. H. Lee. Transient wave analysis in a linear time-dependent material—947
Gohar, M. Kamal. Experimental determinations of the electric field and equipotential surfaces using the heat conduction analogy—805(L)
Golay, Marcel J. E. Maxwell's demon must remain incommunicado—1062(L)
Gold, Louis. Relativistic dynamics of a charged particle in crossed magnetic and electric fields with application to the planar magnetron—683
—— On the nature of the transcendental curves associated with the relativistic trajectories of charged particles—691
—— Direct cellular evaluation of the density of states in phase space and the accurate calculation of Fermi levels —1278
Goldey, James M. (see Hsieh, Hsi-Teh)—302
Goldsmith, W. (see Allen, Wm. A.)—813(L)
Goss, A. J. (see Logan, R. A.)—1551(L)
Grenville-Wells, H. J. Graphical method of evaluating trigonometric functions used in crystal structure analysis. Parts I and II—485
Grossweiner, Leonard I. Erratum: A note on the analysis of first-order glow curves—136
Grundhauser, F. J. (see Dyke, W. P.)—106
Gumbel, E. J. (see Freudenthal, A. M.)—1435(L)
Gumowski, Igor. Further comments on summation of slowly converging series—133(L)
Gurnee, Edward F. Theory of orientation and double refraction in polymers—1232
Gutman, A. S. Modified Luneberg lens—855
—— Errata: Modified Luneberg lens—1553

Hannam, H. J. and A. van der Ziel. On the flicker noise generated in an interface layer—1336
Hatch, A. J. and H. Bartel Williams. Secondary electron resonance mechanism of low-pressure high-frequency gas breakdown—417
Hatcher, E. C., Jr., and A. Leitner. Radiation from a point dipole located at the tip of a prolate spheroid—1250
Hatfield, M. R. and G. B. Rathmann. Constant stress elongation of soft polymers: Plasticizer studies—1082
Haus, H. A. An equivalent circuit for a passive nonreciprocal network—1500
Hayward, Evans and John H. Hubbell. Backscattering of the Co^{60} gamma rays from infinite media—506
Hedberg, R. W. (see Kerns, D. M.)—1550(L)
Heffner, H. (see Clogston, A. M.)—436
Hegyi, I. J. Ferromagnetic spinels with rectangular hysteresis loops—176
Henkels, H. W. and J. Maczuk. Electrical properties of selenium. III. Microcrystalline selenium metal doped—1
Hertzberg, A. and W. E. Smith. Method for generating strong shock waves—130(L)
Higatsberger, M. J., H. L. Demorest, and A. O. Nier. Secondary emission from Nichrome V, Cube, and AgMg alloy targets due to positive ion bombardment—883
Hlynka, I. (see Cunningham, J. R.)—1075
Hoffman, William C. Joint distribution of n successive outputs of a linear detector—1006
Hogan, C. L. (see Van Uitert, L. G.)—925(L)
Hogg, D. C. Electromagnetic field near a dielectric lens—542(L)
Honnold, V. R., F. McCaffrey, and B. A. Mrowca. Studies of rubberlike polymers by nuclear magnetism—1219
Houska, C. R. and B. E. Warren. X-ray study of the graphitization of carbon black—1503
Howard, Lorn L. Sudden change in the arrangement of crystallites in thin evaporated bismuth films—125(L)
—— Errata: Sudden change in the arrangement of crystallites in thin evaporated bismuth films—543
Hsieh, Hsi-Teh, James M. Goldey, and Sanborn C. Brown. Resonant cavity study of semiconductors—302
Hsu, S. S. On the diffraction of x-rays by a twisted crystal lattice—541(L)
Hubbell, John H. (see Hayward, Evans)—506
Hurwitz, H., Jr. (see Zweifel, P. F.)—1241

Huth, J. H. Note on the elastic wedge problem—929(L)
Hutton, Allen Q. and A. W. Nolle. Experimental study of low-frequency effects on the dynamic modulus of a Buna-N rubber—350

Ikehara, Suketoshi. New method of measuring the cathode temperature of indirectly heated vacuum tubes—725
Ivey, Henry F. Erratum: Approximate solutions of the space-charge problem for some unusual electrode geometries—543

Jacobs, Harold, F. A. Brand, W. Matthei, and A. P. Ramsa. Forming point-contact silicon transistors—1406
Jacobs, Ira and E. S. Akeley. Transverse motion of an electron in a constant wave speed section of a linear accelerator—572
Jaffe, B., R. S. Roth, and S. Marzullo. Piezoelectric properties of lead zirconate-lead titanate solid-solution ceramics —809(L)
Jenkins, R. (see Wallick, G. C.)—1491
Johnson, E. R. and J. A. Amick. Formation of single crystal silicon fibers—1204(L)
Johnson, R. D. (see Martin, A. B.)—364

Kalmus, Ernest H. Preparation of aerosols for electron microscopy—87
Kamel, R. (see Yousef, Y. L.)—1064(L)
Kaufman, Irving (see Coleman, Paul D.)—679(L)
Kauzmann, W. (see Tanenbaum, M.)—451
Kay, Alan F. On roots of transcendental equations—811(L)
Kay, Irvin and Joseph B. Keller. Asymptotic evaluation of the field at a caustic—876
Keller, Joseph B. Multiple shock reflection in corners—588
—— (see Kay, Irvin)—876
—— **and I. Kolodner.** Instability of liquid surfaces and the formation of drops—918
—— Geometrical acoustics. I. The theory of weak shock waves—938
Kellogg, Dorothy J. (see Kellogg, Paul J.)—1438(L)
Kellogg, Paul J. and Dorothy J. Kellogg. Entropy of information and the odd ball problem—1438(L)
Kenney, Nancy T. (see Fine, M. E.)—402
Kent, Gordon. Space charge waves in inhomogeneous electron beams—32
Kerns, D. M. and R. W. Hedberg. Propagation constant in rectangular wave guide of finite conductivity—1550(L)
Kerr, J. S., J. S. Schaffner, and J. J. Suran. Effect of a transverse electric field on carrier diffusion in the base region of a transistor—1293
King, Bernard G. (see Scheibe, Elmer H.)—790
Kingston, R. H. Point emitter-junction collector transistor —513
Kisliuk, Paul. Arcing at electrical contacts on closure. Part V. The cathode mechanism of extremely short arcs —897
Kodis, Ralph D. Additional comments on "Diffraction of electromagnetic waves by an aperture in a plane screen" —1342(L)
Kolin, Alexander and Fritz Reiche. Electromagnetic velometry. II. Elimination of the effects of induced currents in explorations of the velocity distribution in axially symmetrical flow—409
—— Centripetal and centrifugal electromagnetophoresis—1065(L)
—— A method for elimination of thermal convection—1442(L)
Kolodner, I. (see Keller, Joseph B.)—918
Koonce, S. Eloise and S. M. Arnold. Metal whiskers—134(L)
Kowaka, M. (see Sugeno, T.)—1063(L)
Krieger, I. M. and S. H. Maron. Direct determination of the flow curves of non-Newtonian fluids. III. Standardized treatment of viscometric data—72
Krieger, I. M. (see Maron, S. H.)—971
Krumbein, A. D. (see Malamud, H.)—591
Kuerti, G. Comment on the summation of series involving roots of transcendental equations and related applications —133(L)
Kunz, K. S. Propagation of microwaves between a parallel pair of doubly curved conducting surfaces—642

Laitone, E. V. Limiting pressure on hydrofoils at small submergence depths—623
Lampard, D. G. Generalization of the Wiener-Khintchine theorem to nonstationary processes—802
Landecker, K. Property of a family of equiangular spirals and its application to some problems of wave propagation —41
Laporte, Otto and E. B. Turner. On the interaction of two plane shocks facing in the same direction—678(L)
Lax, Benjamin and S. F. Neustadter. Transient response of a *p-n* junction—1148
——, **Kenneth J. Button, and Laura M. Roth.** Ferrite phase shifters in rectangular waveguide—1413
Lazarus, D. (see Tomizuka, C. T.)—1443(L)
Leaderman, Herbert. Approximations in linear viscoelasticity theory: Delta function approximations—294
LeBras, Louis R. (see Powell, Allen S.)—757
LeCraw, R. Conway. High-speed magnetic pulsing of ferrites—678(L)
Lee, E. H. (see Glauz, R. D.)—947
Lefker, R. (see Bills, A. E.)—901
Leitner, A. (see Hatcher, E. C., Jr.)—1250
Letaw, Harry, Jr., and John Bardeen. Electrolytic analog transistor—600
Letner, H. R. and S. R. Maloof. Stress measurement by x-ray diffraction—1440(L)
Lewin, L. Diffraction of electromagnetic waves by an aperture in a large screen—1053(L)
Lin, Shao-Chi. Cylindrical shock waves produced by instantaneous energy release—54
Ling, Yang. Electron diffraction study of the structures of antimony electrodeposited on antimony cleavage face—184
Lo, Y. T. Electromagnetic field of a dipole source above a grounded dielectric slab—733
Lock, C. M. (see Starkey, B. J.)—816(L)
Logan, R. A., A. J. Goss, and M. Schwartz. Semiconductor devices made with single crystal germanium-silicon alloys —1551(L)
Longini, R. L. (see McKelvey, J. P.)—634

MacDonald, D. K. C. Information theory and knowledge —619
MacLean, William. Theory of strong electromagnetic waves in massive iron—1267
Machlin, E. S. and W. R. Yankee. Friction of clean metals and oxides with special reference to titanium—576
Machlup, Stefan. Noise in semiconductors: Spectrum of a two-parameter random signal—341
Mackay, R. Stuart. Switching in bistable circuits—424
Maczuk, J. (see Henkels, H. W.)—1
Magness, T. A. Spectral response of a quadratic device to non-Gaussian noise—1357

Malamud, H. and A. D. Krumbein. Measurement of the effect of chlorine treatment on the work function of titanium and zirconium—591
Maloof, S. R. (see Letner, H. R.)—1440(L)
Mandelkern, Leo, F. A. Quinn, Jr., and P. J. Flory. Crystallization kinetics in high polymers. I. Bulk polymers—830
Manheimer, Y. (see Birk, M.)—1208(L)
Mann, Glenn A. and R. D. Spence. Rotation of the microwave polarization in liquid crystals—271(L)
Mapes, Joe M. (see Allen, Wm. A.)—675(L)
Maron, S. H. (see Krieger, Irvin M.)—72
——, **I. M. Krieger, and A. W. Sisko.** Capillary viscometer with continuously varying pressure head—971
Martin, A. B., R. D. Johnson, and Frank Asaro. Diffusion of gold into copper—364
Marvin, R. S., R. Aldrich, and H. S. Sack. Dynamic bulk viscosity of polyisobutylene—1213
Marzullo, S. (see Jaffe, B.)—809(L)
Mason, W. P. (see Shockley, W.)—677(L)
Mathis, H. F. Experimental procedures for determining the efficiency of four-terminal networks—982
Matthei, W. (see Jacobs, Harold)—1406
McCaffrey, F. (see Honnold, V. R.)—1219
McKelvey, J. P. and R. L. Longini. Volume and surface recombination rates for injected carriers in germanium—634
McLaren, E. H. Reproducibility of the freezing temperature of high-purity zinc—808(L)
Medicus, Gustav (see Wehner, Gottfried)—698
Mencher, Alan G. Concerning the use of delta-function source in a problem on elastic waves—804(L)
Meyer, H. I. and A. O. Garder. Mechanics of two immiscible fluids in porous media—1400
Meyer, M. A. and David Middleton. On the distributions of signals and noise after rectification and filtering—1037
Meyer, Robert A. Influence of deuteron bombardment and strain hardening on notch sensitivity of mild steel—1369
Middleton, David. Further remarks on the nature of the statistical observer—127(L)
—— Information loss attending the decision operation in detection—127(L)
——, **W. W. Peterson, and T. G. Birdsall.** Discussion of "Statistical criteria for the detection of pulsed carriers in noise I, II"—128(L)
—— (see Meyer, M. A.)—1037
Mihran, T. G. Scalloped beam amplification—1341(L)
Miller, Kenneth S. Remark on stability—407(L)
Mindlin, R. D. and M. Forray. Thickness-shear and flexural vibrations of contoured crystal plates—12
—— **and H. Deresiewicz.** Thickness-shear vibrations of piezoelectric crystal plates with incomplete electrodes—21
—— **and H. Deresiewicz.** Suppression of overtones of thickness-shear and flexural vibrations of crystal plates—25
—— **and H. Deresiewicz.** Thickness-shear and flexural vibrations of a circular disk—1329
Ming, D. L. and R. W. Thorpe. Transfer function as a tool in the analysis of a resistance-capacitance coupled voltage amplifier—934
Minnick, Robert C. Magnetic switching circuits—479
Mooney, M. On an indeterminate integral in Einstein's theory of the viscosity of a suspension—406(L)
—— **and W. E. Wolstenholme.** Rheological unit in raw elastomers—1098
Morant, M. J. Electron atmosphere in dielectrics—1053(L)
Morduchow, Morris. Method of averages and its comparison with the method of least squares—1260
Morito, Nozomu. On the chromatic field aberration of the magnetic electron lens in the electron microscope—986
Moyer, James W. and William A. Riemen. Heat transfer measurements at sodium-stainless steel interface—400
Mrowca, B. A. (see Honnold, V. R.)—1219
Muller, F. A. (see Warner, A. J.)—131(L)
Muller, M. W. and W. L. Beaver. Application of perturbation theory to the traveling wave tubes—542(L)

Nachman, Joseph F. and William J. Buehler. 16 Percent aluminum-iron alloy cold rolled in the order-disorder temperature range—307
Nahmani, G. (see Birk, M.)—1208(L)
Nelson, C. V. (see Gabor, D.)—413
Nesbitt, E. A., H. J. Williams, R. M. Bozorth. Factors determining in the permanent magnet properties of single crystals of Fe_2NiAl—1014
—— (see Lax, Benjamin)—1148
Nichols, J. B. X-ray and infrared studies on the extent of crystallization of polymers—840
Nichols, P. L., Jr., and A. G. Presson. Heat conduction in an infinite cylindrical medium with heat generated by a chemical reaction—1469
Nielsen, Lawrence E. Effect of crystallinity on the dynamic mechanical properties of polyethylenes—1209
Nier, A. O. (see Higatsberger, M. J.)—883
Nolle, A. W. (see Hutton, Allen Q.)—350
Nordlin, H. G. (see Warner, A. J.)—131(L)
Nowick, A. S. Internal friction and dynamic modulus of cold-worked metals—1129

Olsen, H. L. (see Edmonson, R. B.)—1008
Onat, E. T. and W. Prager. Necking of a tension specimen in plane plastic flow—491

Padden, F. J. and T. W. DeWitt. Some rheological properties of concentrated polyisobutylene solutions—1086
Pai, Shih I. Laminar flow of an electrically conducting incompressible fluid in a circular pipe—1205(L)
Palmer, Wilfred. Electrical characteristics of MnSe and MnTe—125(L)
Papas, Charles H. Thermodynamic consideration of electromagnetic cavity resonators—1552(L)
Papoulis, A. Penetration of an electromagnetic wave into a ferromagnetic material—169
Pavlovic, A. and R. Pepinsky. Reexamination of low-temperature properties of crystalline quartz—1344(L)
Payne, L. E. (see Weiss, G.)—1321
Pearson, G. L. (see Chapin, D. M.)—676(L)
Pearson, John and John S. Rinehart. Hardness plateaus and twinning in exposively loaded mild steel—778
Penner, S. S. Approximate emissivity calculations for polyatomic molecules. I. CO_2—660
Pepinsky, R. (see Pavlovic, A.)—1344(L)
Perkins, James F. Optimal loading of a thermoelectric generator—1058(L)
Persano, A. (see Colli, L.)—429
Peterson, John W. Contact charging between a borosilicate glass and nickel—501
—— Contact charging between nonconductors and metal—907
Peterson, W. W. (see Middleton, David)—128(L)
Pfann, W. G. and W. van Roosbroeck. Radioactive and photoelectric *p-n* junction power sources—1422
Philippoff, Wladimir. Further dynamic investigations on polymers—1102
Pierce, J. R. Coupling of modes of propagation—179
—— Theorem concerning noise in electron streams—931

—— **and W. E. Danielson.** Minimum noise figure of traveling-wave tubes with uniform helices—1163
Pipes, Louis A. Matrix analysis of linear time-varying circuits—1179
Pizzarello, Frank. Vapor phase crystal growth of lead sulfide crystals—804(L)
Plesset, M. S. On the stability of fluid flows with spherical symmetry—96
—— **and S. A. Zwick.** Growth of vapor bubbles in superheated liquids—493
Pohl, Robert G. Cross section of pulled crystals—668
—— Solute redistribution by recrystallization—1170
Post, Daniel. Multiple beam sharpening of photoelastic fringes—1060(L)
Potter, Richard D. Calibration of a nickel-molybdenum thermocouple—1383
Pound, G. M. (see Simnad, M.)—268(L)
Powell, Allen S., Louis R. LeBras, Edward G. Bobalek, and William von Fischer. Improved replica technique for electron microscopy of paint films—757
Prager, W. (see Onat, E. T.)—491
Presson, A. G. (see Nichols, P. L., Jr.)—1469
Preuss, Luther E. Errata: A study of the propagation mode for metallic vapors in shadow casting by vacuum evaporation of Au^{198} and Cr^{51}—136

Quinn, F. A., Jr. (see Mandelkern, L.)—830

Rado, George T. Some magnetostriction relations in materials possessing preferred domain orientations—102
Raisbeck, G. Definition of passive linear networks in terms of time and energy—1510
Ramsa, A. P. (see Jacobs, Harold)—1406
Rappaport, Paul. Methods of processing silver-magnesium secondary emitters for electron tubes—288
Rathmann, G. B. (see Hatfield, M. R.)—1082
Redfield, Alfred G. Electrodynamic perturbation theorem with application to nonreciprocal systems—1021
Reding, F. P. and Alexander Brown. Infrared study of the crystallization of polyethylene—848
Reiche, Fritz (see Kolin, Alexander)—409
Reingold, Irving and Kenton Garoff. Measurements of the gas temperature of a low-pressure RF discharge—537
Reza, F. M. Synthesis without ideal transformers—807(L)
—— RLC canonic forms—297
Rhoads, H. U. (see Bryant, P. J.)—1343(L)
Rice, Philip. Combined slow-wave circuit and beam focusing structure—680(L)
Riemen, William A. (see Moyer, James W.)—400
Rieser, L. M., Jr. (see Blois, M. S., Jr.)—338
Riesz, R. and G. H. Dieke. Analysis and purification of rare gases by means of electric discharges—196
Rinehart, John S. (see Pearson, John)—778
Robinson, L. B. Concept of stability for nuclear reactors—516
Rogers, W. A., R. S. Buritz, and D. Alpert. Diffusion coefficient, solubility, and permeability for helium in glass—868
Rose, A. (see Cope, A. D.)—240
Rosen, Philip. Use of restricted variational principles for the solution of differential equations—336
Rosenstock, Herbert B. Response of pulsed Geiger tube—275
Rosenthal, D. and N. E. Friedmann. Thermal diffusivity of metals at high temperatures—1059(L)
Roth, Laura M. (see Lax, Benjamin)—1413
Roth, R. S. (see Jaffe, B.)—809(L)
Rouse, P. E., Jr. (see Sittel, K.)—1312
Rubin, Robert J. (see Alpher, Ralph A.)—395
—— Propagation of longitudinal deformation waves in a prestressed rod of material exhibiting a strain-rate effect—528
Rumsey, V. H. Kinetics of piles with reflectors—1395
Russell, Paul N. and A. S. Eisenstein. Thermionic emission and electron diffraction from thin films of barium oxide—954
Rutzler, J. E., Jr. (see Skinner, S. M.)—1055(L)
Rynn, N. (see Watkins, D. A.)—1375

Sack, H. S. (see Marvin, R. S.)—1213
Salkovitz, Edward I. (see Smith, Paul L.)—237
Saltzberg, Bernard (see Cohn, George I.)—252
Sandoz, G. (see Stauss, H. E.)—267(L)
Sanyal, G. S. (see Deb, S.)—1196
Savage, R. L. (see Skinner, S. M.)—1055(L)
Savitt, Jacob and R. H. Stresau. Velocity attenuation of explosive-produced air shocks—89
—— **and R. H. Stresau.** Errata: Velocity attenuation of explosive-produced air shocks—1208(L)
——, **R. H. Stresau, and L. E. Starr.** Compression wave velocity experiments with copper—1307
Schafer, J. P. (see Van Uitert, L. G.)—925(L)
Schaffner, J. S. and J. J. Suran. Steady-state solution of the two-dimensional diffusion equation for transistors—863
—— (see Kerr, J. S.)—1293
Scharfman, Howard. Scattering from dielectric coated spheres in the region of the first resonance—1352
Scheibe, E. H., B. G. King, and D. L. Van Zeeland. Loss measurements of surface wave transmission lines—790
Scheidegger, Adrian E. Statistical hydrodynamics in porous media—994
Schlier, R. E. and H. E. Farnsworth. Low-energy electron diffraction investigation of chemisorbed gases on the (100) faces of copper and nickel single crystals—1333
Schubauer, G. B. Turbulent processes as observed in boundary layer and pipe—188
Schultheiss, P. M., C. A. Wogrin, and F. Zweig. Short-time frequency measurement of narrow band random signals in the presence of wide-band noise—1025
Schwartz, M. (see Logan, R. A.)—1551(L)
Seigle, L. L. (see Balluffi, R. W.)—607
—— (see Balluffi, R. W.)—1380
Seiler, J. A. and P. S. Symonds. Plastic deformation in beams under distributed dynamic loads—556
Senftle, F. E. (see Bracken, J. T.)—267(L)
Sevick, J. (see Storer, J. E.)—369
Sewell, J. R. (see Dowling, P. H.)—228
Shader, F. L. (see Sponsler, G. C.)—1271
Sharbaugh, A. H. (see Bragg, J. K.)—382
—— (see Crowe, R. W.)—392
—— (see Crowe, R. W.)—1480
Sheingold, Leonard S. and J. E. Storer. Circumferential gap in a circular wave guide excited by a dominant circular-electric wave—545
Shercliff, J. A. Relation between the velocity profile and the sensitivity of electromagnetic flowmeters—817(L)
Shive, J. N. (see Slocum, A.)—406(L)
Shockley, W. and W. P. Mason. Dissected amplifiers using negative resistance—677(L)
Shreffler, R. G. and R. H. Christian. Boundary disturbances in high-explosive shock tubes—324
—— (see Christian, R. H.)—1341(L)
Sicinski, H. S., N. W. Spencer, and W. G. Dow. Rocket measurements of upper atmosphere ambient temperature and pressure in the 30- to 75-kilometer region—161

Sidles, P. H. and G. C. Danielson. Thermal diffusivity of metals at high temperatures—58
Siegman, A. E. (see Watkins, D. A.)—133(L)
Simnad, M., Ling Yang, and G. M. Pound. Radioactive-shadowing technique and note on the deposition of metal crystals from atomic beams—268(L)
Sirkis, Murray D. (see Coleman, Paul D.)—679(L)
Sisko, A. W. (see Maron, S. H.)—971
Sittel, K., P. E. Rouse, Jr., and E. D. Bailey. Method for determining the viscoelastic properties of dilute polymer solutions at audio-frequencies—1312
Skinner, S. M., R. L. Savage, J. E. Rutzler, Jr. Electrical phenomena in adhesion: Further comments on electron atmospheres—1055(L)
Slocum, A. and J. N. Shive. Shot dependence of *p-n* junction phototransistor noise—406(L)
Smith, C. B. (see Walters, K. C.)—1254
Smith, Jack H. and Martin L. Storm. Generalized off-axis distributions from disk sources of radiation—519
Smith, Paul L. and Edward I. Salkovitz. Plastic deformation of ammonium dihydrogen phosphate—237
Smith, W. E. (see Hertzberg, A.)—130(L)
Smoluchowski, R. (see Couling, S. R. L.)—1538
Smythe, W. R. Resistance of a bar with a transverse hole—930(L)
Spence, R. D. (see Mann, Glenn A.)—271(L)
Spencer, N. W. (see Sicinski, H. S.)—161
Spetner, Lee M. Errors in power spectra due to finite sample—653
Spiegel, Murray R. Applications of the Dirac delta function to the evaluation of certain integrals—1302
Sponsler, G. C. Potential distribution and prevention of a space-charge-induced minimum between a plane secondary electron emitter and parallel control grid—282
—— **and F. L. Shader.** PPI light spot brightness probability distributions—1271
Stark, Louis. Lower modes of a concentric line having a helical inner conductor—1155
Starkey, B. J. and C. M. Lock. Short range propagation of mechanical disturbances in the ground—816(L)
Starr, L. E. (see Savitt, Jacob)—1307
Stauss, H. E. and G. Sandoz. New magnetostrictive material—267(L)
Steele, Earl L. Charge storage in junction diodes—916
Steele, H. L., Jr., and P. J. Walsh. Effect of moving striations on microwave conductivity of a coaxial discharge—1435(L)
Stello, P. E. (see Carman, J. N.)—543(L)
Stone, W. M. On the effect of integration in a pulsed radar, randomly modulated carrier—1543
Storer, J. E. and J. Sevick. General theory of plane-wave scattering from finite, conducting obstacles with application to the two-antenna problems—369
—— (see Sheingold, Leonard S.)—545
Storm, Martin L. (see Smith, Jack H.)—519
Stresau, R. H. (see Savitt, Jacob)—89
—— (see Savitt, Jacob)—1208(L)
—— (see Savitt, Jacob)—1307
Strong, H. M. (see Bundy, F. P.)—1531
—— **and F. P. Bundy.** Measurement of temperatures in flames of complex structure by resonance line radiation. I. General theory and application to sodium line reversal methods—1521
—— **and F. P. Bundy.** Measurement of temperatures in flames of complex structure by resonance line radiation. II. Sodium line reversal by high resolution spectroscopy—1527
Sugar, George R. Estimation of correlation coefficients from scatter diagrams—354
Sugeno, T., and M. Kowaka. Hardening of Pd by cathodic hydrogen—1063(L)
Sumi, Masao (see Udagawa, Kanehisa)—135(L)
Suran, J. J. (see Schaffner, J. S.)—863
—— (see Kerr, J. S.)—1293
Surtees, Walter J. (see Wait, James R.)—553
Swann, W. F. G. Stress and strain (Discussion of Dr. Philippoff's paper—1108
Swanson, John A. Diode theory in the light of hole injection—314
Sweeny, K. H. and R. D. Geckler. Rheology of suspensions—1135
Symonds, P. S. (see Seiler, J. A.)—556

Tadatosi, Hibi and Keiji Yada. High-resolution replicas and their application—712
Tanenbaum, M. and W. Kauzmann. Studies on the creep recovery and annealing of zinc single crystals—451
Tchen, C.-M. Motion of small particles in skew shape suspended in a viscous liquid—463
Telfair, David. Dynamic mechanical and electrical behavior of polymethyl methacrylate—1062(L)
Telkes, Maria. Solar thermoelectric generators—765
—— Power output of thermoelectric generators—1058(L)
Thorpe, R. W. (see Ming, D. L.)—934
Thun, R. (see Boettcher, A.)—926(L)
Tien, Ping King. Focusing of a long cylindrical electron stream by means of periodic electrostatic fields—1281
Tobolsky, A. V. (see Catsiff, E.)—145
—— (see Catsiff, E.)—1092
Tomizuka, C. T. and D. Lazarus. Reproducibility of diffusion measurements: Time of anneal and method of counting radiation—1443(L)
Tomlinson, T. B. On the conductivity of oxide cathode coatings—720
Treupel, H. (see Boettcher, A.)—926(L)
Trolan, J. K. (see Dyke, W. P.)—106
Trump, J. G. (see Aarset, B.)—1365
Turner, E. B. (see Laporte, Otto)—678(L)
Turner, C. H. M. On the concept of an instantaneous power spectrum and its relationship to the autocorrelation function—1347
Twersky, V. Certain transmission and reflection theorems—859

Udagawa, Kanehisa and Masao Sumi. Some remarks on thermal effect in an electron beam on the gain of traveling-wave tubes—135(L)

Vallese, L. M. Diffusion of pulsed currents in conductors—225
van der Maas, G. J. Simplified calculation for Dolph-Tchebycheff arrays—121
van der Ziel, A. Note on shot and partition noise in junction transistors—815(L)
—— (see Hannam, H. J.)—1336
Van Duyne, H. (see Fine, M. E.)—402
van Roosbroeck, W. (see Pfann, W. G.)—1422
Van Uitert, L. G., J. P. Schafer, and C. L. Hogan. Low-loss ferrites for applications at 4000 megacycles per second—925(L)
——, **J. P. Schafer, and C. L. Hogan.** Erratum: Low loss ferrites—1345
Van Zeeland, Donald L. (see Scheibe, Elmer H.)—790
Varnerin, L. J., Jr., and D. White. Ultimate vacuum in a vacuum-enclosed ionization gauge—1207(L)
Visvanathan, S. and J. F. Battey. Some problems in the diffusion of minority carriers in a semiconductor—99

Volkin, Howard C. Effect of inelastic collisions on the slowing-down length of neutrons in a hydrogenous mixture—83
von Fischer, William (see Powell, Allen S.)—757
VonFoerster, H. (see Ernst, E. W.)—674(L)

Wade, G., K. Amo, and D. A. Watkins. Noise in transverse-field traveling-wave tubes—1514
Wait, James R. and Walter J. Surtees. Impedance of a top-loaded antenna of arbitrary length over a circular grounded screen—553
Walker, L. R. Dispersion formula for plasma waves—131(L)
—— Stored energy and power flow in electron beams—615
Wallick, G. C. and R. Jenkins. An analysis of short-time tracer injection in underground formation—1491
Walsh, P. J. (see Steele, H. L., Jr.)—1435(L)
Walters, K. C. and C. B. Smith. Effect of uniform displacement on the stress distribution of a wood plate—1254
Warner, A. J., F. A. Muller, and H. G. Nordlin. Electrical conductivity induced by ionizing radiation in some polymeric materials—131(L)
Warren, B. E. Monochromatic x-rays for single crystal diffuse scattering—814(L)
—— (see Houska, C. R.)—1503
Watkins, D. A. and A. E. Siegman. Note on helix impedance measurements using an electron beam—133(L)
—— **and E. A. Ash.** Helix as a backward-wave circuit structure—782
—— **and N. Rynn.** Effect of velocity distribution on traveling-wave tube gain—1375
—— (see Wade, G.)—1514
Weber, A. H. (see Bryant, P. J.)—1343(L)
Wegener, Peter P. Water vapor condensation process in supersonic nozzles—1485
Wehner, Gottfried K. Momentum transfer in sputtering by ion bombardment—270(L)
—— **and Gustav Medicus.** Sputtering at low ion velocities—698
Weiss, G. and L. E. Payne. Torsion of a shaft with a toroidal cavity—1321
Wert, C. (see Ang, C.)—1061(L)
West, D. C. Electrical phenomena in adhesion. I. Electron atmospheres in dielectrics—1054(L)
Westendorp, W. F. (see Baldwin, G. C.)—1553(L)
Wheelon, Albert D. On the summation of infinite series in closed form—113
White, D. (see Varnerin, L. J., Jr.)—1207(L)
Wick, R. F. Solution of the field problem of the germanium gyrator—741
Williams, H. B. (see Hatch, A. J.)—417
Williams, H. J. (see Nesbitt, E. A.)—1014
Wilson, Wesley G. (see Allen, Wm. A.)—675(L)
Winkler, Eva M. Design and calibration of stagnation temperature probes for use at high supersonic speeds and elevated temperatures—231
Wiseman, G. G. (see Baumann, N. P.)—1391
Wogrin, C. A. (see Schultheiss, Peter M.)—1025
Wolstenholme, W. E. (see Mooney, M.)—1098
Wood, Lawrence A. Crystallization in butadiene-styrene copolymers—851
Woodward, W. B. (see Drucker, D. C.)—510

Yada, Keiji (see Tadatosi, Hibi)—712
Yadavalli, S. V. Tube noise under large transit-time conditions—564
Yamaguchi, Shigeto. Titanium observed by electron diffraction—408(L)
—— Application of Ellis' theory on plural electron scattering to razor edge—811(L)
—— Note on the oxide replica in electron microscopy—927(L)
—— Protective films on magnesium observed by electron diffraction and microscopy—1437(L)
Yang, Ling (see Simnad, M.)—268(L)
Yankee, W. R. (see Machlin, E. S.)—576
Yokobori, Takeo. Delayed yield and strain rate and temperature dependence of yield point in iron—593
Young, D. R. (see Drougard, M. E.)—1166
Yousef, Y. L. and R. Kamel. Elastic relaxation and grain boundary diffusion in cadmium—1064(L)

Zawels, Jakob. Physical theory of new circuit representation for junction transistors—976
Zemanian, Armen H. Approximate method of evaluating integral transforms—262
Zuber, N. (see Forster, H. K.)—474
Zweifel, P. F. and H. Hurwitz, Jr. Transformation of scattering cross sections—1241
Zweig, F. (see Schultheiss, Peter M.)—1025
Zwick, S. A. (see Plesset, M. S.)—493

Subject Index to Volume 25

References with (L) are to Letters to the Editor

Acoustics
Geometrical acoustics. I. Theory of weak shock waves, Joseph B. Keller—938
Adhesion
Electrical phenomena in adhesion. I. Electron atmospheres in dielectrics, D. C. West—1054(L)
Electrical phenomena in adhesion: Further comments on electron atmospheres, S. M. Skinner, R. L. Savage, and J. E. Rutzler, Jr.—1055(L)
Electron atmosphere in dielectrics, M. J. Morant—1053(L)
Aerodynamics (see **Fluid Dynamics** and **Shock Waves**)
Announcements—24, 544, 681, 819
Antennas
Band width of cavity antennas, Marshall H. Cohen—582
Comments on J. H. Crysdale's "Letter to the Editor," G. Bekefi—808(L)
Diffraction of electromagnetic waves by an aperture in a large screen, Comments on, J. H. Crysdale—269(L)
Diffraction of electromagnetic waves by an aperture in a large screen, L. Lewin—1053(L)
Diffraction of electromagnetic waves by an aperture in a plane screen, Additional comments on, Ralph D. Kodis —1342(L)
Electromagnetic field near a dielectric lens, D. C. Hogg—542(L)
General theory of plane-wave scattering from finite, conducting obstacles with application to the two-antenna problems, J. E. Storer and J. Sevick—369
Impedance of a top-loaded antenna of arbitrary length over a circular grounded screen, James R. Wait and Walter J. Surtees—553
Modified Luneberg lens, A. S. Gutman—855
Radiation from a point dipole located at the tip of a prolate spheroid, E. C. Hatcher, Jr., and A. Leitner—1250
Reciprocity theorems in electromagnetic theory, T. H. Crowley—119
Simplified calculation for Dolph-Tchebycheff arrays, G. J. van der Maas—121

Ballistics
Effect produced by oblique impact of a cylinder on a thin target, Wm. A. Allen, Joe M. Mapes, and Wesley G. Wilson—675(L)
Hardness plateaus and twinning in explosively loaded mild steel, John Pearson and John S. Rinehart—778
Spall effects produced by a cylindrical and a spherical charge of high explosive, Wm. A. Allen and W. Goldsmith—813(L)
Biophysics
Determination of the resultant dipole of the heart from measurements on the body surface, D. Gabor and C. V. Nelson—413
Book Reviews—1444, 1554
Books Received—1452, 1556

Colloids
Preparation of aerosols for electron microscopy, Ernest H. Kalmus—87
Computing Techniques and Machines
Ferrites for microwave circuits and digital computers, E. Albers-Schoenberg—152
Ferromagnetic spinels with rectangular hysteresis loops, I. J. Hegyi—176
Magnetic switching circuits, Robert C. Minnick—479
Conductivity (see **Electrical** or **Thermal Conductivity**)

Contact Electrification
Contact charging between a borosilicate glass and nickel, John W. Peterson—501
Contact charging between nonconductors and metal, John W. Peterson—907
Electrical phenomena in adhesion. I. Electron atmospheres in dielectrics, D. C. West—1054(L)
Electrical phenomena in adhesion: Further comments on electron atmospheres, S. M. Skinner, R. L. Savage, and J. E. Rutzler, Jr.—1055(L)
Electron atmosphere in dielectrics, M. J. Morant—1053(L)
Creep (see **Metallurgy**)
Crystals and Crystal Growth
Analysis of quantitative pole-figure data, C. G. Dunn—233
Crystallization in butadiene-styrene copolymers, Lawrence A. Wood—851
Crystallization kinetics in high polymers. I. Bulk polymers, Leo Mandelkern, F. A. Quinn, Jr., and P. J. Flory—830
Distortion of a crystal by point imperfections, J. D. Eshelby—255
Electron diffraction study of the structures of antimony electrodeposited on antimony cleavage face, Ling Yang —184
Formation of single crystal silicon fibers, E. R. Johnson and J. A. Amick—1204(L)
Infrared study of the crystallization of polyethylene, F. P. Reding and Alexander Brown—848
Metal whiskers, S. Eloise Koonce and S. M. Arnold—134(L)
Molecular structure and the crystallinity of long-chain polymers, C. W. Bunn—820
Radioactive-shadowing technique and note on the deposition of metal crystals from atomic beams, M. Simnad, Ling Yang, and G. M. Pound—268(L)
Relationship of first- to second-order transition temperatures for crystalline high polymers, Raymond F. Boyer —825
Reproducibility of the freezing temperature of high-purity zinc, E. H. McLaren—808(L)
Solute redistribution by recrystallization, Robert G. Pohl —1170
Vapor phase crystal growth of lead sulfide crystals, Frank Pizzarello—804(L)
X-ray and infrared studies on the extent of crystallization of polymers, J. B. Nichols—840

Dielectrics and Dielectric Breakdown in Insulators
Cathode effects in the dielectric breakdown of liquids, J. K. Bragg, A. H. Sharbaugh, and R. W. Crowe—382
Dielectric constant and loss measurements on barium titanate single crystals while traversing the hysteresis loop, M. E. Drougard, H. L. Funk, and D. R. Young —1166
Direct-current transients in polymethyl methacrylate and in polystyrene, Paul Ehrlich—1056(L)
Dynamic mechanical and electrical behavior of polymethyl methacrylate, David Telfair—1062(L)
Electric strength and molecular structure of saturated hydrocarbon liquids, R. W. Crowe, A. H. Sharbaugh, and J. K. Bragg—1480
Electric strengths of aliphatic hydrocarbons, R. W. Crowe, J. K. Bragg, and A. H. Sharbaugh—392
Electrical noise pulses from polarized dielectrics, N. P. Baumann and G. G. Wiseman—1391

Dielectrics and Dielectric Breakdown in Insulators (continued)
Reexamination of low-temperature properties of crystalline quartz, A. Pavlovic and R. Pepinsky—1344(L)
Rotation of the microwave polarization in liquid crystals, Glenn A. Mann and R. D. Spence—271(L)
Diffusion (see also **Semiconductors** and **Semiconductor Devices**)
Anisotropy of diffusion in grain boundaries, S. R. L. Couling and R. Smoluchowski—1538
Change of the isotopic abundance ratio within a sphere due to diffusion, J. T. Bracken and F. E. Senftle—267(L)
Conditions for porosity formation during diffusion, R. W. Balluffi and L. L. Seigle—1380
Diffusion coefficient, solubility, and permeability for helium in glass, W. A. Rogers, R. S. Buritz, and D. Alpert—868
Diffusion in bimetal vapor-solid couples, R. W. Balluffi and L. L. Seigle—607
Diffusion of boron and phosphorus into silicon, C. S. Fuller and J. A. Ditzenberger—1439(L)
Diffusion of gold into copper, A. B. Martin, R. D. Johnson, and Frank Asaro—364
Elastic relaxation and grain boundary diffusion in cadmium, Y. L. Yousef and R. Kamel—1064(L)
Reproducibility of diffusion measurements: Time of anneal and method of counting radiation, C. T. Tomizuka and D. Lazarus—1443(L)
Symmetry as a factor in finite difference approximations, C. M. Fowler—293

Elasticity and Inelasticity
Concerning the use of delta-function source in a problem on elastic waves, Alan G. Mencher—804(L)
Dynamic mechanical and electrical behavior of polymethyl methacrylate, David Telfair—1062(L)
Effect of crystallinity on the dynamic mechanical properties of polyethylenes, Lawrence E. Nielsen—1209
Effect of uniform displacement on the stress distribution of a wood plate, K. C. Walters and C. B. Smith—1254
Elastic relaxation and grain boundary diffusion in cadmium, Y. L. Yousef and R. Kamel—1064(L)
Elastic wedge problem, Note on, J. H. Huth—929(L)
Epicentral displacement due to elastic waves in an infinite slab, Comments on the paper of Alan G. Mencher, Arthur S. Ginzbarg—804(L)
Experimental study of low-frequency effects on the dynamic modulus of a Buna-N rubber, Allen Q. Hutton and A. W. Nolle—350
Internal friction and dynamic modulus of cold-worked metals, A. S. Nowick—1129
Interpretation of photoelastic transmission patterns for a three-dimensional model, D. C. Drucker and W. B. Woodward—510
Low-temperature internal friction and elasticity effects in vitreous silica, M. E. Fine, H. Van Duyne, and Nancy T. Kenney—402
Multiple beam sharpening of photoelastic fringes, Daniel Post—1060(L)
New magneto-mechanical torsion experiments, A. W. Cochardt—670
Propagation of longitudinal deformation waves in a prestressed rod of material exhibiting a strain-rate effect, Robert J. Rubin—528
Relation between stress-relaxation studies and dynamic properties of polyisobutylene, E. Catsiff and A. V. Tobolsky—145
Second mode vibrations of the Pochhammer-Chree frequency equation, C. W. Curtis—928(L)
Torsion of a shaft with a toroidal cavity, G. Weiss and L. E. Payne—1321
Torsional pendulum of low thermal inertia, C. Ang and C. Wert—1061(L)
Transient wave analysis in a linear time-dependent material, R. D. Glauz and E. H. Lee—947

Electrical Circuits and Networks
Analyses of basic dielectric amplifier circuits, Shou-Hsien Chow—1297
Analysis of systems involving difference-differential equations, T. M. Burford—1145
Approximate method of evaluating integral transforms, Armen H. Zemanian—262
Circumferential gap in a circular wave guide excited by a dominant circular-electric wave, Leonard S. Sheingold and James E. Storer—545
Definition of passive linear networks in terms of time and energy, G. Raisbeck—1510
Dissected amplifiers using negative resistance, W. Shockley and W. P. Mason—677(L)
Electrodynamic perturbation theorem, with application to nonreciprocal systems, Alfred G. Redfield—1021
Equivalent circuit for a passive nonreciprocal network, H. A. Haus—1500
Experimental procedures for determining the efficiency of four-terminal networks, H. F. Mathis—982
Magnetic switching circuits, Robert C. Minnick—479
Matrix analysis of linear time-varying circuits, Louis A. Pipes—1179
Parallel-connected magnetic amplifiers, Shou-Hsien Chow—216
RLC canonic forms, F. M. Reza—297
Switching in bistable circuits, R. Stuart Mackay—424
Synthesis without ideal transformers, F. M. Reza—807(L)
Transfer function as a tool in the analysis of a resistance-capacitance coupled voltage amplifier, D. L. Ming and R. W. Thorpe—934
Transform method for linear time-varying systems, J. A. Aseltine—761

Electrical Conductivity
Electrical characteristics of MnSe and MnTe, Wilfred Palmer—125(L)
Electrical conductivity induced by ionizing radiation in some polymeric materials, A. J. Warner, F. A. Muller, and H. G. Nordlin—131(L)
Electrical properties of selenium. III. Microcrystalline selenium metal doped, H. W. Henkels and J. Maczuk—1
Measurement of the conductivity of a jet flame, Fred P. Adler—903
Resistance of a bar with a transverse hole, W. R. Smythe—930(L)
Semiconducting films of antimony, Julius Cohen—798

Electrical Contacts
Arcing at electrical contacts on closure. Part IV. Activation of contacts by organic vapor. L. H. Germer—332
Arcing at electrical contacts on closure. Part V. Cathode mechanism of extremely short arcs, Paul Kisliuk—897
Contact charging between a borosilicate glass and nickel, John W. Peterson—501
Current fluctuation phenomena in current-carrying sliding contacts, G. W. Epprecht—1473

Electrical Discharges in Gases
Analysis and purification of rare gases by means of electric discharges, R. Riesz and G. H. Dieke—196
Application of ideal gas theory to the gaseous expansion from an electric spark, R. B. Edmonson, H. L. Olsen, and E. L. Gayhart—1008
Arcing at electrical contacts on closure. Part IV. Activation of contacts by organic vapor, L. H. Germer—332

Dynamics of corona discharge between cylindrical electrodes, L. Colli, U. Facchini, E. Gatti, and A. Persano —429
Effect of moving striations on microwave conductivity of a coaxial discharge, H. L. Steele, Jr., and P. J. Walsh —1435(L)
Fast time analysis of intermittent point-to-plane corona in air. I. Positive point burst pulse corona, M. R. Amin—210
Fast time analysis of intermittent point-to-plane corona in air. II. Positive pre-onset streamer corona, M. R. Amin —358
Fast time analysis of intermittent point-to-plane corona in air. III. Negative point Trichel pulse corona, M. R. Amin—627
Measurement of the conductivity of a jet flame, Fred P. Adler—903
Measurement of temperatures in flames of complex structure by resonance line radiation. I. General theory and application to sodium line reversal methods, H. M. Strong and F. P. Bundy—1521; II. Sodium line reversal by high resolution spectroscopy, H. M. Strong and F. P. Bundy—1527; III. From absolute intensity measurements at high resolution, F. P. Bundy and H. M. Strong —1531
Measurements of the gas temperature of a low-pressure rf discharge, Irving Reingold and Kenton Garoff—537
Momentum transfer in sputtering by ion bombardment, Gottfried K. Wehner—270(L)
Response of a pulsed Geiger tube, Herbert B. Rosenstock —275
Secondary electron resonance mechanism of low-pressure high frequency gas breakdown, Albert J. Hatch and H. Bartel Williams—417
Sputtering at low ion velocities, Gottfried Wehner and Gustav Medicus—698

Electromagnetic Waves

Asymptotic evaluation of the field at a caustic, Irvin Kay and J. B. Keller—876
Certain transmission and reflection theorems, V. Twersky —859
Comments on J. H. Crysdale's "Letter to the Editor," G. Bekefi—808(L)
Coupling of modes of propagation, J. R. Pierce—179
Diffraction of electromagnetic waves by an aperture in a large screen, L. Lewin—1053(L)
Diffraction of electromagnetic waves by an aperture in a large screen, Comments on, J. H. Crysdale—269(L)
Diffusion of pulsed currents in conductors, L. M. Vallese —225
Electromagnetic field near a dielectric lens, D. C. Hogg —542(L)
Electromagnetic field of a dipole source above a grounded dielectric slab, Y. T. Lo—733
General theory of plane-wave scattering from finite, conducting obstacles with application to the two-antenna problems, J. E. Storer and J. Sevick—369
Helix as a backward-wave circuit structure, D. A. Watkins and E. A. Ash—782
Helix impedance measurements using an electron beam, Note on, D. A. Watkins and A. E. Siegman—133(L)
Loss measurement of surface wave transmission lines, E. H. Scheibe, B. G. King, and D. L. Van Zeeland—790
Modified Luneberg lens, A. S. Gutman—855
Penetration of an electromagnetic wave into a ferromagnetic material, A. Papoulis—169
Propagation of microwaves between a parallel pair of doubly curved conducting surfaces, K. S. Kunz—642
Property of a family of equiangular spirals and its application to some problems of wave propagation, K. Landecker—41
Reciprocity theorems in electromagnetic theory, T. H. Crowley—119
Scattering from dielectric coated spheres in the region of the first resonance, H. Scharfman—1352
Simplified calculation for Dolph-Tchebycheff arrays, G. J. van der Maas—121

Electron Beams

Combined slow-wave circuit and beam focusing structure, Philip Rice—680(L)
Crossed electron beam technique for measuring space-charge effects in beams, P. D. Coleman, M. D. Sirkis, and I. Kaufman—679(L)
Dispersion formula for plasma waves, L. R. Walker—131(L)
Focusing of an electron beam by periodic fields, A. M. Clogston and H. Heffner—436
Focusing of high-current electron beams, George Brewer —243
Helix impedance measurements using an electron beam, Note on, D. A. Watkins and A. E. Siegman—133(L)
Scalloped beam amplification, T. G. Mihran—1341(L)
Space charge waves in inhomogeneous electron beams, Gordon Kent—32
Stored energy and power flow in electron beams, L. R. Walker—615
Theorem concerning noise in electron streams, J. R. Pierce —931
Thermal effect in an electron beam on the gain of traveling-wave tubes, Kanehisa Udagawa and Masao Sumi —135(L)

Electron Diffraction

Application of Ellis' theory on plural electron scattering to razor edge, Shigeto Yamaguchi—811(L)
Continuously recording electron diffraction camera for studies of crystal structure transitions, A. Boettcher, R. Thun, and H. Treupel—926(L)
Electron diffraction study of the structures of antimony electrodeposited on antimony cleavage face, Ling Yang —184
Graphical method of evaluating trigonometric functions used in crystal structure analysis. Parts I and II, H. J. Grenville-Wells—485
Low-energy electron diffraction investigation of chemisorbed gases on the (100) faces of copper and nickel single crystals, R. E. Schlier and H. E. Farnsworth—1333
Protective films on magnesium observed by electron diffraction and microscopy, Shigeto Yamaguchi—1437(L)
Thermionic emission and electron diffraction from thin films of barium oxide, Paul N. Russell and A. S. Eisenstein—954
Titanium observed by electron diffraction, Shigeto Yamaguchi—408(L)

Electron Emission

Cathode and anode resistance on the retarding potential characteristics of diodes, Effects of, G. C. Dalman—1263
Conductivity of oxide cathode coatings, T. B. Tomlinson —720
Electron emission from metals under high-energy hydrogen ion bombardment, B. Aarset, R. W. Cloud, and J. G. Trump—1365
Field emission current-density distribution, W. P. Dyke, J. K. Trolan, W. W. Dolan, and F. J. Grundhauser—106
Flicker noise generated in an interface layer, H. J. Hannam and A. van der Ziel—1336

Electron Emission (continued)
Measurement of the effect of chlorine treatment on the work function of titanium and zirconium, H. Malamud and A. D. Krumbein—591
Methods of processing silver-magnesium secondary emitters for electron tubes, Paul Rappaport—288
New method of measuring the cathode temperature of indirectly heated vacuum tubes, Suketoshi Ikehara—725
Organic vapor on the secondary emission of phosphors, Effect of, P. H. Dowling and J. B. Sewell—228
Potential distribution and prevention of a space-charge-induced minimum between a plane secondary electron emitter and parallel control grid, George C. Sponsler—282
Secondary electron resonance mechanism of low-pressure high-frequency gas breakdown, A. J. Hatch and H. B. Williams—417
Secondary emission from Nichrome V, CuBe, and AgMg alloy targets due to positive ion bombardment, M. J. Higatsberger, H. L. Demorest, and A. O. Nier—883
Thermionic emission and electron diffraction from thin films of barium oxide, Paul N. Russell and A. S. Eisenstein—954

Electron and Ion Optics
Chromatic field aberration of the magnetic electron lens in the electron microscope, Nozomu Morito—986
Crossed electron beam technique for measuring space-charge effects in beams, Paul D. Coleman, Murray D. Sirkis, and Irving Kaufman—679(L)
Effect of filament voltage on the plate current of a diode, Note on, Henry S. C. Chen—929(L)
Electron bunches of short time duration, E. W. Ernst and H. Von Foerster—674(L)
Experimental studies of betatron orbit stability, G. C. Baldwin, F. R. Elder, and W. F. Westendorp—1553(L)
Focusing of a long cylindrical electron stream by means of periodic electrostatic fields, Ping King Tien—1281
Focusing of an electron beam by periodic fields, A. M. Clogston and H. Heffner—436
Ion trajectories in the omegatron, Clifford E. Berry—28
Potential distribution and prevention of a space-charge-induced minimum between a plane secondary electron emitter and parallel control grid, George C. Sponsler—282
Relativistic dynamics of a charged particle in crossed magnetic and electric fields with application to the planar magnetron, Louis Gold—683
Transcendental curves associated with the relativistic trajectories of charged particles, On the nature of, Louis Gold—691
Transverse motion of an electron in a constant wave speed section of a linear accelerator, Ira Jacobs and E. S. Akeley—572

Electron Microscope Society of America, Proceedings of the Twelfth Annual Meeting—pp. 1453–1468

Electron Microscopy
Chromatic field aberration of the magnetic electron lens in the electron microscope, Nozomu Morito—986
Decompositions of inorganic specimens during observation in the electron microscope, Robert B. Fischer—894
Electron beam effects on thin evaporated bismuth films, P. J. Bryant, H. U. Rhoads, and A. H. Weber—1343(L)
High-resolution replicas and their application, Tadatosi Hibi and Keiji Yada—712
Improved replica technique for electron microscopy of paint films, Allen S. Powell, Louis R. LeBras, Edward G. Bobalek, and William von Fischer—757
Oxide replica in electron microscopy, Note on, Shigeto Yamaguchi—927(L)
Preparation of aerosols for electron microscopy, Ernest H. Kalmus—87
Protective films on magnesium observed by electron diffractions and microscopy, Shigeto Yamaguchi—1437(L)
Shadowing technique for electron microscopy—a possible substitute for the high-vacuum evaporation technique, A. E. Bills and R. Lefker—901
Spin-coated polyvinyl alcohol replicas for electron microscope use, F. E. Bulette—810(L)
Sudden change in the arrangement of crystallites in thin evaporated bismuth films, Lorn L. Howard—125(L)

Electron Tubes (see also **Space Charge**)
Amplification factor and perveance of an elliptic triode, S. Deb and G. S. Sanyal—1196
Application of perturbation theory to the traveling wave tubes, M. W. Muller and W. L. Beaver—542(L)
Combined slow-wave circuit and beam focusing structure, Philip Rice—680(L)
Coupling modes of propagation, J. R. Pierce—179
Effects of cathode and anode resistance on the retarding potential characteristics of diodes, G. C. Dalman—1263
Effect of velocity distribution on traveling-wave tube gain, D. A. Watkins and N. Rynn—1375
Helix as a backward-wave circuit structure, D. A. Watkins and E. A. Ash—782
Methods of processing silver-magnesium secondary emitters for electron tubes, Paul Rappaport—288
Minimum noise figure of traveling-wave tubes with uniform helices, J. R. Pierce and W. E. Danielson—1163
New method of measuring the cathode temperature of indirectly heated vacuum tubes, Suketoshi Ikehara—725
Noise in transverse-field traveling-wave tubes, G. Wade, K. Amo, and D. A. Watkins—1514
Potential distribution and prevention of a space-charge-induced minimum between a plane secondary electron emitter and parallel control grid, George C. Sponsler—282
Relativistic dynamics of a charged particle in crossed magnetic and electric fields with application to the planar magnetron, Louis Gold—683
Response of a pulsed Geiger tube, H. B. Rosenstock—275
Scalloped beam amplification, T. G. Mihran—1341(L)
Space charge waves in inhomogeneous electron beams, Gordon Kent—32
Thermal effect in an electron beam on the gain of traveling-wave tubes, Some remarks on, Kanehisa Udagawa and Masao Sumi—135(L)
X-ray noise observation using a photoconductive pickup tube, A. D. Cope and A. Rose—240

Electrophoresis
Centripetal and centrifugal electromagnetophoresis, Alexander Kolin—1065(L)
Method for elimination of thermal convection, Alexander Kolin—1442(L)

Emissivity (see **Spectra**)

Errata
Analysis of first-order glow curves, Leonard I. Grossweiner, erratum—136
Approximate solutions of the space-charge problem for some unusual electrode geometries, Henry F. Ivey, erratum—543
Effect of filament voltage on the plate current of a diode, A note on, Henry S. Chen, erratum—1345
Low loss ferrites, L. G. Van Uitert, J. P. Schafer, and C. L. Hogan, erratum—1345
Modified Luneberg lens, A. S. Gutman, errata—1553
Nonlinear diffusion equation applied to the magnetization of saturable reactors, Shou-Hsien Chow, erratum—930(L)

Propagation constant in gentle circular bends in rectangular wave guides—matrix theory. A. T. de Hoop, erratum—136
Study of the propagation mode for metallic vapors in shadow casting by vacuum evaporation of Au^{198} and Cr^{51}, Luther E. Preuss, errata—136
Sudden change in the arrangement of crystallites in thin evaporated bismuth films, Lorn L. Howard, errata—543
Thermal effects in point contact rectifiers, H. L. Armstrong, erratum—136
Vector wave function solution of the diffraction of electromagnetic waves by circular disks and apertures. II. Diffraction problems, Carson Flammer, errata—543
Velocity attenuation of explosive-produced air shocks, Jacob Savitt and R. H. Stresau, errata—1208

Explosives and Explosions
Boundary disturbances in high-explosive shock tubes, R. G. Shreffler and R. H. Christian—324
Compression wave velocity experiments with copper, Jacob Savitt, R. H. Stresau, and L. E. Starr—1307
Hardness plateaus and twinning in explosively loaded mild steel, John Pearson and John S. Rinehart—778
Propagation of explosion-produced air shocks, Note on, M. Birk, Y. Manheimer, and G. Nahmani—1208(L)
Shock propagation in brass, H. Becker—1066(L)
Spall effects by a cylindrical and a spherical charge of high explosive, Wm. A. Allen and W. Goldsmith—813(L)
Velocity attenuation of explosive-produced air shocks, Jacob Savitt and R. H. Stresau—89

Fatigue (see **Plastic Deformation**)

Ferroelectricity
Dielectric constant and loss measurements on barium titanate single crystals while traversing the hysteresis loop, M. E. Drougard, H. L. Funk, and D. R. Young—1166

Ferromagnetic Materials and **Ferrites**
Factors determining the permanent magnet properties of single crystals of Fe_2NiAl, E. A. Nesbitt, H. J. Williams, and R. M. Bozorth—1014
Ferrite phase shifters in rectangular wave guide, Benjamin Lax, Kenneth J. Button, and Laura M. Roth—1413
Ferrites for microwave circuits and digital computers, E. Albers-Schoenberg—152
Ferromagnetic spinels with rectangular hysteresis loops, I. J. Hegyi—176
High-speed magnetic pulsing of ferrites, R. Conway LeCraw—678(L)
Low loss ferrites for applications at 4000 megacycles per second, L. G. Van Uitert, J. P. Schafer, and C. L. Hogan—925(L)
Penetration of an electromagnetic wave into a ferromagnetic material, A. Papoulis—169
16 percent aluminum-iron alloy cold rolled in the order-disorder temperature range, J. F. Nachman and Wm. J. Buehler—307
Theory of strong electromagnetic waves in massive iron, William MacLean—1267

Fluid Dynamics (see also **Shock Waves** and **Turbulence**)
Design and calibration of stagnation temperature probes for use at high supersonic speeds and elevated temperatures, Eva M. Winkler—231
Limiting pressure on hydrofoils at small submergence depths, E. V. Laitone—623
Phenomena associated with supersonic liquid jets, Brian Dunne and Benedict Cassen—569
Stability of fluid flows with spherical symmetry, M. S. Plesset—96
Variational and Galerkin's methods in compressible fluid flow problems, Pei Chi Chou—1551(L)
Water vapor condensation process in supersonic nozzles, Peter P. Wegener—1485

Fluid Flow, Low Speed
Diffusion coefficient, solubility, and permeability for helium in glass, W. A. Rogers, R. S. Buritz, and D. Alpert—868
Direct determination of the flow curves of non-Newtonian fluids. III. Standardized treatment of viscometric data, I. M. Krieger and S. H. Maron—72
Effect of gas slip on unsteady flow of gas through porous media. Part I, J. S. Aronofsky—48
Electromagnetic velometry. II. Elimination of the effects of induced currents in explorations of the velocity distribution in axially symmetrical flow, Alexander Kolin and Fritz Reiche—409
Laminar flow of an electrically conducting incompressible fluid in a circular pipe, Shih I. Pai—1205(L)
Mechanics of two immiscible fluids in porous media, H. I. Meyer and A. O. Garder—1400
Relation between the velocity profile and the sensitivity of electromagnetic flow-meters, J. A. Shercliff—817(L)
Stability of fluid flows with spherical symmetry, M. S. Plesset—96
Statistical hydrodynamics in porous media, Adrian E. Scheidegger—994
Transient flow of non-ideal gases in porous solids—one-dimensional case, J. S. Aronofsky and O. D. Ferris—1289
Turbulent processes as observed in boundary layer and pipe, G. B. Schubauer—188

Friction and Wear
Friction of clean metals and oxides with special reference to titanium, E. S. Machlin and W. R. Yankee—576

Geophysics
Analysis of short-time tracer injection in underground formations, G. C. Wallick and R. Jenkins—1491

Hall Effect
Electrical characteristics of MnSe and MnTe, Wilfred Palmer—125(L)
Solution of the field problem of the germanium gyrator, R. F. Wick—741

Heat Capacity
Thermal diffusivity of metals at high temperatures, D. Rosenthal and N. E. Friedmann—1059(L)

Heat Flow (see **Thermal Conductivity**)

Heat Transfer
Heat transfer measurements at sodium-stainless steel interface, James W. Moyer and William A. Riemen—400

Hydrodynamics (see **Fluid Dynamics**)

Information Theory and Communication Theory
Coincidence of pulse trains, Henry D. Friedman—1001
Entropy of information and the odd ball problem, Paul J. Kellogg and Dorothy J. Kellogg—1438(L)
Information theory and knowledge, D. K. C. MacDonald—619
Information theory and knowledge: Remarks on a paper by D. K. C. MacDonald, A. Gamba—1549(L)
Information theory and uncertainty principle, L. Brillouin—887
Maxwell's demon must remain incommunicado, Marcel J. E. Golay—1062(L)
Negentropy and information in telecommunications, writing, and reading, L. Brillouin—595
PPI light spot brightness probability distributions, G. C. Sponsler and F. L. Shader—1271

Insulators (see **Dielectrics and Dielectric Breakdown**)
Ion Optics (see **Electron and Ion Optics**)

Liquids (see also **Fluid Flow**)
Conduction of heat into a growing vapor bubble, H. Kurt Forster—1067(L)
Growth of a vapor bubble in a superheated liquid, H. K. Forster and N. Zuber—474
Growth of vapor bubbles in superheated liquids, M. S. Plesset and S. A. Zwick—493
Instability of liquid surfaces and the formation of drops, J. B. Keller and I. Kolodner—918
Phenomena associated with supersonic liquid jets, Brian Dunne and Benedict Cassen—569
Luminescence
Brightness waves and transitory phenomena in the quenching of luminescence by alternating electric fields, G. Destriau—67
Effect of organic vapor on the secondary emission of phosphors, P. H. Dowling and J. R. Sewell—228

Magnetic Resonance
Studies of rubberlike polymers by nuclear magnetism, V. R. Honnold, F. McCaffrey, and B. A. Mrowca—1219
Magnetism (see also **Magnetostriction** and **Ferromagnetic Materials**)
Ferrites for microwave circuits and digital computers, E. Albers-Schoenberg—152
Ferromagnetic spinels with rectangular hysteresis loops, I. J. Hegyi—176
New magneto-mechanical torsion experiments, A. W. Cochardt—670
Nonlinear diffusion equation applied to the magnetization of saturable reactors, Shou-Hsien Chow—377
Parallel-connected magnetic amplifiers, Shou-Hsien Chow—216
Theory of strong electromagnetic waves in massive iron, William MacLean—1267
Magnetostriction
Magnetostriction relations in materials possessing preferred domain orientations, George T. Rado—102
Method of measuring magnetostriction, A. W. Cochardt—91
New magnetostrictive material, H. E. Stauss and G. Sandoz—267(L)
Mass Spectrometry
Secondary emission from Nichrome V, CuBe, and AgMg alloy targets due to positive ion bombardment, M. J. Higatsberger, H. L. Demorest, and A. O. Nier—883
Mathematics
Applications of the Dirac delta function to the evaluation of certain integrals, Murray R. Spiegel—1302
Approximate method of evaluating integral transforms, Armen H. Zemanian—262
Direct cellular evaluation of the density of states in phase space and the accurate calculation of Fermi levels, Louis Gold—1278
Elastic wedge problem, J. H. Huth—929(L)
Estimation of correlation coefficients from scatter diagrams, George R. Sugar—354
Generalization of the Wiener-Khintchine theorem to nonstationary processes, D. G. Lampard—802
Graphical method of evaluating trigonometric functions used in crystal structure analysis. Parts I and II, H. J. Grenville-Wells—485
Information loss attending the decision operation in detection, David Middleton—127(L)
Method of averages and its comparison with the method of least squares, Morris Morduchow—1260
Nature of the statistical observer, Further remarks on, David Middleton—127(L)
Period and amplitude of the Van Der Pol limit cycle, Edward Fisher—273
Remark on stability, Kenneth S. Miller—407(L)
Resistance of a bar with a transverse hole, W. R. Smythe—930(L)
Roots of transcendental equations, Alan F. Kay—811(L)
Solution of nonlinear differential equations by the reversion method through the first thirteen terms, George I. Cohn and Bernard Saltzberg—252
Statistical criteria for the detection of pulsed carriers in noise I, II, Discussion of, David Middleton, W. W. Peterson, and T. G. Birdsall—128(L)
Summation of infinite series in closed form, Albert D. Wheelon—113
Summation of series involving roots of transcendental equations and related applications, Comment on, G. Kuerti—133(L)
Summation of slowly converging series, Comments on, Julian H. Braun—132(L)
Summation of slowly converging series, Comments on Gumowski's letters, E. L. Chu—1553(L)
Summation of slowly converging series, Further comments on, Igor Gumowski—133(L)
Symmetry as a factor in finite difference approximations, C. M. Fowler—293
Theory of consolidation for anisotropic materials, M. A. Biot—1385
Transform method for linear time-varying systems, J. A. Aseltine—761
Use of restricted variational principles for the solution of differential equations, Philip Rosen—336
Metallurgy (see also **Diffusion, X-rays, Crystals, Electrical,** and **Magnetic Properties**)
Analysis of quantitative pole-figure data, C. G. Dunn—233
Creep recovery and annealing of zinc single crystals, Studies on, M. Tanenbaum and W. Kauzmann—451
Hardening of Pd by cathodic hydrogen, Takesi Sugeno and Masamichi Kowaka—1063(L)
Influence of deuteron bombardment and strain hardening on notch sensitivity of mild steel, Robert A. Meyer—1369
Magnetostriction relations in materials possessing preferred domain orientations, George T. Rado—102
Necking of a tension specimen in plane plastic flow, E. T. Onat and W. Prager—491
Radiation damage effects on order-disorder in nickel-manganese alloys, Lewis R. Aronin—344
Regrowth of silicon through a low melting zone of silicon-gold eutectic, J. N. Carman, P. E. Stello, and C. A. Bittmann—543(L)
Reproducibility of the freezing temperature of high-purity zinc, E. H. McLaren—808(L)
16 percent aluminum-iron alloy cold rolled in the order-disorder temperature range, Joseph F. Nachman and William J. Buehler—307
Synthesis of x-ray spectrometer line profiles with application to crystallite size measurements, Leroy Alexander—155
Meteorology
Rocket measurements of upper atmosphere ambient temperature and pressure in the 30- to 75-kilometer region, H. S. Sicinski, N. W. Spencer, and W. G. Dow—161
Microwaves (see **Electron Tubes, Resonant Cavities,** and **Transmission Lines**)

Noise
Concept of an instantaneous power spectrum, and its relationship to the autocorrelation function, C. H. M. Turner—1347

Current noise in thermistor bolometer flakes, James J. Brophy—222
Detection of sure signals in noise, R. C. Davis—76
Distributions of signals and noise after rectification and filtering, M. A. Meyer and David Middleton—1037
Effect of integration in a pulsed, radar, randomly modulated carrier, W. M. Stone—1543
Electrical noise pulses from polarized dielectrics, N. P. Baumann and G. G. Wiseman—1391
Errors in power spectra due to finite sample, Lee M. Spetner—653
Flicker noise generated in an interface layer, H. J. Hannam and A. van der Ziel—1336
Flicker noise in germanium rectifiers at very low- and audio-frequencies, D. K. Baker—922
Generalization of the Wiener-Khintchine theorem to nonstationary processes, D. G. Lampard—802
Information loss attending the decision operation in detection, David Middleton—127(L)
Joint distribution of n successive outputs of a linear detector, William C. Hoffman—1006
Minimum noise figure of traveling-wave tubes with uniform helices, J. R. Pierce and W. E. Danielson—1163
Nature of the statistical observer, Further remarks on, David Middleton—127(L)
Noise in semiconductors: Spectrum of a two-parameter random signal, Stefan Machlup—341
Noise in transverse-field traveling-wave tubes, G. Wade, K. Amo, and D. A. Watkins—1514
PPI light spot brightness probability distributions, G. C. Sponsler and F. L. Shader—1271
Short-time frequency measurement of narrow-band random signals in the presence of wide-band noise, P. M. Schultheiss, C. A. Wogrin, and F. Zweig—1025
Shot and partition noise in junction transistors, A. van der Ziel—815(L)
Shot dependence of p-n junction phototransistor noise, A. Slocum and J. N. Shive—406(L)
Spectral response of a quadratic device to non-Gaussian noise, T. A. Magness—1357
Statistical criteria for the detection of pulsed carriers in noise I, II, David Middleton, W. W. Peterson, and T. G. Birdsall—128(L)
Statistical properties of the output of a frequency sensitive device, George R. Arthur—1185
Theorem concerning noise in electron streams, J. R. Pierce—931
Tube noise under large transit-time conditions, S. V. Yadavalli—564
X-ray noise observation using a photoconductive pickup tube, A. D. Cope and A. Rose—240

Nuclear Physics (see also **Nuclear Reactor**)
Backscattering of the Co^{60} gamma rays from infinite media, Evans Hayward and John H. Hubbell—506
Effect of inelastic collisions on the slowing-down length of neutrons in a hydrogenous mixture, Howard C. Volkin—83
Estimating differential scattering cross sections in gases, Tino Ahrens—505
Generalized off-axis distributions from disk sources of radiation, Jack H. Smith and Martin L. Storm—519
Transformation of scattering cross sections, P. F. Zweifel and H. Hurwitz, Jr.—1241

Nuclear Reactor (see also **Nuclear Physics**)
Concept of stability for nuclear reactors, L. B. Robinson—516
Generalized off-axis distributions from disk sources of radiation, Jack H. Smith and Martin L. Storm—519
Kinetics of piles with reflectors, V. H. Rumsey—1395
Kinetics of the circulating-fuel nuclear reactor, William K. Ergen—702

Operations Research
Coincidence of pulse trains, Henry D. Friedman—1001

Optical Properties
Measurements of orientation in polystyrene monofilaments by means of double refraction, R. D. Andrews—1223
Theory of orientation and double refraction in polymers, Edward F. Gurnee—1232

Phase Transformations
Reexamination of low-temperature properties of crystalline quartz, A. Pavlovic and R. Pepinsky—1344(L)

Photoelasticity (see **Elasticity**)

Piezoelectricity
Piezoelectric properties of lead zirconate-lead titanate solid-solution ceramics, B. Jaffe, R. S. Roth, and S. Marzullo—809(L)
Reexamination of low-temperature properties of crystalline quartz, A. Pavlovic and R. Pepinsky—1344(L)
Thickness-shear and flexural vibrations of contoured crystal plates, R. D. Mindlin and M. Forray—12
Thickness-shear vibrations of piezoelectric crystal plates with incomplete electrodes, R. D. Mindlin and H. Deresiewicz—21

Plastic Deformation (see also **Rheology**)
Cross section of pulled crystals, Robert G. Pohl—668
Delayed yield and strain rate and temperature dependence of yield point in iron, Takeo Yokobori—593
Failure and survival in fatigue, A. M. Freudenthal and E. J. Gumbel—1435(L)
Hardness plateaus and twinning in explosively loaded mild steel, John Pearson and John S. Rinehart—778
Necking of a tension specimen in plane plastic flow, E. T. Onat and W. Prager—491
Plastic deformation in beams under distributed dynamic loads, J. A. Seiler and P. S. Symonds—556
Plastic deformation of ammonium dihydrogen phosphate, Paul L. Smith and Edward I. Salkovitz—237
Propagation of longitudinal deformation waves in a prestressed rod of material exhibiting a strain-rate effect, Robert J. Rubin—528

Polymers
Approximations in linear viscoelasticity theory: delta function approximations, Herbert Leaderman—294
Composition of apparent shearing forces during shear degradation of polymers, A. B. Bestul—1069
Constant stress elongation of soft polymers: Plasticizer studies, M. R. Hatfield and G. B. Rathmann—1082
Crystallization in butadiene-styrene copolymers, Lawrence A. Wood—851
Crystallization kinetics in high polymers. I. Bulk polymers, Leo Mandelkern, F. A. Quinn, Jr., and P. J. Flory—830
Direct-current transients in polymethyl methacrylate and in polystyrene, Paul Ehrlich—1056(L)
Dynamic investigations on polymers, Wladimir Philippoff—1102
Dynamic mechanical and electrical behavior of polymethyl methacrylate, David Telfair—1062(L)
Elastoviscous properties of amorphous polymers in the transition region. II. Stress-relaxation of butadiene-styrene copolymers, E. Catsiff and A. V. Tobolsky—1092

Polymers (continued)
Electrical conductivity induced by ionizing radiation in some polymeric materials, A. J. Warner, F. A. Muller, and H. G. Nordlin—131(L)
Experimental study of low-frequency effects on the dynamic modulus of a Buna-N rubber, A. Q. Hutton and A. W. Nolle—350
Flow of melts in "crosshead"-slit dies; criteria for die design, James F. Carley—1118
Infrared study of the crystallization of polyethylene, F. P. Reding and Alexander Brown—848
Method for determining the viscoelastic properties of dilute polymer solutions at audio-frequencies, K. Sittel, P. E. Rouse, Jr., and E. D. Bailey—1312
Molecular structure and the crystallinity of long-chain polymers, C. W. Bunn—820
Relation between stress-relaxation studies and dynamic properties of polyisobutylene, E. Catsiff and A. V. Tobolsky—145
Relationship of first- to second-order transition temperatures for crystalline high polymers, Raymond F. Boyer—825
Rheological properties of concentrated polyisobutylene solutions, F. J. Padden and T. W. DeWitt—1086
Rheological unit in raw elastomers, M. Mooney and W. E. Wolstenholme—1098
Rotational plastometry applied to molten polyethylene, F. D. Dexter—1124
Stress and strain (Discussion of Dr. Philippoff's paper), W. F. G. Swann—1108
X-ray and infrared studies on the extent of crystallization of polymers, J. B. Nichols—840
Preferred Orientation (see **Metallurgy**)

Radiation Effects in Solids
Electrical conductivity induced by ionizing radiation in some polymeric materials, A. J. Warner, F. A. Muller, and H. G. Nordlin—131(L)
Influence of deuteron bombardment and strain hardening on notch sensitivity of mild steel, Robert A. Meyer—1369
Nature of radiation damage in metals, John A. Brinkman—961
Radiation damage effects on order-disorder in nickel-manganese alloys, Lewis R. Aronin—344
Resistivity (see **Electrical Conductivity**)
Resonant Cavities
Band width of cavity antennas, Marshall H. Cohen—582
Measurement of electromagnetic field in resonant cavities by introduction of small metallic rings, Aldo Gilardini—1064(L)
Resonant cavity study of semiconductors, Hsi-Teh Hsieh, J. M. Goldey and S. C. Brown—302
Thermodynamic consideration of electromagnetic cavity resonators, Charles H. Papas—1552(L)
Rheology (see also **Plastic Deformation**)
Rheology symposium papers:—pp. 1069—1144
Composition of apparent shearing forces during shear degradation of polymers, A. B. Bestul—1069
Constant stress elongation of soft polymers: Plasticizer studies, M. R. Hatfield and G. B. Rathmann—1082
Effect of rheological behavior on thermal stresses, Alfred M. Freudenthal—1110
Elastoviscous properties of amorphous polymers in the transition region. II. Stress-relaxation of butadiene-styrene copolymers, E. Catsiff and A. V. Tobolsky—1092
Flow of melts in "crosshead"-slit dies; criteria for die design, James F. Carley—1118
Further dynamic investigations on polymers, Wladimir Philippoff—1102
Internal friction and dynamic modulus of cold-worked metals, A. S. Nowick—1129
Relaxation time spectrum of dough and the influence of temperature, rest and water content, J. R. Cunningham and I. Hlynka—1075
Rheological properties of concentrated polyisobutylene solutions, F. J. Padden and T. W. DeWitt—1086
Rheological unit in raw elastomers, M. Mooney and W. E. Wolstenholme—1098
Rheology of suspensions, K. H. Sweeny and R. D. Geckler—1135
Rotational plastometry applied to molten polyethylene, F. D. Dexter—1124
Stress and strain (discussion of Dr. Philippoff's paper), W. F. G. Swann—1108

Semiconductor Devices
Additional observation on thermal effects in point contact rectifiers, H. L. Armstrong—1345(L)
Charge storage in junction diodes, Earl L. Steele—916
Diode theory in the light of hole injection, John A. Swanson—314
Effect of a transverse electric field on carrier diffusion in the base region of a transistor, J. S. Kerr, J. S. Schaffner, and J. J. Suran—1293
Electrolytic analog transistor, Harry Letaw, Jr., and John Bardeen—600
Flicker noise in germanium rectifiers at very low- and audio-frequencies, D. K. Baker—922
Forming point-contact silicon transistors, Harold Jacobs, F. A. Brand, W. Matthei, and A. P. Ramsa—1406
Germanium diodes from spherical pellets, W. C. Dunlap, Jr.—448
New silicon *p-n* junction photocell for converting solar radiation into electrical power, D. M. Chapin, C. S. Fuller, and G. L. Pearson—676(L)
Physical theory of new circuit representation for junction transistors, Jakob Zawels—976
Point emitter-junction collector transistor, Robert H. Kingston—513
Radioactive and photoelectric *p-n* junction power sources, W. G. Pfann and W. van Roosbroeck—1422
Shot dependence of *p-n* junction phototransistor noise, A. Slocum and J. N. Shive—406(L)
Solution of the field problem of the germanium gyrator, R. F. Wick—741
Steady-state solution of the two-dimensional diffusion equation for transistors, J. S. Schaffner and J. J. Suran—863
Surface leakage current in rectifiers, Melvin Cutler and Hubert M. Bath—1440(L)
Transient response of a *p-n* junction, Benjamin Lax and S. F. Neustadter—1148

Semiconductors
Conductivity of oxide cathode coatings, T. B. Tomlinson—720
Current noise in thermistor bolometer flakes, James J. Brophy—222
Electrical characteristics of MnSe and MnTe, Wilfred Palmer—125(L)
Electrical properties of selenium. III. Microcrystalline selenium metal doped, H. W. Henkels and J. Maczuk—1
Etching of single crystal germanium spheres, Ray C. Ellis, Jr.—1497
Formation of single crystal silicon fibers, E. R. Johnson and J. A. Amick—1204(L)
Germanium diodes from spherical pellets, W. C. Dunlap, Jr.—448
Germanium-stabilized gray tin, A. W. Ewald—1436(L)

Noise in semiconductors: Spectrum of a two-parameter random signal, Stefan Machlup—341
Problems in the diffusion of minority carriers in a semiconductor, S. Visvanathan and J. F. Battey—99
Regrowth of silicon through a low melting zone of silicon-gold eutectic, J. N. Carman, P. E. Stello, and C. A. Bittmann—543(L)
Resistivity striations in germanium crystals, Paul R. Camp—459
Resonant cavity study of semiconductors, Hsi-Teh Hsieh, James M. Goldey, and Sanborn C. Brown—302
Semiconducting films of antimony, Julius Cohen—798
Semiconductor devices made with single crystal germanium-silicon alloys, R. A. Logan, A. J. Goss, and M. Schwartz —1551(L)
Shot and partition noise in junction transistors, Note on, A. van der Ziel—815(L)
Vapor phase crystal growth of lead sulfide crystals, Frank Pizzarello—804(L)
Volume and surface recombination rates for injected carriers in germanium, J. P. McKelvey and R. L. Longini—634

Shock Waves
Boundary disturbances in high-explosive shock tubes, R. G. Shreffler and R. H. Christian—324
Cylindrical shock waves produced by instantaneous energy release, Shao-Chi Lin—54
Equation of state of argon, R. H. Christian and R. G. Shreffler—1341(L)
Geometrical acoustics. I. Theory of weak shock waves, Joseph B. Keller—938
Interaction of two plane shocks facing in the same direction, Otto Laporte and E. B. Turner—678(L)
Interaction of two similarly facing plane shock waves, C. A. Ford and I. I. Glass—1549(L)
Method for generating strong shock waves, A. Hertzberg and W. E. Smith—130(L)
Multiple shock reflection in corners, Joseph B. Keller—588
Normal reflection of shock waves from moving boundaries, Ralph A. Alpher and Robert J. Rubin—395
Propagation of explosion-produced air shocks, Note on, M. Birk, Y. Manheimer, and G. Nahmani—1208(L)
Shock propagation in brass, H. Becker—1066(L)
Velocity attenuation of explosive-produced air shocks, Jacob Savitt and R. H. F. Stresau—89

Sound Wave Propagation
Short range propagation of mechanical disturbances in the ground, B. J. Starkey and C. M. Lock—816(L)
Transmission and reflection theorems, V. Twersky—859

Space Charge
Amplification factor and perveance of an elliptic triode, S. Deb and G. S. Sanyal—1196
Crossed electron beam technique for measuring space-charge effects in beams, P. D. Coleman, M. D. Sirkis, and I. Kaufman—679(L)
Effect of filament voltage on the plate current of a diode, Note on, Henry S. C. Chen—929(L)
Potential distribution and prevention of a space-charge-induced minimum between a plane secondary electron emitter and parallel control grid, George C. Sponsler—282
Space charge waves in inhomogeneous electron beams, Gordon Kent—32

Spectra and Spectroscopy
Approximate emissivity calculations for polyatomic molecules. I. CO_2, S. S. Penner—660

Sputtering (see **Electrical Discharges in Gases**)
Stability of Flow (see **Fluid Dynamics**)

Surface Properties
Low-energy electron diffraction investigation of chemisorbed gases on the (100) faces of copper and nickel single crystals, R. E. Schlier and H. E. Farnsworth—1333
Measurement of the effect of chlorine treatment on the work function of titanium and zirconium, H. Malamud and A. D. Krumbein—591
Momentum transfer in sputtering by ion bombardment, Gottfried K. Wehner—270(L)
Sputtering at low ion velocities, Gottfried Wehner and Gustav Medicus—698
Ultra-high vacuum. II. Limiting factors on the attainment of very low pressures, D. Alpert and R. S. Buritz —202
Volume and surface recombination rates for injected carriers in germanium, J. P. McKelvey and R. L. Longini—634

Thermal Conductivity and Thermal Conduction
Experimental determinations of the electric field and equipotential surfaces using the heat conduction analogy, M. Kamal Gohar—805(L)
Heat conduction in an infinite cylindrical medium with heat generated by a chemical reaction, P. L. Nichols, Jr., and A. G. Presson—1469
Heat transfer measurements at sodium-stainless steel interface, James W. Moyer and William A. Riemen—400
Stationary temperature distribution in an electrically heated conductor, Charles A. Domenicali—1310
Thermal diffusivity of metals at high temperatures, D. Rosenthal and N. E. Friedmann—1059(L)
Thermal diffusivity of metals at high temperatures, P. H. Sidles and G. C. Danielson—58
Transient-flow method for determination of thermal constants of insulating materials in bulk. Part I. Theory, J. H. Blackwell—137

Thermodynamic Properties
Equation state of argon, R. H. Christian and R. G. Shreffler—1341(L)
Measurement of temperatures in flames of complex structure by resonance line radiation. I. General theory and application to sodium line reversal methods, H. M. Strong and F. P. Bundy—1521
Measurement of temperatures in flames of complex structure by resonance line radiation. II. Sodium line reversal by high resolution spectroscopy, H. M. Strong and F. P. Bundy—1527
Measurement of temperatures in flames of complex structure by resonance line radiation. III. From absolute intensity measurements at high resolution, F. P. Bundy and H. M. Strong—1531

Thermoelectricity
Calibration of a nickel-molybdenum thermocouple, Richard D. Potter—1383
Electrical properties of selenium. III. Microcrystalline selenium metal doped, H. W. Henkels and J. Maczuk—1
Optimal loading of a thermoelectric generator, James F. Perkins—1058(L)
Power output of thermoelectric generators, Maria Telkes —1058(L)
Solar thermoelectric generators, Maria Telkes—765

Thin Films
Apparent density of thin evaporated films, M. S. Blois, Jr., and L. M. Rieser, Jr.—338
Electron beam effects on thin evaporated bismuth films, P. J. Bryant, H. U. Rhoads, and A. H. Weber—1343(L)
Electron diffraction study of the structures of antimony electrodeposited on antimony cleavage face, Ling Yang —184

Thin Films (continued)
Improved replica technique for electron microscopy of paint films, A. S. Powell, L. R. LeBras, E. G. Bobalek, and Wm. von Fischer—757
Protective films on magnesium observed by electron diffractions and microscopy, Shigeto Yamaguchi—1437(L)
Radioactive-shadowing technique and note on the deposition of metal crystals from atomic beams, M. Simnad, Ling Yang, and G. M. Pound—268(L)
Semiconducting films of antimony, Julius Cohen—798
Sudden change in the arrangement of crystallites in thin evaporated bismuth films, Lorn L. Howard—125(L)
Transistors (see **Semiconductor Devices**)
Transmission Lines and **Wave Guides**
Circumferential gap in a circular wave guide excited by a dominant circular-electric wave, L. S. Sheingold and J. E. Storer—545
Ferrite phase shifters in rectangular wave guide, Benjamin Lax, Kenneth J. Button, and Laura M. Roth—1413
Loss measurements of surface wave transmission lines, E. H. Scheibe, B. G. King, and D. L. Van Zeeland—790
Lower modes of a concentric line having a helical inner conductor, Louis Stark—1155
Propagation constant in rectangular wave guide of finite conductivity, D. M. Kerns and R. W. Hedberg—1550(L)
Propagation of microwaves between a parallel pair of doubly curved conducting surfaces, K. S. Kunz—642
Turbulence
Turbulent processes as observed in boundary layer and pipe, G. B. Schubauer—188

Vacuum Technique
All-glass valves for use in obtaining ultra high vacua, Richard W. Decker—1441(L)
Ultimate vacuum in a vacuum-enclosed ionization gauge, L. J. Varnerin, Jr., and D. White—1207(L)
Ultra-high vacuum. II. Limiting factors on the attainment of very low pressures, D. Alpert and R. S. Buritz —202
Vaporization (see **Liquids**)
Vibrations
Delta-function source in a problem on elastic waves, Concerning the use of, Alan G. Mencher—804(L)
Epicentral displacement due to elastic waves in an infinite slab, Arthur S. Ginzbarg—804(L)
Second mode vibrations of the Pochhammer-Chree frequency equation, E. W. Curtis—928(L)
Short range propagation of mechanical disturbances in the ground, B. J. Starkey and C. M. Lock—816(L)
Suppression of overtones of thickness-shear and flexural vibrations of crystal plates, R. D. Mindlin and H. Deresiewicz—25
Thickness-shear and flexural vibrations of a circular disk, R. D. Mindlin and H. Deresiewicz—1329
Thickness-shear and flexural vibrations of contoured crystal plates, R. D. Mindlin and M. Forray—12
Thickness-shear vibrations of piezoelectric crystal plates with incomplete electrodes, R. D. Mindlin and H. Deresiewicz—21
Viscosity and Viscoelasticity
Approximations in linear viscoelasticity theory: Delta function approximations, Herbert Leaderman—294
Capillary viscometer with continuously varying pressure head, S. H. Maron, I. M. Krieger, and A. W. Sisko— 971
Dynamic bulk viscosity of polyisobutylene, R. S. Marvin, R. Aldrich, and H. S. Sack—1213
Indeterminate integral in Einstein's theory of the viscosity of a suspension, M. Mooney—406(L)
Method for determining the viscoelastic properties of dilute polymer solutions at audio-frequencies, K. Sittel, P. E. Rouse, Jr., and E. D. Bailey—1312
Motion of small particles in skew shape suspended in a viscous liquid, Chan-Mou Tchen—463
Nature of radiation damage in metals, John A. Brinkman —961
Theory of stress-strain relation phenomena, M. A. Biot— 1385

Wave Propagation (see **Electromagnetic Waves**)

X-Rays, and X-Ray Diffraction
Analysis of quantitative pole-figure data, C. G. Dunn—233
Diffraction of x-rays by a twisted crystal lattice, S. S. Hsu—541(L)
Distortion of a crystal by point imperfections, J. D. Eshelby—255
Graphical method of evaluating trigonometric functions used in crystal structure analysis. Parts I and II, H. J. Grenville-Wells—485
Monochromatic x-rays for single crystal diffuse scattering, B. E. Warren—814(L)
Synthesis of x-ray spectrometer line profiles with application to crystallite size measurements, Leroy Alexander —155
Spurious areas in pole figures, A. H. Geisler—1245
Stress measurement by x-ray diffraction, H. R. Letner and S. R. Maloof—1440(L)
X-ray and infrared studies on the extent of crystallization of polymers, J. B. Nichols—840
X-ray noise observation using a photoconductive pickup tube, A. D. Cope and A. Rose—240
X-ray study of the graphitization of carbon black, C. R. Houska and B. E. Warren—1503

Lockheed announces

formation of its

Physics Research Laboratory

for advanced study in fields of

acoustics and optics

Creation of the Laboratory has created positions for...

Physicists with acoustics backgrounds to perform advanced study on reduction of internal and external aircraft noises, including problems such as:

1. sound transmission loss studies
2. acoustic treatment of enclosures for purposes of noise reduction
3. vibration isolation
4. investigation and analysis of noise sources
5. measuring techniques

Advanced degrees in Physics or Electrical Engineering preferred.

Physicists with optics backgrounds to perform advanced research in:

1. detection
2. searching
3. guidance
4. integration of optics into airplane control systems
5. infra-red tracking

Advanced degrees in Physics or equivalent experience preferred.

Lockheed offers you increased salary rates now in effect; generous travel and moving allowances; an opportunity to enjoy Southern California life; and an extremely wide range of employee benefits which add approximately 14% to each scientist's salary in the form of insurance, retirement pension, sick leave with pay, etc.

Those interested are invited to write E. W. Des Lauriers, Dept. JP-P-12, for an application blank and illustrated brochure describing life and work at Lockheed.

Lockheed

Aircraft Corporation

Burbank California

MISSILE SYSTEMS

Research
and
Development

Inquiries are invited from those who can make significant contributions to, as well as benefit from, a new group effort of utmost importance.

Lockheed

MISSILE SYSTEMS DIVISION

research
and
engineering
staff

LOCKHEED AIRCRAFT CORPORATION

VAN NUYS • CALIFORNIA

ENGINEERS NEEDED FOR RESEARCH AND DEVELOPMENT POSITIONS

in the

Design of electronic instrumentation for underwater ordnance, including high gain amplifiers, conventional filters, power amplifiers, oscillators and detectors in the ultrasonic range.

Analytical and experimental treatment of scientific research problems in the fields of hydrodynamics, acoustics, electronics, network theory, servomechanisms, mechanics, information theory and noise analysis, including analogue and digital computations.

Design of transducers, fundamental problems in underwater acoustics involving transmission, attenuation, reflection, etc. Problems in sound control and noise reduction. Acoustical aspects of systems research including operations research and feasibility studies.

Opportunities for graduate study
Liberal Vacation Policies
Excellent Working Conditions

Write
Personnel Director
THE PENNSYLVANIA STATE UNIVERSITY
ORDNANCE RESEARCH LABORATORY
STATE COLLEGE, PENNSYLVANIA

CAREER OPPORTUNITIES

in

NUCLEAR REACTOR TECHNOLOGY

Our expanding reactor program is creating new, outstanding research and development opportunities for capable young men with appropriate training, experience, or interests in reactor physics, instrumentation, and engineering. These are career openings in a stable, progressive organization involving both Government and industrial applications of atomic energy. Apply now for prompt, confidential consideration to

BATTELLE MEMORIAL INSTITUTE
505 King Avenue
Columbus, Ohio

Gaertner OPTICAL INSTRUMENTATION

A Divided Circle Spectrometer Reading to 1 Second of Arc

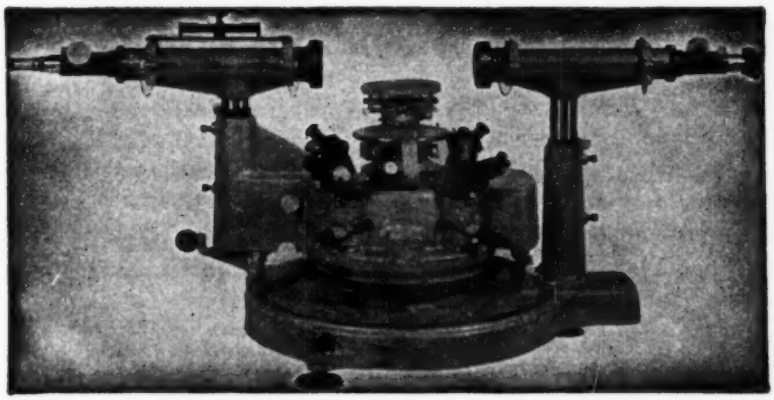

The L124 One Second Spectrometer

L124

Circle Dia.	300 mm
Reading to	1 sec.
Objectives	
Achromatic Triplets	
Dia.	50 mm
E.F.L.	540 mm
Prism Table Dia.	150 mm
Length Eyepiece to Slit	1400 mm
Shipping Weight	400 lbs.

THE L124 IS INTENDED FOR HIGH PRECISION MEASUREMENT OF REFRACTIVE INDEX, DISPERSION AND PRISM AND WEDGE ANGLES. BULLETIN NUMBER 157–52 LISTS DETAILS. REQUEST YOUR COPY.

THE GAERTNER SCIENTIFIC CORPORATION
1246 WRIGHTWOOD AVENUE . CHICAGO 14 . U.S.A.

---

the SYSTEMS ENGINEER at RCA

Systems engineers conduct studies to determine operational requirements . . . create and synthesize military equipment concepts . . . guide development of new integral elements . . . conduct evaluation programs to determine operational effectiveness.

You may qualify! Professional ***ability*** to create and analyze over-all complex systems and ***experience*** in electronic or electro-mechanical systems engineering required.

There are several opportunities now in:

AVIATION ELECTRONICS
INFORMATION HANDLING
COMPUTERS • RADAR
COMMUNICATIONS
MISSILE GUIDANCE

Send a complete resume of your education and experience to:

Mr. John R. Weld, Employment Manager
Dept. B-482L, Radio Corporation of America
Camden 2, New Jersey

RADIO CORPORATION OF AMERICA
ENGINEERING PRODUCTS DIVISION ***CAMDEN, N. J.***

Electronics Engineers

California Institute of Technology JET PROPULSION LABORATORY has desirable positions in the following fields. Applicants must have a minimum of B.S. degree.

•

RELIABILITY GROUP

To work on the reliability of electronic equipment as it concerns electronic circuits.

NEW CIRCUIT ELEMENTS GROUP

To carry on independent research in the construction and application of devices utilizing the phenomena of solid state physics and related fields. Initial assignments might include investigation of new magnetic phenomena, dielectric amplifiers, transistors, or original research leading to the development of a stable frequency standard.

ANTENNA GROUP

Work is particularly concerned with the analysis, development and design of radio frequency transmission and radiating structures.

TELEMETERING ENGINEER

Must be familiar with audio and radio techniques. Instrumentation, transistor circuit design, and noise theory experience desirable.

TEST EQUIPMENT ENGINEER

Must have experience in the design of integrated test equipment employing radar and audio techniques.

GROUND-RADAR ENGINEER

Must know pulse-radar techniques and servo mechanisms.

MISSILE MECHANICAL-ELECTRICAL ENGINEER

Must know gyroscopes and servo mechanisms plus precision machine work.

INERTIAL GUIDANCE ENGINEER

For system analysis and development.

GUIDANCE SYSTEM DESIGN AND ANALYSIS ENGINEERS

Must have experience in one or more of the following fields: noise and filter theory, ballistic and trajectory theory, radio or inertial guidance systems and techniques.

•

Send your summary of qualifications to:

California Institute of Technology
JET PROPULSION LABORATORY
4800 Oak Grove Drive • Pasadena 3, California

PHYSICISTS
ELECTRICAL ENGINEERS
MECHANICAL ENGINEERS

MS or PhD degree preferred

Our openings require technical personnel experienced in:

1. **Solution of physical problems related to infrared instrumentation, or**
2. **Applied research and development on optical instruments.**

If interested in becoming associated with a progressive, scientific instrument company, please submit a detailed resume to the Personnel Manager,

THE PERKIN-ELMER CORPORATION
NORWALK, CONNECTICUT

THE PHYSICAL REVIEW
Thirty Year Cumulative Index
1921 through 1950

Published in two volumes:
Author Index—543 pages
Subject Index—498 pages

This Index was prepared under the direction of Professor J. W. Buchta, Assistant Editor of THE PHYSICAL REVIEW from 1930 to 1950.

This two volume index furnishes a quick answer to who did what and when in this most significant period in the advancement of physics, as expressed in the pages of THE PHYSICAL REVIEW.

Subscribers who have files of the journals will need this index to make them more useful. Other researchers will find the index of great value in literature searches and for ready reference. For all libraries the index is a necessity.

Stiff paper binding.....(2 vols.) $14.00
Cloth binding.....(2 vols.) $16.00

Special Price for APS Members, 1 copy only
Stiff paper binding.....(2 vols.) $10.00
Cloth binding.....(2 vols.) $12.00

AMERICAN INSTITUTE OF PHYSICS
57 East 55 Street New York 22, N. Y.

Engineers and Physicists

Your Move

The men we seek are experts in their specialized fields, capable of filling responsible engineering positions with MELPAR, a leader in research and development. Perhaps one of these men may be you. We invite you to learn about our long-range military and industrial programs.

If you are experienced in one or more of the fields listed below, write us about yourself and let us tell you during a personal interview about our past record of success and how you can successfully fit into our future plans.

- *Network Theory*
- *Microwave Techniques*
- *UHF, VHF or SHF Receivers*
- *Digital Computers*
- *Magnetic Tape Handling Equipment*
- *Radar and Countermeasures*
- *Microwave Filters*
- *Flight Simulators*
- *Subminiaturization Techniques*
- *Electro-Mechanical Design*
- *Packaging Electronic Equipment*
- *Photographic Equipment Design*

Technical Personnel Representative

melpar, inc. *A Subsidiary of the Westinghouse Air Brake Co.*

452 Swann Ave., Dept. JA-7, Alexandria, Virginia or 11 Galen St., Watertown, Mass.

FOR *Research* THROUGH

INTERFEROMETRY

CONSULT

Paul M. McPherson
Precision Instruments
ACTON, MASS.

DESIGNERS and SUPPLIERS of MACH-ZEHNDER INTERFEROMETERS

Research Physicists

FOR SYSTEMS PLANNING AND ANALYSIS IN THE FIELD OF INTERCEPTOR RADAR FIRE CONTROL

At Hughes Research and Development Laboratories unusual attention is devoted to creation and preservation of a professional climate suited to the individual needs and interests of the advanced physicist, mathematician and engineer.

The Laboratories are presently in need of physicists with experience in systems planning and analysis. The work involves military studies of radar fire control systems for supersonic interceptor aircraft. Directly concerned is evaluation of strategic and tactical needs of the services to establish design objectives following a period of systems invention and early paper design down to the "black box" stage—with comparison of possible alternatives leading to recommendations for development.

Considerable analytic effort is also required on advanced projects involving complex interactions of noise, smoothing and prediction, multi-loop nonlinear servos, aircraft dynamics and controls, and the properties peculiar to mixed analog and digital systems.

Scientific and Engineering Staff

Hughes

Culver City, Los Angeles County, California

RESEARCH AND DEVELOPMENT LABORATORIES

Relocation of applicant must not disrupt an urgent military project.

POSITIONS OPEN

Teaching Opportunity
Electronics and Physics

Three positions in electronics engineering as well as advanced physics are open at a rapidly expanding Eastern technological university. Excellent opportunities for the right men. Write, giving experience and qualifications, to

Box 1254, Journal of Applied Physics, 57 E. 55 St., N. Y. 22, N. Y.

ENGINEER RECENT GRADUATE

Master's degree in applied mechanics, or in aeronautical engineering with minor in applied mechanics. Interesting position in the Applied Mechanics Department.

Please send complete resume to
Mr. A. T. Schwab.

BULOVA RESEARCH & DEVELOPMENT LABORATORIES, INC.
62-10 Woodside Ave., Woodside, L. I., New York

A.P.S.—A.A.P.T.
MEETING AND EXHIBIT
Jan. 27, 28, 29, 1955 New York City

An exhibit of technical books, instruments, and apparatus is being scheduled for the combined winter meeting of the American Physical Society and the American Association of Physics Teachers. The exhibit will be located in the East and Blue rooms of the Hotel McAlpin, 34th Street and Broadway. These rooms are adjacent to the registration desk located on the first mezzanine of the hotel. The exhibits will be open each day of the meeting, January 27, 28, 29, 1955, and everyone attending the meeting is cordially invited to visit the exhibits.

Publishers and manufacturers interested in exhibiting should write to Mr. T. Vorburger, Exhibit Manager, 57 East 55th Street, New York 22, N. Y.

ELECTRONIC PHYSICISTS
ELECTRONIC ENGINEERS

OUR STEADILY EXPANDING LABORATORY OPERATIONS
ASSURE PERMANENT POSITIONS AND UNEXCELLED
OPPORTUNITY FOR PROFESSIONAL GROWTH IN

RESEARCH — DEVELOPMENT — DESIGN

ELECTRONIC COUNTERMEASURES
RADAR SYSTEMS
MICROWAVE COMPONENTS
AIRBORNE ANTENNAS
MISSILE GUIDANCE CONTROL SYSTEMS
SOLID STATE PHYSICS
TEST EQUIPMENT

THE EMPLOYMENT DEPT.
ADDRESS INQUIRIES TO FARNSWORTH ELECTRONICS CO.
FORT WAYNE, IND.

PLACEMENT SERVICE REGISTER
OF THE
AMERICAN INSTITUTE OF PHYSICS
to be held in connection with the
American Physical Society Meeting
January 27, 28, 29, 1955
Hotel New Yorker, New York, N. Y.

LOOKING FOR PHYSICISTS?
Universities, institutions, government laboratories, and companies wishing to post notices of positions may send descriptions of the openings on 8½ x 11 paper in multiple copies (*15 required*) to the Institute office, or post them on arrival at the meeting. If you plan to have a representative present, to interview applicants, please indicate his name at the bottom of the job description sheets.

SEEKING A NEW POSITION?
Applicants may obtain registration forms and further information from the Institute office. *Pre-registration is essential.* Complete registration forms must be received at the Institute office by January 10, 1955 to insure their inclusion at this register.

INTERVIEWS.
It is to the advantage of the registrants to be present. Interviews will be arranged between employers' representatives and applicants attending the meeting.

COMPLETE REGISTER of applicants will be available upon request at the meeting and after the meeting at a nominal service charge.

PLEASE REPORT TO THE PLACEMENT OFFICE UPON ARRIVAL AT THE MEETING

AMERICAN INSTITUTE OF PHYSICS, 57 East 55 Street, New York 22, N.Y.

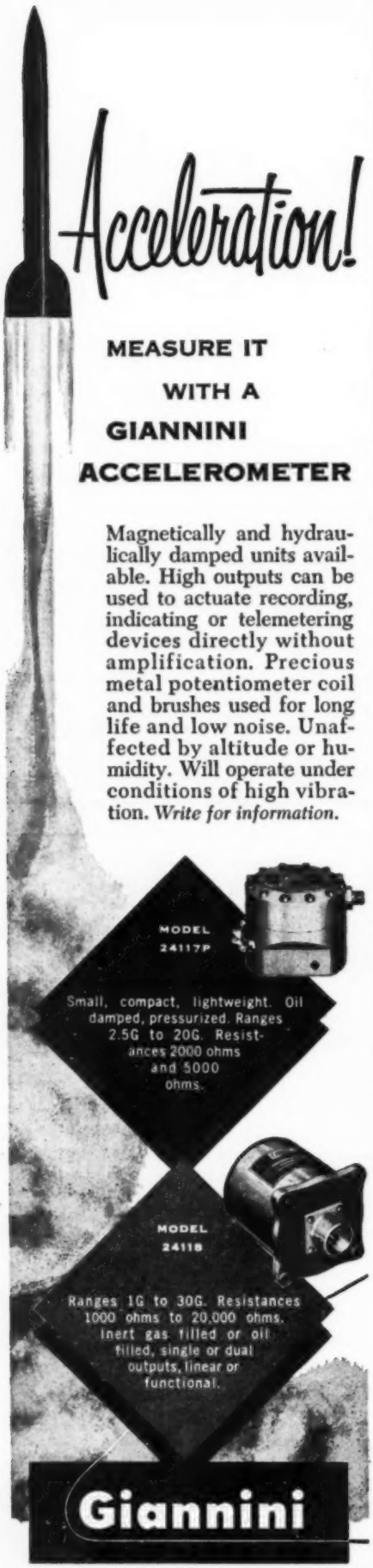
Acceleration!
MEASURE IT
WITH A
GIANNINI
ACCELEROMETER
Magnetically and hydraulically damped units available. High outputs can be used to actuate recording, indicating or telemetering devices directly without amplification. Precious metal potentiometer coil and brushes used for long life and low noise. Unaffected by altitude or humidity. Will operate under conditions of high vibration. Write for information.
MODEL 24117P
Small, compact, lightweight. Oil damped, pressurized. Ranges 2.5G to 20G. Resistances 2000 ohms and 5000 ohms.
MODEL 24118
Ranges 1G to 30G. Resistances 1000 ohms to 20,000 ohms. Inert gas filled or oil filled, single or dual outputs, linear or functional.
Giannini

G. M. GIANNINI & CO. INC.
Airborne Instrument Division
PASADENA 1, CALIFORNIA

INDEX TO ADVERTISERS

Name	*Page*
THE ARNOLD ENGINEERING COMPANY — Alnico Permanent Magnets.	ii
ATOMIC INSTRUMENT COMPANY	Cover 4
BATTELLE MEMORIAL INSTITUTE	xvi
BELL TELEPHONE LABORATORIES	iii
BETA ELECTRIC COMPANY — High Voltage DC power supplies, kilovoltmeters, electronic microammeters, portable projection oscilloscopes and regulated DC power supplies of all types.	x
CALIFORNIA INSTITUTE OF TECHNOLOGY	xviii
CENTRAL RESEARCH LABORATORIES, INC.	xii
COMPUTER COMPANY OF AMERICA — Division of Bruno-New York Industries Corp.	xiii
FARRAND OPTICAL COMPANY	xii
FARNSWORTH ELECTRONICS COMPANY	xxi
GAERTNER SCIENTIFIC CORP.	xvii
GENERAL DYESTUFF CORP.	viii
GENERAL RADIO COMPANY — Manufacturers of electronic measuring instruments; vacuum-tube voltmeters, amplifiers and oscillators; wave analyzers, noise meters and analyzers, stroboscopes, laboratory standards of capacitance, inductance and frequency; impedance bridges, decade resistors and condensers, air condensers and variable inductors; rheostats, Variacs, transformers; other laboratory accessories.	Cover 3
G. M. GIANNINI & CO., INC.	xxii
HUGHES RESEARCH & DEVELOPMENT LABS.	xx
LEEDS & NORTHRUP COMPANY — Manufacturers of Galvanometers, Resistors, Bridges, Condensers, Inductances, Potentiometers, Testing Sets; Temperature Measuring, Recording and Controlling Apparatus; Instruments for Measuring and Controlling Conductivity of Electrolytes and Hydrogen Ion Concentrations.	i
LOCKHEED AIRCRAFT CORP.	xvi, vi, xv
PAUL M. McPHERSON PRECISION INSTRUMENTS	xix
MELPAR, INC.	xix
PENNSYLVANIA STATE UNIVERSITY	xvi
PERKIN-ELMER CORP.	xviii
RADIO CORPORATION OF AMERICA	xvii
THE RAMO-WOOLDRIDGE CORP.	iv
SANBORN COMPANY	vii
F. J. STOKES MACHINE COMPANY	v
SUPERIOR ELECTRIC COMPANY	xi
TRACERLAB, INC.	ix
TRANSRADIO, LIMITED	xii
W. M. WELCH SCIENTIFIC COMPANY — Manufacturers of high-vacuum pumps, both mechanical and diffusion; vacuum gauges; electrical measuring instruments; physics equipment; and other items for the physical and chemical laboratories.	xiv

POSITIONS OPEN

Lamp Engineer—heavy experience in electrical discharge lamps (Mercury) qualified for taking charge of lamp engineering, experimental and design work. **Transformer Designer**—to work on small to medium size transformers for illuminating field. Long established Newark, N. J., lamp manufacturer engaged in both peace time and government contracts. Box 1254B, 57 East 55 St., New York 22, N. Y.

Wide Range
Power Source
For Audio and Radio Frequencies

One of the most widely used G-R Oscillators is the popular Type 1330-A Bridge Oscillator. It is an ideal power source for bridge and antenna measurements, and for general laboratory use. Its features include exceptionally wide range, good power output, excellent stability and low distortion.

★ Three Audio Frequencies: line frequency, 400 c and 1000 c

★ Continuous R-F Coverage: 5 kc to 50 Mc in 8 direct-reading ranges

★ Over One Watt Output

★ Excellent Accuracy: ±5% for 400 and 1000 c; ±2% above and ±3% below 150 kc

★ Low Distortion: 3% Over most of r-f range. Approximately 5% at audio. Envelope less than 6% at 60% modulation and less than 3% at 30% level.

★ Incremental frequency dial indicates increments of 0.1% per division from 5 kc to 15 Mc

★ Small Leakage: stray fields about 50μv per meter 2 feet from oscillator

Type 1330-A Bridge Oscillator: $525.00

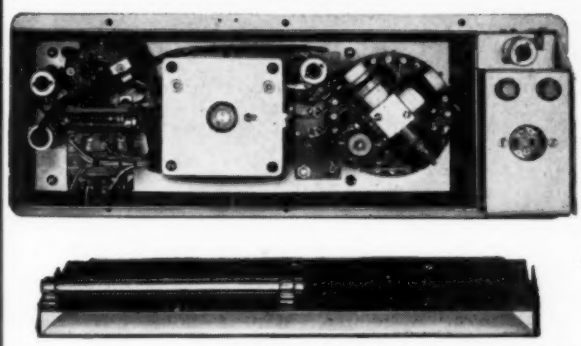

Assembly plugs into heavy brass box. Double shielded cover, filtered leads and shielding sleeves over the four projecting shafts reduce leakage to its lowest minimum.

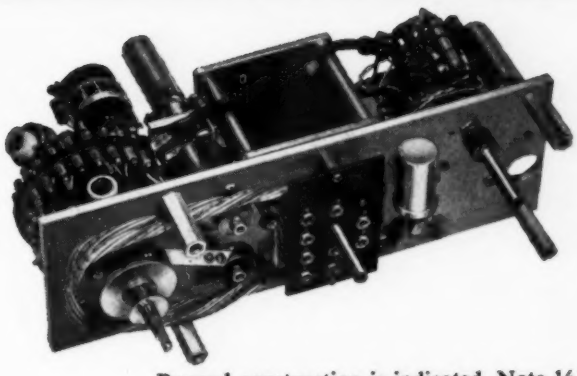

Rugged construction is indicated. Note ½" tuning capacitor tie rods and 3/16" end-plates. Preloaded ball-bearings are used. Entire assembly on ¼" sub-panel for extra rigidity. Servicing and testing cable provided.

We sell direct. Prices shown are NET, f.o.b. Cambridge or W. Concord, Mass.

GENERAL RADIO Company

275 Massachusetts Avenue, Cambridge 39, Massachusetts, U.S.A.

90 West Street NEW YORK 6
8055 13th St., Silver Spring, Md. WASHINGTON, D.C.
920 S. Michigan Avenue CHICAGO 5
1000 N. Seward Street LOS ANGELES 38

ADMITTANCE METERS
AMPLIFIERS
COAXIAL ELEMENTS
DISTORTION METERS
FREQUENCY MEASURING APPARATUS
FREQUENCY STANDARDS
IMPEDANCE BRIDGES
LIGHT METERS
MEGOHMMETERS
MODULATION METERS
MOTOR CONTROLS
NULL DETECTORS
OSCILLATORS
PARTS & ACCESSORIES
POLARISCOPES
PRECISION CAPACITORS
PULSE GENERATORS
R-L-C DECADES
R-L-C STANDARDS
SIGNAL GENERATORS
SOUND & VIBRATION METERS
STROBOSCOPES
TV & BROADCAST MONITORS
U-H-F MEASURING EQUIPMENT
UNIT INSTRUMENTS
VARIACS®
V-T VOLTMETERS
WAVE ANALYZERS
WAVE FILTERS

ATOMIC'S *new and different* SCALERS

using Cold Cathode Tubes

• low current • low heat • long-lived

- new—simpler—more reliable
- exclusive improved circuits (Pat. Applied for)
- use of cold cathode tubes eliminates many hard tubes
- lower power consumption
- cooler operation
- more economical for general radioactivity counting

Model 1031 general purpose, 5 microsecond resolving time, scaler for radioactivity counting

3 MODELS FOR YOUR CHOICE

Model 1031 Pre-set Time Scaler (shown above), with built-in Regulated H. V. Supply, 500-2500 volts

Model 1035 Pre-set Time Scaler identical to Model 1031, except with 1000-5000v. Regulated H. V. Supply

Model 131 Pre-set Time Scaler (shown below) for use with separate H. V. Supply

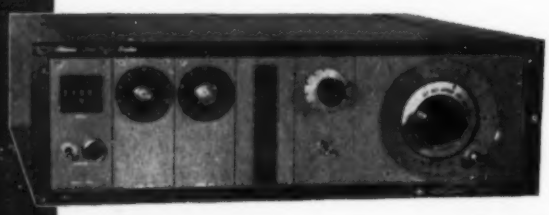

MODEL 131

Atomic offers these additional new scalers for Geiger, Scintillation or Proportional counting . . . more economical instruments with the newest design features . . . may be used with standard Linear Amplifiers, Pulse Height Analyzers and suitable detection devices.

INPUT SENSITIVITY, 0.25v. negative, with adjustable stable discriminator
RESOLUTION, better than 5 microseconds
REGULATED HIGH VOLTAGE SUPPLY, (60 cycle type), 500-2500v. with coarse and fine controls (Model 1031)
SCALE FACTOR, scale of 1000 followed by 4-digit electro-mechanical register
CONTROL: Pre-Set Time or manual with elapsed time to 1 hour
RESET: Single switch resets both register and scaling stages
TIMER: Atomic's Model 960 Dual-Purpose Precision Timer, preset or elapsed time from 1 second up to 1 hour
DIRECT READING "VISUALIZED" COUNT
UNITIZED CONSTRUCTION, functional plug-in units provide simplified circuits of high reliability

Atomic's complete line of "research quality" instruments, including: Scalers, Amplifiers, H. V. Supplies, Analyzers, Scintillation equipment, etc., are described in the new General Catalog. Write for your "registered" copy.

Get complete information on Atomic's new Cold Cathode SCALERS—write today for Bulletin 1031-3.

For full details on Atomic's Standard 10-10 Series Scalers, please request Bulletin 1010-3.

Watch for more new ATOMIC precision instruments for nuclear research.

ATOMIC INSTRUMENT COMPANY

84 MASSACHUSETTS AVE. CAMBRIDGE 39, MASS.

Linear Amplifiers, Scalers, High Voltage Supplies, Scintillation Counters, Count Rate Meters, Coincidence and Anticoincidence Instruments, Differential Pulse Height analyzers, Accessories.

SALES REPRESENTATIVES

H. E. RANSFORD CO. — 2601 Grant Bldg., Pittsburgh 19, Pa.
W. A. BROWN & ASSOCIATES — Alexandria, Virginia
Branch Offices — throughout Southeastern U.S.
PACKARD INSTRUMENT CO. — P.O. Box 428, LaGrange, Ill.
KITTLESON COMPANY — Los Angeles 46, Calif.
Branch Offices — San Francisco, Calif. — Albuquerque, N.M.
RON MERRITT COMPANY — Seattle, Wash.
STRAUS-FRANK COMPANY, Eng. Prod. Div. — Houston, Texas
CANADIAN MARCONI CO. — Montreal, P.Q.
Branch Offices—Toronto—Winnipeg—Vancouver—Halifax